Covalent End-Immobilization of Oligonucleotides onto Solid Surfaces

by

Ivan H. Lee

B. S., Chemical Engineering (1992)

University of California, Berkeley

M. S. in Chemical Engineering Practice (1998)

Massachusetts Institute of Technology

Submitted to the Department of Chemical Engineering
in Partial Fulfillment of the Requirements for the Degree of
Doctor of Philosophy in Chemical Engineering

at the

Massachusetts Institute of Technology
[September 2001]
August, 2001

Signature of Author.... .....
Ivan H. Lee
Department of Chemical Engineering
August 8, 2001

Certified by..... .....
Paul E. Laibinis
Associate Professor of Chemical Engineering
Thesis Supervisor

Accepted by.....
Daniel Blankschtein
Professor of Chemical Engineering
Chairman, Committee for Graduate Students

Covalent End-Immobilization of Oligonucleotides onto Solid Surfaces

by

Ivan H. Lee

Submitted to the Department of Chemical Engineering
On August 8, 2001 in Partial Fulfillment of the
Requirements for the Degree of Doctor of Philosophy in
Chemical Engineering

ABSTRACT

With the completion of the Human Genome Project, the focus of genetics research has shifted towards functional genomics, with emphasis on gene expression and polymorphism studies. To this end, there is rapidly increasing interest in solid-phase, high-throughput, combinatorial microarrays for DNA assays. For this purpose I synthesized oligonucleotides (oligos) stepwise onto derivatized SiO_2 surfaces. Then double-stranded (ds)DNA molecules with "dangling end" oligo overhangs were immobilized onto the oligo surface by hybridization. Photolysis of psoralen crosslinkers covalently immobilized the dsDNA molecules to the oligo surface. The covalently end-attached dsDNA formed brush-like structures where the dsDNA strand could react under conditions resembling the natural solution-state found *in vivo*. This method minimized the possibility of nonspecific surface interactions, and could be developed for site-specific segregation of mixed dsDNA sequences from solution onto surface microarrays.

Oligo surfaces with different densities were synthesized to determine the conditions that optimize dsDNA hybridization. The oligo surface density was controlled by derivatizing the SiO_2 surface with mixed compositions of alkylsilane molecules ($X\text{-}(CH_2)_{11}\text{-}SiCl_3$, X= OH or CH_3). X-ray photoelectron spectroscopy was used in conjunction with commercially available iodine-labeled nucleotides for quantifying oligo surface densities and stepwise reaction (coupling) efficiencies. ^{32}P-radiolabeled complementary oligos and dangling-end dsDNA sequences also were used to determine hybridization yields and efficiencies. The experimental results clearly indicated that oligo coupling efficiency increased with decreasing oligo surface density, and also with increased coupling time. Consequently, I maximized the yield of full-length surface oligos by manipulating these reaction conditions. In addition, hybridization efficiency was inversely related to oligo surface density, and total hybridization yield was achieved at an oligo surface density of between 2 and 4 x 10^{-11} moles/cm^2. The oligo surfaces were found to be thermally stable and reusable for performing multiple hybridization experiments on glass slides.

dsDNA with 5' oligo overhangs were generated by PCR with a customized oligo primer. The dsDNA molecules were successfully immobilized onto oligo surfaces, at surface densities of approximately 2 x 10^{-13} moles/cm^2. The spatial addressability of patterned oligo surfaces was demonstrated. Psoralen crosslinking was observed to proceed at 30-80% efficiency, compared to optimal 50% efficiency in solution phase. Upon heating the end-immobilized dsDNA unraveled to form covalently end-immobilized ssDNA probes with sequence lengths up to 390 bp that were employed in hybridization studies.

Thesis Supervisor: Paul E. Laibinis
Title: Associate Professor of Chemical Engineering

To my father, Chu-Yuan Lee, whose generous and unwavering support helped me to complete this humble endeavor.

Acknowledgements

It has been a long journey through time and space to complete my research MIT. Many people have helped me along the way, and I am indebted to their generosity. Though it may be incomplete, I will try my best to acknowledge them:

My thesis advisor, Prof. Paul E. Laibinis, for his continued guidance, support, and critiques in all aspects of my research. I met Paul by Armstrong-inspired serendipity, and to date I still cannot find a more knowledgeable, dedicated, and thoughtful advisor. His research and analysis skills are matched by his unwavering principles for being an objective and unbiased scientist and academic. It is my fortune to have worked with him.

My thesis committee member and advisor on a collaborative project with the Department of Biology at MIT, Prof. Leonard S. Lerman, for his insights and inspirations on the myriad details of my project. Leonard possesses unmatched breadth of knowledge in chemistry, engineering, math, biology, electronics, explosives, machining skills, philosophy, history.....you get the picture. Leonard is always happy to share his skills and experience with me, imparting his wisdom with sharp wit and lots of patience.

My thesis committee members-Profs. Hammond, and Lauffenburger, for their support and advice from their respective fields concerning my research.

My colleagues in the Laibinis group, Kane, Mark, Namyong, Seokwon, Ben, and Richard-to each and every one of you thanks for imparting your hard-earned knowledge in organic synthesis, surface characterization, and graduate life in general to a new group member who had a tendency for reading while in motion and dozing at his desk. Your help was invaluable to me. Special thanks to Namyong, with whom I've had many a long conversation on topics unrelated to research. True friends help their buddies stay sane.

Also to other group members Jiehyun, Tseh-Hwan, Manish, James, Dan, and Vikas. Thanks for sharing your good humor and friendship, introducing a new social aspect to 66-425, you have made life in the lab quite pleasant, to my surprise.

My associates in the Department of Biology at MIT, Dr. Kathy Hogan and Jeremy Lambert, who taught me how to be a biologist. Jeremy introduced and trained me on the skills and techniques required for biological research, while Kathy helped me truly understand how to approach and analyze issues in biology. She also provided me with the template DNA need for my research, as well as priceless background information that I initially lacked in the field. Kathy carries part-time duties as a collaborator, and full time duties as a friend.

My fellow combatants in Practice School, Mitch, Tamara, Hua, Stephanie, Robert, Brian, and Ash, who showed me that it is possible to competently and efficiently solve engineering problems in one month in the real world (outside MIT) and to have tons of fun at the same time, if 100 hour weeks and 100 page reports are one's idea of fun.

Finally, but most importantly, my father Chu-Yuan Lee, and my son Jonathan Lee, my motivation for being at MIT and completing my dissertation. My father first encouraged me to pursue graduate studies, and ever since I entered MIT he has been an tireless supporter to me in every way, and I owe my work here to his generosity. Jonathan has been with me for the past 2.5 years, behaving remarkably well and tolerating my occasional retreats into research insanity in the duration. Thank you.

List of Figures

Chapter 1 figures

Chapter 2 figures

Chapter 3 figures

Chapter 4 figures

Appendix I figures

List of Tables

Chapter 1: Introduction

1.1 Evolution of biological research

1.1.1 DNA sequencing

Ever since *Watson and Crick* determined the structure of deoxyribonucleic acid (DNA) in 1953 (Figure 1-1), the mapping and decoding of the estimated 30,000 to 60,000 genes in the human genome has been one of the most important goals of modern biological research. Previously, genetic phenotypes were only deduced by the selective breeding of animals or plants, which was a limited and narrow method for studying the variations and mutations that occur in the genetic code. However, through the meticulous efforts of numerous researchers, scientists were able to deduce the rules of DNA base-pair hybridization, the mechanisms of DNA transcription (to mRNA) and translation (to proteins), the relationships between the 3-nucleotide (nt) long DNA codons and their corresponding amino acids, and the codes for the "start" and "stop" transcription commands[1,2]. These encouraging developments in the fundamental understanding of DNA function motivated the biological community to embark on the mission of decoding the human genome. This undertaking could not proceed until the appropriate enabling technologies discussed below were developed.

1.1.2 DNA amplification

The critical issues in DNA sequencing are DNA separation and purification, DNA amplification, and the sequencing method itself. Various protocols have been developed to obtain a purified DNA sample from the chemically complex environments of cell

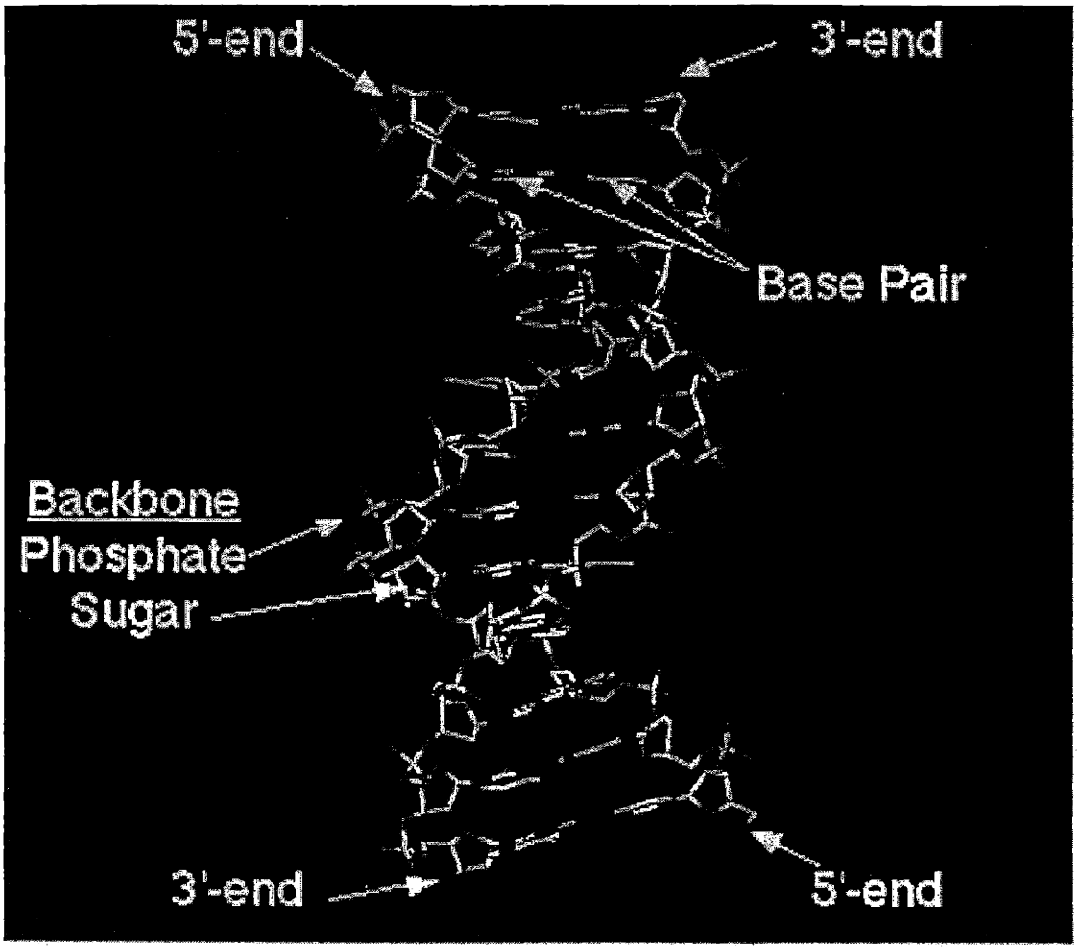

Courtesy of Griffith et al., Introduction to Genetic Analysis, 2000

Figure 1-1. Structure of the DNA double helix. The two ssDNA strands are oriented in an antiparallel fashion (3' end of one strand to the 5' end of its complementary strand). The hybridization occurs through the formation of hydrogen bonds between matched base pairs (**A**denine-**T**hymine, **C**ytosine-**G**uanine). The double helix structure is a result of the specific conformations induced by the base pair hydrogen bonds, and the favorable thermodynamics from base stacking. The nucleotide bases are surrounded by a negatively charged phosphate backbone.

nuclei or mitochondria; however, the obtained DNA quantities are too minute for effective characterization by existing methods. The first bottleneck for DNA sequencing was the ability to produce a sufficient sample of DNA. This shortcoming was first overcome by Recombinant DNA techniques. Restriction endonucleases were used to cut the DNA chain at specific sequence sites. The resulting short DNA segments (donor DNA) had short oligo overhangs ("sticky ends") created by the endonuclease action. DNA plasmid rings (vectors) were designed with specific sequence (restriction) sites that were also cut open by endonucleases to expose oligo overhang sequences complementary to the sticky ends of the donor DNA. The donor DNA could be incorporated into the vector through hybridization of the complementary sticky ends, and the two DNA segments could be permanently linked together using the enzyme DNA ligase. In turn, the plasmid vectors containing the donor DNA are introduced (transformed) into a bacterium such as *E. coli*. As the bacteria are cultured in biofermentation reactors and proliferate, the DNA is amplified accordingly[2,3].

Later, researchers discovered certain thermophilic DNA polymerases in bacteria that live in thermal vents. The enzymes from these bacterial strains could function at high temperatures close to the boiling point of water. One example is Taq polymerase. Thus, the thermophilic polymerases operated at temperatures at which the two DNA strands in the double helix separate, or "melt", into two complementary single strands. At about the same time as the discovery of thermophilic DNA polymerases, new methodologies were developed that enabled the stepwise chemical synthesis of oligonucleotide (oligo) chains by a solid phase manner similar to the *Merrifield* approach for synthesizing polypeptides on polymeric supports. The oligos were synthesized stepwise on controlled pore glass (CPG) supports using a steadily evolving series of reaction chemistries that were developed during this time. Upon completion of the synthesis, in this approach the prepared oligos are cleaved from the support, isolated, and then purified. The synthesized oligos can be labeled with radioactive or fluorescent tags and used as DNA probes in hybridization reactions. Among the various synthesis chemistries, the most reliable

methodology is the 5' dimethyltrityl (DMT) protected phosphoramidite chemistry for linking together nucleotides developed by *Caruthers*[4,5].

Muller utilized the advances in stepwise oligo synthesis and polymerase reactions to create a synthetic protocol for DNA amplification, the polymerase chain reaction (PCR)[6,7]. In this process, two oligo chains of 20-25 nt length are produced by a stepwise process of solid phase synthesis on CPG supports. The sequences of the synthesized oligo chains are designed to be complementary to the two ends of the targeted DNA segment (the template) and are called "primers". The template DNA is combined with the two complementary primer sequences (in molar excess to ensure that the single-stranded (ss) template DNA strands prefer to hybridize with the oligo primers), and a thermophilic polymerase such as Taq. The mixture is subjected to repeated temperature cycles to facilitate melting of the template DNA (at ~ 95 °C), primer annealing (to hybridize the primers to the template ssDNA at ~ 55-62 °C), and polymerase extension of the remaining ssDNA chain from the 3' end of the primer (at ~ 72 °C). This process is repeated many times to produce roughly a doubling in the amount of the template DNA with each cycle. The PCR reactions readily resulted in DNA amplification scales on the order of millions after 2-3 hours and about 28-33 thermal cycles. PCR is now performed routinely in automated, programmable thermocycler machines, and has effectively solved the sample size problem.

1.1.3 DNA sequencing

The sequencingof DNA is often accomplished using gel-based electrophoresis. In the process, the DNA to be sequenced is first amplified by PCR and then cut into smaller fragments with nucleases. The DNA fragments are introduced into a polymeric hydrogel (agarose or crosslinked acrylamide), which is immersed in a buffer solution. An electric potential is applied to the gel, creating an electric field that induces the negatively charged DNA segments to move along the gel towards the positive electrode, and to separate on the gel according to their length.

Two approaches have been used to generate the nuclease sites along the DNA chain. *Maxam-Gilbert* introduced a method whereby the DNA samples are reacted with chemicals that selectively modify one of the four nucleotides - adenine (A), cytosine (C), guanine (G), and thymine (T) along the DNA sequence. The sample is split into 4 aliquots, and each aliquot is exposed to one of the four chemical modifiers. Next, an exonuclease is combined with the modified DNA for a limited time. The modified nucleotides serve as target sites for enzymatic cleavage. Because of the imposed time limitation, the exonuclease is only able to partially digest the DNA chain, resulting in a collection of DNA fragments of random length, each cleaved at the chemically modified sites. The enzymatically-digested samples are then loaded onto a polyacrylamide gel and undergo electrophoresis. The four aliquots, each cut into fragments at a different specific nucleotide (A, T, G, or C), are loaded onto the gel in parallel. During the electrophoresis the digested DNA fragments are separated according to their length, and the DNA sequence is read by moving in the direction of increasing DNA fragment length. The DNA sequence is identified by electrophoresis by determining which one of the four nucleotides was cut for each different fragment length [1,8].

More recently, *Sanger* introduced an alternative method to that of Maxim and Gilbert, that employed dideoxyribonucleotide triphosphates (ddNTP)[1,9]. Unlike regular deoxyribonucleotide triphosphates (dNTP), the ddNTPs lacked 3' hydroxyl groups. This chemical alteration prevented the enzymatic addition of more nucleotides at the 3' end of any ddNTP molecule; however, the ddNTP could be incorporated at its 5' end into a DNA chain. In addition, the ddNTPs are labeled with different fluorescent tags. In one reaction, minute quantities of fluorescent-labeled ddATP are added to a regular mixture of dNTP for PCR. The ddATP competes with regular dATP for incorporation into the DNA chain during the amplification reaction. Since the ddATP prevents further extension in the 3' direction, the polymerization reaction stops at random lengths along the DNA chain, ending for each sequence with a terminal ddATP. The PCR reaction is repeated on the initial DNA sample using the other ddNTPs (T, C and G). Then the four ddNTP-labeled DNA fragments are loaded in parallel on a polyacrylamide gel and separated

according to their length by electrophoresis. The gel is characterized by fluorescence with the appropriate excitation wavelengths, one for each ddNTP. As for the Maxim-Gilbert sequencing technique, the gel is read in the direction of increasing chain length. The DNA sequence is then determined by identifying the characteristic fluorescent signature of each ddNTP at the different DNA chain lengths on the gel.

In addition to the resolution of these critical technical bottlenecks during the past few decades, rapid improvements have been made in the automation and integration of the complete sequencing process[10-13] based on the Sanger fluorescent ddNTP approach, and in the creation of powerful bioinformatics software[14-17] to organize, interpret, manipulate, and store the enormous amounts of generated experimental data. These techniques drastically increased the pace of DNA sequencing, and with the added pressure of competition in gene sequencing by Celera (who wanted patents for their sequenced genome), the government sponsored International Human Genome Sequencing Consortium (IHGSC) completed a rough draft of the entire genome in 2001, a few years ahead of schedule, when Celera and IHGSC jointly announced a rough draft of the human genome[156,157].

1.1.4 Genomics and physiological functions

Though over 90% of the sequence of the entire human genome has been decoded[156,157], the deciphering and translation of the genomic data to protein amino acid sequences and the determination of their functions (i.e. functional genomics) are just beginning. Functional genomics is a much less straightforward process as compared to DNA sequencing due to the incredible complexity of the human body. Each biological function is regulated and implemented by a collection of genes, which complicates the problem of establishing causal relationships. In addition, gene expression affects physiological processes at many levels, including mRNA expression, protein expression,

biological functions at the cellular level, and phenotype expression. However, the procession is nonlinear and often the levels are interrelated in complicated ways.

Analysis of sequenced genomic DNA revealed that 97% of the DNA in the human genome consists of noncoding, or "junk" DNA[2]. Of the remaining coding regions (primary transcripts) are separated into introns (the part of the primary transcript that is removed by splicing during RNA processing) and exons (the part of the primary transcript that is expressed as mRNA and tRNA)[2]. The exons are the major determining factor in protein synthesis. Also, during the transcription of DNA into mRNA, the transcription may start at a different nucleotide along the gene sequence and create an alternative "reading frame" for generating mRNA. Thus, the shift in reading frames could result in the ability of one gene to become transcribed into multiple proteins[2]. In addition, many genes may act in concert to affect a particular metabolic pathway. Furthermore, most expressed proteins undergo extensive post-translational modifications[18,19] before they become active. For some of these modifications, portions of the peptide chain are removed by splicing reactions during the process. Thus, the final amino acid sequences of a functional protein or enzyme may no directly match its mRNA or genomic DNA counterpart.

The above phenomena that affect the final protein sequence further obscure the picture between DNA and protein structures. Consequently, there is a large discrepancy between my present knowledge of the genomic DNA sequence and full understanding of gene expression and the effects of genetic mutations. There also remain conceptual and functional gaps between genomics and proteomics, as well as between proteomics and the expressed phenotypes. Therefore, the first question is how to best approach genomics research. Gene expression is observable at the mRNA, protein, and cellular levels. Many researchers argue correctly that both cell function and protein expression are closer to accurately explaining physiological processes than is gene expression. However, present constraints in obtaining adequate samples and problems in devising reliable and sensitive characterization techniques have significantly hindered progress for such analysis.

1.1.5 Comparison between studies of genomics, proteomics and whole cells

Because of the variables created by post-translational protein modifications, it is helpful to study either living cells or proteins directly, in order to obtain a clear picture of many biological mechanisms. Despite this preference for detection, proteomics research is not yet practical due to the delicate structure and functional relationship of all enzymes. For example, a slight change in the conformation of an enzyme could readily result in its deactivation or its loss in specificity[18,20]. More importantly, there is no synthetic protocol equivalent to PCR for amplifying protein amounts. Because of the lack of generated protein sample available for study, the development of extremely sensitive characterization techniques would be needed for obtaining proteomics data. Otherwise, proteins expressed at low levels would be missed, resulting in inaccurate or incomplete interpretations of biological functions. In comparison, a single PCR run can amplify a DNA sample by a factor of 10^6. This amplification greatly enhances the ability to detect the presence of small numbers of mRNA copies in a cell and effectively improves the sensitivity and accuracy of experiments directed toward DNA over those directed toward protein analysis.

At present, researchers are studying protein expression in whole cells using labels such as green fluorescent protein (GFP)[21-23]. The genomic sequence for GFP is known and cloned genes are available. In this approach, the GFP genomic sequence is spliced adjacent to the genomic sequence of a target protein. The hybrid GFP-target protein genetic material is then cloned into a cell line. During the transcription of the protein, the GFP sequence is also transcribed, resulting in a hybrid containing GFP linked to the target protein. Therefore, when the target protein is expressed the fluorescent signature of GFP is provided for detection. An advantage of using whole cells for proteomics studies lies in the ability to observe the location of the expressed protein within the cell. This information is critical since there are various organelles in a cell and the ability to trace the route of a protein from its sources is helpful in determining its function. In addition, many whole cell studies are designed for living cells, allowing researchers to observe

biological processes *in vivo* instead of *in vitro*. The *in vivo* capability increases the accuracy of data interpretation. However, whole cell studies are technically unpractical due to the extreme difficulty of effectively characterizing multiple reactions or pathways simultaneously within living cells.

As an alternative, biologists realized that the decoded genome could provide a foundation for researching the mechanisms of many biological functions. One approach is to observe how the level of gene expression throughout the genome is affected by a change in environmental conditions. Another area of research is determining the effects of mutations on phenotypes and their mechanistic contribution to genetic and metabolic processes. Thus, many present researchers focus on DNA probes as a practical starting point for genetics research, with a particular emphasis on studying gene expression and polymorphisms (mutations).

In addition to now having an almost complete library of genomic DNA available for reference and access to DNA amplification by PCR, the relative simplicity of the structural conformations and binding rules for DNA as compared to amino acids make them better candidates for intensive manipulation and study in the lab. The four bases of DNA consist of two purines, G and A, and two pyrimidines, C and T, and are shown in Figure 1-2. Of these bases, there is a highly specific binding or hybridization between A and T and between C and G. The hybridizations occur through hydrogen bonding (see Figure 1-3) to provide base-pairing. Of these two pairs, the GC hybrids are more thermodynamically stable compared to AT hybrids, partially by virtue of having an extra hydrogen bond in their assembly (three vs. two), and predominately by more favorable base stacking[1]. The specific base-pair hybridizations coupled with base stacking along a DNA chain provide the thermodynamic stability necessary to produce the signature double helix structure of double-stranded DNA (dsDNA)

Besides the regularity and simplicity of DNA hybridization, an additional advantage of centering research on DNA is its reliance on only four bases in its

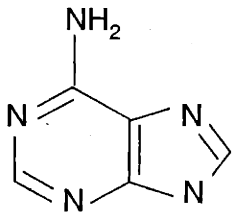

Adenine

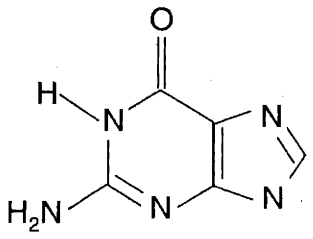

Guanine

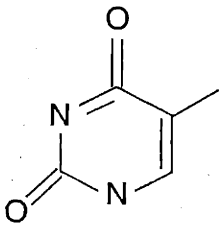

Thymine

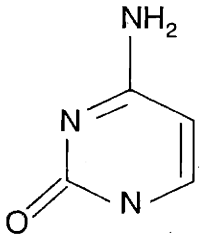

Cytosine

Figure 1-2. Structures of the four DNA bases: Adenine (A), Guanine (G), Thymine (T) and Cytosine (C).

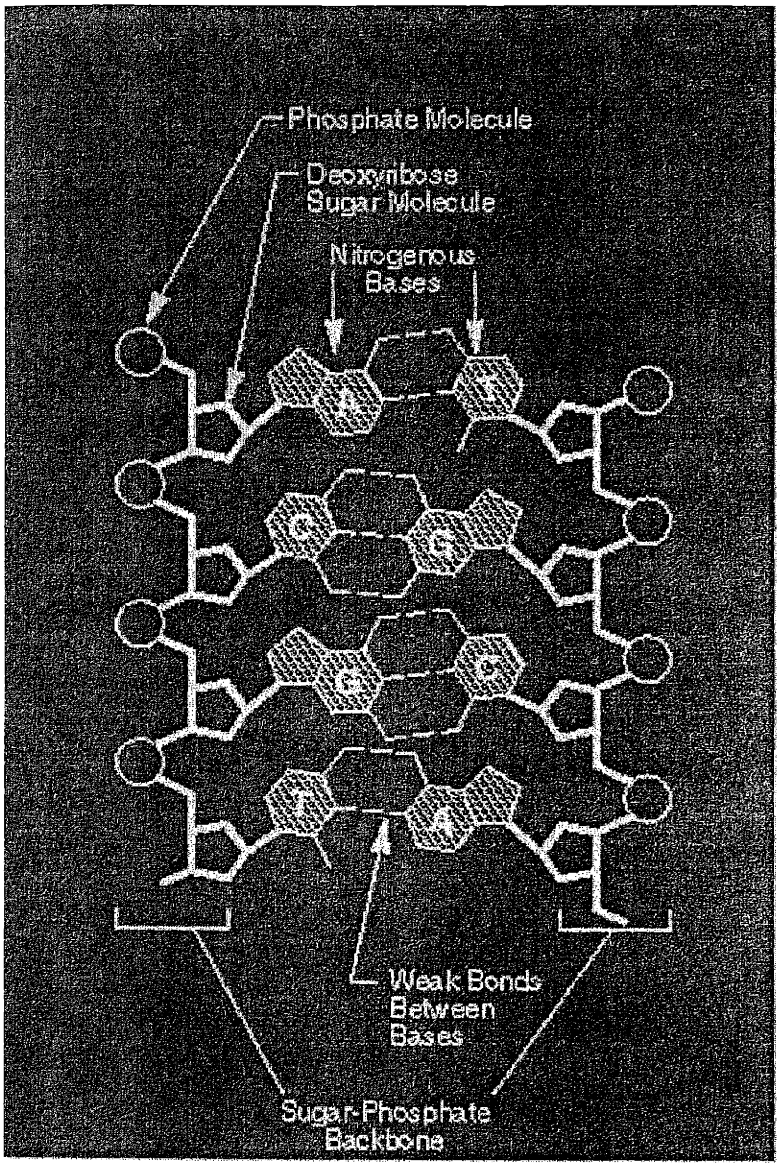

Courtesy of R. E. Dickerson, 1983, Sci. Am. ***249*** *, 94*

Figure 1-3. Base pair structures in the DNA duplex. The A-T hybrids are held together by two hydrogen bonds, while the G-C hybrids are held together by three hydrogen bonds.

sequence (compared to the 20 possible amino acids in proteins). In addition, the phosphate backbone of dsDNA chains provide them with physical and chemical properties similar to those of a negatively charged polyelectrolyte polymer chain, with certain conformational restrictions resulting from the added rigidity of the double helix structure. Although some departures from the standard dsDNA double helix structure may be induced by alternative base-pair schemes (Hoogsteen, Reversed Hoogsteen, Reversed Watson Crick, Wobble)[1], hybridization conditions, and specific DNA sequences occasionally form certain secondary and tertiary structures (such as Z-DNA, cruciforms, and triplexes)[1] the general structural properties and binding relationships of DNA are much more consistent and well understood. Therefore the basic rules for connecting the structures and functions of DNA are easier than for proteins[24]. Thus, DNA is the primary candidate in genomics research from a structural and operational standpoint.

1.1.6 From a linear approach to a combinatorial system

Originally, research in functional genomics consisted mainly of studies using living organisms as research models. Mutated genes were introduced by transfection techniques, or certain genes were deleted ("knocked out")[2] in cell lines or animals. The resulting phenotypes were studied to determine the functions of the introduced or removed genes. The use of animal models and knock out/transfection techniques yielded valuable information regarding the functions of some genes and their expressed enzymatic reactions. This information helped researchers ascertain some of the mechanisms and pathways underlying a variety of basic biological functions. In addition, knock out studies also provided valuable insight about the effects of genetic mutations; however, the work is labor-intensive, time consuming, and limited in scope. For simple organisms such as *E. coli,* the relationships between genomic DNA and phenotypes were

relatively straightforward and were in most cases directly correlated. However, for more complex multicellular organisms with differentiated cells, the relationships were nonlinear. It was often difficult to pinpoint a particular gene as responsible for a certain function, since usually a collection of genes is involved, not all of which are directly observed or known. Therefore, after the sequencing of genomic DNA, there was a shift in research strategy from a linear, evolutionary approach to a combinatorial approach, using genomic DNA libraries to simultaneously determine, *in vitro*, the genes expressed in a cell or bacteria under various stimuli. Scientists hoped to obtain an overall picture of all the genes involved in a particular biological operation using the combinatorial approach, and then use the information to deduce the role of each gene and its contribution to the underlying mechanisms. Consequently, the focus of functional genomics has turned toward the development of effective combinatorial DNA assays.

1.2 Evolution of DNA assays

1.2.1 Design considerations for DNA amplification

As the focus of DNA research turned toward functional genomics, and in particular to the development of combinatorial *in vitro* DNA assays, selection of characterization techniques and assay design became central issues. Certain characteristics of DNA analysis had to be considered and resolved. The first obstacle for analysis was that only minute quantities of target DNA are available for an assay. To successfully characterize such samples, the target DNA had to be amplified by many orders of magnitude. In addition, miniaturization would be a requirement for providing a combinatorial assay system that could simultaneously assay the thousands of DNA sequences present in the human genome from only a limited amount of target DNA. Finally, highly sensitive transduction methods had to be employed for detecting and

measuring the individual signals emitted from each element within a miniaturized combinatorial DNA assay.

Fortunately, the amplification of the target DNA proved to be relatively straightforward. In a now routine process, mRNA is first extracted and purified from the cells of interest. Then, the enzyme reverse transcriptase is used to convert the mRNA to a single-stranded complementary DNA (cDNA) chain. Next, the cDNA is amplified by PCR protocols using radiolabeled or fluorescently labeled dNTPs to create larger amounts of a labeled version of the target DNA. This protocol is called the reverse transcription-PCR or RT-PCR method[6].

1.2.2 Characterization techniques

In terms of approaches for measuring DNA levels, a variety of methods have been developed for attaching radioactive, fluorescent, colorimetric or chemiluminescent labels to either the target or the probe DNA[25,26] and measuring the labeled species. For example, radiolabeled DNA sequences are detected by autoradiography, and are quantified by a phosphoimager or a liquid scintillation counter. Although radiolabeled DNA is measured consistently by these methods, there is a trend toward a reduction in the usage of radioactive materials for such analyses in order to decrease the health risks associated with the use of radioactive materials.

Fluorescence and chemiluminescence provide convenient alternatives to radioactivity. Fluorescent molecules emit light at a characteristic wavelength when excited by a lower wavelength light source. In contrast, chemiluminescent species produce light as a result of chemical process. Specific enzymes such as alkaline phosphotase or horseradish peroxidase are used to catalyze a redox reaction that supplies electrons to induce a photon emission from a chemical such as luminol that is provided in the solution. In both procedures, sensitive photoelectric equipment such as photomultiplier tubes (PMT) or charge-coupled devices (CCD) are used to characterize

and measure the amount of light emitted by the labeled DNA. A notable advantage of using fluorescent and chemiluminescent labels is the significant levels of signal amplification that can be achieved from the process. The amplified signal results in a higher detection sensitivity for DNA as compared to radioactive molecules, and enables access to measurement thresholds that approach the attamole scale[27]. However, though highly sensitive, it is more difficult to accurately quantify an amount of labeled DNA from a measured photonic signal. In fluorescent systems, there is variability in the signal due to quenching effects leading to a decrease in the quantum yield, and photobleaching of the fluorophore. For chemiluminescence, variations in the reaction conditions can affect the enzyme activity and thus change the generated signal. In addition, artifacts introduced by background noise from the assay substrate or other chemical species can also cause measurement problems. The consistency of measurements between sample lots is also suspect due to variations in the measurement conditions and detector efficiencies. Because of these factors, fluorescent and chemiluminescent DNA assays are therefore usually only semiquantitative. However, a quantitative measurement of gene expression in a combinatorial DNA assay is critical for obtaining a more accurate picture of the effect of each gene on a physiological function. Thus, the assay design must take into account the limitations of the present characterization techniques.

1.2.3 A combinatorial instead of a linear approach to DNA assays

Designing a direct, feasible and reliable DNA assay paradigm is somewhat difficult, since many biological functions are the result of scores of enzymes operating in concert with the proper signaling and regulation pathways. This immensely complex, interactive and dynamic system is not easily modeled by linear progression but is much more amenable to a combinatorial approach where all the possibly related genes for a reaction are studied.

As noted earlier, initial DNA assays were linear in nature. The classic method of Southern blotting[28,29], invented by *Southern*, used electrophoresis to separate target DNA on a hydrogel according to their chain lengths. After electrophoresis, wet cellulose

or nylon sheets were placed over the gel and pressure was applied. The target DNA sequences were adsorbed onto the cellulose or nylon sheets by capillary action. The immobilized target DNA is then challenged by radioactively labeled oligo probes in a buffer solution. If the probe sequence is complementary to a specific target DNA, the radiolabeled oligos become immobilized onto the sheet the location of the target DNA. The sheet is characterized by autoradiography to determine the location of the labeled oligo. This identification technique indicates the presence of a certain gene in the target DNA sample. This assay strategy was so successful that it spawned a series of similar protocols known as Northern blotting (for RNA)[29,30], Western blotting (for proteins)[30] and Northwestern blotting (for protein-RNA interactions)[30]. Despite these notable features, the gel-based, sequential methodology was still fairly time-consuming, labor intensive, restricted in scope, and difficult to automate or miniaturize.

Instead, genomics researchers sought to determine the level of gene expression for a certain biological function simultaneously over the entire genome. This combinatorial approach would generate a more accurate picture of the various details that occur during a biochemical process as compared to a linear assay. One such example is glucose metabolism, which is incredibly complex and often requires the action of scores of enzymes acting in concert. Often the enzymes react in a cascade, with several subsequent steps occurring before the metabolism is complete. In addition, the enzymes act to regulate each other, or are regulated by chemical signals from other enzymes.

A combinatorial DNA assay could identify the genes involved in such a complication reaction, and also determine the expression level for each gene. In addition to providing more complete information on the biological system, a parallel assay process is more economical than a sequential array, saving time, money, manpower, and most importantly the valuable DNA sample. Therefore, researchers devised a powerful characterization algorithm utilizing a combinatorial library of the complete genome as the best approach for gene expression studies. Furthermore, a combinatorial DNA assay could be developed on a solid-state substrate, utilizing techniques similar to those used for high throughput screening (HTS) of potential drugs. HTS drug screens often use very

large combinatorial libraries of small molecules or oligopeptides immobilized onto a solid surface. The solid phase systems offer various advantages over liquid systems: they are easier to fabricate, miniaturize, and pattern, and existing immobilization techniques used to attach proteins or antibodies to a solid surface could also be employed for DNA probes. Researchers designed solid phase combinatorial DNA assays, using patterned "microarrays" of genomic DNA probes to characterize gene expression[31-46].

1.2.4 Choice of substrate for DNA assays

Although polymer fibers and sheets as well as derivatized polystyrene microtitre plates were initially tested and considered as substrates for DNA assays[27,47-54], silicon and glass surfaces quickly emerged as the superior support for producing microarrays[25,55-60]. Glass is cheap, transparent to visible light, and relatively easy to machine, modify and pattern with existing techniques. Silicon chips, the foundation of the semiconductor industry, are readily patterned by microlithography and etching techniques to produce complex surface features in the sub-micron range. In addition to their stable and robust physical properties, glass and silicon chips both possess a native oxide surface layer that can be reacted with a variety of organosilane compounds to form a surface film with certain desirable surface chemical and physical properties. In addition, the silicon substrate itself may contain dopants that render it electrically conductive, and this property may be used for localizing DNA molecules at desired surface sites by the application of an electric field, as demonstrated by the innovative array system produced by Nanogen[61-64].

Beyond the use of silicon as a microarray substrate, there have been significant advances in performing biochemical operations such as DNA sequencing[65-74], PCR amplification[75-79], and electrophoresis in microcapillary channels[80-86] on silicon chips. An ultimate goal is to integrate these techniques onto a single chip[87-92], and consequently simplify and streamline the DNA sequencing process further.

1.2.5 Other developments: system design, automation, bioinformatics

Researchers and manufactures chose a solid-state microarray format as the primary DNA assay strategy. In addition, after some experimentation, silica and silicon substrates have emerged as the dominant platform. Then other related developments in the system hardware and software helped to improve the overall system performance. First, most new assay systems were designed as integrated packages that optimized process efficiency, and were highly automated to further decrease the time and manpower associated with operations. In addition, microlithography and other patterning techniques common in the semiconductor chip industry were used to produce miniaturized arrays at the micron scale. Also, powerful new computer software was developed to help interpret and analyze the large amounts of raw data generated by the DNA assays[14-16]. The software would then identify the promising candidate genes that had a high probability of participating in any particular biological process as targets for further, more detailed studies. This methodology is called "data mining", and efforts related to the analysis and interpretation of DNA expression data lead to the creation of a new and popular discipline, bioinformatics, a field that is attracting increasing numbers of computer scientists, mathematicians, and electrical engineers into traditional biological research, resulting in a more diverse and interdisciplinary research environment.

1.2.6 DNA assays for polymorphism detection

There have been a number many advances in the design and application of combinatorial solid phase DNA arrays for characterizing gene expression. In contrast, the formulation of an effective DNA assay for detecting single nucleotide polymorphisms (SNP) remains a more challenging objective[58,93,94]. On average, there is one SNP for every 1 kb of genomic DNA in human beings, and certain SNPs are the cause of hereditary diseases or specific phenotypes. Since humans are essentially an outbred (as opposed to inbred) species, and since the inbreeding and testing methodology widely employed in animal models is obviously both unethical and illegal when pertaining to humans, the primary resource for detection of the genes responsible for various genetic

diseases is by traditional population genetics. This procedure involves extensive statistical research and requires the genetic screening of a large number of individual to be effective[2].

An appropriate HTS method for targeting individuals with a specific suspect SNP, or for screening a general population to determine the types and numbers of existing polymorphisms to correlate with known phenotypes, would be very helpful to this effort. Alhough traditional sequencing methods such as denaturing gradient gel electrophoresis[95-97] can detect single base-pair mutations, and new systems such as TaqMan™ [98,99] and denaturing high performance liquid chromatography (DHLPC)[100-102] have been developed, they remain limited in scope and are used primarily for confirming the existence of a known mutation point from the target DNA.

The bottleneck to SNP research is the difficulty in discerning the minute chemical and physical differences between two genomic DNA sequences with a single base pair mismatch. Genomic DNA sequences are long (over 1 kb) and a single mismatch anywhere along the chain would hardly cause a change in the thermodynamic stability or other physical or chemical aspects of the DNA chain. Therefore, it is difficult to confirm the existence of an SNP within a gene and to determine its location in a DNA sequence. Although the above-mentioned SNP detection methods have been commercialized and provide benefits, researchers have yet to devise a SNP detection system that can identify a SNP at an *unknown* point along the genomic DNA chain. A variety of new strategies are being pursued for SNP detection, including approaches that use the small differences in T_m (melting temperature, the temperature at which the DNA duplex unravels into single strands) [103] between a DNA homoduplex and a heteroduplex with an SNP. Once a reliable and consistent SNP detection protocol is developed, the next step will be to design of a solid-phase DNA microarray type SNP assay format based on this strategy for the high-throughput parallel screening of many different genomic DNA sequences simultaneously for SNPs.

1.3 Surface modification through the used of organic thin films

1.3.1 Chemical modification of solid substrates

As mentioned above, researchers have developed high throughput combinatorial DNA assaying based on generating solid-state microarray systems, with typically silicon or glass as the substrate for the arrays. Appropriate immobilization chemistries must be used to localize the probe DNA onto their surfaces at the desired sites and at very high densities for these systems to achieve the necessary sensitivity and resolution. The attachment chemistry should be thermally and chemically stable so that the DNA assay could be reused. In addition, miniaturization is critical to improving the performance of the DNA microarray. As the surface features of the DNA assay approaches the micron level, the surface-to-volume ratio increases dramatically. Consequently, so does the importance of controlling the solid/liquid interfacial properties. Therefore, another requirement for surface modification chemistries is the ability to prevent nonspecific DNA adsorption on the substrates through the appropriate choice of physical properties (interfacial energy, electric charge). Therefore, the silicon or silica substrates must be modified chemically to create the proper physical or chemical properties. Reactive groups are introduced to facilitate chemical attachment of the probe DNA to the surface. Functional groups with certain surface energies or electric charges may be employed to prevent unwanted nonspecific adsorption of the target DNA to the solid substrates. This dramatically improves the signal to noise ratio during characterization.

Finally, controlling the density of reactive surface sites in critical to the performance of the DNA assay. For quantitative analysis the amount of DNA probes on the assay surface should be larger than the target DNA in solution to theoretically guarantee 100% hybridization of the target DNA to the surface. On the other hand if the DNA probe surface density is too high steric hindrance may prevent efficient hybridization. Therefore the chemical modification of the silicon and silica surfaces must be able to produce DNA attachment sites with controlled surface density in order to

optimize the system performance. It is crucial to choose the right surface modification chemistry, the correct modification technique, and the appropriate reactive functional group for DNA probe attachment. A straightforward method for modifying the surface properties of silicon or glass is to coat the substrates with an organic film with the desired physical or chemical properties.

1.3.2 Organic films for surface modification

Organic films are used extensively to modify the properties of solid surfaces[104]. Examples range from surface protection (latex paints), nonwetting surfaces (Teflon), adhesion (epoxy glues), separation (chromatography beads and membrane filters), patterning devices (polymer photoresists), and reactive surfaces (immobilized organic catalysts or enzymes). Polymeric organic films are adsorbed onto solid surfaces from a latex solution emulsion (paint). Also, coating techniques such as spin coating or dip coating are commonly used. These methods create a phyisorbed film onto an inorganic interface. The relatively thick films (above the micron level) tend to dramatically change the optical and physical properties (such as the heat transfer coefficients and index of refraction) of the system. The difference in physical properties could significantly affect the characterization of the surfaces, or introduce background signals. More importantly, most coated polymer films are not covalently bound to the surfaces and thus are less stable to mechanical, chemical or thermal effects. When incorporated in a microarray system, even a minute amount of desorbed coating could contaminate the sample or destroy some the probe DNA pixels on the surface, rendering the data collection incomplete. Therefore, coated polymer films are less desirable for production of the highly sensitive and miniaturized DNA microarrays.

1.3.3 Organosilane films on glass or silicon substrates

To minimize the effects of organic films on the silicon and silica substrates, the film thickness has to be reduced, perhaps even to the nanoscale level. In addition, the film

must be covalently bound to the substrate in improve its stability. One of the first examples for this type of very thin, covalently attached organic films is the modification of glass fibers with thin organosilane films for producing fiberglass composites with organic polymers such as epoxies and polyesters. The glass surfaces were derivatized with a very thin layer of end functionalized organosilane molecules ($X\text{-}(CH_2)_n\text{-}OR_3$, where X = $CHCH_2O$, OH or NH_2, n = 3-12, R = CH_3 or CH_3CH_2). The silane groups form a covalent attachment to the glass surface through a condensation reaction. The end groups of the organosilane molecules are now exposed at the interface. These exposed functionalities are usually reactive groups such as epoxy, hydroxy or amino group. They take part in the polymerization reaction and serve to bind covalently with the polyester or epoxy resins. The reaction creates a light-weight composite that combines the toughness of polymers with the tensile strength of glass. The organosilane compounds are covalently bound to the glass surface and thus were highly stable. Furthermore, continuous improvements in the deposition protocols for functionalized organosilane compounds has led to the formation relatively thin (< 5 molecular layers) organic films with fairly consistent surface properties onto silicon or glass surfaces. Consequently researchers regularly use organosilanes to modify glass or silicon surfaces for attaching DNA probes[50,58,105-111],. But structurally organosilanes tend to form multilayered gel-like structures, which are less ordered and uniform than monolayer films. Therefore though they are less useful for the research and studies of interfacial effects, which are important to understanding how to prevent nonspecific DNA adsorption.

1.3.4 Organic monolayer films

The first monolayer thick organic films were Langmuir-Blodgett films[104]. Surfactant molecules in an aqueous solution congregate at the water/air interface to form a sparse surfactant layer (coverage < 1 monolayer). The surfactant layer was compressed by lateral pressure until it forms a densely packed organic film of roughly monolayer thickness across the water/air interface. This organic monolayer film was then transferred onto a solid surface, forming a well-ordered monolayer that could be used to study

interfacial phenomena. What researchers discovered was that surface physical and chemical properties (such as interfacial energy and electric charge) could be modified with just a monolayer-thick film. However, Langmuir-Blodgett films are physisorbed and lack the chemical or thermal stability to withstand some experimental conditions and characterization techniques. Therefore researchers tried to develop a chemisorbed monolayer film for improved stability.

The idea of using self-assembly to form a monolayer film was first demonstrated by *Zisman*, who exposed metal and metal oxide surfaces to a variety of long-chained amines, carboxylic acids and primary amides in organic solvents. The long-chained molecules adsorbed onto the surfaces to form oriented monolayer films with surface properties very similar to Langmuir-Blodgett films. The driving force for the formation of the monolayer films lay in the thermodynamic driving force generated by the large interfacial energy between the solvent and the metal/metal oxide substrate. The polar functional groups (amines, amides, carboxylic acid) of the amphiphilic molecules adsorbed onto the high-energy surfaces, while the nonpolar methyl tails were orientated away from the substrate to expose a low energy surface to the organic solvent. These self-assembled organic films were easier to produce, but still lacked the required energy of adsorption or stability.

Subsequently, *Nuzzo* and *Allara* developed a new approach for self-assembly by immersing gold surfaces into n-alkanethiol solutions[112,113]. Due to the high affinity between sulfur and gold, the thiol groups at one end of the alkanethiol chain ($X\text{-}(CH_2)_n\text{-}SH$) are chemisorbed onto the gold surfaces to form densely packed, well-ordered self-assembled monolayers (SAM) [114]. These nanometer-thick organic surface films are produced under ambient conditions and readily modify the physical and chemical properties of the gold surface. Therefore alkanethiol SAMs are model organic surfaces for research in interfacial phenomena.

Researchers synthesized alkanethiol molecules with various functional groups at their ω-end (such as hydroxy, carbonyl, amino, amide, ethylene glycol) and used them to

form SAMs for studying interfaces. The data from contact angle experiment with water indicated that monolayer thickness was sufficient to alter the physical properties of the underlying surface. Also, researchers discovered that desired surface properties such as hydrophilicity, hydrophobicity, and chemical reactivity could be obtained by choosing the appropriate end-functionalized alkanethiol species. Some SAMs with reactive end groups were also used for surface reactions such as peptide coupling. In addition, *Whitesides et al* have discovered that by manipulating the solution compositions of two SAM species they could produce "mixed monolayers" with controlled compositions and homogenous surface properties[115]. By using mixed monolayers to control surface properties such as hydrophilicity, researchers can gain insight on which surface conditions could facilitate or prevent nonspecific DNA adsorption, an untoward surface effect for DNA microarrays. In addition, mixed SAMs containing both reactive and inert species could be used to determine how the surface density of reactive sites affects the attachment, and hybridization efficiency of immobilized DNA probes.

However, the thermal and mechanical stability of the chemisorbed alkanethiol SAMs are substantially lower than covalently attached organic films such as the organosilane/silicon system. The instability of alkanethiol SAMs limited their practical applications, especially for modifying the glass or silicon substrates used for making DNA microarrays. Therefore, although alkanethiol SAMs are readily used for surface studies, the end-functionalized organosilane films covalently attached to silicon surfaces are still the primary candidate for generating DNA microarrays .

1.3.5 Surface characterization techniques

Various classic surface characterization techniques are utilized for studying thin organic films (both alkanethiol SAMs on gold and organosilanes on silicon). Common methods include ellipsometry, contact angle measurements, Fourier transform infrared spectroscopy (FTIR), X-ray photoelectron spectroscopy (XPS), atomic force microscopy (AFM), and surface plasmon resonance (SPR). Researchers developing DNA

microarrays also occasionally rely on such techniques to provide them with data on their solid substrates.

1). Ellipsometry is an optical characterization technique used to measure organic film thickness by measuring the changes that the film's index of refraction (N_f=1.45-1.52) imposes on the index of refractive for the underlying reflective surface (gold, silicon, silver, copper). Researchers use ellipsometry to quantify organosilane films, alkanethiol SAMs, DNA adlayers created by nonspecific adsorption, and even the thickness of oligonucleotide chains synthesized on a silicon surface[116,117].

2). Contact angle measurements are used to qualitatively determine the surface energy of an organic film by measuring the angle a liquid droplet forms with the underlying solid surface. For instance, contact angles for water higher than 90° indicate a hydrophobic surface, while low contact angle suggest a surface is hydrophilic. Contact angle measurements can also be used to evaluate the homogeneity of a surface, or to confirm surface modification through changes in the contact angle after a reaction. If quantification is necessary Young's equation may be used to calculate the solid/vapor interfacial energy.

3). FTIR is used for identifying functional groups in organic compounds in solution and in solids. Different functional groups absorb IR radiation at distinct wavenumbers (cm^{-1}). and dissipate the energy through vibration. Thus it is possible to discern the presence of various functional groups by scanning the sample over a range of IR wavenumbers and observing the absorption peaks. However, due to the very small amount of sample and high background signal from the metal/metal oxide substrates, it is impossible to characterize most nanometer-thick organic surface films by transmission IR. Instead, the incident IR beam is reflected off the reflective substrates at a grazing angle (80° to the surface normal). The low incidence angle maximizes exposure of the organic film to the IR beam, while the reflectance method minimizes the background from the metal/metal oxide substrate. Therefore grazing angle reflectance IR can discern the functional groups present in an organic film adsorbed on the surface, including DNA molecules[118].

4). XPS is a highly sensitive measurement technique for surface elemental analysis[105,116]. A monochromatic X-ray beam strikes atoms, ejecting core electrons.

The core electrons are ejected from atoms up to a depth of around 50 Å from the sample surface, and collected by an analyzer. Each element produces electrons with a characteristic binding energy, which are measured to determine the identity, quantity, and the ionic state of the sample. For alkanethiol SAM studies XPS data is also used to determine the film thickness and surface coverage. The theory is based on the attenuation of the XPS signal of the metal substrate (Au) brought upon by the SAM film. As film thickness or coverage increases, so does the level of signal attenuation for the underlying substrate. In addition, it is possible to determine the composition of "mixed monolayer" organic films by XPS by using a mixture of organic molecules, one of which contains a label such a halogen species. The composition is critical when evaluating the proper density of surface reactive sites for optimizing DNA probe immobilization and hybridization efficiency. XPS has proven a sensitive and versatile tool for characterizing organic thin films.

4). AFM is a microscopy technique with nanometer scale resolution, and is commonly used for surface imaging[119 120,121]. AFM drags a highly sensitive piezoelectric cantilever over the surface of interest. A reflect laser beam is used to calibrate the position of the cantilever, and the sample height is adjusted during the scan to ensure that the position of the cantilever is unchanged. The changes in the height of the sample correspond to the organic film thickness. AFM is commonly used to generate high-resolution images of various nanoscale surface features made by the adsorption of organic films onto patterned surfaces. AFM instruments have also been modified to act as a force probe to determine the force constants of molecular interactions at the atomic scale.

5). SPR is a novel optical technique applied extensively by biologists to study the adsorption of various biomolecules onto surfaces[116,118,122-128]. An incident beam creates a resonance wave (plasmon wave) on a metal/metal oxide substrate. The intensity of the plasmon wave reaches a maximum at a certain incident angle for each substrate material. The angle of maximum resonance shifts due to the presence of organic adlayers on the substrate. The shift in angle is correlated to the thickness of the surface film. SPR manufacturers claim sub-Angstrom resolution, but the strength of SPR lies in the ability to observe adsorption dynamics in real-time. SPR also measures surface reactions such as

DNA hybridization under flow conditions, which is not feasible with most DNA microarrays. SPR is useful for real-time *in situ* characterization of adsorption kinetics, but claims of sub-Å resolution for the SPR data are still in question.

1.3.6 Applications of thin organic films

Thin film technology is readily integrated into the development of biotechnology, especially in the areas of separations, biosensors, and bioreactors. In general, for genomics applications, the sample sizes are small (nano to microliter scale). Therefore, there it is more effective to perform biochemical reactions (enzymatic reactions, PCR, DNA sequencing), bioassays (gene expression and SNP analysis, immunology screens, paternal tests, pathogen screens) and separation (electrophoresis, chromatography) on a very small scale, such as on microarrays or in microfluidic devices. These systems are manufactured on glass or silicon substrates using lithography techniques developed for the semiconductor industry.

In addition, most biological probes are labeled with highly fluorescent or chemiluminescent molecules that can provide enormous signal amplification, thereby increasing the sensitivity and detection limits for biosensors. Due to the large surface-to-volume ratios inherent to these microscale devices and the signal amplification abilities of many bioprobes, it is critical to control unwanted nonspecific adsorption of biomolecules onto the solid surfaces of the sensors or reactors, resulting in contamination and high background noise. This problem could be prevented by modifying the solid surfaces with organic films that express the appropriate functional groups for inhibiting the nonspecific adsorption of certain biomolecules such as DNA, proteins, lipid molecules, or polysaccharides.

This surface modification approach could be taken a step further by using mixed organic films containing reactive moieties that can selectively immobilize the biomolecules of interest, while other functional groups in the mixture prevent nonspecific

adsorption to the surface. These modified surfaces can be used to reduce sample loss from adsorption during liquid transport in microfluidic devices. Appropriate surface modification also prevents enzymes from adsorbing and denaturing during biochemical reactions, thus maintaining the enzyme's activity. Surfaces that inhibit nonspecific adsorption of the labeled target biomolecules reduce background signal, effectively improving the signal-to-noise in bioassays. Modified surfaces can also prevent the competitive adsorption of unwanted chemical species onto a surface in place of the target species, thereby improving the performance of a competitive bioassay, or possibly the separation efficiency for small-scale chromatography and electrophoresis.

Furthermore, these organic films could be used to construct a solid-state bioassay by providing a reactive surface for the specific attachment of biological probes. The surface reactive site density may be modified to control the surface density of the probe. Thus it is possible to optimize bioassay efficiency by minimizing the steric effects of the surface probes on the target-probe binding. Most biomolecule binding sites are highly specific and depend on the conformation and orientation of both the target and probe. Also, target biomolecules come in a range of sizes and shapes. Thus, for each specific bioassay, there is an optimal surface probe density that provides the appropriate steric conditions for the target-probe interactions to proceed unhindered. By using mixed organic films researchers can tailor the surface probe density according to their needs.

The advantages of implementing thin film technology for producing solid-state combinatorial DNA assays are mostly practical. Compared to the thick adsorbed polymer films, thin organic films are easy to produce and more robust. Morever, monolayer thick films possess highly uniform and controllable surface properties. Also, the density of reactive surface sites for thin organic films is consistently quantified with various surface techniques such as XPS. This enables researchers to obtain an optimal surface DNA probe density that maximizes hybridization efficiency and the amount of probes available for reaction. In addition, other functional groups in a mixed thin film are incorporated to prevent nonspecific adsorption of the target DNA. The resulting DNA assay would have

higher signal-to-noise ratios and increased sensitivity, with minimal false positives due to contamination.

1.4 Current methods for producing solid-phase DNA microarrays

1.4.1 Affymetrix oligo arrays

For gene expression studies, two major production philosophies have been developed for making DNA microarrays on glass substrates. The first was developed and commercialized by *Fodor et al.* at Affymetrix[129-132]. Their microarray design closely resembles a system proposed by *E. M. Southern*. The Affymetrix chips are produced by the same solid-phase oligo synthesis methodology used to make PCR primers. However, the 5' end of the phosphoramidite nucleotides used for the oligo synthesis are protected by a photolabile NVOC group, instead of the usual acid-labile dimethyl trityl (DMT) groups. This innovation allows the immobilized nucleotides to become deprotected by photolysis (see Figure 1-4). Affymetrix used photolithographic masks (common in the semiconductor industry) as a template to create the desired surface patterns. Upon illumination only the nucleotides that are exposed to light are deprotected, and consequently they are available for subsequent nucleotide addition. Since there are four nucleotide bases (A, T, G and C), four photolithographic masks and four illumination-synthesis cycles are required to complete each nucleotide addition step. Therefore $4n$ masks are required to produce an n mer. However, the mask allow for 4^n possible combinations for the oligo sequences synthesized on the surface. If the pixel sizes are small (<100 microns per side), then it is possible to create an oligo array with thousands of different sequences per cm^2

Usually Affymetrix generates arrays of 20 – 25 nt oligo probes after around 100 illumination-synthesis cycles. The array is usually challenged by fluorescently labeled target dsDNA in characterized with a CCD or PMT. For gene expression arrays the target DNA is the RT-PCR product amplified from mRNA purified from sample cells. These

DNA sequences are composed of the exons of the genomic DNA, and are about 300 bp to 1 kb in length. Since the surface oligo probes on the chip are only a fraction of this size, the array is designed to include many oligo probe sequences, each complementary to a segment of the target DNA sequence. This guarantees the specificity of the microarray for detecting a specific target DNA sequence. For example, for a 300 bp length target DNA sequence 8 complementary oligo probes are generated on the surface. Another design strategy is to surround the "match" oligo probe (complementary to a portion of the target DNA) with a collection of other "mismatch" oligo chains. Each of these oligo chains has a single mismatch along its length. The mismatched oligo sequences act as controls to improve the stringency of hybridization by minimizing the possibility of generating false positive signals.

The Affymetrix chip is fairly efficient at screening large numbers of target DNA sequences in parallel for gene expression studies. However, due to the hybridization issues mentioned above, extensive amounts of time and computer support are required to design the myriad collection of oligo sequences necessary for accurate and stringent characterization results. This causes a substantial increase in the cost and delivery time for Affymetrix chips, especially custom-designed ones. Also, although the fluorescence signal-to-noise assay (S/N) ratios are acceptable the assay is only semi-qualitative. Thus the chips could readily screen for the genes that are expressed during a biological function. But actual measurements of the expression levels are less reliable. Also, there is a lack of consistency and large degrees of spread in the signal intensities for the same target DNA sample between different production lots, hindering the meaningful comparison of readings between samples. This is a critical problem since many gene expression experiments rely on comparing the difference between gene expression levels in cells as the environmental conditions are varied. Finally, the NVOC-protected nucleotides used by Affymetrix have a lower stepwise oligo addition (coupling) efficiency compared to regular DMT-protected nucleotides. Thus each pixel in the array could contain a large proportion of oligo chains that are less than full length. The decreased synthesis efficiency results in both decreased oligo sequence fidelity and also

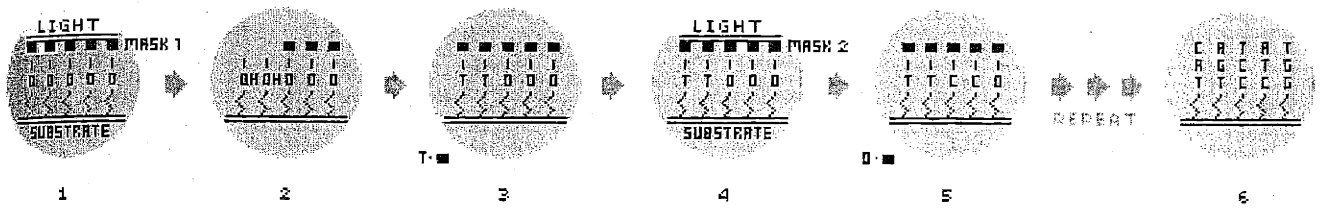

Courtesy of Affymetrix

Figure 1-4. Graphic overview of the photoactivated oligonucleotide synthesis protocol used to produce Affymetrix DNA chips. (1) A silicon substrate is derivatized with a protected hydroxysilane film. The protecting groups are photolabile and are removed upon illumination through a photolithographic mask; (2) after washing only the illuminated protecting groups are removed to expose the reactive hydroxy groups; (3) the 1st nucleotide (T) is added to the exposed sites; (4) illumination with a 2nd mask deprotects the hydroxy groups at other sites; (5) a different nucleotide base (C) is added; (6) the illumination-synthesis cycle is repeat for other nucleotides to stepwise synthesize oligo sequences with addressable locations on the substrate.

lower quantities of oligo probes available for hybridization with the target. This problem degrades the overall performance efficiency of the array.

1.4.2 Pat Brown microspot arrays

Brown et al. at Stanford University developed an alternative protocol for producing a DNA microarray. His design was based on 300 – 1000 bp long dsDNA probes [40-44,133] instead of on the short chain oligos used by Affymetrix. First, glass slides are coated with a layer of polylysine molecules. Since lysine amino acids have amine side chains, the polylysine surface contains a positive charge density, due to partialprotonation of the amine groups. The dsDNA probes are produced by PCR, and loaded onto metal pins. The DNA solution is held by capillary forces in an indented groove that runs along the length of the pin. The metal pins strike the polylysine-coated slides sharply, depositing a small droplet of DNA solution about 250-400 μm in diameter. As the solution dries the probe DNA is adsorbed onto the polylysine surface due to the electrostatic interactions between the negatively charged dsDNA phosphate backbone and the positively charged amine side chains of the polylysine layer.

The adsorbed dsDNA strands are then rapidly heated to their melting temperature (T_m), causing the DNA duplex to separate into ssDNA strands. The chip is quenched with ethanol to prevent reannealing of the ssDNA strands. Next, the chip was illuminated with short wavelength (254 nm) ultraviolet (UV) light to immobilize the ssDNA probes onto the underlying polylysine surface. Researchers believe the immobilization is due to the formation of a covalent crosslink between the thymine nucleotides of the ssDNA and the polylysine chain. This treatment resulted in the formation of immobilized ssDNA probes with lengths equivalent to their complementary target dsDNA in solution.

The microspot array also measures fluorescence from labeled target dsDNA produced by RT-PCR. The target DNA is heated until it unravels into ssDNA, and then the solution is quickly contacted with the microarray slides. The target DNA hybridizes

with the probe DNA on the surface and is characterized by confocal microscopy. For gene expression assays the characterization process is more complex. First, two sets of cell lines are grown. One line is grown under "standard" conditions, the other with a perturbation in one environmental variable. The purified mRNA samples from both cell lines are amplified by RT-PCR but labeled with different fluorescent probes. The two fluorescent probes (usually Cy3 and Cy5) have equivalent quantum yields but are excited at different wavelengths. In addition, a small amount of DNA sequence from a different species is added to the target DNA solutions prior to PCR. This DNA is not amplified and acts as an internal standard.

A microarray slide is immersed in each DNA solution until hybridization is complete. Then the slides are scanned with a confocal microscope. Each slide also contains a microspot containing a DNA sequence complementary to the internal standard DNA present in the target solutions. The signal from this spot is used to normalize the perturbated sample fluorescence intensity to that of the standard sample. When the normalized intensities are equal the level of gene expression hasn't changed. If the intensity for the perturbated sample is higher than the standard the gene is being expressed at higher level. This methodology, called two-tone fluorescence microscopy, identifies which genes are activated or repressed during a change in an environmental condition. It also provides a semi-quantitative analysis of the expression level.

The Brown methodology produced microspot arrays of long chain ssDNA probes adsorbed and crosslinked onto a coated glass surface (see Figure 1-5). The process is readily automated and creates glass slides with about 2000 spots containing different DNA probe sequence, and has been commercially adapted by many companies including Incyte. In addition, improvements have been made on the liquid delivery system and the coating for the glass slides. Now the probe DNA solutions can be spotted onto the slide using inkjet printing technology or by delivery through plastic capillary tubes. Corning produces a glass slide coated with a thin adlayer of chemisorbed γ-amino propyl silane that replaces the original polylysine coating.

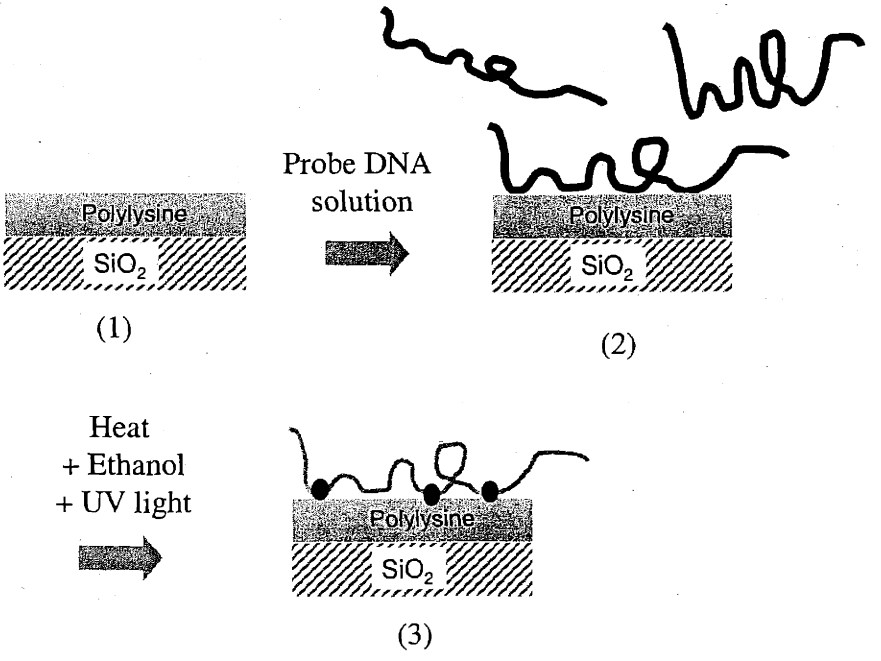

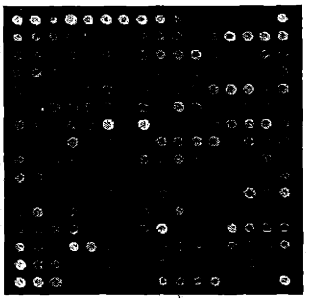

Courtesy of Incyte Genomics

Figure 1-5. Graphic overview of the Pat Brown microspot array protocol. (1) A glass surface is coated with a layer of positively charged polylysine molecules; (2) dsDNA is generated by PCR, and nonspecifically adsorbed onto the polylysine surface from solution. (3)The adsorbed dsDNA is heated to unravel into probe ssDNA strands. The surface is quenched with ethanol to prevent the ssDNA strands from reannealing, and the ssDNA strands are crosslinked to the polylysine by UV photolysis. The attachment sites are shown as dark ovals. Underneath is a representative false color fluorescence confocal microscope image of a 20 x 20 pixel microspot array using Cy5 labeled target DNA.

Though cheaper, easier and quicker to produce than the Affymetrix chips, the microspot arrays also have various drawbacks. Like the Affymetrix chips, the microspot arrays suffer from inconsistencies and large amounts of error spread between different production lots. In addition, the probe DNA is attached onto the polylysine surfaces at multiple points, which drastically reduces hybridization efficiency to the target DNA (0.1%). In addition, due to the multiple point attachment, only small segments of the probe DNA chain are available for hybridization. This immobilization method increases the possibility of mismatches due to partial hybridization of the probe DNA to target DNA. Indeed, high overall background noise has been frequently observed when using microspot arrays. Regardless of their shortcomings, both the above approaches and systems represent the current state-of-the-art and are commonly utilized in both academic and industrial functional genomics research.

1.4.3 Methods for immobilizing oligo probes onto solid surfaces

Improved DNA immobilization techniques are being actively explored, and a large number of competing protocols with different approaches have been studied. Researchers have attempted different strategies to immobilize oligo chains from solution onto a variety of solid materials[49,108,109,111,118,134-140]. Currently oligo chains can be synthesized with a variety of chemical moieties on their 3' or 5' ends using standard phosphoramidite chemistry. These include potential linker functions such as amino groups[47,48,58,105,108,140], thiol groups[106,116,135], and biotin[122,123], as well as numerous fluorescent tags.

After cleavage from the solid-phase CPG support, these oligo chains are purified and then covalently attached onto surfaces by a large collection of specialized bifunctional crosslinkers [47,105-107,140-142] routinely used for conjugating proteins. One commonly used crosslinker is gluteraldehyde[105,108,140]. Alternately, coupling reactions used for peptide synthesis such as dicyclocarbodiimide (DCC) and 1-ethyl-3-(3-

dimethylaminopropyl) carbodiimide hydrochloride (EDC)[27,94,105,109] are used to create activated esters, which react with amine groups on a surface. Another common approach uses the highly specific biotin-avidin interaction[94,111,122,123,127] ($K_d=10^{-15}$ M) commonly associated with the production of enzyme linked immunosorbent (ELISA) assays used for immunological screens. The solid supports used in these protocols are usually modified with functionalized organosilanes (on glass)[50,58,105-111], ammonia plasma (on polypropylene)[51,52], or adsorbed streptavidin (on nylon and polystyrene)[27,47,49,94,122,123].

1.4.4 Methods for immobilizing oligos in polymer gels at the surface

On the other hand, some researchers have modified the solid substrate with organosilanes containing acrylic end groups. Regular acrylamide monomers along with a small proportion of amine or thiol-linked monomers acrylamide monomers are added to the surface. Polymerization is induced to form an acrylamide gel that is covalently bound to the surface[53,54]. The gel contains copolymers with amine or thiol groups, which can react with bifunctional crosslinkers or with oligos containing a chemical linker. In another case Mosaic Technologies developed Acrydite™-linked oligos[110]. The Acrydite™ linker is a acrylic group that is attached to the 5' end of an oligo chain during standard solid phase stepwise synthesis. These oligo "monomers" are mixed with regular acrylamide monomers and with acrylic surfaces during polymerization. The acrylic linker participates in the reaction, resulting in oligo chains directly incorporated into the surface gel as copolymers[50,55].

1.4.5 Questions raised by alternative oligo immobilization strategies

Though all the above studies resulted in successful oligo or dsDNA immobilization, many issues remain unresolved. Although most bifunctional crosslinkers

are chosen for their specificity, many contain reactive groups that could crosslink with functional groups on the nucleotide instead of with the 5' linker group. This phenomena introduces the possibility of side reactions between the amino groups on the nucleotide bases and the bifunctional crosslinkers[27,49]. In addition, oligos and dsDNA are usually dissolved in water, which in many reactions acts as a competitor that quenches the surface reaction sites. The large excess of water molecules (55 M) compared to the solvated oligo chains (μM) further decreases the amount of successful oligo or dsDNA immobilization reactions to surface groups like activated esters or isocyanate groups. In addition, nonspecific DNA adsorption is sometimes a problem for the organic surfaces immersed in an aqueous buffer[58,126,143]..

An alternative would be to change to aprotic solvents such as formamide, or dimethyl formamide (DMF), to which oligo chains possess limited solubility. However, the low solubility results in unfavorable reaction kinetics. Furthermore, the solvation of highly polar polyelectrolytes in less polar solvents creates a thermodynamic driving force that favors the partitioning of the oligo chains onto the solid surface, resulting in substantial nonspecific adsorption instead of covalent attachment.

Finally, none of the crosslinking methods offers a reliable method to control the surface density of the immobilized oligos, which could be critical for DNA hybridization at the surface. It is possible that the packing density of the oligo surfaces may induce steric factors that affect hybridization kinetics, efficiency, and stringency, as well as the thermodynamic stability of the hybridized dsDNA duplex. However, due to the inconsistent oligo surface densities obtained using the various approaches mentioned above, no systematic studies have yet been conducted on the relationship between the surface density of the immobilized oligos and DNA surface hybridization.

1.4.6 Methods for immobilizing DNA onto surfaces

The majority of researchers try to produce surface arrays of short chain (10 to 30 nt) oligo probes, with functions similar to the Affymetrix system. In contrast, relatively few groups have chosen to compete with *Brown's* technique of attaching longer (over 100 nt/bp) ssDNA/dsDNA chains onto solid surfaces. Some notable exceptions include *Guschin* et al., who used sodium periodate to oxidize the pentose ring of the 3' nucleotide in a ssDNA chain[144]. The sugar ring opens to form two aldehydes, which react with surface amino groups via gluteraldehyde chemistry. Mosaic Technologies tried inducing PCR at the surface by first derivatizing silicon surfaces with organosilanes containing an acrylic group. Then Acrydite™-linked oligos are copolymerized with a polyacrylamide gel at the surface. The acrylic surface groups react with acrylamide monomers to covalently immobilize the gel, along with the oligos, to the silicon surface. The immobilized oligo chain act primers for PCR amplification. The amplified dsDNA molecules are immobilized onto the surface by hybridizing with the surface oligos. Still other groups have tried immobilizing a long ssDNA strand to the surface by hybridizing one end to an immobilized oligo chain. The ssDNA strand acts as a template, and the oligo acts as a primer for a DNA polymerase extension reaction. The polymerase would fill in the DNA strand complementary to the ssDNA template to generate an immobilized dsDNA chain.

The groups that used acrylamide chemistry relied on relatively thick (1 μm), polymer gels as their substrates, which sterically hindered access of target DNA in solution to the probe ssDNA (often entangled within the polymer network). The steric hindrance could result in lower DNA hybridization efficiencies at the surface. In most cases hybridization was demonstrated using only short oligo chains (25 nt), instead of full-length dsDNA exons produced by RT-PCR, as the target. Therefore it is difficult to determine the actual hybridization efficiency of full-length target DNAs to the surface DNA probes. In addition to problems with the surface structure of the polymer gels, there is an inherent lack of control over the surface densities of the oligo chains incorporated in the surface gel during the polymerization reaction. The density of oligos incorporated in the gel is crucial to the amount of dsDNA synthesized (by PCR) at the gel surface.

As for the polymerase method, restriction endonucleases were utilized to preferentially cut the immobilized dsDNA product at a particular site. The presence of DNA fragments with the correct length and restriction site in the elution buffer demonstrated that the polymerase reaction was successful. However, questions remained on how to consistently control the surface density of both the initial oligo chains and the polymerized long-chain dsDNA. Furthermore, due to steric effects an upper limit of about $1e^{-14}$ moles/cm^2 would have to be imposed on the dsDNA surface density, to allow for the bulky polymerase enzyme to function properly.

1.5 Motivation and fundamental design philosophy

Despite the ongoing interest and research in variations of either the Affymetrix or *Brown* approaches for DNA immobilization, there is a lack of substantial progress or improvement in the area of quantitative solid-state DNA bioassays. The bottlenecks could be due to limitations on the philosophies of both approaches, which appear to be polar opposites. Perhaps a methodology that incorporates portions of both approaches and occupies the middle group between them would be better suited for improving the existing techniques[105,145]. The DNA immobilization strategy I propose demonstrates such a combination. My first goal was to attach oligonucleotides onto a solid surface such as silica with controlled surface density and optimal sequence fidelity. I followed the stepwise oligo synthesis protocol using standard phosphoramidite chemistry[51,117,146], but at the same time I control the oligo surface density by manipulating the amount of reactive hydroxy groups available to the incoming phosphoramidites. In turn, the surface hydroxy group density was controllable by modifying the underlying silica surface with organic thin films of differing compositions. Next, novel characterization techniques were explored to achieve the sensitivity and specificity necessary to effectively quantify the oligo surface coverage. Further in-depth studies were conducted on how the oligo surface density affects the oligo sequence fidelity, as well as the appropriate reaction conditions and synthesis protocols that would ensure that the sequence fidelity is optimized.

Once the oligo surfaces were properly synthesized, characterized and optimized, they will be utilized to systematically study the effects of oligo surface density on DNA surface hybridization kinetics, quantities and stability. Particular emphasis was placed on possible steric and structural factors. Next, I determined the optimal oligo surface density and reaction conditions for DNA surface hybridization.

Upon completion of this phase immobilized long-chain dsDNA onto the surface. The attachment chemistry was the exquisitely specific base-pair interactions of DNA hybridization itself, with the surface oligos acting as the "glue" that serves to immobilize the dsDNA onto the solid surface. In addition, the discrete surface oligo sequences act with lock-and-key type specificity to localize different dsDNA exons from solution onto the surface in a spatially addressable manner. The dsDNA was produced by PCR, with a customized primer containing a 10 nr oligo overhang with a sequence complementary to one of the surface oligo sequences. The oligo overhang acts as a "sticky end" for surface attachment of the dsDNA. In addition, there is a psoralen moiety at the 5' end of the oligo overhang which may be photolyzed by long wavelength UV light (365 nm) to form a covalent bond that crosslinks the dsDNA with the surface oligo chain[147-149]. Heating of the immobilized dsDNA to its T_m released one ssDNA strand and exposed the other ssDNA strand, which is covalently attached to the solid surface at one end. My next goal was to immobilize the ssDNA probes at surface densities high enough to produce a brush-like structure (see Figure 1-6). The end-immobilized ssDNA probe is not adsorbed onto the solid substrate at multiple points and will behave as if it were in solution phase when solvated [145]. Therefore its complete and continuous length is available for hybridization to the target DNA in solution, vastly increasing DNA surface hybridization kinetics, efficiency and stringency. Furthermore, if the amount of DNA probes on the surface is in excess of the target DNA in solution, and if the surface DNA hybridization efficiency is high, it is possible to obtain consistent and quantitative empirical data, which is the ultimate goal of this project.

The focus of my thesis was to devise appropriate surface modification and oligo synthesis protocols for the formation of oligo surfaces with controlled surface density and high sequence fidelity, and the covalent, site-specific attachment of long chain dsDNA to this solid surface via DNA hybridization. The performance the system I devised is dependent on many factors such as the structure and density of the synthesized oligo surfaces or the immobilized DNA probes. At every phase of the experimental design there are a number of variables to consider (See Figure 1-7). Consequently, I conducted systematic research to determine the appropriate oligo surface density as well as the proper hybridization and photolysis conditions for optimizing the amount of dsDNA end-immobilized to the surface. If successful, the approach I proposed will result in a low cost, highly flexible solid-state platform capable of specific, site-directed end-attachment of probe DNA for the quantitative characterization of gene expression levels in genetic research. Development of patterning approaches to produce an oligo microarray, as well as further modifications in the hybridization technique such as electric focusing[64,150] are reserved for future research.

1.6 Possible applications for my DNA immobilization technology

There are a variety of possible applications for the system I devised at each stage of the development process. Research on how the physical and chemical properties of a surface are affected by surface modification using derivatized organic thin films can be utilized to develop barrier films that resist DNA adsorption, or to produce surfaces that facilitate DNA adsorption. Thin organic films with chemically active functional groups can be used as a substrate to covalently immobilize other biomolecules (than DNA) such as proteins and antibodies. Immobilized oligo surfaces with controlled density and high sequence fidelity can be used for research on the kinetics and thermodynamics of DNA surface hybridization[105]. The oligo surfaces could also be used in affinity chromatography columns for DNA separation, and as short-chain DNA probes for solution phase oligo detection.

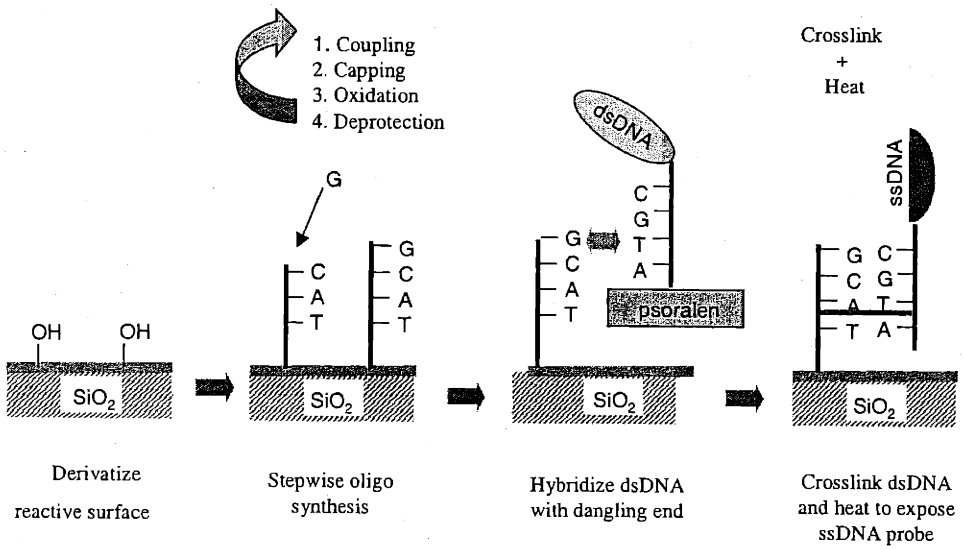

Figure 1-6. General strategy for end-immobilizing dsDNA to a solid surface. (1) silicon surface is derivatized with thiol-terminated silane thin films; (2) oligos are synthesized stepwise onto the silane layers; (3) a dsDNA strand with oligo overhang and psoralen linker is attached to the surface by hybridizing with the synthesized surface oligos; (4) after UV photolysis to crosslink one ssDNA strand and heating to remove the other ssDNA strand a covalently bound end-immobilized ssDNA probe is formed.

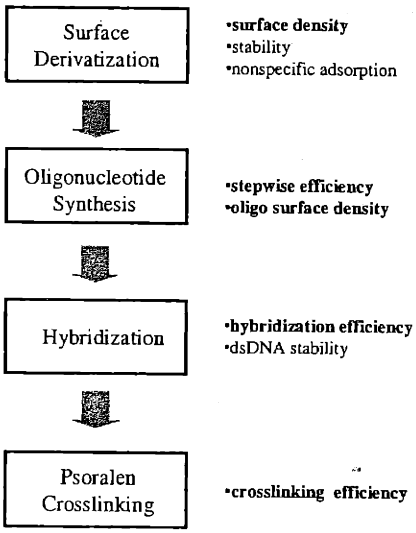

Figure 1-7. Experimental design for the production of end-immobilized dsDNA chains on a solid surface and the considerations involved at each step of the process.

In addition, a combinatorial array of end-immobilized dsDNA strands may be used to study DNA-protein interactions[122-124,151], or to screen small molecules, peptide nucleic acids (PNA)[152], or other biologically active compounds for potential pharmaceutical applications[105,153 154]. dsDNA surface arrays can also be utilized for SNP detection by comparing of the shift in the melting curve and T_m between DNA homoduplexes and heteroduplexes[95-97].

If the surfaces are heated to produce end-immobilized long-chain ssDNA probes, possible applications include gene expression assays, or clinical screens for pathogens[34] (by detecting the presence of their characteristic DNA sequences in biological sample). Regardless of the applications, the general theme of my system was to provide a flexible, economical and universal solid-state diagnostic platform that can be tailored to characterize the DNA sequences of particular interest to the end-user. The oligo chips would be manufactured in a prepatterned microarray format, and supplied to the user with the surface oligo sequences mapped out in detail. With knowledge of the surface oligo sequences, the user could then custom-synthesize PCR primers with the appropriate "sticky end" oligo overhangs complementary to any particular surface oligo sequence, and then amplify the relevant dsDNA probes through standard PCR procedures. When a solution mixture of the dsDNA probes with oligo overhangs contacts the oligo chip the dsDNA probes will diffuse throughout the surface but only hybridize only at specific sites according to the discrete codes on their "sticky ends", creating a self-assembled microarray of dsDNA probes. Then UV photolysis crosslinks the attached dsDNA probes to the surface via psoralen chemistry, creating a customized and spatially addressed solid-state array of DNA probes. All the end-user requires for producing these flexible and customized DNA microarrays are the patterned oligo chips, an automated oligo synthesizer or a reliable oligo source, and a PCR thermocycler. Finally, as demonstrated by *Christof et al.* [155], it is possible to attach other bioactive molecules such as enzymes and antibodies in an addressable manner. Thus, by extension, the patterned oligo surface arrays can be modified to accept a variety of different biomolecules and act as a flexible, multifunctional biosensor that can be tailored to the needs of the patient or the researcher.

1.7 References

1) R. R. Sinden, *DNA Structure and Function*; 1 ed.; Academic Press: New York, 1994.

2) A. J. F. Griffiths; J. H. Miller; D. T. Suzuki; R. C. Lewontin; W. M. Gelbart *An Introduction to Genetic Analysis*; 6 ed.; W. H. Freeman and Company: New York, 1996.

3) J. Sambrook; E. F. Fritsch; T. Maniatis *Molecular Cloning: A Laboratory Manual*; 2 ed.; Cold Spring Harbor Laboratory Press: Cold Spring Harbor NY, 1989.

4) L. J. McBride; M. H. Caruthers *Tetrahedron Letters* **1983**, *24*, 245-248.

5) S. L. Beacage; M. H. Caruthers *Tetrahedron Letters* **1981**, *22*, 1859-1862.

6) H. Erlich *PCR Technology: Principle and Applications for DNA Amplification*; W. H. Freeman and Company: New York, 1992.

7) R. K. Saiki *Science* **1988**, *239*, 487-491.

8) A. M. Maxam; W. Gilbert *Meth. in Enzymol.* **1980**, *65*, 449-560.

9) F. Sanger *Science* **1981**, *214*, 1205-1210.

10) L. M. Smith; S. Fung; M. W. Hunkapiller; T. J. Hunkapiller; L. E. Hood *Nuc. Acids Res.* **1985**, *13*, 2399-2412.

11) L. M. Smith; J. Z. Sanders; R. J. Kaiser; P. Hughes; C. Dodd; C. R. Connell; C. Heiner; S. B. H. Ken; L. E. Hood *Nature* **1986**, *321*, 674-679.

12) L. E. Hood; M. W. Hunkapiller; L. M. Smith *Genomics* **1987**, *1*, 201-212.

13) T. Hunkapiller; R. J. Kaiser; B. K. Koop; L. E. Hood *Science* **1991**, *254*, 59-67.

14) B. Ewing; P. Green *Genome Res.* **1998**, *8*, 186-194.

15) B. Ewing; L. Hillier; M. C. Wendl *Genomic Res.* **1998**, *8*, 175-185.

16) D. Gordon; C. Abajian; P. Green *Genome Res.* **1998**, *8*, 195-202.

17) C. Fields *Trends in Biotechnol.* **1996**, *14*, 286-289.

18) H. Lodish; A. Berk; S. L. Zipursky; P. Matsudaira; D. Baltimore; J. Darnell *Molecular Cell Biology*; 4 ed.; W. H. Freeman and Company: New York, 2000.

19) F. B. Perler; M. Q. Xu; H. Paulus *Curr. Opin. Chem. Biol.* **1997**, *1*, 292-299.

20) A. Fersht *Enzyme Structure and Mechanism*; 3 ed.; W. H. Freeman and Company:

New York, 1999.

21) B. Cubitt; R. Heim; S. R. Adams; A. E. Boyd; L. A. Gross; R. Y. Tsien *Trends In Biol. Sci.* **1995**, *20*, 448-455.

22) R. H. Stauber; K. Horie; P. Carney; E. A. Hudson; N. I. Tarasova; G. A. Gaitanaris; G. N. Pavlakis *Biotechniques* **1998**, *462-470.*

23) D. C. Youvan; M. E. Michel-Beyerle *Nature Biotechnol.* **1996**, *14*, 1219-1220.

24) C. Branden; J. Tooze *Introduction to Protein Structure*; Garland:, 1999.

25) M. Eggers; M. Hogan; Reich., R. K.; J. Lamture; D. Ehrlich; M. Hollis; B. Kosicki; T. Powdrill; K. Beattie; S. Smith; R. Varma; R. Gangadharan; A. Mallik; B. Burke; D. Wallace *Biotechniques* **1994**, *17.*

26) P. Tijssen *Hybridization with Nucleic Acid Probes Part II: Probe labeling and hybridization techniques*; Elsevier: New York, 1993; Vol. 24.

27) S. R. Rasmussen; M. R. Larsen; S. E. Rasmussen *Anal. Biochem.* **1991**, *198*, 138-142.

28) E. M. Southern *J. Mol. Biol.* **1975**, *98*, 508.

29) D. C. Darling; P. M. Brickell *Nucleic Acid Blotting, The Basics*; IRL Press: New York, 1994.

30) B. D. Hames *A Practical Approach*; Oxford Press: London.

31) D. Meldrum *Genomic Res.* **2000**, 1288-1303.

32) D. Meldrum *Genome Res.* **2000**, 1288-1303.

33) M. Lee; D. R. Walt *Anal. Chem.* **2000**, *282*, 142-146.

34) J. Cheng; P. Fortina; S. Surrey; L. J. Kricka; P. Wilding *Mol. Diag.* **1996**, *1*, 183-199.

35) C. H. Mastrangelo; M. A. Burns; D. T. Burke *Proc. IEEE* **1998**, *86*, 1769-1787.

36) A. Marshall; J. Hodgson *Nat. Biotechnol.* **1998**, *16*, 27-31.

37) A. P. Blanchard; S. H. Friend *Nat. Biotechnol.* **1999**, *17*, 953.

38) D. R. Walt *Science* **2000**, *287*, 451-452.

39) J. C. McDonald; D. C. Duffy; J. R. Anderson; D. T. Chiu; H. Wu; O. J. Schueller; G. M. Whitesides *Electrophoresis* **2000**, *21*, 27-40.

40) M. Schena *BioEssays* **1996**, *18*, 427-431.

41) D. Shalon; S. J. Smith; P. O. Brown *Genome Res.* **1996**, *6*, 639-645.

42) J. L. DeRisi; V. R. Iyer; P. O. Brown *Science* **1997**, *278*, 680-686.

43) A. M. Castellino *Genome Res.* **1997**, *7*, 943-946.

44) J. R. Pollack; C. M. perou; A. A. Alizadeh; M. B.; A. Pergamenschikov; C. F. Williams; S. S. Jeffrey; D. Botstein; P. O. Brown *Nat. Genet.* **1999**, *23*, 41-46.

45) P. Linsley; A. Blanchard; J. Burchard; E. Coffey; H. Dai; Y. He; T. Hughes; A. Jones; S. Kobayshi; A. Lee *Microb. Comparat. Genomics* **1999**, *4*, 90.

46) E. M. Southern *Trends in Genomics* **1996**, *12*, 110-115.

47) J. A. Running; M. S. Urdea *Biotechniques* **1990**, *8*, 276-&.

48) P. Balaguer; B. Terouanne; P. Allibert; P. Cros; A-M. Boussioux; B. Mandrand; J. C. Nicolas *Mol. and Cell. Probes* **1993**, *7*, 155-159.

49) H. Bunemann; P. Weshoff; R. G. Hermann *Nuc. Acids Res.* **1982**, *10*, 7163-7180.

50) V. A. Efimov; A. A. Buryakova; O. G. Chakhmakhcheva *Nuc. Acids Ress* **1999**, *27*

51) R. S. Matson; J. Rampal; S. L. Pentoney, J.; Philip D. Anderson; P. J. Coassin *Anal. Biochem.* **1995**, *224*, 110-116.

52) R. S. Matson; J. B. Rampal; P. J. Coassin, P. J. *Anal. Biochem.* **1994**, *217*, 306-310.

53) E. N. Timofeev; S. V. Kochetkova; A. D. Mirzabekov; V. L. Florentiev *Nuc. Acids Res.* **1996**, *24*, 3142-3148.

54) D. Proudnikov; E. Timofeev; A. Mirzabekov *Anal. Biochem.* **1998**, *259*, 34-41.

55) A. Muscate; F. Natt; A. Paulus; M. Ehrat *Anal. Chem.* **1998**, *70*, 1419-1424.

56) W. D. Volkmuth; R. H. Austin *Nature* **1992**, *358*, 600-602.

57) M. Yang; R. Y. C. Kong; N. Kazmi; A. K. C. Leung *J. of the Chem. Soc. of Japan* **1998**, 257-258

58) Z. Guo; R. A. Guilfoyle; A. J. Thiel; R. Wang; L. M. Smith *Nuc. Acids Res.* **1994**, *22*, 5456-5465.

59) L. A. Chrisey; G. U. Lee; E. O'Ferrall *Nuc. Acids Res.* **1996**, *24*, 3031-3039.

60) U. Maskos; E. M. Southern *Nuc. Acids Res.* **1992**, *20*, 1679-1684.

61) C. F. Edman; P. Mehta; R. Press; C. A. Spargo; G. T. Walker; M. Nerenberg *J. Investig. Med.* **2000**, *48*, 93-101.

62) R. Radtkey; L. Feng; M. Muralhider; M. Duhon; D. Canter; D. DiPierro; S. Fallon; E. Tu; K. McElfresh; M. Nerenberg *Nucleic Acids Res.* **2000**, *28*, E17.

63) L. Westin; X. Xu; C. Miller; L. Wang; C. F. Edman; M. Nerenberg *Nat. Biotechnol.* **2000**, *18*, 1815-1818.

64) C. F. Edman; D. E. Raymond; D. J. Wu; Eugene Tu; R. G. Sosnowski; W. F. Butler; M. Nerenberg; M. J. Heller *Nuc. Acids Res.* **1997**, *25*, 4907-4914.

65) H. Swerdlow; B. J. Jones; C. T. Wittwer *Anal. Chem.* **1997**, *69*, 848-855.

66) H. Tan; E. S. Yeung, *Anal. Chem.* **1998**, *70*, 4044-4053

67) D. J. Harrison; K. Fluri; K. Seller; Z. Fan; C. S. Effenhauser; A. Manz *Science* **1993**, *261*, 895-897.

68) S. C. Jacobson; L. B. Koutny; R. Hergenroder; A. W. Moore Jr.; J. M. Ramsey *Anal. Chem.* **1994**, *66*, 3472-3476

69) A. T. Woolley; R. A. Mathies *Proc. Natl. Acad. Sci. USA* **1994**, *91*, 11348-11352

70) K. Morishima; T. Fukuda; F. Arai; K. Yoshikawa *Microflow system and transportation of DNA molecule by dielectrophoretic force utilizing the conformational transitions in the higher order structure of DNA molecule.*: Nagoya, Japan, 1997.

71) D. Schmalzing; A. Adourian; L. Koutny; L. Ziaugra; P. Mastudaira; D. Ehrlich *Anal. Chem.* **1998**, *70*, 2303-2310

72) J. R. Scherer; I. Kheterpal; A. Radhakrishnan; W. W. Ja; R. A. Mathies **1999**, *20*, 1508-1517.

73) S. R. Liu; Y. N. Shi; W. W. Ja; R. A. Mathies *Anal. Chem.* **1999**, *71*, 566-573.

74) Y. N. Shi; P. C. Simpson; J. R. Scherer; D. Wexler; C. Skibola; M. T. Smith, a.; R. A. Mathies *Anal. Chem.* **1999**, *71*, 5354-5361.

75) M. A. Burns; C. H. Mastrangelo; T. S. Sammarco; P. F. Mann; J. R. Webster; B. N. Johnston; B. Foerster; D. K. Jones; Y. Fields; A. R. Kaiser *Proc. Natl. Acad. Sci. USA* **1996**, *93*, 5556-5561.

76) J. Cheng; M. A. shoffner; G. A. Hvichia; L. J. Kricka; P. Wilding *Nuc. Acids Res.* **1996**, *24*, 380-385.

77) M. U. Kopp; A. J. Mello; A. Manz *Science* **1998**, *280*, 1046-1048.

78) M. A. Northrup; D. Hadley; P. Landre; S. Lehew; J. Richards; P. Stratton *Anal. Chem.* **1998**, *70*, 918-922.

79) L. A. Christel; K. Petersen; W. McMillan; M. A. Northrup *Nucleic acid concentrations and PCR for diagnostic applications.*; D. J. Harrison, and A. van der Berg Ed.; Kluwer Academic Publishers: Boston, 1998.

80) J. Z. Zhang; Y. Fang; J. Y. Hou; H. J. Ren; R. Jiang; P. Roos; N. J. Dovichi *Anal. Chem.* **1995**, *67*, 4589-4593.

81) J. Bashkin; M. Bartosiewicz; D. Roach; J. Leong; D. Barker; R. Johnston *J. Capill. Electrophor.* **1996**, *3*, 61-68.

82) S. A. Soper; S. M. Ford; Y. Xu; S. Qi; S. McWhorter; S. Lassiter; D. Patterson; R. C. Bruch *J. Chromatogr. A* **1999**, *853*, 309-324.

83) S. McWhorter; S. A. Soper *Electrophoresis* **2000**, *21*, 1267-1280.

84) E. Carrilho; M. C. Ruiz-Martinez; J. Berka; I. Smirnov; W. Goetzinger; A. W. Miller; D. Brady; B. L. Karger *Anal. Chem.* **1996**, *68*, 3305-5513.

85) I. Kheterpal; R. A. Mathies *Anal. Chem.* **1999**, *71*, 31A-37A.

86) Q. Gao; E. S. Yueng *Anal. Chem.* **2000**, *72*, 2499-2506.

87) R. H. Service *Science* **1998**, *282*, 399-401.

88) L. J. Kricka *Nat. Biotechnol.* **1998**, *16*, 513-514.

89) O. Hofmann; D. Che; K. A. Cruickshank; U. R. Muller *Anal. Chem.* **1999**, *71*, 678-686.

90) D. Figeys; D. Pinto *Anal. Chem.* **2000**, *72*, 330A-335A.

91) G. Ekstrand; C. Holmquist; A. E. Orlefors; B. Hellman; A. Larson; P. Andersson *Microfluidics in a rotating CD*; A. van der Berg, W. Olthuis, and P. Bergveld, Ed.; Kluwer, Academic Publishers: Boston, 2000.

92) G. Yershov; V. Barsky; Belgovskiy., A.; E. Kirillov; E. Kreindlin; I. Ivanov; S. Parinov; D. Guschin; A. Drobishev; S. Dubiley; A. Mirzabekov *Proc. Natl. Acad. Sci.* USA **1996**, *93*, 4913-4918.

93) L. Picoult-Newberg; T. Ideker; M. Pohl; S. Taylor; M. Donaldson; D. Nickerson; M. T. Boyce-Jacino *Genome Res.* **1999**, *9*, 167-174.

94) T. T. Nikiforov; R. B. Rendle; P. Goelet; Yu-Hui Rogers; M. L. Kotewicz; S. Anderson; G. L. Trainor; M. R. Knapp *Nuc. Acids Res.* **1994**, *22*, 4167-4175.

95) R. M. Meyers; T. Maniatis; L. S. Lerman *Meth. in Enzymol.* **1987**, *155*, 501-527

96) R. M. Meyers; N. Lumelsky; L. S. Lerman; T. Maniatis *Nature* **1985**, *313*, 495-498.

97) E. S. Abrams; S. E. Murdaugh; L. S. Lerman *Genomics* **1990**, *7*, 463-475.

98) M. S. Ibrahim; R. S. Lofts; P. B. Jahrling; E. A. Henchal; V. W. Weedn; M. A. Northrup; P. Belgrader *Anal. Chem.* **1998**, *70*, 2013-2017.

99) K. K. Callaghan; S. J. Clayton; J. C. Fox; S. Little *Amer. J. of Human Genet.* **1997**, *61*, 332.

100) T. Shinka; T. Naroda; T. Tamura; Y. Nakahori *J. of Human Genet.* **2001**, *46*, 263-266.

101) E. Klein; G. Wierich; H. Brauch *Human Genet.* **2001**, *108*, 376-384.

102) W. Z. Xiao; P. J. Oefner *Human Mut.* **2001**, *17*, 439-474.

103) J. W. Nelson; F. H. Martin; I. Tinoco Jr. *Biopolymers* **1981**, *12*, 2509-2531.

104) A. Ulman *An Introduction to Ultrathin Organic Films from Langmuir-Blodgett to Self-Assembly*; Academic Press: Boston, 1991.

105) M. Yang; M. E. McGovern; M. Thompson *Anal. Chimica Acta* **1997**, *346*, 259-275.

106) M. J. O'Donnell; K. Tang; H. Koster; C. L.Smith; C. R. Cantor *Anal. Chem.* **1997**, *69*, 2438-2443.

107) L. A. Chrisey; C. Elizabeth, O. F.; J. S. Barry; C. S. Dulcey; J. M. Calvert *Nuc. Acids Res.* **1996**, *24*, 3040-3047.

108) J. A. Ferguson; T. C. Boles; C. P. Adams; D. R. Walt *Nature Biology* **1996**, *14*, 1681-1684.

109) L. Henke; P. A. E. Piunno; A. C. McClure; U. J. Krull *Anal. Chimica Acta* **1997**, *344*, 201-213.

110) F. N. Rehman; M. Audeh; E. S. Abrams; W. H. Philip; M. Kenney; T. C. Boles *Nuc. Acids Res.* **1999**, *27*, 649-655.

111) A. P. Abel; M. G. Weller; G. L. Duveneck; M. Ehrat; H. M. Widmer *Anal. Chemi.* **1996**, *68*, 2905-2912.

112) R. G. Nuzzo; F. A. Fusco; D. L. Allara *J. Amer. Chem. Soc.* **1987**, *109*, 2358-2367.

113) C. D. Bain; E. B. Troughton; Y. Tao; J. Evall; G. M. Whitesides; R. C. Nuzzo, R. G. *J. Amer. Chem. Soc.* **1989**, *111*, 321-335.

114) P. E. Laibinis; B. J. Palmer; S. W. Lee; G. K. Jennings *The Synthesis of Organothiols and their Assembly into Monolayers on Gold*; A. Ulman, Ed.; Academic Press: Boston, 1998; Vol. 24, pp 1-41.

115) K. L. Prime; G. M. Whitesides *Science* **1991**, *252*, 1164-1167.

116) T. M. Herne; M. J. Tarlov *J. Amer. Chem. Soc.* **1997**, *119*, 8916-8920.

117) U. Maskos; E. M. Southern *Nuc. Acids Res.* **1992**, *20*, 1679-1684.

118) M. Boncheva; L. Scheibler; P. Lincoln; H. Vogel; B. Akerman *Langmuir* **1999**, *15*, 4317-4320.

119) G. U. Lee; L. A. Chrisey; R. J. Colton *Science* **1994**, *266*, 771-773.

120) Y. Fang; J. H. Hoh *J. Amer. Chem. Soc.* **1998**, *120*, 8903-8909.

121) M. Ueda; H. Iwasaki; O. Kurosawa.; M. Washizu *J. Applied Phys.* **1999**, *38*, 2118-2119.

122) I. D. Parsons; B. Persson; A. Mekhalfia; G. M. Blackburn; P. G. Stockley *Nuc. Acids Res.* **1995**, *23*, 211-216.

123) K. Bondeson; A. Frostell-Karlsson; L. Fagerstam; G. Magnusson *Lactose repressor-operator DNA interactions: kinetic analysis by a surface plasmon resonance biosensor,* Academic Press **1993**, 245-251.

124) H. Wu; W. P. Yang; C. F. Barbas III *Proc. Natl. Acad. Sci. USA* **1995**, *92*, 344-348.

125) S. Schouten; P. Stroeve; M. L. Longo *Langmuir* **1999**, *15*, 8133-8139.

126) C. Bamdad *Biophys. J.* **1998**, *75*, 1997-2003.

127) P. Nilsson; Bjorn Persson; M. Uhlen;P. -A Nygren *Anal. Biochem.* **1995**, *224*, 400-408.

128) M. Yang; H. C. M. Yau; H. L. Chan *Langmuir* **1998**, *14*, 6121-6129.

129) S. P. A. Fodor; R. P. Rava; X. C. Huang; A. C. Pease; C. P. Holmes; C. L. Adams *Nature* **1993**, *364*, 555-556.

130) M. Chee; R. Yang; E. Hubbell; A. Berno; X. C. Huang; D. Stern; J. Winkler; D. Lockhart; M. S. Morris; S. P. A. Fodor *Science* **1996**, *274*, 610-614.

131) R. J. Lipshutz; S. P. A. Fodor; T. R. Gingeras; D. J. Lockhart *Nat. Genet. Suppl.* **1999**, *21*, 20-24.

132) A. Pease; D. Solas; E. J. Sullivan; M. T. Cornin; C. P. Holmes; S.P.A. Fodor *Proc. Natl. Acad. Sci. USA* **1994**, *91*, 5022-5026.

133) D. Shalon; S. J. Smith; P. O. Brown, P. O. *Genome Res.* **1996**, *6*, 639-645.

134) M. Eggers; M. Hogan; R. K. Reich; J. Latmure; D. Ehrlich; M. Hollis; B. Kosicki; T. Powdrill; K. Beattie; S. Smith; R. Varman; R. Gangadharan; A. Mallik; B. Burke Wallace *Biotechniques* **1994**, *17*, 516-525.

135) R. Levicky; T. M. Herne; M. J. Tarlov; S. K. Satija *J. Amer. Chem. Soc.* **1998**, *120*, 9787-9792.

136) J. N. Kremsky; J. L. Wooters; J. P. Dougherty; R. E. Meyers; M. Collins; E. Brown, *Nuc. Acids Res.* **1987**, *15*, 2891-2909.

137) D. A. Nickerson; R. Kaiser; S. Lappin; J. Stewart; L. Hood; U. Landergren *Proc. Natl. Acad. Sci. USA* **1990**, *87*, 8923-8927.

138) T. T. Nikforov; Y. H. Rogers *Anal. Biochem.* **1995**, *227*, 201-209.

139) P. A. E. Puinno; R. H. E. Hudson; H. Cohen; M. J. Damha; U. J. Krull *Anal. Chem.* **1995**, *67*, 2635-2643.

140) C. R. Graham; D. Leslie; D. J. Squirrell *Biosen. and Bioelect.* **1992**, 487-493.

141) L. A. Chrisey; C. E. O'Farrell; B. J. Spargo; C. S. Dulcey; J. M. Calvert *Nuc. Acids Res.* **1996**, *24*, 3040-3047.

142) G. U. Lee; C. E. O'Ferrall; L. A. Chrisey *Nuc. Acids Res.* **1996**, *24*, 3031-3039.

143) S. C. Tsang; Z. Guo; Y. K. Chen; M. L. H. Green; H. Allen O. Hill; Trevor W. Hambley; J. S. Peter *Agnew. Chem. Int. Ed. Engl.* **1997**, *36*, 2198-2120.

144) D. Guschin; G. Yershov; A. Zaslavsky; A. Gemmell; V. Shick; D. Proudnikov; P. Arenkov; A. Mirzabekov *Anal. Biochem.* **1997**, *250*, 203-211.

145) M. J. O'Donnell-Maloney; C. L. Smith; C. R. Cantor *Trends in Biotechnol.* **1996**, *14*, 401-407.

146) P. A. E. Piunno; J. Watterson; C. C. Wust; U. J. Krull *Anal. Chimica Acta* **1999**, *400*, 73-89.

147) H. Gamper; J. Piette; J. E. Hearst *Photochem. and Photobiol.* **1984**, *40*, 29-34.

148) G. D. Cimino; H. B. Gamper; S. T. Isaacs; J. E. Hearst *Ann. Rev. Biochem.* **1985**, *54*, 1151-1193.

149) J. W. Tessman; S. T. Isaacs; J. E. Hearst *Biochemistry* **1985**, *24*, 1669-1676.

150) R. G. Sosnowski; E. Tu; William F. Butler; J. P. O'Conell; M. Heller *Proc. Natl. Acad. Sci. USA* **1997**, *94*, 1119-1123.

151) R. A. Potyrailo; R. C. Conrad; A. D. Ellington; G. M. Hieftje *Anal. Chem.* **1998**, *70*, 3419-3425.

152) M. Egholm; O. Buchardt; L. Christensen; C. Behrens; S. M. Freier; D. A. Driver; R. H. Berg; S. K. Kim; B. Norden; P. E. Nielsen *Nature* **1993**, *365*, 566-568.

153) H. Su; Patrick Williams; M. Thompson *Anal. Chem.* **1995**, *67*, 1010-1013.

154) C. Debouck; P. N. Goodfellow *Nat. Genet. Suppl.* **1999**, *21*, 48-50.

155) M. N. Christof; L. Bolt; B. Ceyhan; D. Bhlom *Anal. Biochem.* **1999**, *268*, 54-63.

156) International Human Genome Project Consortium *Nature* **2001**, 490, 860-921

157) Venter et al., Celera *Science* **2001**, 291, 1304-1351

Chapter 2: Groundwork and directions

2.1 Background

Oligos can be synthesized with various 3' or 5' end "linkers" (such as biotin, thiol and amine) which can act as reactive sites for chemical crosslinking reactions. As described in chapter 1, researchers have devised a variety of reaction chemistries to immobilize the oligo linkers to a solid surface. Some examples include using the highly specific biotin/streptavidin interaction (K_d = 10^{-15} M^{-1}), glutaraldehyde, and other bifunctional crosslinkers (traditionally used to conjugate proteins or antibodies with various labels or each other), and peptide coupling reactions using coupling agents such as DCC and EDC. The above immobilization reactions were carried out at about 0.5 μM oligo solution concentration in an aqueous buffer at room temperature, often without surfactants. Radioactive or fluorescent tags (added during the oligo synthesis reaction, or with post-synthesis enzymatic reactions) were used to label the immobilized oligos. Researchers reported from $1x10^{-14}$ to $5x10^{-11}$ moles/cm^2 oligo surface densities, and generally low (<1%) nonspecific adsorption or side reactions (for example reactions involving the amino groups on the nucleotide bases rather than the amino linker on an oligo chain), with the occasional exception. The resulting attachments were covalent in nature and were thermally stable. On the other hand, thiol-linked oligos specifically adsorbed onto gold surfaces with a high affinity, creating oligo surfaces with approximately $1x10^{-13}$ moles/cm^2 densities. This attachment is not covalent and consequently is not thermally stable above 90°C for long periods of time.

From the above success in immobilizing oligos onto surfaces led to the logical conclusion that perhaps it is possible to use the same approaches to immobilize a longer (300-1000 bp) dsDNA chain onto a surface. Oligo primers with 5' linkers could be synthesized. The oligo would be incorporated into the dsDNA chain using PCR. The

resulting dsDNA would have an extended biotin, thiol or amino linker available for reaction with specific functional groups on the surface. Radioactive nucleotides (^{32}P-dCTP) incorporated in the dsDNA backbone during PCR would be used to label the dsDNA strands, for detection using a liquid scintillation counter. Thus I adopted various oligo immobilization protocols to try and attach dsDNA onto surfaces.

The first step was to identify potential candidate chemistries for attaching dsDNA onto surfaces. A long chain dsDNA is structurally different from a short oligo. Therefore, certain constraints must be considered. First, the molecular weight of my target dsDNA chain is at least 50-100 higher than a single strand oligo. Therefore the proportion of nonreactive sites to reactive sites on a dsDNA molecule is also proportionately larger compared to an oligo chain. Also, the diffusivity of the dsDNA chain is lower than an oligo chain. Thus, the overall reactivity of dsDNA solutions with a concentration equivalent to an oligo solution (0.5 μM) is lower. Optimizing the concentration of dsDNA in solution will help to improve the surface immobilization. Since dsDNA is only significantly soluble in water, aqueous buffers were the only choice for the dsDNA immobilization reactions. However, since water is a protic solvent and therefore may participate in many of the reaction protocols mentioned above, it is important to try and maximize the amount of dsDNA solvated in the buffer. Also, I had to choose chemistries that are more specific towards the amino, biotin or thiol linkers on the dsDNA strand to reduce the side reactions produced by the water molecules.

A second consideration of the long length of the dsDNA chain is that for an equal number of collisions/interactions with a surface site, the dsDNA chain has a much higher probability of nonspecific interactions versus a specific (covalent bond formation) interaction due to the high ratio of inert/reactive sites across its length. One possible nonspecific reaction is adsorption. Many researchers have reported about a 1% occurrence of nonspecific adsorption for surface immobilization reactions involving oligos, in the absence of surfactants[1-4]. Though this may seem trivial for a short chain oligo (10-25 nt single strand), if 1% of the surface sites each adsorb a much larger dsDNA molecule the effects are much more significant. In addition, due to its polymeric

nature once a dsDNA is nonspecifically adsorbed onto a surface the other bases along its chain are brought into close proximity to the surface, increasing the possibility of further adsorption reactions. Therefore, the nonspecific adsorption of long chain dsDNA onto surface is an important topic that merits detailed study before trying to covalently attach dsDNA onto surfaces.

Furthermore, the general trend of in the biotechnology industry, in particular the biosensor area, is towards nanoscale production and operation. As the dimensions of emerging DNA sequencing, amplification, purification systems steadily decrease, and with the introduction of numerous DNA microarrays with sub-micron surface features, the surface-to-volume ratio increases dramatically. Consequently DNA interactions at the liquid-solid interface become critical to the efficiency and performance of micron and sub-micron scale systems, and must be taken into account during their design. For instance high-energy surfaces may facilitate nonspecific DNA adsorption and result in product loss for a PCR chip, or impede DNA resolution during microcapillary electrophoresis. On the other hand, the cDNA microarrays developed by Brown require thermally stable surfaces that optimize nonspecific DNA adsorption onto a glass substrate. More sophisticated control of surface properties is required for a microscale gene delivery method, the biolistic gun[5-8]. For this system the DNA intended to transfect cells are adsorbed onto micron sized metal pellet, which are then propelled into the cell cytoplasm by high-pressure gas. To minimize cell mortality and optimize the DNA transfection efficiency, a surface coating must be designed for the pellets that prevents pellet agglomeration, and also optimizes intracellular DNA desorption under physiological conditions.

It is evident that DNA interactions with solid surfaces should be studied in detail to provide insight for the design of microscale solid-phase biochemical systems[9-14]. The challenge is to develop a straightforward, flexible model organic surface that can quantify DNA adsorption under various conditions, and the final goal is to modify the surface properties to control DNA adsorption and desorption. End (ω)-functionalized alkanethiol self-assembled monolayers (SAM) on gold substrates have been effectively utilized for

studying the surface properties of organic films such as interfacial energy and wettability, and have potential applications in surface pacification, corrosion prevention, and microlithography. Alkanethiols spontaneously form densely packed, well-ordered monolayers onto flat crystalline gold surfaces under ambient conditions. The resulting SAM films possess consistent surface properties that are readily characterized by a variety of techniques such as X-ray photoelectron spectroscopy (XPS), grazing-angle reflectance IR, ellipsometry and wetting measurements. Studies using end-functionalized alkanethiol SAMS to prevent nonspecific adsorption of proteins have been performed, the results indicating the oligo ethylene glycol (EG) moieties are capable of resisting protein adsorption. Some evidence indicates that EG groups may also prevent DNA adsorption[12]. In addition, researchers have utilized hydroxy-terminated alkanethiol SAMs to prevent DNA adsorption onto surfaces[15]. However, at present there are no systematic studies on how the surface properties affect nonspecific DNA adsorption, using functionalized SAMs as model surfaces.

More importantly, the ω-functional group of the alkanethiol SAM is exposed at the interface and simulates the chemical and physical surface properties of a corresponding bulk solid phase. Consequently, surface properties such as hydrophilicity and electric charge are controllable by simple manipulation of the ω-functional groups and composition of the solution phase alkanethiols. The resulting modified surfaces can then be used to study, and subsequently control, nonspecific DNA adsorption, and perhaps even control desorption of the DNA adlayer under certain conditions.

I synthesized or collected a variety of ω-functionalized alkanethiols and formed SAMs on gold substrates to serve as model organic films for studying nonspecific DNA adsorption at different solution temperatures, pH, DNA concentrations, salt concentrations, and surfactant species. A simplified schematic describing the SAM system is shown in Figure 2-1. Ellipsometry and FTIR were used to quantify and compare the adlayer amount, and wetting measurements were used to characterize the changes in surface energy that occurred during DNA adsorption. Possible mechanisms, and physical or chemical properties that pertain to DNA adsorption were proposed and

discussed, and subsequently modified SAM surfaces were designed using alkanethiol mixtures to test my hypothesis. The resulting trends for DNA adsorption with regards to hydrophilicity and electrostatic charges generally agreed with my findings on monolithic organic surfaces. Therefore I concluded that DNA adsorption is controllable through modifying the surface properties by the appropriate choice of surface chemical species and their composition.

2.2 Studies of nonspecific DNA adsorption onto solid surfaces

2.2.1 SAM formation

Gold (Au) surfaces were immersed in 1 mM end-functionalized alkanethiol solutions for 24 hours at room temperature. SAMs were formed on Au with the following surface functional groups: methyl (CH_3), amine (NH_2), hydroxy (OH), carboxylic acid (CO_2H), 1-hydroxy tetraethylene glycol (EG4), amide ($C{=}ONH_2$), dimethyl amine ($N(CH_3)_2$), and dimethyl amide ($C{=}ON(CH_3)_2$). The ellipsometric thickness, contact angles of water, and characteristic IR peaks for each surface are shown in Table 2-1.The SAM thicknesses were measured by ellipsometry, and the degree of error between samples was determined to be ±2Å. The contact angles of water for each surface were measured to determine the interfacial energy of the surfaces. High advancing angle (θ_a) values (>90°) are indicative of nonwetting, hydrophobic, low energy surfaces. On the other hand, hydrophilic, high-energy surfaces have low θ_a values (<30°). The extent of hysteresis (difference between θ_a and retreating angle (θ_{ret})) is affected by the heterogeneity of the SAM surface. The low hysteresis values for all seven SAM surfaces (<20°) indicated that they were well ordered and homogenous. The margin of error for the contact angle measurements was determined to be ±2°. FTIR spectra were taken for each of the SAM surfaces and confirmed the presence of the appropriate surface groups. The incident IR beam is directed by mirrors to contact the sample at "grazing" angle (80° from the surface

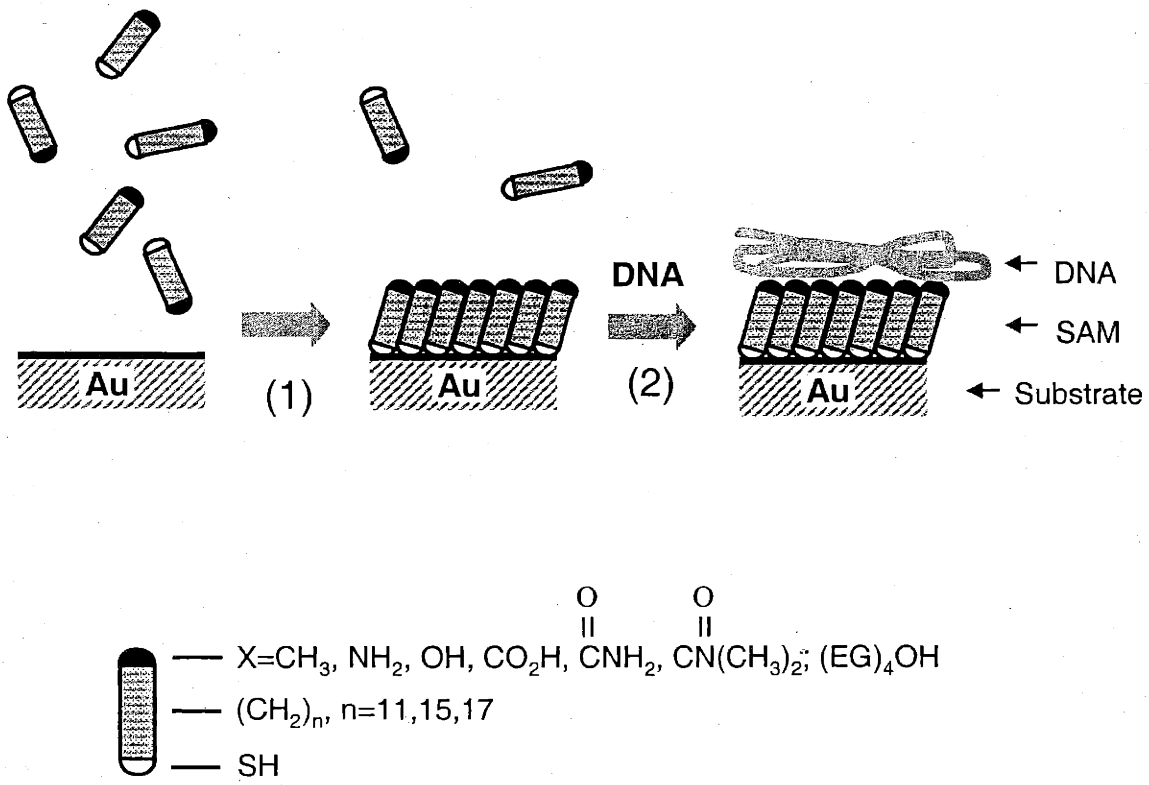

Figure 2-1. Experimental procedure for DNA adsorption studies. (1) Surface modification of gold substrates by self-assembly of end-functionalized alkanethiols. (2) Nonspecific adsorption of DNA from buffer solution onto modified organic surfaces.

Table 2-1. Ellipsometric thicknesses and contact angles of water for various ω-functionalized alkanethiol SAMs on gold substrates.

Adsorbate $HS(CH_2)_nX$ X=	Monolayer Thickness (Å)	θ_a of water (degrees)
$-CH_3$	23	115
$-CO_2H$	18	15
-OH	11	24
$-N(CH_3)_2$	11	72
$-(EG)_4OH$	23	62
$-C{=}ON(CH_3)_2$	11	66
$-NH_2$	13	56
$-C{=}ONH_2$	12	53

normal). The low incidence angle maximizes the contact between the IR beam and the thin organic films (10-50 Å) formed on the Au surfaces. The IR beam is reflected by the Au surface to a very sensitive MCT detector. In addition, a high number of scans (1024) are taken to improve the resolution of the IR spectra. The FTIR spectra were also used as background references for the DNA adsorption experiments.

2.2.2 DNA adsorption from 1 mg/ml TE solution

The initial DNA adsorption experiments were performed at a solution concentration of 1 mg/ml because it represents the upper limit for most applications

involving DNA. The solution pH was titrated to 7.4, the physiological pH of human serum. The SAM surfaces were immersed in the DNA solutions for 24 hours under ambient temperature and pressure, then rinsed with water. Ellipsometry measurements taken of the SAM surfaces before and after immersion in the DNA buffer solution indicated adlayer formation onto CH_3 and NH_2 surfaces. Wetting measurements indicated that θ_a for the CH_3 surface decreased from 115° to 72°, while θ_a for the NH_2 surface remained constant about 54°. The decrease in contact angle for the CH_3 SAM surface suggests an increases the surface energy. This result is expected for the adsorption a negatively charged DNA molecule onto an originally hydrophobic surface. An increase in the hysteresis between θ_a and θ_{ret} to >30° indicated that the adlayers on the CH_3 and NH_2 surfaces were more heterogeneous and less well ordered. dsDNA behaves like a semi-rigid polyelectrolyte, and would attach to the surfaces to form a heterogeneous, disordered adlayer.

FTIR spectra were taken of the adlayers on the CH_3 and NH_2 surfaces to confirm their identity. DNA chains had the following characteristic peaks: N-H stretch (amine) at 3320 cm^{-1}, C=O stretch (amide I) at 1680 cm^{-1}, N-H bend (amide II) at 1540 cm^{-1}, P=O stretch at 1226 cm^{-1} and P-O stretch at 987 cm^{-1}. In addition, XPS provided further evidence of DNA adsorption. XPS is a highly sensitive technique used for elemental analysis of solid surfaces. X-ray beams travel through extremely high vacuum (10^{-8} Torr) to bombard surface atoms, ejecting core level electrons. The kinetic energy of the ejected electrons is measured to determined the binding energy of the surface atoms, which is different for each element. The presence of DNA on the surface was confirmed by detection of phosphorous Phosphorous is abundant in a DNA molecule as part of its backbone, but is rare in the general environment. Thus it is a highly specific indicator for DNA. Phosphorous has a characteristic binding energy of 399 eV, but has a very low photoionization cross-section. Therefore more scans (64 scans vs. the general 4-8 scans) were needed to obtain an acceptable signal to noise ratio. The XPS and IR evidence was further supported by subsequent DNA adsorption experiments using radiolabeled dsDNA. The 390 bp long dsDNA strands were produced by PCR, and ^{32}P-dCTP was incorporated during the reaction. Various SAM surfaces were immersed in the

radiolabeled dsDNA solution for 24 hours, then characterized by a Geiger counter. Significant signal intensities were observed for the CH_3 and NH_2 surfaces, confirmation that DNA adsorption had occurred.

Initial ellipsometry and IR measurements suggested there was possible DNA adsorption onto $N(CH_3)_2$ surfaces. However, immersion of $N(CH_3)_2$ surfaces in a control solution containing only the TE buffer species produced the same ellipsometry and IR data as the DNA solutions. This indicated that the data obtained were most likely due to artifacts. Consequently no further experiments were conducted with $N(CH_3)_2$ as a candidate surface. Control experiments for the other functionalized surfaces immersed in TE buffer solution only showed no signs of ellipsometric thickness increase or artifactual peaks in the IR spectra.

It was theorized that perhaps some DNA in the buffer solution was being partitioned to the water/air interface, where it would adsorb onto the SAM coated gold substrate while the sample was being removed from the buffer solution. The adsorption mechanism is analogous to the methodology for producing Langmuir-Blodgett organic films on solid substrates. To test this hypothesis, CH_3 and NH_3 samples were immersed in a 1 mg/ml DNA solution for 24 hours at ambient conditions. Next, the DNA solution was diluted 1000 fold before the samples were removed, to prevent the formation of a DNA layer at the water/air interface. The samples were removed from the diluted solution and characterized by ellipsometry and FTIR. There was no difference in the amount of DNA adsorbed onto the surfaces under the above conditions, confirming that the DNA adsorption is occurring in solution. Another question was whether changes in the sample wash conditions would affect the DNA adsorption values. Samples with DNA adlayers (from immersion in 1 mg/ml DNA solutions for 24 hours at ambient conditions) were rinsed with a variety of buffer solutions. The number of washes and the strength of the fluid flow were also varied. The DNA adlayer thickness was measured by ellipsometry and FTIR to determine whether there was a difference in the thickness for different washing methods. However, the DNA adlayer thickness was consistent for a certain surface functional group regardless of the number or washes or the type of wash solution,

suggesting that the sample wash does not play a critical role in the amount of DNA adsorbed onto a surface.

No adsorption of DNA was evidenced for the OH, CO_2H, EG4, $C{=}ONH_2$ and $C{=}N(CH_3)_2$ surfaces after immersion in 1 mg/ml DNA solution (TE buffer, pH=7.4) for 24 hours at ambient conditions. The results suggest that these surfaces may be candidates to prevent nonspecific DNA adsorption. Finally, DNA readily adsorbed with monolayer coverage onto unmodified bare gold and bare silicon surfaces. However, silicon surfaces cleaned with a 12.5wt% NaOH solution for two hours resisted DNA adsorption. The cleaned silicon surfaces were very hydrophilic ($\theta_a < 15°$), possibly due to surface hydroxyl groups created by the reductive chemical environment of the base bath. The uncleaned bare silicon surfaces had a more hydrophobic surface ($\theta_a = 85°$), perhaps due to the adsorption of trace hydrocarbon contaminants from the ambient air. Thus the DNA may adsorb onto the hydrocarbon surface rather than the silicon surface itself.

2.2.3 DNA adlayer thickness

DNA adsorption onto organic surfaces was quantified by ellipsometry, and by the strong amide I peak intensity at 1680 cm^{-1} in the FTIR spectra. To obtain more information on the consistency and reproducibility of the FTIR and ellipsometry measurements, DNA was adsorbed from a 1 mg/ml solution (TE buffer, pH=7.4) onto CH_3 and NH_2 surfaces at different conditions, and the data were compared. The measurement values for both FTIR and ellipsometry were normalized using measurement values at a DNA solution concentration of 0.5 mg/ml on a NH_2 surface as the reference point. The difference in the height of the normalized FTIR and ellipsometry columns is proportional to the discrepancies between the two characterization methods. From Figure 2-2 it is evident that at higher salt concentrations the difference is higher. The same trend was reflected in similar comparisons performed on the CH_3 surface. The maximum difference between FTIR and ellipsometry measurements for DNA adlayer thickness on all surfaces was 25%. In general, the FTIR intensities were more consistent (within ±10%

difference) for different runs, while ellipsometry measurements had error margins of up to ±20%, especially at high salt concentrations. The overall trends of the FTIR and ellipsometry data were fairly consistent. Therefore it is possible to use both methods as complementary techniques to measure DNA adsorption onto organic surfaces and to determine trends.

2.2.4 Relationship of DNA solution concentration and adsorption

The effect of DNA solution concentration on DNA adsorption was studied on CH_3 and NH_2 surfaces. The 1 mg/ml DNA stock solution was serially diluted in TE buffer (pH=7.4) down to 2μg/ml concentration. CH_3 and NH_2 surfaces were immersed in the various DNA solutions for 24 hours at ambient conditions, and DNA adsorption was characterized by ellipsometry and FTIR. The results are shown in Figure 2-3. The DNA adsorption profile was fitted with a Langmuir-type adsorption isotherm:

$$\theta = K_c C / 1 + K_c C$$

Where θ = fractional surface coverage, C = DNA solution concentration (mg/ml), and K = adsorption constant. The DNA adsorption profiles did not perfectly fit the Langmuir-type model[15-19] frequently proposed by researchers who studied dsDNA adsorption. Some isotherms fit the data points from the lower concentration values (<0.1 mg/ml) while deviating for the higher concentration values. If the curves are fit to the higher concentration values then the lower concentration model values are too low as compared to the experimental values. Possibly this is due to the large molecular weight (ave. value ~ 10^7 Daltons), which could cause even a few partially adsorbed dsDNA molecules to generate a large negative electric charge density at the solid interface. The negative would repulse incoming dsDNA molecules from making contact with the solid surface, thus hindering the adsorption and counteracting the thermodynamic driving force for adsoption (increased solution concentration). Consequently, the dsDNA adsorbs less readily at higher concentrations than a traditional Langmuir model would indicate.

On the other hand, the K_c values for DNA adsorption onto CH_3 and NH_2 surfaces were consistently between 20 to 100 ml/mg, or approximately 0.2-1 x 10^8 M^{-1} for an average DNA M.W. = 10^7 Daltons. This value is about 20-100 times higher than the $1.5x10^6$ M^{-1} value determined for thiol-linked 718 bp dsDNA adsorbed onto gold surfaces[20]. One reason for the difference in Kc values is the large difference (20 times) in the M.W. between the DNA molecules used in the two studies. My DNA is longer and heavier so it can achieve the same surface coverage at lower solution concentrations compared to the shorter, thiol-linked DNA. In addition, the maximum DNA solution concentration for my study, 10^{-7} M, is about 100 times higher than the concentrations used in the Nelson study. This suggests that at higher solution concentrations nonspecific DNA adsorption may actually dominate surface interactions, even over specific DNA chemisorption reactions such as the thiol-gold system.

Initially, the amount of adsorbed DNA rapidly increased with solution concentration. Then, at DNA solution concentrations over 0.1 mg/ml the DNA adlayer thickness leveled out, suggesting that the adsorption thickness has an asymptotic upper limit, possibly at monolayer coverage. This result is supported by the ellipsometry data showing a maximum thickness increase of about 20 Å for DNA adsorbed onto CH_3 and NH_2 surfaces at solution concentrations from 0.1 mg/ml to 1 mg/ml. Since the diameter of the DNA double helix is 20 Å, it is reasonable to assume that DNA adsorption reaches monolayer coverage for solution concentrations over 0.1 mg/ml. This adsorption behavior is also observed during the formation of polyelectrolyte multilayers on solid surfaces[9,21-27]. Both anionic and cationic polymer chains consistently adsorbed onto surfaces in approximately monolayer level coverage over a range of solution concentrations. It is likely that the polyelectrolyte adlayer inhibits further polyelectrolyte adsorption due to electrostatic repulsion between the like charges. The negatively charged DNA molecules resemble anionic polymers, thus the adsorption of DNA possibly also follows the general adsorption behavior of polyelectrolytes.

The adsorption of DNA onto CH_3 and NH_2 surfaces, even at low solution concentrations, suggests that these surfaces are not appropriate solid substrates for

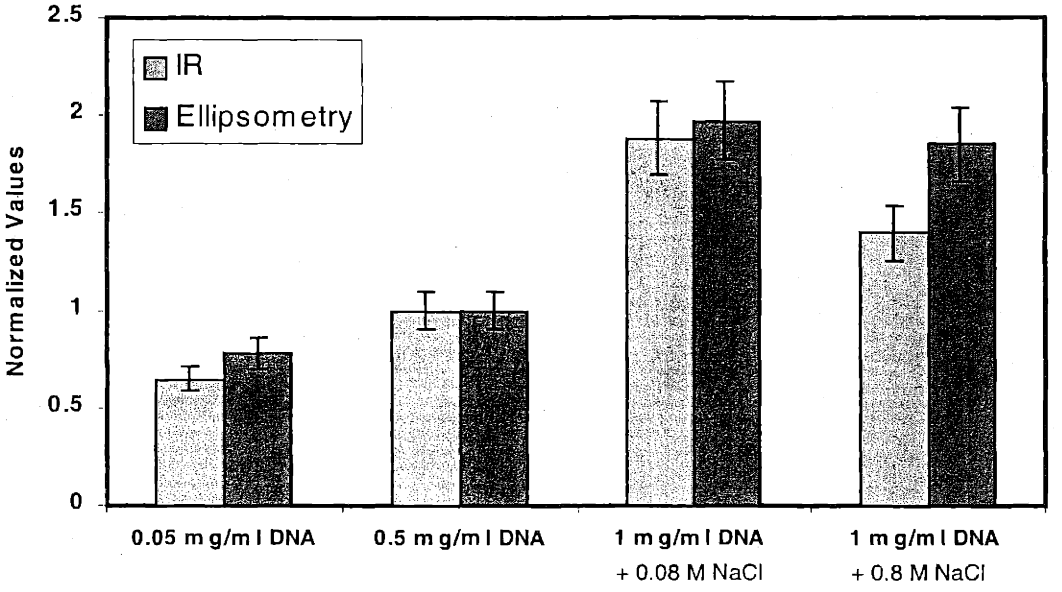

Figure 2-2. Comparison of the relative amounts of adsorbed DNA on $Au/S(CH)_{17}CH_3$ surfaces as determined by ellipsometry and FTIR spectroscopy. The values for a technique were normalized to those obtained at 0.5 mg/ml DNA solution concentration (set to 1.0). The results indicated that the maximum difference between the measured amounts determined by ellipsometry and FTIR is 25%.

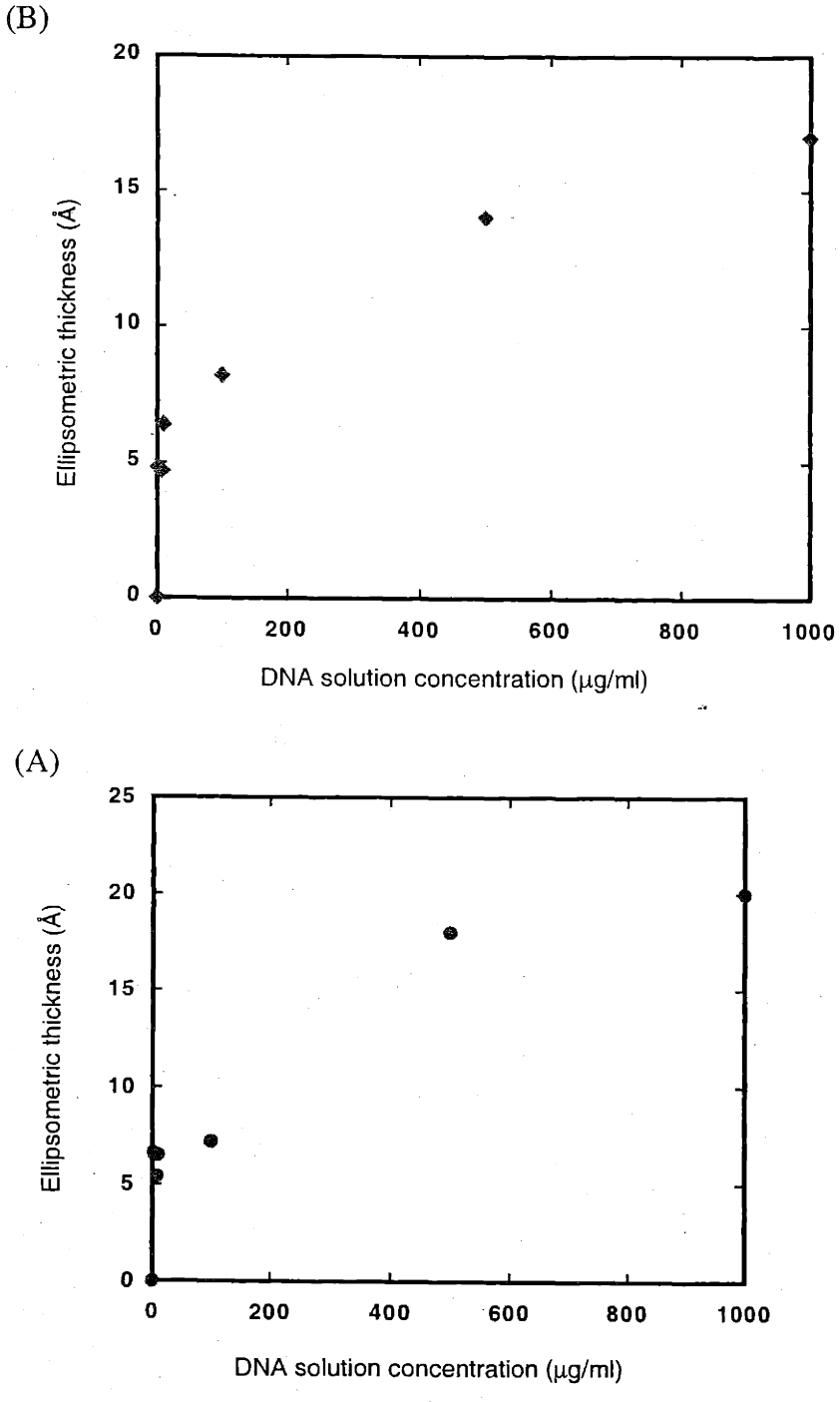

Figure 2-3. Relationships between DNA adlayer thickness and DNA solution concentration for adsorption onto: (A) CH_3, and (B) NH_2 surfaces. DNA was dissolved in TE buffer (pH=7.4, 0.01 M NaCl), and adsorption occurred at room temperature for 24 hours.

(C)

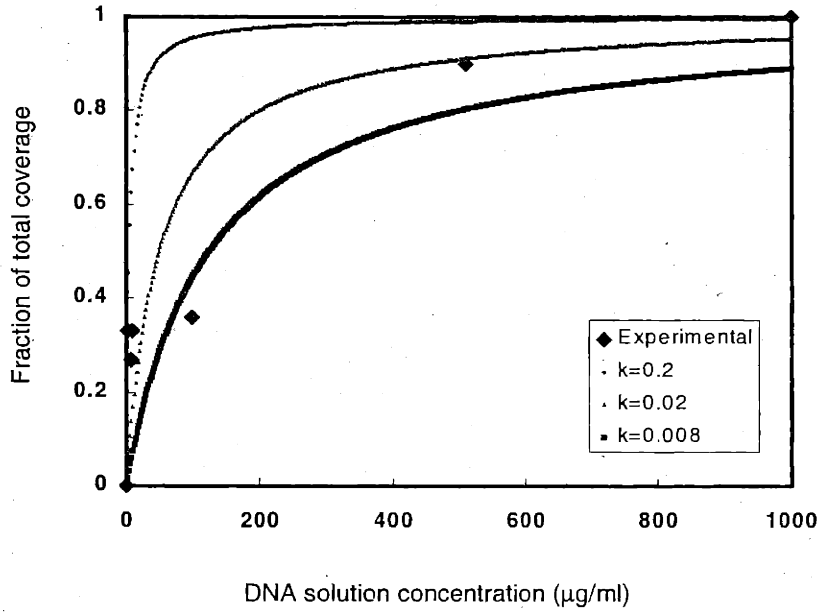

(D)

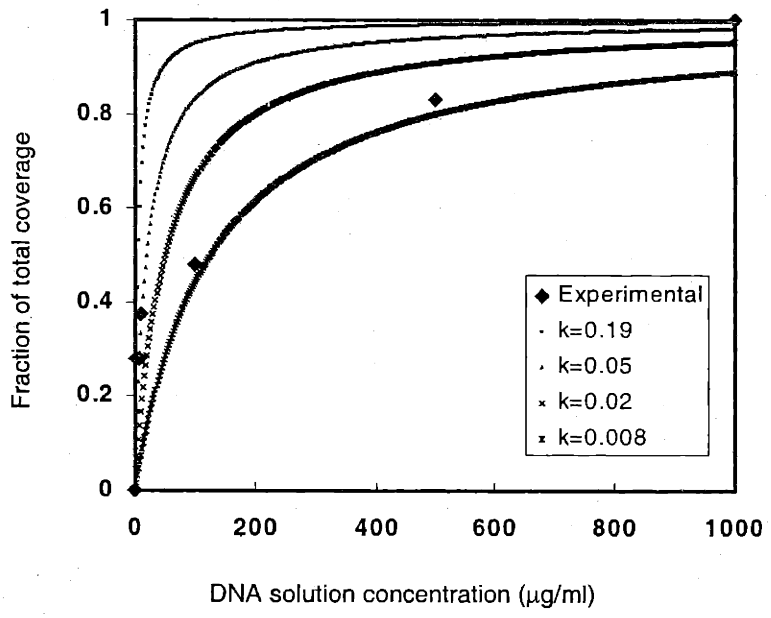

Figure 2-3. The DNA coverage on (c) CH_3 surfaces and (d) NH_2 surfaces are fit with Langmuir model adsorption isotherms.

biochemical applications where nonspecific DNA adsorption is unwanted. Currently, the storage and reaction vessels used in most biological research laboratories are made of glass or hydrocarbon (HC)-based polymers such as polystyrene, polyethylene and polypropylene. HC polymers are prevalent because they are cheap, and are easy to manufacture. In addition, the nonwetting surface properties of HC polymers are favorable when handling aqueous samples in the μl range. This is because aqueous solutions do not spread on the hydrophobic surfaces and are easily removed, preventing sample loss. On the other hand, it is evident that CH_3 surfaces are susceptible to a high degree of nonspecific DNA adsorption. The unwanted DNA adsorption could result in product loss from the liquid phase, or untoward contamination of a solid phase. In fact, the salmon sperm DNA used in this study is routinely used to prevent nonspecific adsorption of sample DNA on the polymer or glass surfaces commonly used as storage and reaction vessels. The salmon sperm DNA forms a barrier layer by adsorbing on the solid surface, and prevents further DNA adsorption using the rationale of electrostatic repulsion.

Perhaps it is possible to directly modify surfaces with organic films with certain functional groups to achieve the same effect as a sacrificial DNA adlayer. In addition, in-depth research on the surface properties that prevent nonspecific DNA adsorption may also be helpful in its prevention. For instance, the information obtained from such studies may be used to design polymer blends with the appropriate surface species and composition to prevent DNA adsorption. On the other hand, CH_3 and NH_2 surfaces may be used to facilitate DNA adsorption onto surfaces from dilute solutions. For instance, an NH_2 surface could be used to replace the current polylysine substrate developed by Brown *et al.* for cDNA microspot arrays. Glass microscope slides are coated with a fairly thick layer of polylysine. These surfaces are difficult to produce with consistent quality. Perhaps a thin organic film covalently attached onto the glass surfaces may serve the same purpose. Different applications have differing requirements with respect to DNA adsorption. Therefore it is critical to understand the surface properties that affect DNA adsorption and how to modify the surfaces appropriately for the relevant application.

2.2.5 DNA adsorption kinetics

DNA was adsorbed from a 1 mg/ml solution (TE buffer, pH=7.4) onto a CH_3 surface at ambient conditions. The DNA adlayer was measured by ellipsometry over an immersion time range from 5 minutes 48 hours, and the results are shown in Figure 2-4. Clearly, DNA adsorbs fairly rapidly, with about 25% of the final adlayer amount being adsorbed during the first 5 minutes of contact between the solution and the surface. After about 24 hours the adsorption reaches equilibrium levels and asymptotes. No further adsorption occurs after longer time periods. It is less clear on how to effectively model the DNA adsorption kinetics using traditional adsorption models for small molecules, since the long DNA chains adsorb onto the surface at multiple points. Also, due to its polymeric properties the footprint of each adsorbed DNA molecule may vary widely. Consequently it is uncertain on how to determine the number of surface adsorption sites available at any certain time.

For surface assays that utilize long chain (>100 bp) DNA probes it is desirable to immobilize one end of the DNA strand onto the surface, preferably in a covalent manner. Thus the whole length of the surface DNA probe is available for hybridization to the target DNA in solution. The basic approach for end-immobilizing long chain DNA probes requires some type of chemical reaction. As mentioned above, long chain DNA molecules possess a large ratio of inert to reactive sites. Therefore, it is critical to maximize the DNA solution concentration to improve the probability of a favorable reaction occurring on the surface. In such concentrations nonspecific DNA adsorption is rapid enough to compete with the immobilization reaction and reduce the number of reactive surface sites available for directed DNA end-attachment. Or, an end immobilized DNA chain could quickly adsorb onto the surface at multiple points, drastically reducing its hybridization efficiency and stringency. Therefore nonspecific DNA adsorption is not negligible from a kinetics standpoint during DNA surface immobilization reactions.

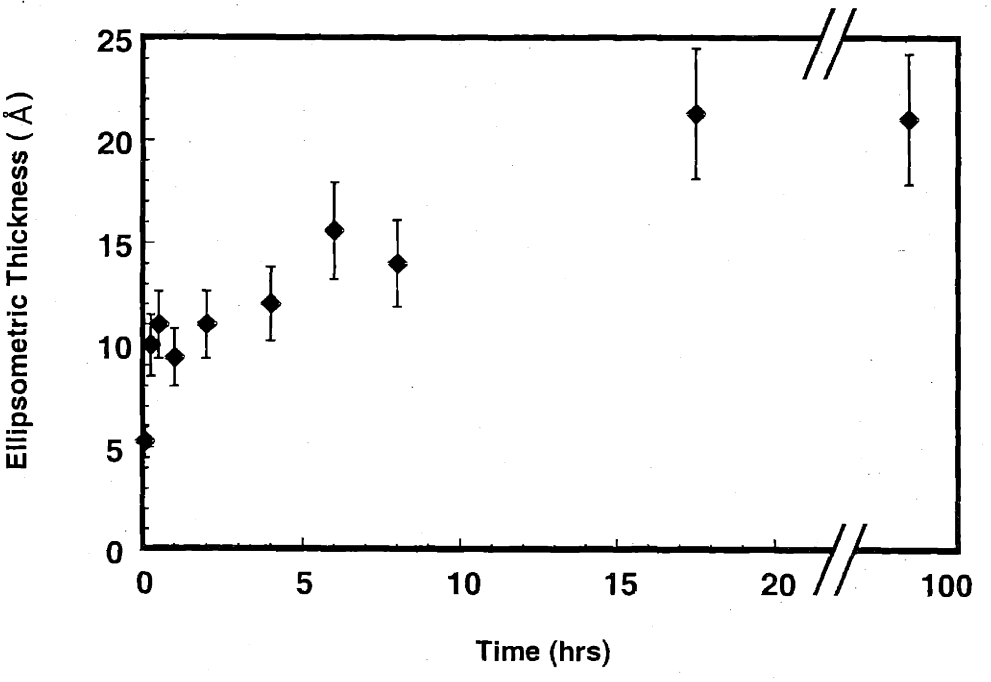

Figure2- 4. Kinetics of DNA adsorption from solution (1 mg/ml concentration in TE buffer, pH=7.4, 0.01 M NaCl) onto $Au/S(CH)_{17}CH_3$ surface at room temperature. The results indicated that DNA adsorption was rapid, with 25% of the final amount adsorbed within 5 minutes and 50% adsorbed within 30 minutes.

2.2.6 Mechanisms of DNA adsorption

The CH_3 surface is hydrophobic, as evidenced by the nonwetting (>90°) θ_a of water. However, the θ_a of water for the CH_3 surface decreased from 115° to 72° after DNA adsorption. The interfacial energy between the CH_3 surface and water is high, and consequently there is a thermodynamic driving force to lower it to achieve a minimum energy state. The decrease in θ_a of water for the CH_3 surface to wetting (<90°) after DNA adsorption suggests that the DNA adlayer effectively lowered the surface energy due to its hydrophilic, negatively charged phosphate backbone. The DNA molecules behave similarly to surfactants that aggregate at interfaces to minimize the interfacial energy. Furthermore, when I correlated the hydrophobicity of the various organic SAM surfaces with the relative amount of adsorbed DNA, I found the general trend of decreasing DNA adsorption with decreasing contact of water (see Figure 2-5). This strongly suggests that DNA adsorption is strongly affected by the interfacial energy of the organic surface with water. In addition, it indicates that DNA is thermodynamically driven to adsorb onto more hydrophobic surfaces.

For NH_2 surfaces there is no change in the contact angles, suggesting there is no thermodynamic driving force for DNA adsorption. However, the NH_2 surface is partially protonated to NH_3^+ at pH = 7.4. Therefore, DNA adsorption is due to electrostatic attraction between the positively charged NH_3^+ surface groups and the negatively charged phosphate backbone of the DNA chains. This hypothesis is supported by DNA adsorption experiments in 1 mg/ml TE buffer at pH=9.0 and pH =6.0 (at room temperature for 24 hours). The results of these experiments are shown in Figure 2-6. At higher pH there was less protonated NH_3^+ on the surface and the DNA adlayer decreased by approximately 80%.

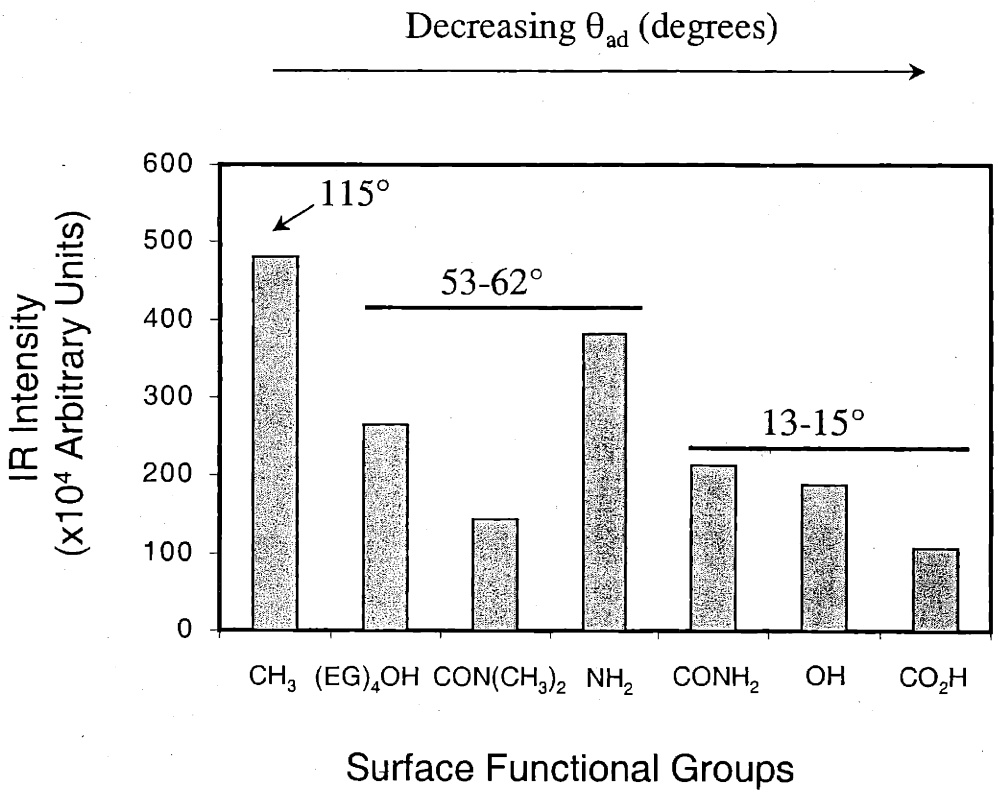

Figure 2-5. DNA adsorption from 1 mg/ml solution (TE buffer, pH=7.4, 0.01 M NaCl) onto various organic surfaces ($Au/S(CH_2)_nX$, n=11,15). Adsorption occurred over 24 hours at room temperature. The amount of DNA adsorption increased with increasing hydrophobicity.

On the other hand, at pH=6.0 and 7.4 there was no DNA adsorption onto the CO_2H surface, but at pH=9.0 an 8 Å DNA adlayer was observed. This result suggests that at pH=9.0, when all the CO_2H groups are deprotonated to CO_2^- ions, electrostatic repulsion from the negatively charged surface prevents DNA adsorption. However, at pH=6 when most of the CO_2H groups are protonated, DNA adsorbs onto the CO_2H surface in the absence of electrostatic repulsion.

The results from the above experiments using NH_3 and CO_2H surfaces demonstrate that electrostatic interactions are one of the deciding factors in whether DNA will adsorb onto a surface. This hypothesis is supported by literature on DNA interactions with charged surfaces[28]. Positively charged NH_3^+ ions facilitate DNA adsorption[12], while negatively charged CO_2^- ions prevent DNA adsorption. The results also suggest that perhaps it is possible to control DNA adsorption onto electroactive surfaces by varying the pH of the buffer and also the charge polarity of the surface chemical species. Finally, the different adsorption mechanisms for DNA onto CH_3, NH_2, and CO_2H surfaces suggest that the mechanics of DNA adsorption are complex and may be due to a combination of intermolecular attractions, including Van der Waals forces, hydrogen bonding, and electrostatic forces, and that the driving force for DNA adsorption is mainly due to thermodynamic considerations, especially for the hydrophobic CH_3 surfaces.

The mechanism for EG4 resistance of DNA adsorption is somewhat different from the regular considerations of intermolecular forces, since it is theorized that the repulsive force is entropic in nature. Polyethylene glycol polymers (PEG) are commonly used in the medical devices, especially for transplants, because they are biocompatible and do not elicit an immune response from the recipient body. The main reason for the lack of immunological response is due to the inability of cell interaction or adhesion to the PEG surface.

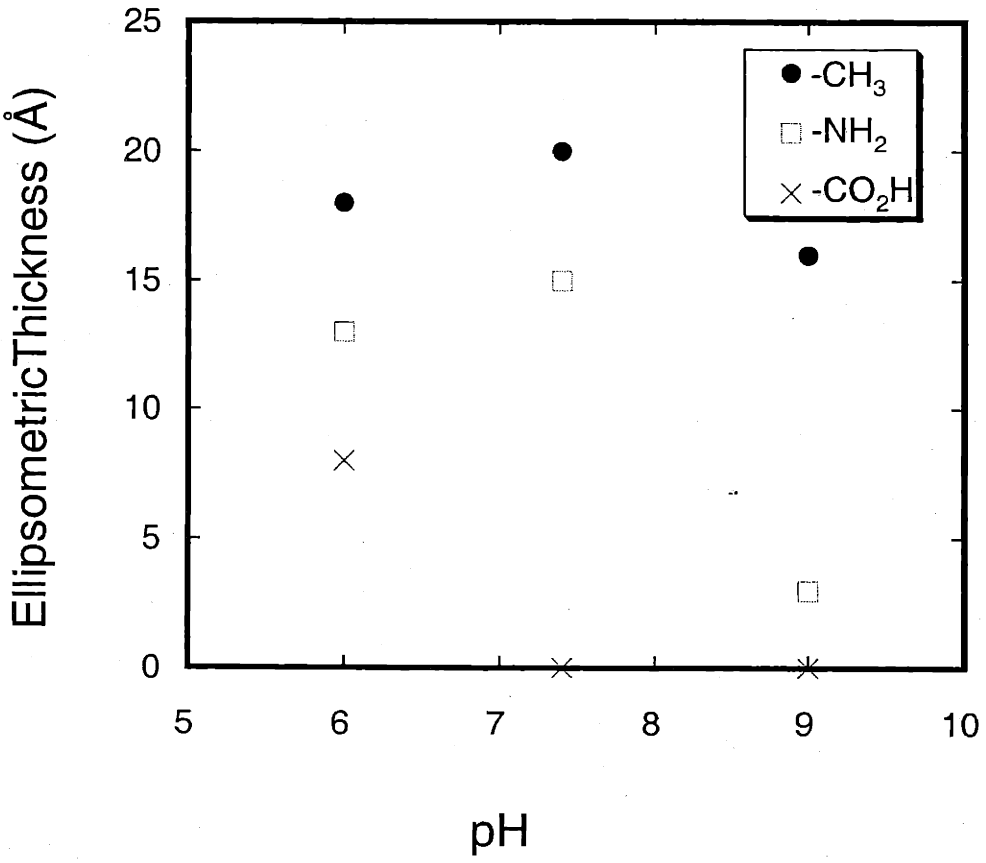

Figure 2-6. The effect of pH on the adsorption of DNA onto various organic surfaces. DNA is dissolved at 1mg/ml concentration in TE buffer (pH=7.4, 0.01 M NaCl), and all surfaces are immersed in DNA solution for 24 hours at room temperature.

This phenomena effectively renders the PEG coated surfaces undetectable by the immune system. Therefore the body does not reject the implant. Efforts were made to reproduce this effect using a short chain alkanethiol SAM with an EG terminal group. The EG terminated thin films were very successful in inhibiting the nonspecific adsorption of many proteins[29-31]. Though the alkane chains form well ordered, densely packed surface structures, the EG groups were less ordered and therefore possessed a large amount of entropy. Adsorption of a large molecule such as a protein or DNA would restrict the random motion of the EG groups and thus decrease the entropy of the system, resulting in a thermodynamically unfavorable state. Consequently the EG groups act like "entropy springs" that repulse molecules from the surface and thus prevent nonspecific adsorption. Alkanethiol SAMs on Au with more than 2 EG groups effectively passivated the surface from protein adsorption. But silane films on silicon are less ordered and less dense, so more EG groups are necessary to prevent protein adsorption. This is probably because the overall entropy of such a disordered silane film is much larger compared to an alkanethiol surface. Thus, the decrease in entropy due to nonspecific adsorption of proteins or DNA onto the EG terminated surface would have less thermodynamic impact on the silane system. An EG4 functionalized alkanethiol SAM resisted DNA adsorption unless very high (>1.37 M) salt concentrations were present, suggesting that at lower salt concentrations the EG4 surfaces are adequate to prevent DNA adsorption. However, more DNA adsorption studies should be conducted using EG4 functionalized films on silica surfaces to see whether the lower surface density and decreased order of silane films degrade their ability to resist adsorption.

2.2.7 Controlled DNA adsorption through surface modification

From the previous section I noted that DNA adsorbed onto hydrophobic CH_3 surfaces, subsequently reducing the surface's interfacial energy with water. This effect was evidenced by the drop in the contact angle of water for CH_3 surfaces after formation

of the DNA adlayer. In addition, the hydrophilic OH surface (θ_a<15°) resisted DNA adsorption at 1 mg/ml, possible due to the lack of a thermodynamic driving force or other intermolecular forces favorable to adsorption. These results suggested that I could control DNA adsorption by altering the hydrophilicity or interfacial energy of a surface. Mixed alkanethiol monolayers with terminal CH_3 and OH groups were used to explore this hypothesis.

Alkanethiol solution mixtures (10 mM) were prepared in ethanol. The solutions contained 0 to 100% 1-hydroxyundecanethiol (OH thiol), with the balance 1-methylundecanethiol (C12 thiol). The two alkanethiols are of similar length to ensure that the resulting SAM is of uniform height. Previous studies of mixed monolayers indicated that the surface composition is homogenous, with both functional groups randomly and evenly distributed on the surface. However, the solubility of the end-functionalized alkanethiols in ethanol differed (OH thiol is favored due to hydrogen bonding with ethanol molecules). Consequently, the mixed SAM surface composition deviated from a linear correlation with the solution OH thiol concentration (the OH surface fraction is lower). XPS was utilized to measure the oxygen content (binding energy=532 eV) of the mixed SAMs over a range of OH compositions. The values were normalized, with the XPS oxygen signal from a 100% OH SAM as the standard. The resulting calibration curve for surface OH composition against the solution OH thiol concentration is shown in Figure 2-7a. In addition, wetting measurements were performed with MQ water, and the contact angles are shown in Figure 2-7b.

(A)

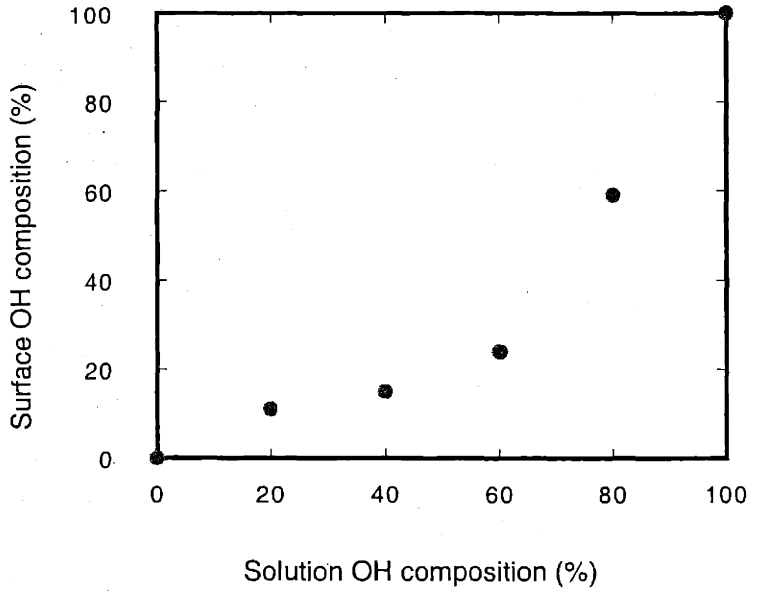

(B)

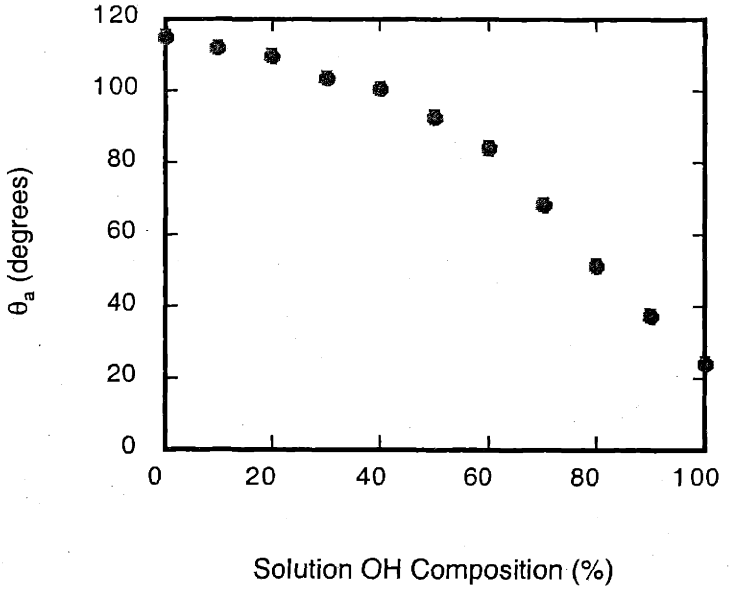

Figure 2-7. Characterization of mixed monolayers by XPS and contact angles of water. (a) Surface composition of mixed SAMs formed on Au surfaces from solution mixture of $CH_3(CH_2)_{11}SH$ and $HO(CH_2)_{11}SH$. Deposition time was 24 hours, at room temperature. Surface composition was determined by XPS. (b) Advancing contact angles of water on the mixed monolayer SAM surfaces.

The adsorption profile in Figure 2-6a is similar to the results of previous studies of mixed alkanethiol SAMs, evidencing a nonlinear relationship between OH content on the surface and in solution. The C12 thiol preferentially adsorbed onto the gold surface, possibly due to differences in solubility in the 95% ethanol solution. The decreasing contact angle with increasing OH fraction matched the theoretical prediction that the surface hydrophilicity increased with increasing surface OH content, and is supported by previous studies performed on mixed alkanethiolate monolayer on gold substrates by *Laibinis* and *Whitesides*[54].

The amount of DNA adsorbed onto the mixed monolayer surfaces under a variety of solution conditions is shown in Figure 2-8. It is clear that the amount of DNA adsorbed decreases with increasing OH content (hydrophilicity). This general trend further supports the hypothesis that DNA adsorption is related to the interfacial energy of the organic surface. As the surface energy increases, the thermodynamic driving force for DNA adsorption decreases. The results also demonstrate that it is possible to control the amount of DNA adsorbed on a surface by manipulating the surface species and composition to obtain the appropriate characteristics.

From ellipsometry data and FTIR spectra it was observed that the mixed monolayer surface resisted DNA adsorption when surface OH content was higher than 80%. This suggests that mixed OH-CH_3 surfaces designed to prevent nonspecific DNA adsorption should be hydrophilic in nature with a high proportion of OH groups. Finally, it was noted that for solutions with increased NaCl concentrations the amount of DNA adsorbed increased, suggesting that increased salt concentration may facilitate DNA adsorption.

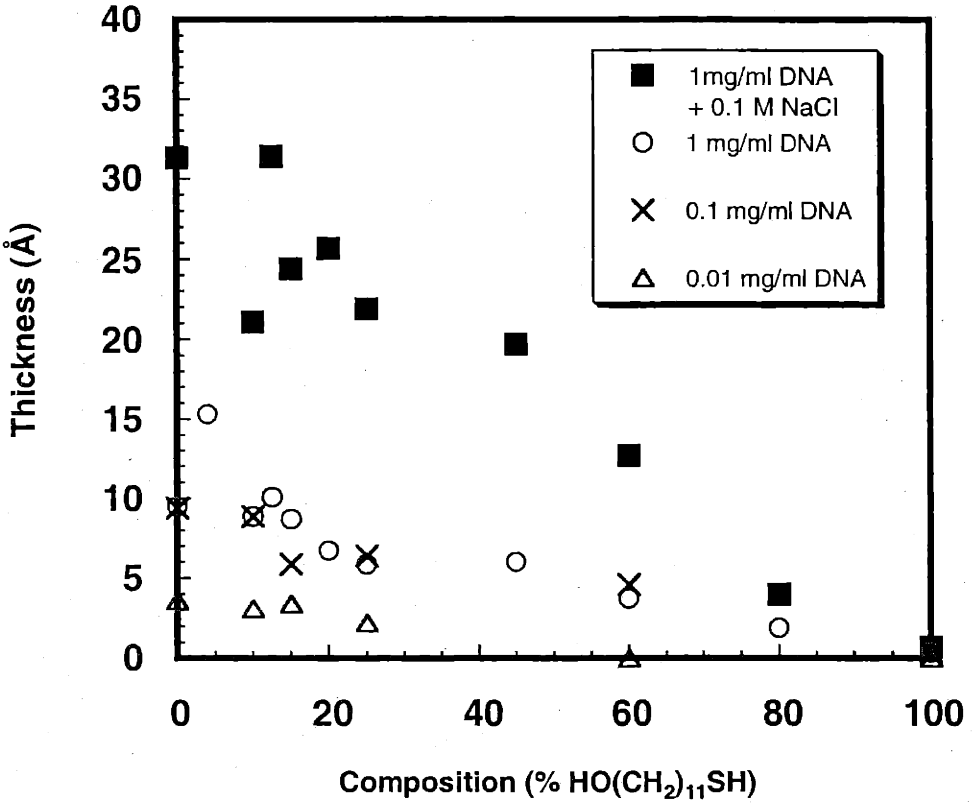

Figure 2-8. DNA adsorption onto mixed CH_3 and OH-terminated alkanethiol monolayers. DNA adlayer thickness decreased with increasing OH fraction. DNA adsorption was prevented when OH composition exceeded 80%.

2.2.8 DNA adsorption and salt concentration

As the salt concentration was increased for DNA solutions in TE buffer, (pH=7.4, 24 hour immersion in room temperature), DNA adsorption occurred on previously resistant surfaces. At 0.137 NaCl concentration, DNA adsorbed onto OH, CO_2H, $C{=}ONH_2$ and $C{=}ON(CH_3)_2$ surfaces, while DNA adsorbed onto EG4 surfaces at 1.37 M NaCl concentration. For CH_3 and NH_2 surfaces, DNA adlayer thicknesses increased by up to 25% in buffer solutions with high salt concentrations. At very high NaCl concentration (5 M), DNA adsorbed on all the surfaces surveyed, and the adlayer thicknesses are shown in Table 2-2. The surfaces are arranged in order of decreasing θ_a (increasing hydrophilicity). A general trend of decreased DNA adsorption with increased surface hydrophilicity was observed, which further supports the above hypothesis that the interfacial energy of the surface with water affects DNA adsorption. However, it was surprising that at high salt concentrations DNA even adsorbed onto the usually resistant EG4 surfaces, which have been utilized to prevent protein adsorption and were considered for general prevention of DNA adsorption.

Table 2-2. Effect of on DNA adsorption onto various organic surfaces. The blue-shaded boxes indicate DNA adsorption onto a surface. The DNA solution concentration was 1 mg/ml in TE buffer, pH=7.4. The adsorption reaction proceeded at room temperature for 24 hours.

NaCl conc. (M)	Surface Functional Group					
	CH_3	NH_2	CO_2H	$CONH_2$	OH	$(EG)_4OH$
0.01						
0.137						
1.37						
5						

There are many possible reasons for the indiscriminate adsorption of DNA onto all the surfaces at high salt concentrations. First, the increased concentration of ions in the DNA solution increases the dielectric constant of the buffer solution, thereby decreasing its ability to solvate the organic, albeit polyionic, DNA molecules. Consequently, the K_{ow} of DNA increased and the DNA molecules partitioned favorably into the organic (solid) phase. This type of "salting out" effect is commonly observed for organic molecules dissolved in aqueous solutions. In addition, the solution ions may screen the negative charges on the DNA phosphate backbone from the electrostatic repulsion from a similarly charged surface such as CO_2^-. Thus, a negatively charged surface would not repulse the solution DNA as effectively. Furthermore, the ionic screening increases the DNA radius of gyration towards a fully extended form. Consequently, more nucleotides on the DNA chain become exposed and available for surface interaction, resulting in an increased probability for the formation of a surface adsorption point. DNA in buffer solutions with

a very high (5 M) salt concentration even adsorbed onto a previously formed DNA adlayer, which was thought to be resistant to further adsorption due to electrostatic repulsion. The second DNA adlayer was not stable and desorbed with a rigorous water wash, suggesting that the driving force for the DNA adsorption was mainly due to the increased salt concentration and the resulting screening and "salting out" effects. A similar effect is used in the "glass milk" method[32,33] of separating DNA from solution. In this method the DNA is first solvated in a buffer solution with a high salt concentration (3 M NaI). Then a suspension of micron size glass (silicon oxide) beads are added to the DNA solution. The high salt concentration forces the DNA to partition onto the surfaces of the glass beads. Then the adsorbed DNA is removed from the glass surfaces by immersing them in a low salt buffer, so that the DNA now partitions favorably into the liquid phase. Previous literature had determined the quantity of adsorbed DNA as 0.2 $\mu g/cm^2$ of bead surface, or the equivalent of about 5 to 6 adlayers of DNA[34]. This result suggests that a high salt concentration indeed forces DNA to adsorb even onto existing DNA adlayers. Also, about 90% of the adsorbed DNA was removed by resuspension in the low salt buffer. This result matches my observation that the second DNA adlayer was removed by a sustain water (low salt concentration) wash.

A general conclusion is that salt concentration profoundly affects DNA adsorption and may negate the advantages of utilizing DNA-resistant surfaces such as OH and EG4. Therefore it is imperative to minimize solution salt concentration for applications where nonspecific DNA adsorption is unwanted unless other methods are available to inhibit DNA adlayer formation.

2.2.9 Temperature, buffer species, surfactants and DNA chain length

Further DNA adsorption experiments were conducted at 1 mg/ml concentration for 24 hours, under different temperatures or with different buffer species. No significant changes in DNA adsorption behavior were observed in the temperature range from 0° to 70° C, and variations in DNA adlayer thickness on CH_3 and NH_2 surfaces were within

15% by ellipsometry. The results suggest that DNA adsorption is unchanged at temperatures between 0° and 70° C. For experiments where the TE buffer was replaced by phosphate, SSC or 10 mM sodium perchlorate solutions, there was no observable difference in DNA adsorption behavior. This indicated that the buffer moeities do not compete for surface sites or otherwise affect DNA adsorption.

However, the addition of an anionic surfactant, SDS (0.1 wt% in 5 x SSC buffer) prevented DNA from adsorbing onto all seven surfaces studied. The solution concentration of SDS at 0.1wt% was higher than the critical micelle concentration (CMC). It is possible that micelles formed around the DNA molecules in solution, effectively lowering their surface energies and passivating them. In addition, some SDS molecules may have competitively adsorbed onto the surfaces. These adsorbates could resist DNA adsorption by electrostatic repulsion and by removing the thermodynamic driving force. In addition, SDS molecules could competitively displace adsorbed DNA from a surface. Therefore surfactants such as SDS can be utilized to prevent nonspecific DNA adsorption regardless of surface composition. In addition, SDS prevented DNA adsorption onto surfaces even at high salt concentrations. This result is important for hybridization reactions, which are facilitated by high salt buffers. However, due to its strong surfactant properties SDS will readily denature proteins and deactivate enzymes, and thus cannot be utilized for any immobilization reactions involving proteins, such as an avidin-biotin system, or if the target DNA has an enzymatic probe such as horseradish peroxidase (HRP) or alkaline phosphotase (AP).

Further studies were conducted with DNA strands sheared into shorter chains using ultrasound. After 30 minutes of sonication, the DNA chain length was determined from agarose gel electrophoresis to average around 700-1200 bp, or 4-6% of the original length. Ellipsometry and FTIR measurements indicated that the thickness of short chain DNA adlayers on CH_3 and NH_2 surfaces were on average 10-15% higher than for long chain DNA. In addition, at 1 mg/ml concentration a small amount (5 Å) of short chain DNA adsorbed onto the OH surface, which was resistant to adsorption of long chain

DNA. The modest increase in DNA surface affinity may be due to the increased solution mobility of the shorter DNA chains, causing them to diffuse more rapidly to the surface.

However, the results from dsDNA adsorption in general seemed to contradict many previous papers where oligos were being attached to the surface. Most of these studies suggested that oligos (10-25 nt long) adsorb to only about 1% of the available surface sites, even in the absence of surfactants such as SDS. However, for my studies dsDNA adsorbed onto CH_3 and NH_2 surfaces with monolayer coverage at solution concentrations equivalent to oligos (0.1-1 μM). This suggests that the amount of DNA adsorption onto surfaces is size dependent[35,36]. One reason for the increased surface coverage for adsorbed dsDNA is probably its large molecular weight (long chain length). At similar concentrations even short chain dsDNA (700-1200 bp) is about 100 times longer than oligos. Therefore, even if only 1% of the dsDNA chains in solution adsorb onto the surface (the equivalent of oligo adsorption), 100% surface coverage (monolayer thickness) is quickly achieved. Also, since the dsDNA chain is much longer, many more nucleotides contact the surface for every collision between a dsDNA molecule and a surface. This phenomenon effectively increases the collision efficiency. Finally, the double helix structure of dsDNA makes it more rigid then the freely rotating oligos. Thus when a dsDNA chain adsorbs onto a surface at one point, the remaining nucleotides in the dsDNA chain remain in close proximity to the surface and are more likely to adsorb too. Consequently, the dsDNA adsorbs onto the surface at multiple points, which increases the thermodynamic stability of the immobilized dsDNA chain. Therefore, in general long chain dsDNA adsorb onto surfaces at much higher densities compared to oligos.

2.2.10 DNA adlayer stability

DNA adlayers (adsorbed from 1 mg/ml solution concentration in TE buffer, pH=7.4, 1.37 M NaCl) on CH_3, NH_2, OH, $C{=}ONH_2$, CO_2H and EG4 surfaces were subjected to a wide range of chemical and mechanical disturbances to study the adlayer stability. All desorption experiments were run for 24 hours to ensure the systems reached

equilibrium and were not kinetically limited. The results are tabulated in Table 2-3. Less than 25% of the adsorbed DNA was removed by heating in TE buffer to 70° C, vigorous mechanical agitation (magnetic stirring), addition of Triton X-100 surfactant, or to changes in solution pH, buffer species, and salt concentration. After the initial loss no further DNA desorption was observed upon repeating the disturbances, suggesting that DNA adsorption is irreversible. The only exception that affected DNA adlayer stability was the addition of 0.1wt% SDS surfactant solution[37]. The DNA adlayers on CH_3 surfaces were completely removed after 24 hours immersion in SDS solution, while the DNA adlayer thickness on NH_2 surfaces decreased only by 25-50%, and little effect was observed for the other surfaces studied. A possible mechanism for DNA desorption in SDS solution is displacement by the competitive adsorption of SDS onto the surfaces. The experimental results suggest that addition of SDS surfactants at concentrations above CMC can remove adsorbed DNA from a hydrophobic surface, but have limited effects on charged or hydrophilic surfaces.

On the other hand, previous literature had shown that certain salts such as phosphates could desorb oligos from surfaces[2,38]. The mechanism for desorption is competitive displacement of the oligo by a smaller phosphate through an exchange reaction. Again, there are contradictory results between dsDNA and oligos. A possible explanation lies in the difference in size. The long chain dsDNA adsorbs onto surfaces at multiple points. Therefore even if a phosphate molecule successfully displaces one of the dsDNA adsorption points, many still remain to immobilize the chain to the surface. However, the shorter oligo chains may only attach to the surface at one or two points, and therefore the oligos are more readily removed by exchange reactions.

Table 2-3. The effects of various experimental conditions on the desorption of DNA adlayers from $Au/S(CH_2)_{11}X$ surfaces, where $X = CH_3$ or NH_2.

Variable	Range	Amount of desorbed DNA from surface	
		$-CH_3$	$-NH_2$
Agitation by magnetic stirring	-	<25%	<25%
Heat + agitation	Up to 70° C	<25%	<25%
NaCl + phosphate	1M	None	None
NaCl + pH change	1M, pH=6-9	<25%	<25%
Surfactants	0.1 wt% Triton X-100	None	None
	0.1 wt% SDS	~100%	25-50%

Previously there was a proposal to deliver DNA into cells for gene therapy using a biolistic gun. For this gene delivery method to work, it was critical to develop a surface that DNA will desorb from under certain biological conditions (such as temperature or pH). The overall stability of the DNA adlayer and the lack of DNA desorption under various conditions diminishes the potential for using functionalized SAMs as a system for gene delivery. Since changes in temperature, pH and salt concentrations are all ruled out for DNA desorption, other possible mechanisms should be explored such as exploiting the shear force created by the DNA-coated pellets when they penetrate the cell membrane or cytoplasm. However, excess shear could damage the DNA material.

Or perhaps DNA hybridization could by applied to immobilize the DNA onto the surfaces of the beads. Since hybridization is temperature sensitive, an alternative is to derivatize the pellet surfaces with oligo chains. One approach uses thiol-linked oligos mixed with OH thiols to modify gold pellets. The therapeutic DNA is designed and cloned with an additional sequence that is recognized and cleaved by certain restriction endonucleases to produce an oligo overhang. The overhang sequence is complementary to the immobilized oligo, and the sequence T_m is lower than the physiological temperature (37 °C). The DNA is then hybridized to the surface oligo at a low temperature (4 °C) and high salt concentration (1 M). Then the pellets are washed with cold ethanol to precipitate the DNA. Once delivered into the cytoplasm, the DNA desorbs from the pellet because the body temperature is higher than the T_m of oligo attachment site. This proposal is perhaps a subject for future research in biolistic gene delivery methods.

2.2.11 Conclusions

The objective of this study was to determine the conditions and mechanisms for nonspecific DNA adsorption onto various organic surfaces, and to control nonspecific DNA adsorption by manipulation of the surface moeities and composition. For solution concentrations <1 mg/ml at pH=7.4 DNA was observed to adsorb onto CH_3 and NH_2 surfaces. The DNA adlayer thickness increased with solution concentration and followed a Langmuir-type isotherm with K_c values of between 30 to 100 ml/mg, suggesting that CH_3 and NH_2 surfaces are not suitable for biological applications where nonspecific DNA adsorption is unfavorable. DNA adsorption kinetics was fairly rapid, with 25% of the final (monolayer) thickness adsorbed within the first 5 minutes. Thus, for DNA surface hybridization or surface attachment reactions nonspecific DNA adsorption kinetics could become a significant source of competition for surface sites, and cannot be neglected.

It was hypothesized that for CH_3 surfaces the driving force for DNA adsorption was thermodynamic. The DNA adlayer was more hydrophilic and decreased the interfacial energy of the surface with water. On the other hand, DNA adsorption on NH_2 surfaces was probably due to electrostatic interactions between the protonated NH_3^+ surface groups and the negatively charged DNA backbone. In addition, experiments conducted at different pH levels indicated that DNA also adsorbs conditionally on CO_2H surfaces. For CO_2H surfaces DNA adsorption is prevented at pH=9.0 due to repulsion of DNA by the negatively charged CO_2^- anions. The experiments conducted on NH_2 and CO_2H surfaces at different pH values suggested that DNA adsorption is also dependent on electrostatic interactions. Therefore DNA adsorption can be facilitated or inhibited by providing the surface with the appropriate electric charge. In addition, the results indicated that the mechanics of DNA adsorption are complex.

OH surfaces inhibited DNA adsorption at low salt concentrations, perhaps due to its hydrophilic nature. EG4 surfaces readily prevented nonspecific DNA adsorption at salt concentrations lower than 1.37 M, probably due to an "entropy spring" type repulsion mechanism, and are another potential option for surface modification to prevent DNA adsorption. By studying which surfaces prevent or facilitate DNA adsorption, it may be possible to modify surfaces to control it.

I immersed Au substrates in mixed monolayers of CH_3 and OH SAMs, to create surfaces that simulated a range of hydrophilicity and interfacial energies. These surfaces were used to study the effect of interfacial energy on DNA adsorption. It was observed that in general the amount of adsorbed DNA decreased with increased hydrophilicity, supporting the hypothesis that DNA adsorption is thermodynamically driven and reduces the surface's interfacial energy with water. The mixed monolayer studies also demonstrated that I could control DNA adsorption by manipulating the surface species and composition. The studies also supported the hypothesis that hydrophilic surfaces can prevent nonspecific DNA adsorption.

DNA adsorption did not depend on temperature or buffer species, but was affected profoundly by increased salt concentrations and surfactants. Salt concentrations above 1.37 M facilitated DNA adsorption onto originally resistant surfaces such as OH and EG4. On the other hand 0.1wt% SDS surfactant in solution prevented DNA adsorption on all surfaces. These two extremes of solution conditions overrode surface considerations. Thus, solution factors such as salt concentration or surfactants may be applied in situations where unconditional DNA adsorption (or its prevention) is absolutely necessary.

Once formed, DNA adlayers are generally stable, and resistant to higher temperature, changes in pH, mechanical stirring, and nonionic surfactants. Immersion in an anionic SDS surfactant solution facilitated desorption from hydrophobic CH_3 surfaces but had less impact on charged or hydrophilic surfaces. The large size of the dsDNA chain significantly affected its adsorption behavior, as opposed to the short chain oligos studied in previous literature. dsDNA adsorbed at much higher coverage onto surfaces, and the resulting adlayers were more stable. Unlike oligos, dsDNA will adsorb onto surfaces in the absence of surfactants. And once adsorbed the DNA is not removable by small molecules such as phosphates, nor does it desorb into low salt solution.

Although for my proposed application (covalent end-immobilizing of dsDNA onto surfaces) nonspecific DNA adsorption is undesirable, there are other instances where is it critical to develop surfaces that optimize DNA adsorption. One example is developing a replacement substrate for polylysine for producing cDNA microspot arrays using the *Brown* protocol. Based on the results from my studies of DNA adsorption onto NH_2 surfaces, I hypothesized that similar adsorption values could be achieved using amino-terminated alkylsilane (NH_2 silane) films formed on silica surfaces. Vikas Mehta and I conducted DNA adsorption studies with ^{32}P radiolabeled and fluorescently labeled (Cy3 or Cy5) PCR product dsDNA. I prepared NH_2 terminated silane films with various lengths (N-(2-aminoethyl)-3-aminopropyltrimethoxylsilane and N-(6-aminohexyl)aminopropyltrimethoxysilane) on silica surfaces by immersing cleaned silica in 0.1wt% silane solutions (in 95% ethanol). I confirmed with autoradiographs that the

PCR product readily adsorbed irreversibly onto amine coated glass and silicon surfaces. From confocal microscopy I obtained signal-to-noise ratios of 200 to 1000 for the fluorescently labeled dsDNA adsorbed onto NH_2 silane surfaces. The above results suggest that monolayer-thick NH_2 terminated silane films could replace polylysine as a substrate for DNA adsorption. This conclusion was further supported by the recent commercial introduction (Corning, NY) of glass slides coated with γ-amino propyl silane (GAPS) adlayers to replace polylysine coated slides as the standard support for producing cDNA microspot arrays.

In conclusion, this study has shown that nonspecific DNA adsorption occurs rapidly via a combination of intermolecular forces and mechanisms to form stable adlayers on organic surfaces. Furthermore, the research results demonstrate that the amount of DNA adsorption can be controlled by an appropriate choice of surface species and composition. From the above results I concluded that the prevention of nonspecific DNA adsorption is critical for successfully end-immobilizing long dsDNA onto a surface with a brush-like structure and high packing density ($> 10^{-13}$ moles/cm^2 for ~ 500 bp length). Therefore I had to either develop a system with surface moieties that prevents nonspecific dsDNA adsorption, or one that tolerates the introduction of surfactants such as SDS in the reaction solution without inhibiting the surface attachment chemistry, or both. Many surface attachment chemistries require hydrophobic surface groups, or NH_2 surfaces, both of which facilitate nonspecific DNA adsorption.

Therefore, I decided to add 0.1-0.2wt% of SDS to all DNA buffer solutions to prevent nonspecific adsorption. SDS is generally inert to the reaction chemistries proposed for immobilizing dsDNA onto surfaces, and it has proven to effectively prevent nonspecific dsDNA adsorption on various organic surfaces, even in high salt conditions. With the question of how to prevent nonspecific DNA adsorption solved, the next step was to choose the best immobilization strategy to producing a brush-like dsDNA surface.

2.3 Covalent attachment of dsDNA onto surfaces

2.3.1 Noncovalent dsDNA attachment protocols

The DNA adsorption experiments had shown that certain surface moities such as hydroxyl and EG effectively prevent nonspecific dsDNA adsorption. It also showed that once adsorbed dsDNA is difficult to remove, which highlighted the importance of prevention. Finally, the studies showed that the presence of SDS in the DNA solution inhibits DNA adsorption onto surfaces. In addition, SDS does not participate in any of the reactions used to covalently attach dsDNA onto surfaces. Thus, it was added at a 0.1wt% concentration in all of the aqueous buffers used in the different reactions.

After the question of preventing nonspecific DNA adsorption was resolved, attachment chemistries were evaluated and chosen. 5' oligo primers for the candidate dsDNA sequence "Hbglb" (partial sequence of gene for producing hemoglobin, 390 bp length, provided by Dr. Kathy Hogan) were ordered with the following 5' linkers: biotin, thiol and amino. The dsDNA was amplified by PCR to produce dsDNA chains with a 5' biotin, thiol or amino linker. ^{32}P-dCTP was also incorporated into the dsDNA chain during PCR to characterize the quantity of dsDNA attached to the surface. The biotin/streptavidin reaction was first chosen because of the highly specific interaction between the two molecules ($K_d = 10^{-15}$ M^{-1})[39]. A former associate in the MIT biology department, Jeremy Lambert, performed studies on immobilizing radiolabeled dsDNA onto surfaces containing streptavidin molecules. The biotin-linked dsDNA PCR product was immobilized onto the streptavidin-coated surfaces at a density of approximately 10^{-14} moles/cm^2. The density achieved was less than the desired amount of at least 10^{-13} to 10^{-12} moles/cm^2. More importantly, upon heating to 90°C the dsDNA was desorbed from the surface. Although surface immobilized dsDNA strands also have possible application, I required that the attachment chemistry be thermally stable to produce an ssDNA probe upon heating. Thus further efforts were needed to improve the stability of the biotin/streptavidin system.

Previous studies with biotin/streptavidin indicated that the interaction was thermally stable up to 120°C, so it was unlikely that this was the cause of the dsDNA desorption. Later it was surmised that instead the 4 subunits of the streptavidin tetramer separated under heating, causing the streptavidin molecule to dissociate and to release the biotin-linked dsDNA from the surface. A specially modified streptavidin molecule crosslinked with glutaraldehyde was ordered to try and retain the attached dsDNA on the surface. The glutaraldehyde was supposed to react with free amine groups in the streptavidin molecule and thus covalently bound the subunits together. However, studies conducted with this modified streptavidin molecules still did not prevent dsDNA desorption. Consequently this approach was not pursued.

Next, I tried adsorbing thiol-linked dsDNA onto gold surfaces following a protocol devised by Tarlov for immobilizing thiol-linked oligos (see Figure 2-10)[15,40]. The key aspect of Tarlov's proposal was the use of hydroxy-terminated alkanethiol groups as "backfiller" groups to displace any nonspecifically adsorbed oligos from gold surface via competitive adsorption. The backfiller alkanethiols also passivated the gold surface against future nonspecific adsorption from the oligo chains. The passivation mechanism is the formation of a hydroxy-terminated alkanethiol SAM on the gold surface. Previous research and the above-mentioned SAM studies indicated that hydroxy surfaces effectively prevent nonspecific dsDNA and oligo adsorption. This strategy was adopted and revised by first producing the thiol-linked dsDNA using PCR. An oligo primer with a 5' thiol linker was added to provide the dsDNA with a reactive group. ^{32}P-dCTP was added during PCR to produce radiolabeled dsDNA molecules. The PCR product was purified by chromatography with a (centrifugal) spin column, and the dsDNA concentration determined using UV-VIS spectroscopy at λ_{abs} = 260 nm.

The thiol linker on the dsDNA is susceptible to oxidation. The disulfide product is less reactive towards a gold surface. Thus, the thiol-linked dsDNA was reduced using 1mM dithiothreitol (DTT)[2]. The DTT was removed by extraction with an organic solvent, and the reduced dsDNA was purified by ethanol precipitation. Finally, the dsDNA was resuspended in a Tris-EDTA buffer at a concentration of 50 μg/ml. SDS (0.1wt%) was

added to prevent nonspecific adsorption of the DNA when it contacted the gold surface. The thiol-linked dsDNA solution was allowed to sit for 30 minutes on the gold surface. Then a 1 mM solution of hydroxy undecanethiol in 95% ethanol was added to passivate the gold surface.

The dsDNA on the surface was characterized by incorporating radioactive ^{32}P dCTP groups to the dsDNA chain during PCR amplification of the sample, and quantified with a liquid scintillation counter. The results indicated that dsDNA was immobilized onto the surface at a density of about 10^{-13}moles/cm^2. To test whether the immobilized DNA was attached at a single point, the dsDNA surface was immersed in a 40 wt% formamide/ 7 M urea solution. The formamide/urea mixture acts as a denaturant to facilitate DNA melting[41,42]. In this case the denaturant solution lowered the effective heated T_m of the Hbglb sequence to approximately 45°C, compared to approximately 90°C in regular TE buffer. An intercalating fluorescent dye, oxazole yellow (YOPRO™, λ_{ex} = 488 nm, λ_{em} = 510 nm) was also added to the denaturant solution at a 10^{-7} M concentration[43]. The fluorescence intensity of YOPRO™ is amplified 50 to 100 times in dsDNA versus in solution, due to the favorable orientation of the intercalated dye[41].

The dsDNA sample was heated from 40°C to 70°C at a constant rate over 30 minutes. An Argon laser was used to excite the YOPRO™ dye and a photomultiplier tube (PMT) was used to measure the fluorescence signal during the temperature ramp. A melting curve was constructed with the PMT data. A typical melting curve for a particular dsDNA sequence in solution should have a sharp transition with a small temperature difference (ΔT <1° C)[41]. If the dsDNA is end-immobilized and not attached to a surface at multiple sites, it should behave similar to a solution phase dsDNA chain and also have a sharp transition. The melting curve obtained from the PMT data is represented in Figure 2-9. There is a fairly sharp transition with a ΔT of about 2° C, indicating that a significant proportion of the dsDNA is actually end-immobilized.

However, since the ΔT was greater than 1°C, some of the immobilized dsDNA is not behaving like end-immobilized product. The question was whether this remainder

was dsDNA adsorbed on the surface at multiple points, or dsDNA desorbed from the surface due to the elevated temperature. Follow-up thermal stability studies of thiol-linked dsDNA attached to gold surfaces showed over 50% of the immobilized dsDNA was lost after heating the sample in a TE buffer solution at 70° C for 15 minutes. Since this temperature was lower than the dsDNA T_m, the dsDNA was clearly desorbing from the surface instead of melting. Clearly the thermal stability of the thiol-linked dsDNA/gold system was unacceptable for heating the immobilized dsDNA above its T_m to generate an ssDNA probe.

I tried to improve the thermal stability of the thiol-linked dsDNA by modifying the gold surface with a thin layer of vapor-deposited elemental mercury, since research literature suggested a strong affinity for mercury to gold and sulfur[44]. The details of this study are presented in Appendix I, but the overall result was negative. There was no increase in the thermal stability of alkanethiols adsorbed onto mercury-coated gold surfaces. Consequently this particular approach was reserved for generating immobilized dsDNA strands only.

2.3.2 Covalent dsDNA attachment protocols

Next, the covalent attachment methodologies (for oligos) were carefully considered. As mentioned above, dsDNA is only soluble in significant amounts in water[45], so any chemical reactions should be feasible in aqueous solvent, and preferably specific towards the DNA linker rather than water. The following systems were chosen: the attachment of amino-linked dsDNA onto glutaraldehyde derivatized surfaces via the formation of a Schiff base (imine group); reaction of an amino-linked dsDNA with surface epoxy groups via a ring opening reaction; and peptide coupling chemistry of amino-linked dsDNA to carboxy groups on a surface using the water-soluble EDC coupling agent (see Figure 2-10).

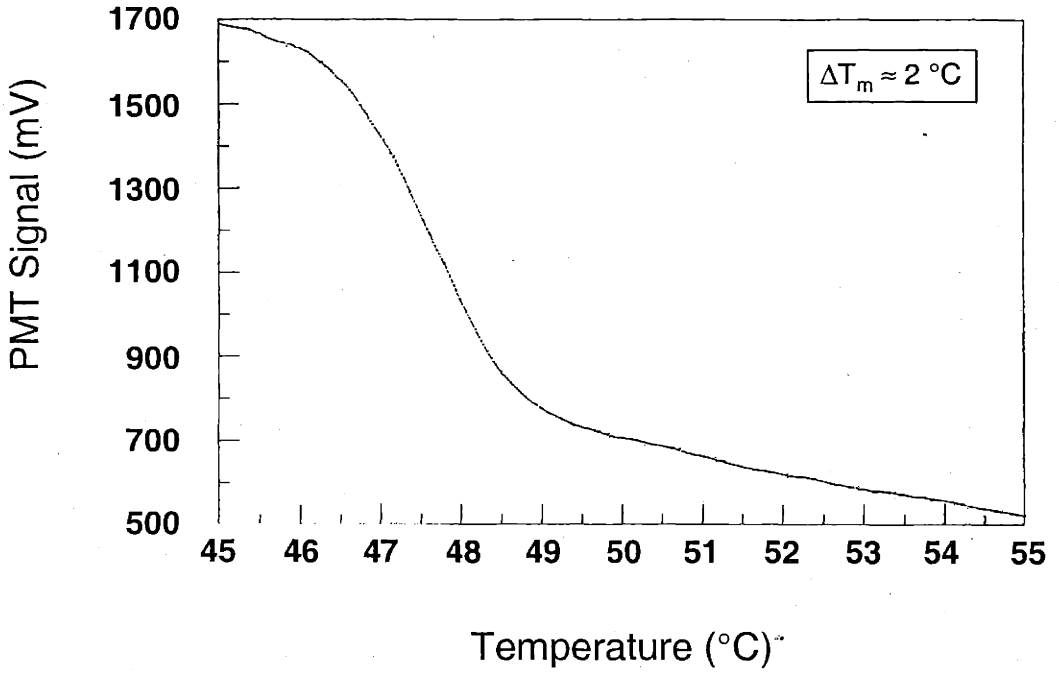

Figure 2-9. Melting curve of surface-immobilized dsD (5' thiol-linked Hbglb sequence, 390 bp) on Au in a 40% formamide/7 M urea denaturant solution with 0.1 μM YOPRO™ dye. The sample was heated from 40 to 70 °C at 1.3 °C/min, excited with an Argon laser (488 nm). The fluorescence was measured with a PMT. The curve has a rather sharp transition at 45 °C, with a ΔT of about 2 °C, indicating that significant dsDNA is end-immobilized to the surface.

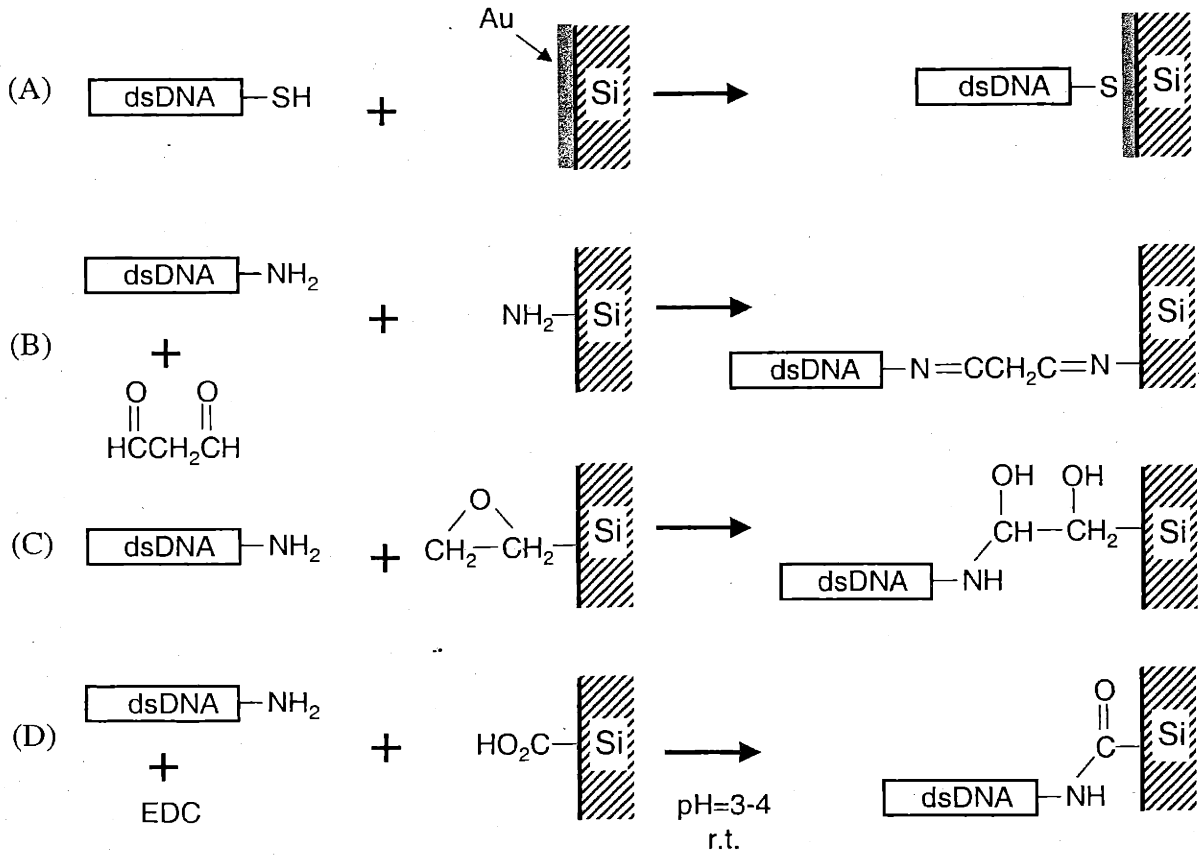

Figure 2-10. Various strategies for immobilizing dsDNA onto solid surfaces. (A) adsorption of thiol-terminated dsDNA onto a gold coated silicon surface; (B) attachment of amino-terminated dsDNA to an amino surface with glutaraldehyde; (C) attachment of amino-terminated dsDNA to an epoxy surface via ring opening nucleophilic addition; (D) attachment of amino-terminated dsDNA attached to a carboxyl surface using the coupling agent EDC.

The glutaraldehyde linkers are commonly used for conjugation of proteins and antibodies in an aqueous buffer[46]. The aldehyde groups are more specific towards amino groups than to water, so there is less likelihood of side reactions occurring with the aqueous solvent. The epoxy ring opening reaction was used by *Southern* to attach amino-linked oligos onto a silicon surface[47,48]. It is also specific for the nucleophilic amine group and has low reactivity towards water. EDC is similar to DCC, another coupling reagent used for Merrifield stepwise peptide synthesis on polymer supports. Unlike DCC, EDC is soluble and active in aqueous solvents, and has been used to conjugate proteins dissolved in buffer solutions[46]. However, EDC may also react with water and carboxy groups, producing another carboxy group and exhausting itself in the process. Thus water competes with amines for coupling with the carboxy groups, but the reaction kinetics for water is slower than for amines.

For this set of reactions amino-linked oligo primers were purchased, and to produce amino-linked dsDNA via PCR. Again, ^{32}P-dCTP was incorporated in the reaction to provide a radiolabel. The PCR product was purified with a spin column and suspended in a Tris buffer (pH=8.5). Next, gold surfaces were immersed in 1 mM amino or carboxyl terminated alkanethiol solutions overnight to produce SAMs with amine and carboxyl groups exposed on the surface. The epoxy surfaces were generated by reacting an epoxy terminated alkylsilane to a silicon surface following a protocol published by *Southern*[48].

For the glutaraldehyde reaction an aqueous 10wt% glutaraldehyde solution was mixed[46]. The amine surfaces were immersed in the glutaraldehyde solution at room temperature for one hour to produce aldehyde-covered surfaces, then rinsed with water and ethanol and dried with N_2. The amino-linked dsDNA was suspended in TE buffer at 0.5 μM concentration, and 0.1wt% SDS was added to prevent nonspecific DNA adsorption. The aldehyde surfaces were immersed in the dsDNA solution at room temperature for 6 hours before washing 2 times with water and dried with N2. For the epoxy ring opening reaction amino-linked dsDNA was suspended in TE buffer at 0.5 μM

concentration with 0.1wt% SDS to prevent nonspecific DNA adsorption. The epoxy surfaces were immersed in the dsDNA solution for 6 hours at room temperature, then rinsed twice with water and dried with N_2. For the EDC coupling reaction an aqueous 0.5wt% EDC solution was prepared with pH=4.0 and with 0.1wt% SDS. The amino-linked dsDNA was suspended in this solution at a concentration of 0.1 μM. Carboxy surfaces were immersed in the EDC-dsDNA solution at room temperature for 6 hours before being washed and dried.

In all the above cases liquid scintillation counting was used to characterize the samples and determine the amount of radiolabeled dsDNA immobilized onto the surfaces. Measurement of a diluted aliquot of amino-linked dsDNA solution indicated an activity of 6,000cpm/μg dsDNA. However, all the samples showed only a background radioactivity of approximately 50-70 cpm regardless of the attachment chemistry. In addition, the radioactive signal of the control sample was also approximately 50 cpm, suggesting that the immobilization reactions were all unsuccessful. Even if immobilized dsDNA was considered the source of all the radioactive signal intensity from the samples, the maximum amount of dsDNA on the surface is about 10^{-14} moles/cm^2. This is one order of magnitude lower than a monolayer surface coverage of 390 bp length dsDNA ($2x10^{-13}$ moles/cm^2), and two orders of magnitude lower than my goal of 10^{-12} moles/cm^2. Since the dsDNA surface coverage must be higher than one monolayer to achieve the desired brush-like orientation, it is obvious that all the above attachment methods fall short. The main reason for the lack of reactivity may be due to the length of the dsDNA molecule. The long chain length not only results in slower diffusion rates, but also drastically decreased the number of effective collisions with the surface, since only one out of 780 nucleotides on the surface is reactive (the amino linker group), compared to a 1 in 1o to 25 ratio for oligos with amino linkers. Therefore the covalent reactions are kinetically unfavorable. The long reaction times required for significant dsDNA immobilization are not only impractical, but also increase the possibility of side reactions between the surface entities with water. Such untoward reactions could reduce the number of active surface sites available for immobilizing amino-linked dsDNA, further reducing the reaction efficiency.

A final area of consideration is bifunctional crosslinkers. A large variety of bifunctional crosslinkers have been developed for conjugating proteins and antibodies[46]. As mentioned in Chapter 1, research groups have reported high densities of immobilized oligos ($2x10^{-12}$ to $5x10^{-11}$ moles/cm^2)[1,49-53] using crosslinkers such as ethylene glycol *bis*(succinimidylsuccinate) (EGS), N-succinimidyl(4-iodoacetyl)aminobenzoate (SIAB), N-(γ-Maleimidobutyryloxy) succinimide ester (GMBS), and 1,4-phenylene diisocyanate (PDC). The basic strategy is to first produce an amine surface by derivatizing glass or silicon surfaces with amino-terminated alkylsilanes. Then the amine surface is further modified by introduction of the crosslinker. Finally, the surface is immersed in a solution of amino or thiol linked oligo chains to complete the immobilization. The crucial factor for successful immobilization should be the choice of the functional group that reacts with the oligo chain. Preferably the chosen reactive is specific to an amine group (succinate, isocyanate) or thiol group (iodo, maleimido) but is slightly reactive or unreactive towards water.

Jeremy Lambert (MIT biology) tried using GMBS to immobilize thiol-linked dsDNA PCR product to a silicon surface. He derivatized a silicon surface with an amino-terminated alkylsilane, and added GMBS in an organic solvent. The succinate group reacted with the amine surface to immobilize the GMBS. Next, he immersed the surfaces in an aqueous solution of thiol-linked, radiolabeled dsDNA. The scintillation counting results were at background level, suggesting that the dsDNA immobilization strategy was unsuccessful. Another colleague, Vikas Mehta from the Laibinis lab tried immobilizing oligos onto a silicon surface using bifunctional crosslinkers similar to GMBS and SIAB. He also prepared silicon surfaces derivatized with an amino-terminated alkylsilane, to which he immobilized the crosslinkers. Then he immersed the samples in a thiol or amino linked oligo solution (TE buffer, pH=7.4) with 0.1% SDS to prevent nonspecific adsorption. The oligos were labeled with a radioactive ^{32}P tag and characterized by liquid scintillation counting. The radiation was at background level, suggesting that little immobilization occurred. The maximum density of dsDNA on the surface would be about 10^{-14}-10^{-15} moles/cm^2. The low surface density was possibly due to side reactions

with water, so the experiments were repeated with the oligos dissolved in an organic solvent, formamide. In this case, the radioactive signal was initially very high, but after repeated rinsing with SDS it fell back to near background level. The decrease in radiation signal after rinsing indicated that the oligos were immobilized to the surface by nonspecific adsorption rather than by covalent attachment. A crosslinker with a photoactivated (265-275 nm) azide group, N-5-Azido-2-nitrobenzoyloxysuccinimide (ANB-NOS), was also tried without success. The conclusion was that if the experiments using bifunctional crosslinkers could not be recreated with amino or thiol linked oligos, then it was very unlikely that it would succeed with a much longer and massive dsDNA chain.

2.3.3 Conclusion

By now it was evident that it is very difficult to covalently attach a long dsDNA chain to a surface due to possible side reactions with the solvent water Also, the lower diffusion rates (in solution) and collision efficiencies of polymeric dsDNA chains may reduce the immobilization reaction efficiency. Any proposed immobilization strategy must involve a highly specific attachment chemistry that is not affected by water or SDS. Oligos immobilized onto a surface can act as a highly discriminating "sticky glue" to immobilize dsDNA (with a complementary oligo overhang) onto a surface. Also, immobilized oligos can help prevent nonspecific DNA adsorption. Finally, a collection of different dsDNA sequences may be localized onto desired locations on a surface by applying the exquisitely specific DNA hybridization rules. DNA with oligo overhangs will be immobilized (by hybridization) to complementary oligo sequences located at discrete surface sites, creating an array via a self-assembly mechanism.

An important aspect of my research is to study how oligo surface density affects the efficiency and kinetics of DNA surface hybridization. The final goal of such studies is not only to gain insight on how to produce oligo surfaces with better hybridization qualities, but also to optimize the quantity of dsDNA end-immobilized to the surface. The

methods developed for immobilizing oligos using bifunctional crosslinkers are unable to control the surface density of the oligo chains. However, it is possible to adjust the oligo surface density by synthesizing oligos stepwise onto surfaces with controlled reactive site densities. In turn, the density of reactive surface sites could be modified by the formation of organic thin films with particular functional groups and solution compositions. The development and application of synthesized oligo surfaces with controlled density is the main topic for the following chapter.

2.4 Experimental Section

Materials: Gold shot (99.99%) and chromium-coated tungsten filaments were obtained from American Precious Metals Co. (East Rutherford, NJ) and R.D. Mathis (Long Beach, CA), respectively. Salmon sperm DNA (MW =10-15 million Daltons, 15% Na cations, 10% water and <3% residual amino acids) and phosphate buffer saline (PBS) tablets were obtained from Sigma. Tris (hydroxymethyl)aminomethane (Tris), ethylenediaminetetraacetic acid (EDTA), 0.495 N hydrochloric acid (HCl), glutaraldehyde, and octadecanethiol were obtained from Aldrich. Sodium dodecyl sulfate (SDS) and Triton X-100 were obtained from Sigma. Sodium citrate, and sodium chloride (NaCl) were obtained from Mallinkroft. (3-Glycidoxypropyl) triethoxysilane was purchased from Gelest. Sodium perchlorate was obtained from Fisher Scientific Co. Ethyl alcohol (95%, Pharmco) was reagent grade. MilliQ (MQ) water at 18.2 MΩ resistance was supplied on-site from a Millipore filtration apparatus.

Dodecanethiol, 1-hydroxyundecanethiol, 1-carboxypentadecanethiol, 1-aminoundecanethiol, 1-amido undecanethiol, and methyl [1-mercapto,undec-11-yl] tetra ethylene glycol (EG4) were prepared from previous studies. 1-N,N dimethylamido undecanethiol and 1-N,N dimethylamino undecanethiol were prepared in the lab by organic synthesis. N-(2-aminoethyl)-3-aminopropyltrimethoxylsilane, and N-(6-aminohexyl) aminopropyltrimethoxysilane were purchased from Gelest Inc. (Tullytown, PA).

Template dsDNA sequences were cloned and purified by Dr. Katherine Hogan from the Lerman Lab at the MIT Biology department. α^{32}P dCTP was purchased from New England Nuclear Biosciences (Boston, MA). Taq polymerase (activity = ?????) and dNTPs were purchased from GIBCO BRL/Life Technologies, or Roche Molecular Biochemicals (Indianapolis, IN). YOPRO dye was purchased from Molecular Probes (Eugene, OR). Custom synthesized oligos with linkers were purchased from The Great American Gene Company (Ramona, CA).

Solution preparation: For surface modification, solutions of approximately 10 mM end-functionalized alkanethiols ($X\text{-}(CH_2)_nSH$, $X=CH_3$,, NH_2, $C=ONH_2$, $C=ON(CH_3)_2$, CO_2H, OH, *and* $(OCH_2CH_2)_4OCH_3$) in ethyl alcohol were prepared.

For DNA adsorption studies, solutions of 0.1 μg/ml to 1 mg/ml DNA were prepared in the following aqueous buffers: Tris-EDTA (TE) buffer with 10 mM Tris and 1 mM EDTA, titrated to pH=7.4 with HCl; phosphate buffer saline (PBS) buffer, with 10 mM sodium phosphate, 0.137 M NaCl and pH=7.4; 5X sodium saline citrate (SSC) buffer with 0.08 M sodium citrate and 0.8 M NaCl. Surfactants (0.1 wt% SDS or Triton X-100) or NaCl salt were added as needed.

Sample preparation: Chromium (100 Å) and gold (1000 Å) were sequentially evaporated at 1.5 Å/s and 4 Å/s, respectively, onto 100 mm silicon <100> wafers (Silicon Sense) in a diffusion-pumped vacuum chamber at an operating pressure of 2×10^{-6} torr. The wafers were cut into 1 cm x 3 cm slides, washed with ethyl alcohol, and dried with N_2.

The gold surfaces were modified by immersion in the end-functionalized alkanethiol solutions for 24 hours. The SAM-covered slides were removed from solution, washed with ethyl alcohol and dried with N_2. The SAM-covered slides were then immersed in DNA solution for 24 hours, washed with MQ water, and dried with N_2.

PCR reaction: The reaction was carried out in an Ericomp (San Diego, CA) DeltaCyclerI™, or an Applied Biosystems (Foster City, CA) GeneAmp® PCR system

9700 thermocycler, with the following temperature profile: initial heating to 94° C for 3 minutes; followed by 28 thermal cycles, each cycle consisting of 3 steps: a melting step at 94° C for 30 seconds, then an annealing step at 55° C for 30 seconds, then an enzymatic reaction step at 72° C for 30 seconds; next, the solution is held at 72° C for 7 minutes to complete the reaction, then cooled and held at 4° C indefinitely.

Recipe

2.5µl 10 x PCR buffer (with 2mM $MgCl_2$)
2.5µl 10x $dNTP_{(aq)}$ solution for labeling reaction
(2.5mM each of dATP, dGTP, and dTTP with 2mM dCTP)
1µl plasmid prep template DNA (Hbglb or SRY sequence)
1µl 5' PCR primer oligo
1µl 3' PCR primer oligo
1µl α^{32}P labeled dCTP
0.5µl Taq polymerase (in ethylene glycol)
15.5µl ddH_2O

DTT reduction

An aliquot of thiol-linked dsDNA in Tris buffer (pH=8.0) was mixed with DTT using the following recipe:

50 µl dsDNA solution
7.5 µl 10 x DDT solution
7.5 µl 10 x PBS buffer
10 µl ddH_2O

The mixture was left at room temperature overnight. The DTT was removed by extraction with 3 x 100 µl aliquots of ethyl acetate.

Ethanol precipitation

For every volume of sample add 0.1 volume of 3M aqueous sodium acetate, and 2 volumes of 100% neat ethanol in a 1.5 ml microfuge tube. Leave the ethanol mixture at –20°C for 24 hours, then spin it in a microfuge at 10,000 g for 15 minutes. Remove the supernatant liquid phase by micropipette, taking care not to remove the precipitated DNA at the bottom of the microfuge tube. Next, add 500 µl of 70% ethanol solution to wash the DNA sample. Leave the sample on ice for 5 minutes, then spin in microfuge at 10,000 g for 7 minutes. Remove the supernatant solution phase, then air dry sample in the tube and resuspend with the appropriate buffer.

Spin column purification

The crude PCR product was purified using a Qiagen (Valencia, CA) PCR purification kit, according to the protocols provided. A or Eppendorf microfuge was used at 10,000 g, and the purified DNA product was eluted in Tris buffer (pH=8.5). The purified samples were stored at 4° C.

UV-VIS Absorbance Spectroscopy

Measurements were conducted using a Varian (Mulgrave, Australia) Cary 1E UV-Visible Spectrophotometer. The blank sample was 1 ml of ddH_2O in a quartz cuvette. All DNA samples were diluted in ddH_2O to a volume of 1ml. The sample absorbance spectra was measured from wavelengths of 240 to 300 nm. The conversion factor was 50 µg/O.D.

Methods of characterization: General instrumental parameters and methods for characterization of SAMs by ellipsometry, wetting measurements, FTIR and XPS are as follows:

Ellipsometry

The alkanethiol SAM film thickness was determined using a Gaertner L116A automatic ellipsometer equipped with a He-Ne laser (λ = 632.8 nm) at an incident angle of 70° and refractive index of 1.45 for the organic film. Baseline index of refraction measurements for the bare gold substrates were taken immediately after washing the gold surfaces with ethanol and drying with N_2. After immersion in the alkanethiol solutions, SAM thickness was determined using "Delta" calculation mode. Three measurements were taken at three different locations on the sample, and the results were averaged to obtain the final value. Reproducibility across a sample was ±2 Å.

Wetting Measurements

Advancing contact angles were measured on static drops of water or hexadecane with a Ramé-Hart manual goniometer equipped with a video camera and computer monitor for viewing the drops. Contact angles were advanced of retreated at a rate of 1 μL/s prior to measurement with a MicroElectapipette syringe (Matrix Technologies, Lowell, MA). The pipette tip remained in the drop during measurement. Both sides of the liquid drops were measured across three different locations on the sample, and the results averaged. Reproducibility across a sample was ±3°.

Fourier Transform Infrared Spectroscopy

IR spectra were obtained in a single reflection mode with a Bio-Rad FTS 175 infrared spectrometer and Universal Reflectance Attachment. The p-polarized light was incident at 80° from the surface normal, and the reflected light was detected with a liquid nitrogen-cooled narrow-band MCT detector. Spectral resolution was $2cm^{-1}$ after triangular apodization. Spectra were referenced to those of SAMs prepared from octadecanethiol-$_{d37}$ on gold with 1024 scans were performed on both sample and

reference. Peak heights were determined by smoothing the spectra baselines, then offsetting the baseline values to zero for comparison.

X-ray photoelectron spectroscopy

XPS spectra were obtained with a Surface Science Instruments Model X-100 spectrometer using a monochromatized Al Kα x-ray source (elliptical spot of 1.0 mm x 1.7 mm) and a concentric hemispherical analyzer (pass energy = 50 eV). The detector angle with respect to the surface parallel was 35°. Peak positions were referenced to $Au(4f_{7/2})$ = 84.00 eV and were fit with 80% Gaussian/20% Lorentzian profiles and a Shirley background to obtain integrated peak intensities.

Liquid Scintillation Counting

^{32}P radioactivity was measured using an LKB 1217 Rackbeta liquid scintillation counter (Wallac, Gaithersburg, MD). Samples were immersed in 10 ml of LiquiScint radiofluorescent solution (National Diagnostics, Atlanta, GA), and measured for 30 seconds.

Epifluorescence detection

A 2 mW (class 2) Uniphase (San Jose, CA) model 2212-4SL Argon laser (λem = 488 nm) was used to excite DNA chains labeled with either fluorescein or YOPRO™ (oxazole yellow) dyes. The incident beam angle was approximately 70 degrees to the surface normal. A PMT was used to characterize the sample fluorescence. The PMT was a Model #RF1/S MKII from Thorn EMI (CA), run using software developed by Lawson Ltd. (??). A custom-made light isolation box for the PMT apparatus was designed by an associate in biology, Greg, and the complete laser-CCD-PMT imaging setup was custom-built on an optical bench and enclosed in a dark room.

Confocal microscopy

For imaging dsDNA labeled with cyanine dyes such as Cy3 (λ_{ex} = 552 nm, λ_{em} = 570 nm) and Cy5 (λ_{ex} = 643 nm, λ_{em} = 667 nm), a ScanArray 3000 (GSI Lumonics, Billerica, MA) or ScanArray 5000 (GSI Lumonics) confocal microscope was used. The ScanArray 2000 was used for imaging glass samples since the objective lens could only be manually adjusted. The objective lens for the ScanArray 5000 was computer-controlled and thus it was used to scan samples on silicon chips, as long as the thickness was less than 2 mm, the tolerance of the sample holder. The laser intensity was set at 60%, and the PMT efficiency at 70% for the imaging runs.

Organic Synthesis

1 N, N dimethyl amido undecene: 1 equivalent (eq) of undecenoyl chloride was added dropwise, over 30 minutes, to dimethyl amine (4 eq) in anhydrous tetrahydrofuran (THF) in an ice bath under inert nitrogen, with the excess dimethyl amine used as a proton scavenger. After stirring overnight, the reaction was quenched with water. After addition of $NaHCO_{3(aq)}$ and ether to form a two-phase mixture, the layers were separated, and the aqueous phase extracted thrice with ether. The organic phase was washed with saturated $NaCl_{(aq)}$ with 0.25 M NaOH. The organic phases were combined and concentrated under reduced pressure. Column chromatography (10% ethyl acetate/hexanes) yielded the title compound (95% yield). ^{1}H NMR, δ 6.0 (t 1 H), δ 5.2 (d 2 H) δ 3.2 (m, 6 H), δ 2.2 (t, 2 H), δ 1.9 (t, 4 H), δ 1.4-1.6 (m, 10 H).

1 N, N dimethyl amido undecane thioacetate: A mixture of 1 N, N dimethyl amido undecene (1 eq), thioacetic acid (4 eq), and 10 mg of 2,2'-Azobisisobutyronitrile (AIBN) in THF were photolyzed for 4 hours with a medium-pressure Hg lamp. After stirring overnight, the reaction was quenched with water. After addition of saturated $NaHCO_{3(aq)}$ and chloroform to form a two-phase mixture, the layers were separated, and the aqueous phase extracted thrice with chloroform. The organic phase was washed with saturated

$NaCl_{(aq)}$ with 0.25 M NaOH. The organic phases were combined and concentrated under reduced pressure. Column chromatography (30% ethyl acetate/hexanes) yielded the title compound 1 N, N dimethyl amido undecane thioacetate (65% yield). ^{1}H NMR, δ 2.85 (m, 6 H), δ 2.3 (m, 3 H), δ 2.2 (t, 2 H), δ 1.6 (t, 4 H), δ 1.3-1.6 (m, 12 H).

1 N, N dimethyl amido undecane thiol. 1 N, N dimethyl amido undecane thioacetate. was refluxed in 0.02 M potassium carbonate in methanol overnight, and quenched with glacial acetic $acid_{(aq)}$. After addition of saturated $NaHCO_{3(aq)}$ and chloroform to form a two-phase mixture, the layers were separated, and the aqueous phase extracted thrice with chloroform. The organic phase was washed with saturated $NaCl_{(aq)}$ with 0.25 M NaOH. The organic phases were combined and concentrated under reduced pressure. Column chromatography (40% ethyl acetate/hexanes) yielded the title compound (90 % yield). ^{1}H NMR, δ 2.9 (m, 6 H), δ 2.5 (t, 2 H), δ 2.3 (t, 2 H), δ 1.6 (t, 6 H), δ 1.2-1.4 (m, 10 H).

1 N, N dimethyl amido undecane thiol: Lithium aluminum hydride (LAH, 2 eq) was added dropwise to 1 N, N dimethyl amido undecane thioacetate (1 eq) of dry THF in an ice bath under nitrogen gas, After stirring for 3 hours the reaction was quenched with 5 eq of water then suction filtered. The LAH served to reduce the amide to an amine, and to deprotect the thiol. Column chromatography (100% methanol) yielded the title compound (35 % yield). ^{1}H NMR, δ 2.5 (t, 1 H), δ 2.4 (t, 2 H), δ 2.2 (m, 6 H), δ 1.6 (t, 2 H), δ 1.45 (t, 2 H), δ 1.4-1.6 (m, 14 H).

2.5 References

(1) Z. Guo; R. A. Guilfoyle; A. J. Thiel; R. Wang; L. M. Smith, L. M. *Nuc. Acids Res.* **1994**, *22*, 5456-5465.

(2) L. A. Chrisey; G. U. Lee; E. O'Ferrall, *Nuc. Acids Res.* **1996**, *24*, 3031-3039.

(3) C. Bamdad *Biophys. J.* **1998**, *75*, 1997-2003.

(4) T. T. Nikforov; Y. -H Rogers *Anal. Biochem.* **1995**, *227*, 201-209.

(5) S. A. Johnston; P. Q. Anziano; K. Shark; J. C. Sanford; R. A. Butow *Science* **1988**, *240*, 1538-1541.

(6) J. B. Miller; F. M. Boyce *Trends in Genetics* **1995**, *11*, 163-165.

(7) F. D. Smith; P. R. Harpending; J. C. Sanford *J. Gen. Microbiol.* **1992**, *138*, 239-248.

(8) R. S. Williams; S. A. Johnston; M. Riedy; M. DeVit; S. G. McElligot; J. C. Sanford *Proc. Natl. Acad. Sci. USA* **1991**, *88*, 2726-2730.

(9) Y. M. Lvov; Z. Lu; J. B. Schenkman; X. Zu; J. F. Rusling *J. Am. Chem. Soc.* **1998**, *120*, 4073-4080.

(10) J. Wang; X. Cai; G. Rivas; H. Shiraishi; N. Dontha *Biosen. and Bioelec.* **1997**, *12*, 587-599.

(11) J. Wang; M. Jiang; T. W. Nilsen; R. C. Getts *J. Am. Chem. Soc.* **1998**, *120*, 8281-8282.

(12) S. Schouten; P. Stroeve; L. M. Longo *Langmuir* **1999**, *15*, 8133-8139.

(13) H. Su; P. Williams; M. Thompson *Anal. Chem.* **1995**, *67*, 1010-1013.

(14) M. Ueda; H. Iwasaki; O. Kurosawa; M. Washizu *J. of Appl. Phys.* **1999**, *38*, 2118-2119.

(15) R. Levicky; T. M. Herne; M. J. Tarlov; S. K. Satija *J. Amer. Chem. Soc.* **1998**, *120*, 9787-9792.

(16) A. W. Adamson *Physical Chemistry of Surfaces*; John Wiley and Sons: New York, 1990.

(17) A. Pease; D. Solas; E. J. Sullivan; M. T. Cornin; C. P. Holmes; S. P. A. Fodor *Proc. Natl. Acad. Sci. USA* **1994**, *91*, 5022-5026.

(18) M. Eggers; M. Hogan; R. K. Reich; J. Latmure; D. Ehrlich; M. Hollis; B. Kosicki; T. Powdrill; K. Beattie; S. Smith; R. Varman; R. Gangadharan; A. Mallik; B. Burke; D. Wallace *Biotechniques* **1994**, *17*, 516-525.

(19) J. B. Latmure; K. L. Beattie; B. E. Burke; M. D. Eggers; D. J. Ehrlich; R. Fowler; M. A. Hollis; B. B. Kosicki; R. K. Reich; S. R. Smith; R. S. Varma; M. E. Hogan *Nuc. Acids Res.* **1994**, *22*, 2121-2125.

(20) M. Yang; H. C. M. Yau; H. L. Chan *Langmuir* **1998**, *14*, 6121-6129.

(21) Y. Lvov; G. Decher; G. Sikhorukov *Macromolecules* **1993**, *26*, 5396-5399.

(22) F. Caruso; H. Lichtenfeld; M. Giersig; H. Mohwald, H. *J. Amer. Chem. Soc.* **1998**, *120*, 8523-8524.

(23) P. T. Hammond; G. M. Whitesides *Macromolecules* **1995**, *28*, 7569-7571.

(24) S. L. R. Barker; M. J. Tarlov; H. Canavan; J. Hickman; L. E. Locascio *Anal. Chem.* **2000**, *72*, 4899-4903.

(25) H. G. M. van de Steeg; M. A. Cohen Stuart; A. de Keizer; B. H. Bijsterbosch *Langmuir* **1992**, *8*, 2538-2546.

(26) R. Bijlsma; A. A. van Well; M. A. Stuart *Physica B* **1997**, *234-236*, 254-255.

(27) N. G. Hoogeveen; M. A. Cohen Stuart; G. J. Fleer; M. R. Bohmer *Langmuir* **1996**, *12*, 3675-3681.

(28) I. G. Pashev; S. I. Dimitrov; D. Angelov *Trends in Biol. Sci.* **1991**, *16*, 323-326.

(29) K. L. Prime; G. M. Whitesides *J. Amer. Chem. Soc.* **1993**, *115*, 10714-10721.

(30) R. M. Nyquist; A. S. Eberhart; L.A. Silks III; Z. Li, X. Y.; B. I. Swanson *Langmuir* **1999**, A-H.

(31) S. W. Lee; P. E. Laibinis *Biomaterials* **1998**, *19*, 1669-1675.

(32) B. Vogelstein; D. Gillespie *Proc. Natl. Acad. Sci. USA* **1979**, *76*, 615-619.

(33) M. J. Carter; I. D. Milton *Nuc. Acids Res.* **1993**, *21*, 1044.

(34) V. G. Cheung; M. Morley; F. Aguilar; A. Massimi; R. Kucherlapati; G. Childs *Nat. Genet. Suppl.* **1999**, *21*, 15-19.

(35) P. B. Gaspers; C. R. Robertson; A. P. Gast *Langmuir* **1994**, *10*, 2699-2704.

(36) R. D. Tilton; A. P. Gast; C. R. Robertson *Biophys. J.* **1990**, *22*, 1321-1326.

(37) S. R. Rasmussen; M. R. Larsen; S. E. Rasmussen *Anal. Biochem.* **1991**, *198*, 138-142.

(38) H. Bunemann; P. Weshoff; R. G. Hermann *Nuc. Acids Res.* **1982**, *10*, 7163-7180.

(39) L. Chalet; E. J. Wolf *Arch. Biochem. Biophys.* **1964**, *108*, 1-5.

(40) T. M. Herne; M. J. Tarlov *J. Amer. Chem. Soc.* **1997**, *119*, 8916-8920.

(41) N. Katherine Hogan; L. S. Lerman, personal communication, 1999-2000

(42) J. Sambrook; E. F. Fritsch; T. Maniatis *Molecular Cloning: A Laboratory Manual*; 2 ed.; Cold Spring Harbor Laboratory Press: Cold Spring Harbor NY, 1989.

(43) M. A. Marino; J. M. Devaney; P. A. Davis; J. E. Girard *J. Chromatogr. B. Biomed. Sci. Appl.* **1999**, *732*, 365-374.

(44) A. K. Rappe; C. J. Casewit; K. S. Colwell; W. A. Goddard III; W. M. Skiff *J. Am. Chem. Soc.* **1992**, *114*.

(45) R. R. Sinden *DNA Structure and Function*; 1 ed.; Academic Press: New York, 1994.

(46) G. T. Hermanson *Bioconjugate Techniques*; Academic Press: New York, 1996.

(47) E. M. Southern; U. Maskos; J. K. Elder *Genomics* **1992**, *13*, 1008-1017.

(48) U. Maskos; E. M. Southern, E. M. *Nuc. Acids Res.* **1992**, *20*, 1679-1684.

(49) V. A. Efimov; A. A. Buryakova; O. G. Chakhmakhcheva *Nuc. Acids Res.* **1999**, *27*.

(50) M. J. Kozal; N. Shah; N. Shen; R. Yang; R. Fucini; T. C. Merigan; D. D. Richman; D. Morris; E. Hubbell; M. Chee; T. Gingeras *Nat. Med.* **1996**, *2*, 753-759.

(51) M. J. O'Donnell; K. Tang; H. Koster; C. L. Smith; C. R. Cantor *Anal. Chem.* **1997**, *69*, 2438-2443.

(52) F. N. Rehman; M. Audeh; E. S. Abrams; W. H. Philip; M. Kenney; T. C. Boles *Nuc. Acids Res.* **1999**, *27*, 649-655.

(53) L. A. Chrisey; C. E. O'Farrell; B. J. Spargo; C. S. Dulcey; J. M. Calvert *Nuc. Acids Res.* **1996**, *24*, 3040-3047.

(54) P. E. Laibinis; G. M. Whitesides *J. Am. Chem. Soc.* **1992**, 114, 1990-1995

Chapter 3: Surface Oligo Synthesis

3.1 Introduction

3.1.1 Considerations for generating oligo surfaces

As mentioned in Chapter 1, there are two major approaches for immobilizing oligos onto a surface. The first requires attachment of an end-functionalized oligo chain onto a reactive surface. Examples include the use of amino, mercapto, and biotin-terminated oligo groups. Though successful oligo attachment and hybridization have been reported, there are issues regarding consistency, nonspecific adsorption and side reactions that still need to be addressed. The other technique is simply the direct stepwise synthesis of the oligos onto a flat surface. Research has been conducted by *Southern* and *Fodor* on the synthesis of oligo sequences on silicon surfaces, using photolabile protecting groups and photolithography to create a high-density microarray. Although the direct synthesis method seems more straightforward and simpler, there are also problems regarding the consistency, reproducibility, and cost of the product.

Regardless of the production technique, there are several common factors critical to the design and production of an immobilized oligo surface assay. Of foremost importance is the total amount of target DNA that can be hybridized to the surface oligo chains, the "hybridization yield", and the selectivity, which may be affected by different conditions such as the density and orientation of the surface oligos, and various reaction conditions during oligo synthesis or attachment. To study the effects of the above conditions and determine how to obtain the highest hybridization yield, it is imperative to design a consistent, reproducible, and flexible oligo surface. In addition, highly sensitive and quantitative surface characterization techniques must be designed to accurately

determine the amount of oligos on the surface. Other considerations are the chemical stability and possible recycle of the oligo surface array, and ease of production.

Although the alkanethiol SAMs formed on gold surfaces could be used as model organic surfaces to study the adsorption of DNA molecules and to provide insight on how to modify a solid surface to conditionally prevent or facilitate nonspecific DNA adsorption, it was not a suitable method for immobilizing long chain dsDNA strands due to its lack of thermal stability at 90° C, the necessary temperature for the dsDNA strands to unravel, revealing the long chain ssDNA probe used in the approach I proposed.

Short chain oligos have been directly immobilized onto gold surfaces and have been used as hybridization assays, with some claims of thermal stability at higher temperatures. However, the dsDNA formed by the oligo chains and their targets were typically only 20 bp in length and thus didn't require heating at 90° C for long periods of time. An alternative surface modification chemistry was needed that provided the same basic characteristics of alkanethiol SAMs, such as the formation of monolayer films with reproducible surface properties, and consistent and quantifiable surface coverage, under ambient conditions. In addition, the alternative SAM system would be chemically and thermally stable, perhaps due to formation of a covalent bond between the organic species and the underlying inorganic substrate.

3.1.2 Modifying silicon surfaces with organosilane compounds

One particular candidate system was the organosilane chemistry used to modify glass surfaces for producing fiberglass composites. The detailed chemistry is still unclear but it is surmised that the silanes are first hydrated into silanols, which then react with a silicon oxide (silica) surface, forming a covalent bond, as shown in Figure 3-1. In addition to reacting with the silica surface, the silanol chains can also crosslink with each other to form polymeric networks on the surface, thereby increasing the chemical stability of the organic film. The crosslinking results in the formation of less densely packed surface films with decreased order and nonuniform orientation, and the possible

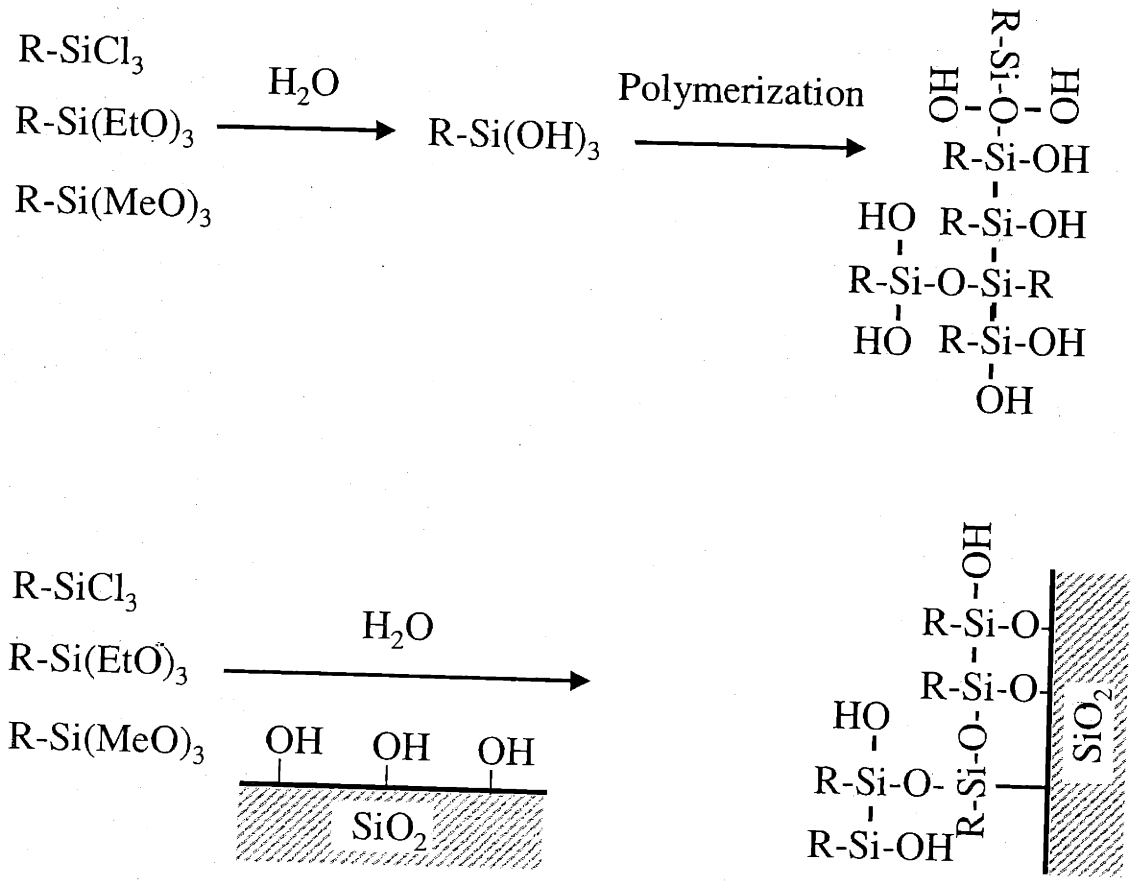

Figure 3-1. Steps in the formation of silane monolayers. The silane group is hydrolyzed to silanol groups, which react with either hydroxy groups on the substrate or with other silanols to form crosslinked silane surface films.

formation of multilayer gel-like structures, which are undesirable from an engineering or characterization viewpoint. On the other hand, there are a variety of organosilane groups with differing degrees of reactivity, including the extremely reactive chlorosilanes, and also ethoxysilanes and methoxysilanes, which are less reaction. By carefully controlling the reaction conditions such as silane concentration, solvent and reaction time, it is still possible to form organic thin films with fairly consistent packing densities and uniform surface properties approximately one monolayer thick on silica substrates under ambient conditions. As mentioned before, researchers have developed a variety of protocols for derivatizing glass surfaces using various functionalized organosilane compounds, to create reactive surfaces that immobilize biomolecules onto the surface. An example is the long-chain alkylamino silanes that are used as the starting point for stepwise oligo synthesis on controlled-pore-glass (GPC) supports. In addition to the complexity and decreased uniformity of the surface film properties, traditionally silane films have been difficult to characterize due to optical transparency of the glass substrates.

For my research I have chosen to use <100> orientation polished silicon chips for my solid substrate. A native oxide layer about 50 Å in thickness provides the covalent attachment sites for the organosilanes, while the underlying reflective silicon surface can be used for ellipsometry measurements. In addition, the relatively flat silicon surface provides a more accurate determination of surface energy using contact angle measurements, because the liquid contact angles are affected by both surface roughness and heterogeneity. Also, the silicon chips are easy to cut and shape compared to glass slides, and chemical dopants in the silicon chips make them semiconductors and thus more readily characterized by XPS. Fluorescence imaging tests conducted on silicon surfaces with silane adlayers showed very low levels of background noise, demonstrating the potential of the surfaces for epifluorescence spectroscopy.

The only shortcoming of the silicon chips is that the surface reflectivity is not high enough to efficiently reflect an IR beam at grazing angles. Consequently reflectance IR cannot be used to characterize the characteristic functional groups on the silane surface film. Alternative approaches for IR spectroscopy were evaluated, including

transmission IR and attenuated total reflectance (ATR) spectroscopy using a specially designed silicon crystal, and also depositing a highly reflective aluminum oxide layer onto the silicon substrate. The spectra obtained from transmission IR studies had very high background noise that covered the signal from the silane film, and the ATR system was too expensive, complex and time consuming for practical characterization, and the aluminum oxide surface were severely lacking in chemical stability and tended to desorb from the surface upon reaction with organosilane molecules in solution. Regardless of this minor difficulty in characterization, the overall chemical and physical surface properties of the silane films assembled onto polished and cleaned silicon surfaces made it my platform on which to perform the stepwise oligo synthesis necessary to produce the surface attachment sites for immobilizing dsDNA strand using the methodology I proposed.

3.1.3 Method of approach

I began by evaluating various silane chemistries to determine the best candidates for forming reactive surface films with controllable surface density. The consideration of surface density arose from the hypothesis that the hybridization efficiency of target oligo in solution with the immobilized surface oligo chains was dependent on steric factors and electrostatic repulsion, both of which are determined by the surface density of immobilized oligos, which in turn was directly related to density of reactive sites in the silane adlayer. Methods were developed to control this surface density using techniques analogous to the mixed monolayer protocols introduced by *Whitesides*[1]. I produced model oligo surface arrays by direct stepwise oligo synthesis onto a flat silicon surface chemically derivatized by a SAM of end-functionalized silanes. By manipulating the density of reactive sites on the SAM surface, I controlled the oligo surface density, and studied how it affected the stepwise reaction efficiency, and also the hybridization yield to complementary solution-phase oligo chains.

In addition, I utilized a sensitive surface characterization technique, XPS and specially labeled nucleotide bases to quantify the surface density of the reactive sites on

the silane SAM surface, and the surface oligo density under various reaction conditions, and utilized the results to determine the optimal conditions that maximized the sequence fidelity of the surface oligo chains. Then, by manipulating the silane film compositions I using a mixed SAM methodology, I created surface oligo films with a controlled surface density, which were used to systematically study the steric and the hybridization yield with labeled complementary oligos in solution. To my knowledge, only limited research has been completed on the effect of oligo surface density on DNA hybridization efficiency at the surface, and most of the studies were not systematic but rather confined to one or two randomly generated data points. I wanted to determine the oligo surface density that optimizes DNA hybridization at the surface, and to produce silane SAMs with the appropriate hydroxy composition to effectively control the oligo surface density for both optimal sequence fidelity and hybridization efficiency. Finally, research was conducted on the stability and recycle efficiency of the synthesized oligo array, since an easily stored and reusable oligo surface would be more practical and economical.

3.2 Materials and procedures

3.2.1 Materials

(3-Glycidoxypropyl) triethoxysilane (GOPS), N- [3-trimethoxysilylpropyl]-4-hydroxy butyramide, and 3-iodo-propyltrimethoxysilane were obtained from Gelest Inc. (Tullytown, PA). Octyltrichlorosilane was purchased from United Technologies, Inc (Bristol, PA), and 20wt% piperidine in dimethyl formamide was purchased from Protein Technologies, Inc (NY). Undecenyl alcohol, trichloroacetyl chloride, diisopropylethyl amine, trichlorosilane, anhydrous THF, chloroplatinic acid, 28 wt% ammonium hydroxide (NH_4OH), methanol, and trifluoroacetic anhydride were purchased from Aldrich (Milwaukee, WI). Gold pellets were supplied from American Precious Metals, and chromium wires were supplied by R. D. Mathis and Company (Long Beach, CA). Hexanes, acetonitrile, potassium carbonate (K_2CO_3) and potassium iodide crystals were purchased from Mallinckrodt (Paris, KE), and all phosphoramidites and reagents used for oligonucleotide synthesis, and empty TWIST™ columns were purchased from Glen

Research (Sterling, MA). Silicon chips were purchased from Recticon Corp. (Pottstown, PA), deionized (Resistance = 18.2 MΩ) water was provided by a MilliQ deionization system (Millipore Corp., Bedford, MA). Terminal transferase reaction kits were supplied by New England Biolabs (Beverly, MA), and ^{32}P radiolabeled dCTP nucleotides were supplied by NEN Life Sciences (Boston, MA).

3.2.2 Formation of silane monolayers

A schematic description of the silane monolayer formation is shown in Figure 3-2. The SiO_2 surfaces were prepared by cutting 3 cm x 1 cm chips from <100> silicon wafers. The silicon chips were immersed for 2 hours at room temperature in a base bath consisting of 40 g NaOH in 150 ml MQ water and 200 ml 95% ethanol, then rinsed with MQ water followed by ethanol, and then dried with a nitrogen gas stream. The cleaned silicon samples were then immersed in solution of various end-functionalized alkylsilanes under ambient temperature and pressure. The silicon samples were immersed for 16 hours in an acidic (pH=3.0-4.0) 5wt% $GOPS_{(aq)}$ solution to form GOPS SAMs; for 16 hours in a solution of 0.5 wt% N-[3-trimethoxysilylpropyl]-4-hydroxy butyramide in 95% ethanol to produce OH silane SAMs; and for 1 hour in 10 µl/20 ml solutions of mixed alkyltrichlorosilanes and trichloroacetyl (TCA) alkyltrichlorosilanes in dry xylene to create mixed monolayers with both methyl and acetyl groups exposed on the surface. The derivatized silicon samples were then removed and rinsed with their respective neat solvents followed by ethanol, and dried with a nitrogen gas stream. The silane adlayer thickness was determined by ellipsometry, and the surface energies were characterized by wetting measurements with MQ water. Subsequently, the epoxy ring of the GOPS SAM was opened by heating the oligo chips to 90° C in pH=3 water for 3 hours to produce two hydroxy groups. The TCA protecting groups on the mixed trichlorosilane SAMs were removed by immersing in 0.05 M K_2CO_3 in a to 1 water methanol mixture for 15 minutes, exposing the hydroxyl group.

A. Pure monolayer approach

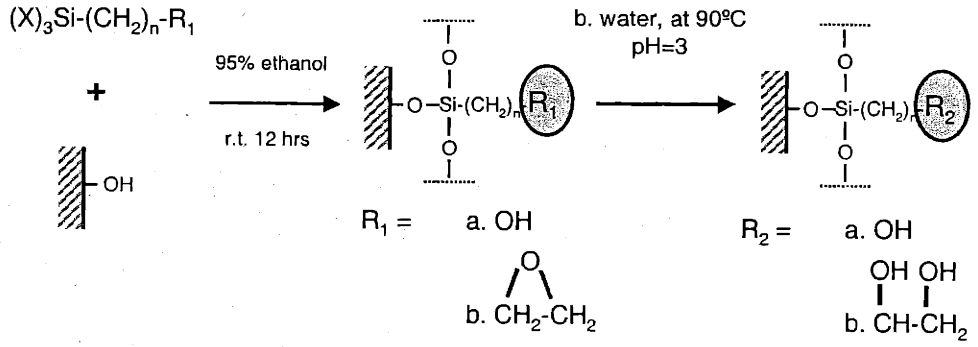

B. Mixed monolayer approach

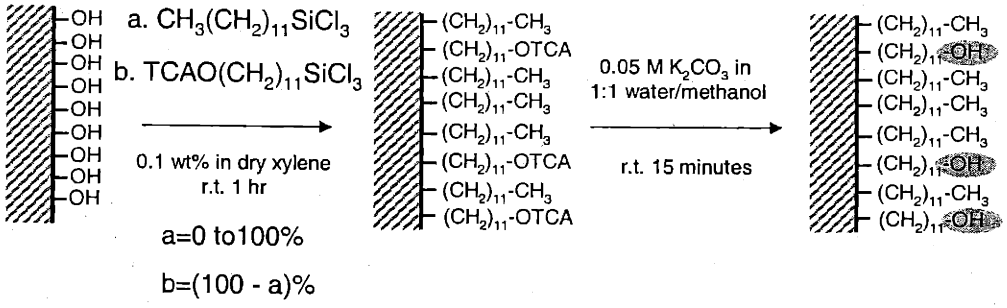

Figure3-2. Summary of the various protocols for the formation of silane SAMS with GOPS, OH, and TCA TCS silane.

3.2.3 Synthesis of oligos, Ultramild® protecting groups

Oligos were synthesized stepwise by the phosphoramidite protocol using an Applied Biosystems ABI392/394 automated oligonucleotide synthesizer. Silicon chips were cut to about 0.5 x 0.5 cm^2 slides to fit inside a 1-μmole-sized TWIST™ synthesis column. Reaction conditions such as coupling time and capping procedures were manipulated by designing custom synthesis cycles and sequences. The automated ammonium hydroxide induced cleavage step was canceled. Instead, the oligo chips were removed from the synthesizer, washed sequentially with acetonitrile, acetone and ethanol, and dried with nitrogen. The base protecting groups were removed by 0.05 M K_2CO_3 in anhydrous methanol, and 20wt% piperidine in dimethyl formamide (pip/DMF) was used remove the cyanoethyl groups.

3.2.4 Preparation of XPS standard iodine on gold substrate

Polycrystalline gold films on silicon were prepared by thermal evaporation as described previously. The films were immersed in a 100 mM aqueous potassium iodide solution for 24 hours at room temperature to produce an adsorbed iodide monolayer on gold that was used as an XPS reference for quantifying iodide surface concentrations. After immersion, the samples were rinsed with MQ water and dried with a stream of nitrogen. This procedure produces a surface that contains a surface density of iodine atoms of 9.1 x $10^{-10}/cm^2$.

3.2.5 Radiolabelling and scintillation counting

Oligo sequences complementary to the surface oligos were purchased from commercial sources (The Great American Gene Company, Ramona, CA). Then α-^{32}P dCTPs were attached to the 3' end of the oligo by the terminal transferase enzymatic ligation reaction performed for one hour at 37° C in an Ericomp PowerBlock™ thermocycler. The radiolabelled oligo was prepared in various concentrations in 8 x saline sodium citrate (SSC) buffer with 0.1wt % sodium dodecyl sulfate (SDS). The oligo surfaces were immersed in the radiolabelled oligo solutions for 24 hours at 4°C, then removed and rinsed with 4° C Tris-EDTA buffer (ph=7.4) and dried with nitrogen gas.

^{32}P radioactivity was measured using an LKB 1217 Rackbeta liquid scintillation counter (Wallace, Gaithersburg, MD). Samples were immersed in 10 ml of LiquiScint radiofluorescent solution (National Diagnostics, Atlanta, GA), and measured for 30 seconds.

3.2.6 Synthesis of protected hydroxyl-terminated trichlorosilanes

Trichloroacetyl undecene: One equivalent (eq) of undecenyl alcohol (Aldrich) was added dropwise to 1.1 eq of trichloroacetyl chloride (Aldrich) in dry THF, under nitrogen, with 1 eq of diisopropylethyl amine added as a proton scavenger. After 24 hr the mixture was worked up with 1 eq of water, and the product solution was filtered, then washed with dry hexane and concentrated under reduced pressure to yield the titled product (80% yield). ^{1}H NMR δ 5.8 (t, 1 H), δ 5.0 (d, 2 H), δ 4.3 (t, 2 H), δ 2.0 (t, 2H), δ 1.7 (t, 2H), δ 1.3-1.45 (m, 10 H).

Trichloroacetyl undecyl trichlorosilane: 1 eq of was trichloroacetyl undecene was combined with 4 eq of trichlorosilane (Aldrich) and 5 mg of chloroplatinic acid, under nitrogen[2]. The reaction was left for 24 hours. The solution was concentrated under reduced pressure to yield the titled product (35% yield). 1H NMR δ 4.1 (t, 2 H), δ 3.6 (t, 2H).δ 2.0 (t, 2H), δ 1.7 (t, 2H), δ 1.3-1.45 (m, 10 H).

Trifluoroacetyl undecene: One equivalent (eq) of undecenyl alcohol was added dropwise to 1.1 eq of trifuoroacetyl chloride (Aldrich) in dry THF, under nitrogen, with 1 eq of diisopropylethyl amine added as a proton scavenger. After 24 hr the mixture was worked up with 1 eq of water, and the product solution was filtered, then washed with dry hexane and concentrated under reduced pressure to yield the titled product (80% yield). ^{1}H NMR δ 5.8 (t, 1 H), δ 5.0 (d, 2 H), δ 4.3 (t, 2 H), δ 2.0 (t, 2H), δ 1.7 (t, 2H), δ 1.3-1.45 (m, 10 H).

Trifluoroacetyl undecyl trichlorosilane: 1 eq of was tricfluoroacetyl undecene was combined with 4 eq of trichlorosilane (TCA) and 5 mg of chloroplatinic acid (Aldrich), under nitrogen. The reaction was left for 24 hours. The solution was concentrated under reduced pressure to yield the titled product (35% yield). 1H NMR 1H NMR δ 4.1 (t, 2 H), δ 3.6 (t, 2H).δ 2.0 (t, 2H), δ 1.7 (t, 2H), δ 1.3-1.45 (m, 10 H).

3.3 Results and discussion for silicon derivatization

3.3.1 Formation of silane monolayers

The silicon surfaces were cleaned with a base bath. The base solution contained 12.5wt% NaOH in a mixture of water and ethanol, and the samples were immersed for 2 hours in the bath before they were removed and washed sequentially with water and ethanol. The recipe was adopted from a protocol that *Brown* developed to clean glass slides before adsorption of a polylysine coating. A basic solution is contrary to the acidic solutions used by many researchers to clean glass substrates prior to silane SAM formation. However, the basic solution had dual purposes: not only did it effectively remove organic contaminants from the surface, but it was a strong reducing agent that created hydroxy groups on the native silicon oxide surface that could readily reacted with the silane compounds in solution to form silane adlayers. The only concern was that the base would damage the thin (20-50 Å) native oxide layer, and this was prevented by limiting the exposure time of the silicon samples to the base bath to less than 2 hours.

I used a variety of organosilane reagents to produce SAMs with varying hydroxyl content, where the hydroxyl groups are the active sites for the attachment of activated phosphoramidites in the stepwise oligo synthesis reaction. In particular, I used both GOPS and hydroxyl-terminated alkoxysilanes for comparison with previous literature involving surface oligo synthesis. In addition, I also prepared surfaces expressing a controlled mixture of hydroxyl and methyl groups by immersing the silicon surfaces in mixtures of two trichlorosilanes containing methyl and TCA protected hydroxyl end groups. The TCA groups were removed with a mild base to expose the hydroxyl groups. The silane adlayers were characterized by ellipsometry to measure their film thickness, and by wetting measurements with water to measure their hydrophilicity. Table 3-1 displays these results.

3.3.2 GOPS SAMs

GOPS SAMs were used by *Southern* to form the reactive sites for his patterned oligo synthesis scheme using traditional phosphoramidite chemistry. Upon heating in an acidic aqueous solution (pH = 3 - 4), the epoxy ring opened to form a glycol group that could react with the incoming activated phosphoramidites. I produced GOPS SAMs with thickness of 8-10 Å, compared to 1-2 Å for control surfaces immersed in water solution only. Since the GOPS chain contains 10 atoms, this thickness constitutes monolayer to sub-monolayer coverage. I attempted to use XPS to characterize the surface density of the GOPS chains. The formation of a thin surface film was supported by XPS spectra, where derivatized samples exhibited a Si (2p) peak at 154 eV that was not present for untreated samples. This new peak is due to the siloxane bond that attaches the silane chain to the silica surface. However, there was difficulty in quantifying the surface coverage due to the high background oxygen signal from the native silicon oxide layer underlying the SAM film.

Table 3-1. The thickness of GOPS silane, OH silane and TCA silane SAMs measured by ellipsometry; the contact angles were determined by a manual goniometer.

Species	Ellipsometric Thickness (Å)	θ_a of water	θ_{ret} of water
Bare SiO2	1±1	<10	-
OH silane	15±3	50	-
Glycidyl silane			
Before Deprotection	12±2	55	-
After Deprotection	12±2	33	-
TCA silane			
Before Deprotection	20±3	98	81
After Deprotection	20±3	71-98	48-55

Trifluoroacetyl chloride was used to label the glycol groups for XPS, but though there was a definitive fluorine signal suggesting the existence of hydroxyl groups on the surface, there is the possibility that some of the due to steric hindrance and reaction efficiency not all of the hydroxy groups would react with the trifluoroacetyl chloride to form the fluorinated ester label. In addition, there was no XPS standard for fluorine available to extrapolate the surface density from my XPS data. Therefore I tried an alternative approach to estimate the silane surface density, using a 3-iodopropyl triethoxysilane SAM. After immersion in a 0.5 wt% solution in ethanol for 24 hours, a 6 Å silane adlayer was formed on the silicon surface, corresponding to approximately monolayer coverage. Next, an iodine surface standard was produced by immersing a gold surface in a 0.1 M $KI_{(aq)}$ solution. The iodine adsorbs onto the gold to form a monolayer with a surface coverage of $9.1x10^{-10}$ moles/cm^2. The iodinated silane SAM and the iodine standard were simultaneously quantified by XPS. The resulted indicated that the silane adlayers had a surface density of approximately $7.2x10^{-11}$ moles/cm^2, which is approximately 80% of the density compared to a densely packed alkanethiol SAM on gold. This is expected since the footprint of a silane chain is larger than an *n*-alkanethiol due to the silicon oxide bonds formed by the crosslinked silane chains. The footprint of the GOPS silane should even be higher due to the epoxy ring, resulting in lower surface densities, but since the ring opens to form a glycol a very dense layer of hydroxy groups is expected.

The GOPS SAM was immersed in acidic (pH = 3) aqueous solution and heated to 90° C to open the epoxy ring and generate the glycol group. After heating the sample were characterized with ellipsometry with no change in the adlayer thickness, suggesting that the SAM is stable to heating in acidic solutions. More vigorous conditions (5 days at 90° C) did not result in any change in the film thickness, confirming the thermal stability of the silane SAM. Before ring opening the GOPS SAM had a θ_a of 55°, which decreased to 33° after heating, suggesting that the reaction was successful and that the decrease in contact angle was due to the presence of the hydrophilic hydroxy groups exposed on the surface at a high density.

3.3.3 OH terminated silane SAM

OH silanes were chosen by *Fodor* to derivatize their silicon surfaces to create the reactive sites for their oligo synthesis using photolabile 5' OH deprotecting groups. With the OH silane, the 15-20 Å thickness observed by ellipsometry indicated monolayer coverage. The θ_a for water was at about 45-55°, which was higher than the 33° observed for glycol surfaces. The increased hydrophobicity suggests that there are less hydrophilic hydroxy groups on the surface, or perhaps that the surface is more disordered resulting in more hydrophobic methylene moieties also becoming exposed on the surface. Further analysis would be performed on OH silane surfaces using XPS, in the following section.

3.3.4 Mixed trichlorosilane SAMs

Silicon surfaces were exposed to solution mixtures of dodecyl trichlorosilane and trichloroacetyl (TFA) or trifluoroacetyl (TCA) undecyl trichlorosilane (TCS) to produce SAM with mixed surface compositions. The approach was analogous to the mixed alkanethiol SAM system used to study and control nonspecific DNA adsorption in Chapter 2. I observed that contrary to the monolayer coverage obtained using alkanethiol SAMs, the thickness of mixed TCS SAMs varied with immersion times. For immersions times lower than 1 hour the SAM thickness was approximately 25-30 Å, corresponding to a monolayer level surface coverage. However, as immersion times increased the thickness increased, until at 8 hour immersion the adlayer thickness was above 100Å, in the multiplayer film regime. This was expected because TCS is much more reactive then the triethoxy or trimethoxy silanes and thus more extensive crosslinking between silane chains occur, resulting in gel-like structures over longer reaction times. Therefore the reaction times for TCS were limited to 30 to 60 minutes to prevent multilayer formation. Also, in general the kinetics of TFA TCS SAM formation were more rapid compared to the TCA TCS SAMs, possibly due to the lower chemical stability of the TFA protecting group, which is more readily removed by trace amounts of residual water to prematurely expose the hydroxy group, resulting in unwanted crosslinking side reactions.

XPS was utilized to characterize the fluorine signal of the mixed methyl and trichloroacetyl (TCA) terminated SAMs, and the results are presented in Figure 3-3. Although I did not determine the surface coverage of the silane adlayer, by normalizing the fluorine signal intensity of the various samples to the intensity of a 100% TCA TCS SAM surface, I were about to correlate the surface compositions of TCA groups with the proportion of TCA undecyl TCS in the solution mixture. From Figure 3-3 it is evident that the relationship between the solution and surface composition of TFA groups is close to linear. Though similar to the plot of OH group solution versus surface compositions in mixed alkanethiol SAM systems, the increased linearity strongly suggests that the chemisorption reaction kinetics of the methyl and TCA terminated TCS with a silicon surface are very similar.

The θ_a of the mixed TCS SAMs were approximately 95° to 100°, suggesting that a hydrophobic low energy surface is formed. However, the large hysteresis (>30°) also indicates that the mixed TCS SAMs are more heterogeneous than their alkanethiol counterparts, which is expected. The surfaces were deprotected by immersion in a 0.05 M K_2CO_3 in 1:1 methanol/water solution (pH = 10) for various times, and the base was observed to rapidly and visibly degrade the TCS surface for immersion times over 1 hour at room temperature. Measurement results from ellipsometry actually showed a large increase in the adlayer film thickness, an anomaly possible created by a drastic change in the index of refraction of the silicon surface due to etching by the base solution. XPS studies using iodopropyl silane SAMs confirmed that the silane chains were being removed from the silicon surface, probably do to base induced hydrolysis of the siloxane bond attaching the silane chain to the native silicon oxide surface layer. This result strongly suggested that the silane surfaces were sensitive to basic environments, and that exposure to bases should be minimized. Further studies showed that the TCA and TFA protecting groups were effectively removed by 15 minutes immersion, without significant damage to the underlying mixed TCS adlayer. This was confirmed by a decrease in the θ_a in water from above 95° to around 72°. The decrease was probably due to the exposure of the hydrophilic hydroxy groups, causing an increase in the surface energy of the mixed TCS SAM. Also, from XPS the fluorine signal (1s) at 270eV disappeared for all surface

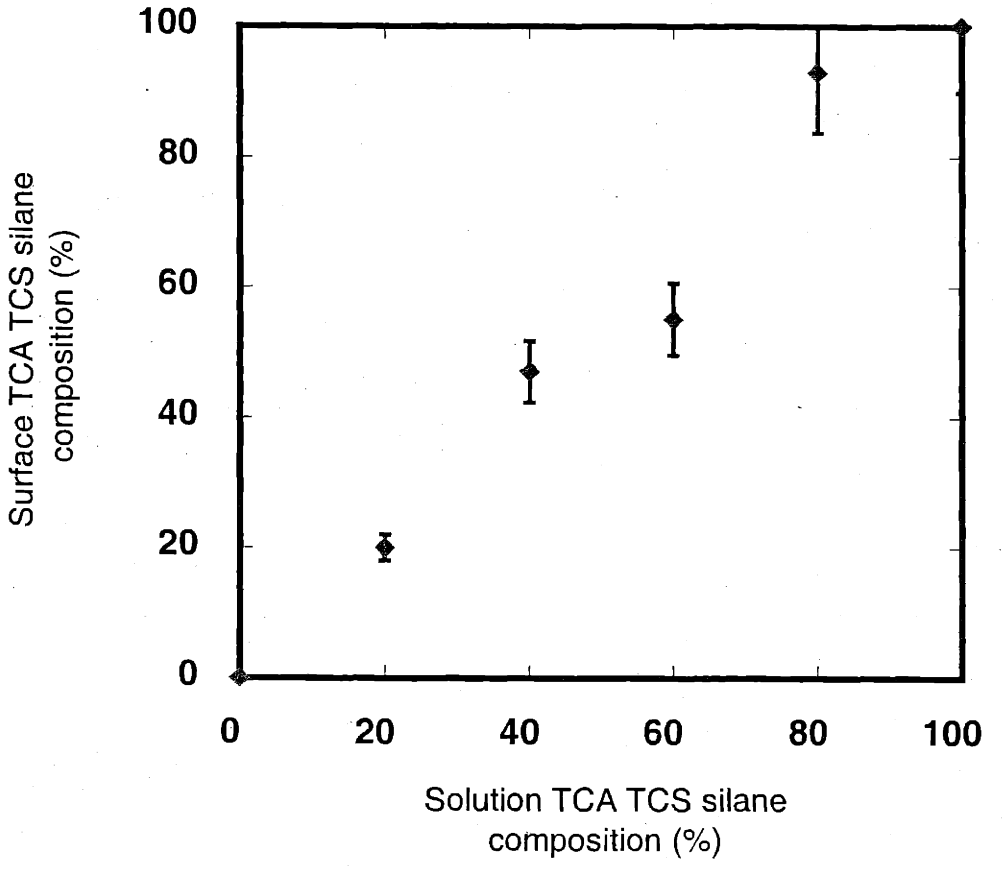

Figure 3-3. Relationship between the solution and surface composition for films prepared from mixed solution of TCA TCS and dodecyl TCS. The TCA silane coverage was determined by the XPS measurement of the chlorine signal at 199 eV. There is a linear relationship between the proportion of TCA TCS silane in solution and on the surface.

compositions of mixed TCA TCS adlayers after 15 minutes immersion in the basic solution.

For homologous organic surfaces the θ_a values in MQ water should decrease with increasing surface composition of the hydrophilic hydroxyl group. Therefore the deprotected mixed hydroxy-methyl TCS surfaces should be expected to possess the lowest hydroxyl surface compositions due to their high θ_a angles. However, comparison of the XPS fluorine (199 eV) signals indicated that the hydroxyl surface densities of mixed TCS surfaces were approximately linearly related to the solution TCA TCS compositions. I surmise that the θ_a values are higher for the mixed hydroxyl-methyl TCS surfaces are higher because they are more homogeneous and consequently the hydrophobic methyl groups are more exposed to the MQ water interface and thus cause an increase in the θ_a values. On the other hand the glycol and OH silane surfaces are less ordered and more heterogeneous, resulting in higher surface energies and consequently lower θ_a values. This hypothesis was supported by the hysteresis values of the glycol and OH silane surfaces, which were significantly higher than for the mixed hydroxyl-methyl TCS surfaces.

3.3.5 Surface oligo density

The previous studies provided valuable information on the thickness and surface properties of various silane adlayers on silicon surfaces. However, there was a lack of instructive data on the surface coverage of the reactive hydroxy groups in the various SAM films. More importantly, since the motivation for derivatizing the silicon surfaces with thin silane films is to create the platform for stepwise oligo synthesis, perhaps the more relevant question would be how to determine the surface density of oligos rather than the surface hydroxy group density. Since the footprint of a phosphoramidite is much larger than a hydroxy group, it is clear that not all the surface hydroxy groups will actually form a covalent bond with the incoming phosphoramidite. Consequently, the surface oligo density should be significantly lower than the hydroxy density, and the

effective oligo density should be the target of my investigations. Thus, I decided add a single labeled nucleotide onto the silane surfaces by automated phosphoramidite oligo synthesis chemistry. Since the stepwise reaction efficiency of the oligo synthesis reaction should not be expected to reach 100%, the density of this 1st nucleotide would represent the maximum possible density for an oligo surface synthesized on any of the above silane adlayers. After determining how the various silane surfaces affect the oligo surface density, I would design a silane SAM system capable of controlling the surface oligo density.

3.3.6 XPS with iodinated phosphoramidites

The next question is how to accurately quantify the minute amounts of 1st nucleotide spread on a single silane monolayer. The most direct method is to use a labeled phosphoramidite. Radioactively labeled phosphoramidites were not available, neither were enzymatic labels such as horseradish peroxidase (HRP) or alkaline phosphotase (AP). Although the signal amplification characteristics of the HRP and AP molecules were desirable for increasing the measurement sensitivity and minimum threshold level, there was a lack of reliable crosslinking chemistries that could attach the enzyme labels efficiently onto the immobilized phosphoramidites, and trying to attach the label to the phosphoramidite prior to the oligo synthesis is prohibitively complex and expensive. In addition, there is no guarantee that the enzyme activity and signal amplification are consistent enough to provide quantitative results.

Another possibility is fluorescent dyes such as fluorescein, rhodamine and the Cy3 and Cy5 dyes from the cyanine family. These fluorophores are all commonly applied in biological research are commercially available as labels on the phosphoramidites. The fluorescent dyes are also inherently amplifiable under continuous laser light stimulation. However, fluorescent labels could become degraded by photobleaching, and furthermore, like HRP and AP the measured fluorescent signal intensity is often not consistent enough to provide quantititative data.

Another approach was to try an enzymatic reaction to add a radioactive nucleotide to the 1st nucleotide immobilized onto the silane surfaces. One candidate was T4 polynucleotide kinase, which phosphorylates oligos or DNA with a 5' hydroxy end, by transferring a ^{32}P molecule from a γ-^{32}P dCTP nucleotide to the 5' end of a nucleotide, consuming 2 ATP molecules in the process. The process was effective in the solution phase, but when performed on the surface a strong level of radioactive background appeared, the result of significant nonspecific adsorption of γ-^{32}P dCTP onto the surface. Sometimes the background noise from controls were higher than the samples, and the nonspecific adsorption could not be prevented by adding SDS since the enzymes would be denatured and thus deactivated by the strong surfactant.

In addition, since the enzyme reaction required a specific orientation between the protein and the nucleotides, it was doubted whether the restricted mobility of immobilized 1st nucleotides would provide adequate space and flexibility for the reaction to occur. Thus this approach was dropped.

XPS could be used to quantify the surface 1st nucleotide density, provided there is a proper label and a suitable measurement standard. I chose iodine labeled phosphoramidites since they were commercially available, and the photoionic cross-section area of an iodine molecule is quite large, at $3_{d3/2}$ (618 eV) and at $3_{d5/2}$ (630) eV, compared to the area at $5_{d5/2}$ (84 eV) and at $5_{d7/2}$ (87 eV) for gold, resulting in very high signal intensities that improves the measurement sensitivity and threshold detection levels. In addition, since iodine is rarely present in the ambient environment, using iodine as the label drastically decreases the possibility of sample contamination and increases the specificity of the method.

Finally, research done by *Weaver* provided the necessary surface standard for quantifying the iodine surface coverage. Weaver conducted studies on iodine monolayers adsorbed onto <111> gold surfaces using electrochemistry, STM and XPS[3]. He found that after immersing gold samples in a 0.1 M $KI_{(aq)}$ solution for 24 hours at ambient conditions[4-6], the iodide anions oxidized to iodine, forming a bond with gold atoms

simultaneously, creating iodine adlayers on the gold surface with a defined ($\sqrt{3}$ x $\sqrt{3}$)R30 lattice structure[5,6], 0.33 monolayer surface coverage, and 5 Å separation between the iodine atoms. From STM images Weaver determined the surface density of the iodine layer to be 9.1 x 10^{-10} moles/cm^2.

My approach was to attach the iodine-labeled nucleotide to the silane surfaces, then characterize labeled surfaces along with the KI standard by XPS, and ratio the XPS iodine intensities of the samples to the standard to determine the oligo surface coverage. To prevent possible differences in XPS signal intensity due to possible fluctuations in the X-ray beam strength between different experimental runs, an internal standard was needed. I used octadecane (C18) thiol SAM on gold as the internal standard since numerous previous studies and my own experimental data have shown that the C18 thiols consistently formed well-ordered SAMs with highly uniform film thickness and orientation. The SAM formed a pacifying barrier to film that resisted adsorption of organic contaminants from the environment, which were easily removed by an ethanol wash. And although the C18 SAM did attenuate the gold signal, due to its uniform surface properties the gold signal should be independent of the C18 SAM properties and directly proportional to the X-ray beam strength.

By comparing both the KI standard and C18 SAM internal standard for each run, I was able to normalize the data and thus compare XPS data from different runs with an appropriate degree of accuracy. From the XPS data I were able to calculate the surface iodine density, and from this value extrapolate the surface 1st nucleotide density. The experimental results allowed us to evaluate the different silane SAM formation strategies and their effect on the 1st nucleotide surface density, and subsequently choose the appropriate silane systems for the studies I had to perform on the synthesized oligo surfaces. A sample representation of the XPS spectra for iodine on various surfaces is shown in Figure 3-4.

3.3.7 Surface coverage of deprotected GOPS SAMs

I used an iodine-labeled uracil (U) phosphoramidite to label the ring opened GOPS surfaces, then rinse the samples with acetonitrile, acetone and ethanol, followed by a 24 hour immersion wash in 0.2wt% SDS to remove any nonspecifically adsorbed U nucleotides. The XPS spectra showed two iodine peaks at 622 eV ($3_{d3/2}$)and 623 eV($3_{d5/2}$), which are slightly shifted from the elemental iodine peaks at 618 eV and at 630 eV. The shift is due to the different ionic state of the iodine, which is covalently attached to the U nucleotide. The 1st nucleotide surface densities were obtained by normalizing the iodine signal from each sample to that from a reference sample (an iodide-treated gold films) that had a known surface iodine concentration of 9 x 10^{-10} moles/cm^2. The 1st nucleotide surface density was determined by XPS to be 1.22 x 10^{-10} moles/cm^2, about one sixth of the surface coverage for a silane monolayer (7.2 x 10moles/cm^2). The lower surface coverage is reasonable because the footprint of a nucleotide is significantly larger than a hydroxy group. There was no increase in the 1st nucleotide surface coverage with increased oligo synthesis reaction times up to a factor of 6, or with repeated reactions, suggesting that the maximum possible oligo packing density has been achieved using the GOPS SAM. The high density is possibly due to the high density of glycol groups formed during the epoxy ring opening reaction. Each glycol group has to hydroxy groups, doubling the potential active surface sites for oligo synthesis.

3.3.8 Surface coverage of OH silane SAMs

From XPS data I determined that the surface 1st nucleotide coverage was about 4.8 x 10^{-10} moles/cm^2, or approximately 40% of the coverage compared to GOPS SAM surfaces. The lower 1st nucleotide coverage suggests that the OH silane SAM forms with a lower OH surface coverage, resulting in a lower 1st nucleotide surface density. This conclusion was supported by the previous contact angle measurements that suggest the OH silane surface was more heterogeneous and more hydrophobic, suggesting that the surface OH group packing density was lower than deprotected GOPS SAMs. Next, I studied the kinetics of the OH silane SAM formation by ellipsometry, and by XPS using

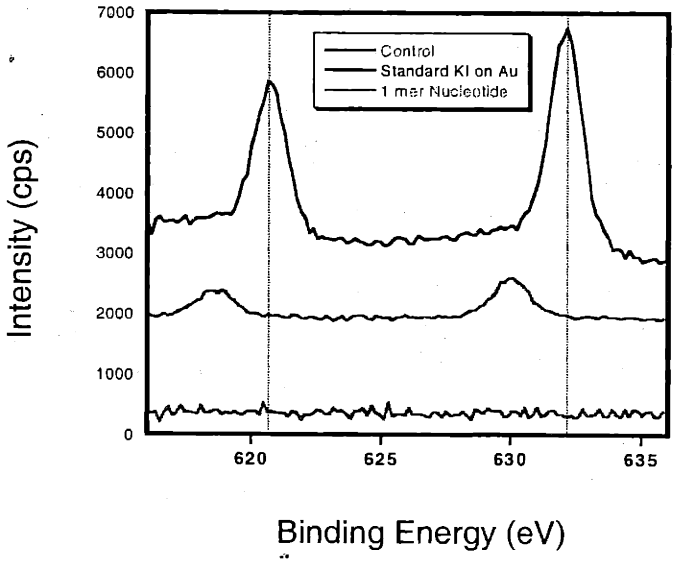

Figure 3-4. Typical iodine XPS spectra with characteristic peaks at 620 and 633 eV. The standard (top) spectra consists of a 0.33 monolayer of iodine on Au<111>; the 1mer nucleotide (middle) spectra is the 1st nucleotide attached to an OH silane SAM; the control (bottom) is a 1st nucleotide synthesis onto a bare, clean silicon surface.

the iodinated U phosphoramidites. The results are shown in Figure 3-5a. The ellipsometry results show an increase in film thickness leveling of after eight hours immersion time to about one monolayer thickness, while the XPS shows that the 1st nucleotide surface coverage reaches a maximum at eight hours immersion time, with a surface density of about $1.2x10^{-10}$ moles/cm^2, or about the same density as the 1st nucleotide surfaces synthesized on the deprotected GOPS surfaces.

However, sometimes after 16 hours of immersion time the 1st nucleotide surface density drops to the 40-50% coverage value of 4.8-6.1 x 10^{-10}, matching my previous readings. While in other instances there is little (10-20%) or no decrease in the density of surface reactive sites from the maximum coverage of about $1.2x10^{-10}$ moles/cm^2. The decrease in 1st nucleotide surface density should be due to a decrease in surface OH group density. But the OH silane film thickness did not decrease with time, suggesting that the lower OH surface coverage was due to some type of rearrangement or chemical reaction that deactivated some of the OH groups. Though the mechanism is still unclear, it is possible to have chemical side reactions occur since the hydroxy end group on the silane is theoretically reactive towards the siloxane groups on other chains, effectively deactivating the hydroxy group on the surface. The 1st nucleotide surface density on OH silane surfaces wasn't consistent between runs after 16 hours of immersion, so I needed a methodology that formed SAMs with consistent and controllable surface hydroxy group surface density. Subsequently, I tried to form mixed silane SAMs using solution mixtures with various proportions of octyl triethoxy silane and OH silane.

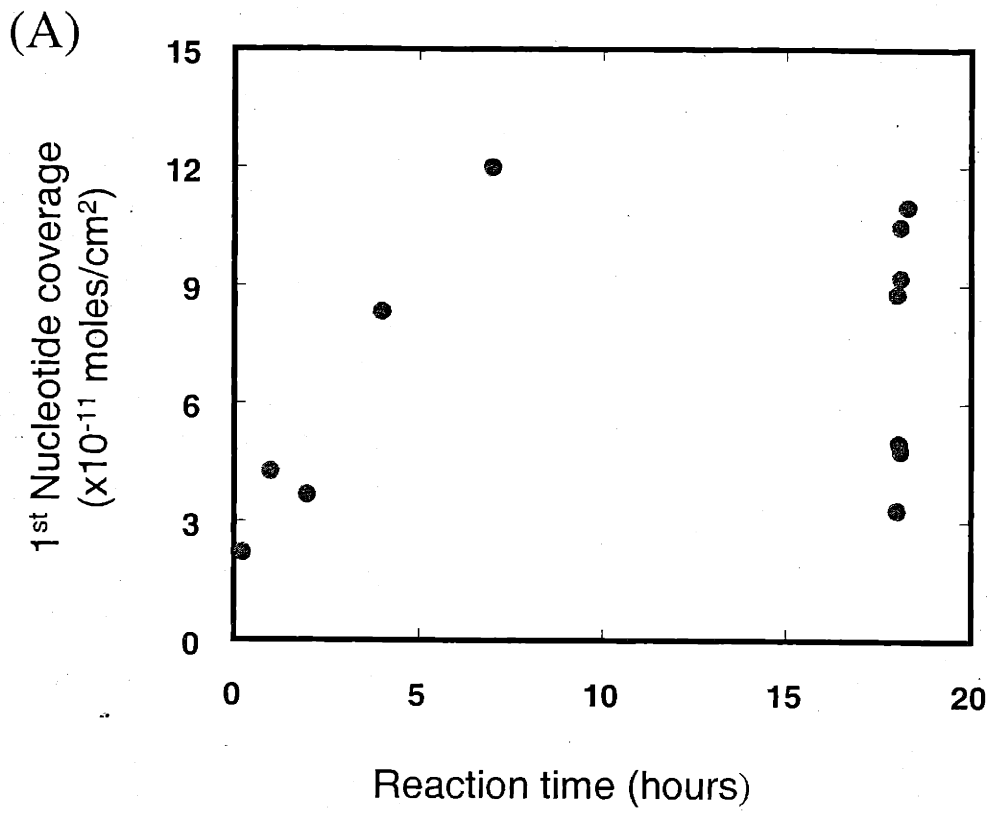

Figure 3-5. XPS iodine signal of 1st nucleotide added onto OH silane SAMs: (a) the surface coverage with respect to immersion time of the substrate in 0.5 wt% OH silane solution shows a decrease in coverage at 18 hours immersion time

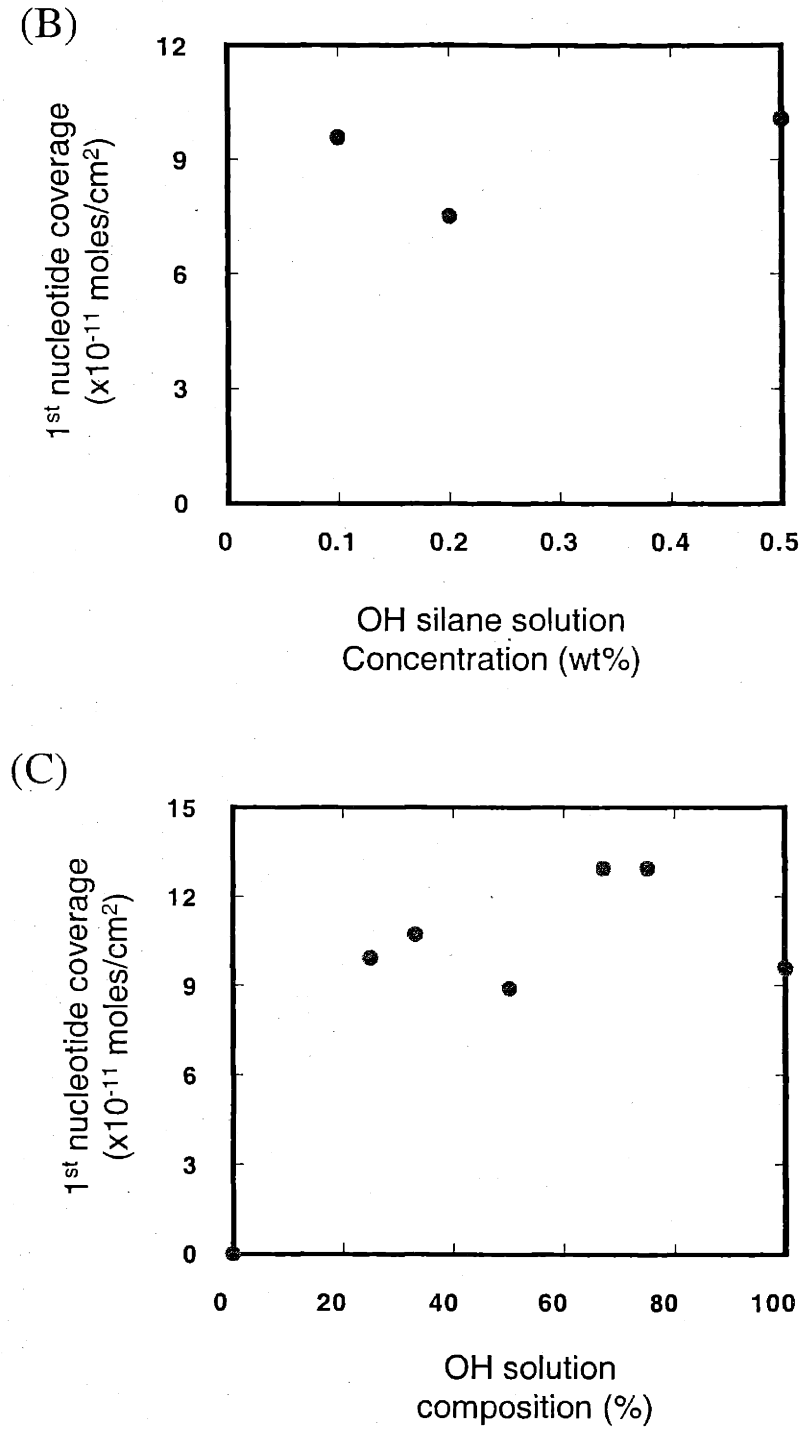

Figure 3-5. XPS iodine signal of 1st nucleotide added onto OH silane SAMs: (b) the surface coverage does not change significantly with varying OH silane concentration, (c) nor with different OH silane compositions in a mixed OH silane-octyl triethoxysilane SAM.

Previous studies have shown that the octyl triethoxy silanes display a low reactivity towards silica surfaces and require catalysts to facilitate silane formation. I theorized that perhaps the octyl silanes could crosslink with the OH silanes in solution to form oligomers, which would then attach to the surface. Silane surfaces were synthesized using mixtures of OH silane and a dodecyl triethoxysilane in solution to test this theory, and used XPS with I-UPA to characterize the 1st nucleotide surface coverage and the results are shown in Figure 3-5b. Regardless of the composition of methyl-ended triethoxysilanes there was no change in the resulting 1st nucleotide surface density, and a solution of 100% octyl triethoxy silanes failed to produce a surface film. The results suggest that the kinetics of the silane surface attachment reaction are much more rapid than the crosslinking reaction between the silicon species in the silane chains, and thus the surface reaction is the dominant deciding factor for the surface film composition.

3.3.9 Surface coverage of mixed TCS silane SAMs

From the studies using mixed triethoxysilanes, I concluded that the surface reaction kinetics were the deciding factor for formation of silane SAMs. Other competitive factors that could influence the surface SAM composition include the relative solubility of the different silanes in the organic solvent, which could thermodynamically favor the partitioning of certain silane species to the hydrophilic SAM surface; and also the reactivity of the silane chains towards each other, which was determined to be much lower than their reactivity towards the surface. Therefore I needed to develop silanes that are very reactive towards the silica surface and rapidly form adlayers with controlled compositions despite possible differences in solubility, and I chose TCS molecules as the candidates. Experiments showed that octadecyl, dodecyl and octyl TCS species in dry xylene rapidly formed monolayer films on silicon surfaces. Contact angle measurements indicated that the monolayers were hydrophobic, with θ_a above 115°, and the low hysteresis (15°-20°) suggested the SAM structures were fairly homogeneous.

Therefore I proposed using mixed methyl and hydroxy terminated TCS molecules to form SAMs with varied hydroxy group densities. However, since the TCS group is highly reactive towards any hydroxy groups I used TCA and TFA protecting groups to prevent side reactions from occurring. Clean silicon surfaces were immersed xylene solutions containing mixtures of octyl and TFA or TCA TCS species, at a concentration of 1μl/ml for 1 hour, under ambient conditions. Although TCS is very hygroscopic I found that SAM formed readily in ambient air as long as the solvent was dry. The reaction mechanism was also hydrolysis of the TCS groups to silanol groups, possibly with residual water adsorbed on the silicon surfaces as well as traces in the organic solvent. The silanols would then quickly react with hydroxy groups on the native oxide surfaces, produced in the reducing environment of the base bath used to clean the silicon chips. Subsequent immersion in a basic solution would remove the protecting groups to expose the hydroxy groups. I ran experiments using both TFA and TCA TCS species to produce the hydroxy surface groups, but I found that the TFA protecting group is less stable compared to TCA groups, thus I focused more on TCA TCS for mixed monolayer studies.

After forming the mixed methyl/hydroxy TCS SAMs I characterized the 1st nucleotide surface density using XPS and iodinated U phosphoramidite. The results are show in Figure 3-6. The 1st nucleotide surface density showed an approximately linear relationship with the solution composition of the TCA silanes used to form the mixed SAM films. The direct relationship between the 1st nucleotide surface density and the proportion of TCA silanes in solution suggests that the TCS silanes are much more reactive towards the silicon surface, and that the adlayer formation kinetics far outweigh any thermodynamic differences in the solubility of the different TCS silane species. In other words SAM formation using TCS is driven by reaction kinetics, and the kinetics of the methyl terminated TCS is very similar to the TFA or TCA TCS. The experimental

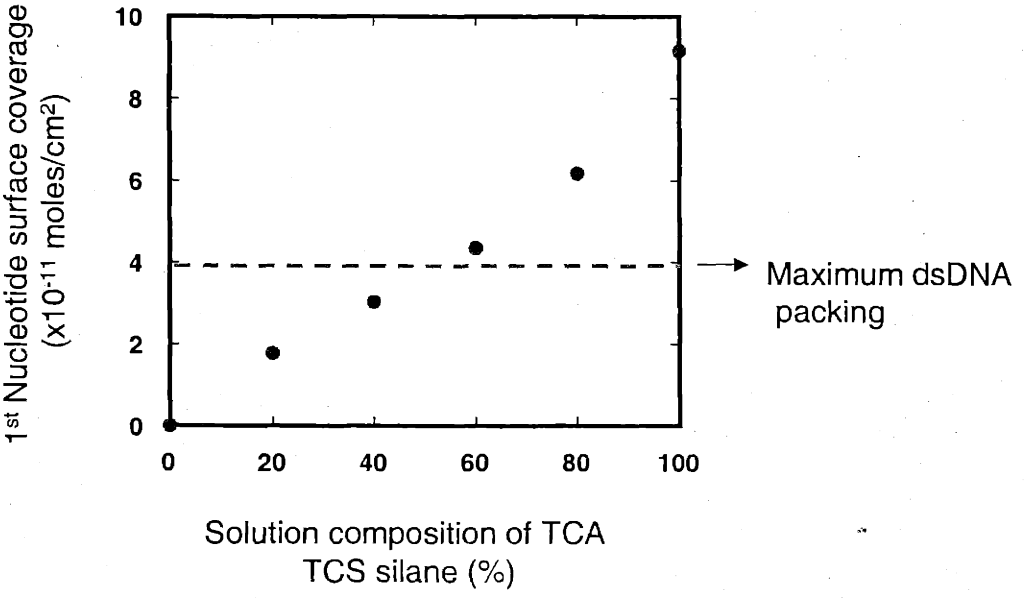

Figure 3-6. 1st nucleotide surface coverage versus TCA solution composition. The relationship between 1st nucleotide surface coverage and the proportion of TCA TCS silane in a mixture of TCA and dodecyl TCS silanes is approximately linear. The blue dashed line represents the theoretically calculated maximum packing density for vertically oriented dsDNA duplexes on a surface, assuming an effective hydrodynamic radius of 13Å.

results clearly indicate that the mixed TCA strategy provides an ability to tailor the surface hydroxyl content and consequently to control the surface density of immobilized nucleotides by simple changes in the solution composition of silane used to provide sites for surface attachment. I note that the maximum surface density of uracil on a pure TCA-derived surface was about 80% that on a glycol-terminated surface. This difference may result from the glycol groups having two hydroxyl groups per silane chain that are available for reaction and might allow a 1st nucleotide surface coverage.

The XPS experiments using iodine labeled U to determine the 1st nucleotide surface density demonstrated the ability to control the oligo surface density by the appropriate choice of silane SAM systems and by using the proper silane solution compositions. However, since my proposal to end-immobilize dsDNA onto the surface requires hybridization of a solution phase oligo to a immobilized oligo to form a short dsDNA double helix, I need to carefully consider the affect of the surface oligo density on the hybridization efficiency. The diameter of the dsDNA double helix is 20 Å, which is at least twice the footprint of an immobilized nucleotide. In addition, the DNA hydrodynamic radius is dependent on the solution ion concentration, since the DNA backbone is negatively charged. At 1M salt concentrations the effective DNA diameter is approximately 21 Å[7]. Therefore a densely packed oligo surface may not provide the necessary space in order to the solution phase complementary oligo to form a double helix.

In addition to the steric hindrance caused by the surface oligo chains, there is electrostatic repulsion between the negatively charged oligos that may further inhibit hybridization on the surface. The electrostatic repulsion may be minimized by performing the hybridization reaction in buffers with high concentrations (>1M) of sodium ions. The salts screen the negatively charged oligo chains and greatly reduce the effective hydrodynamic radius of the dsDNA. However, the physical space available for hybridization in a brush like array of immobilized oligos should present a definite limit on the amount of DNA hybridized onto the surface. I determined the theoretical maximum packing density for dsDNA on a surface by modeling the double helix as a 26

Å x 26 Å square, and assumed the maximum packing would occur when the squares were adjacent to one another. Although modeling the double helices as 26 Å diameter cylinders and using a close-packed hexagonal structure would increase the packing density, the squares were a more realistic representation due to the residual electrostatic repulsion effects and other possible defects in the lattice.

Using this footprint I estimated that the maximum number of dsDNA that could be packed vertically onto a surface was 3.2×10^{-11} moles/cm^2. This value is shown as a dashed line in Figure 3-6, and is only about one third of the maximum packing observed for single nucleotides on a 2 D silane surface. The lower dsDNA packing density suggests that a very dense oligo surface density is not necessary for efficient DNA hybridization at the surface, and that perhaps the densely packed oligo chains could even inhibit or prevent hybridization from taking place due to unfavorable steric and electrostatic effects. Furthermore, it is possible that the steric hindrance from a densely packed surface could interfere with the stepwise oligo synthesis reaction and reduces the reaction efficiency, thereby decreasing the yield of full length oligo chains with the correct sequence synthesized on the SAM surface. Therefore I decided to use all the above silane SAM systems to conduct a systematic study of the effect of surface hydroxy density of the silane SAM on the fidelity and yield of the synthesized oligo chains, as well as on DNA hybridization on the surface.

3.4 Stepwise synthesis of oligo layers

3.4.1 Oligo synthesis overview

After producing and characterizing the various hydroxyl surface films on silicon surfaces, oligonucleotide chains were synthesized on these reactive surfaces by standard phosphoramidite chemistry using an automated oligo synthesizer. The synthesis cycle consists of four basic steps, detritylation, coupling, capping and oxidation, and the reaction chemistry is diagrammed in detail in Figure 3-7. First, the acid labile dimethyl

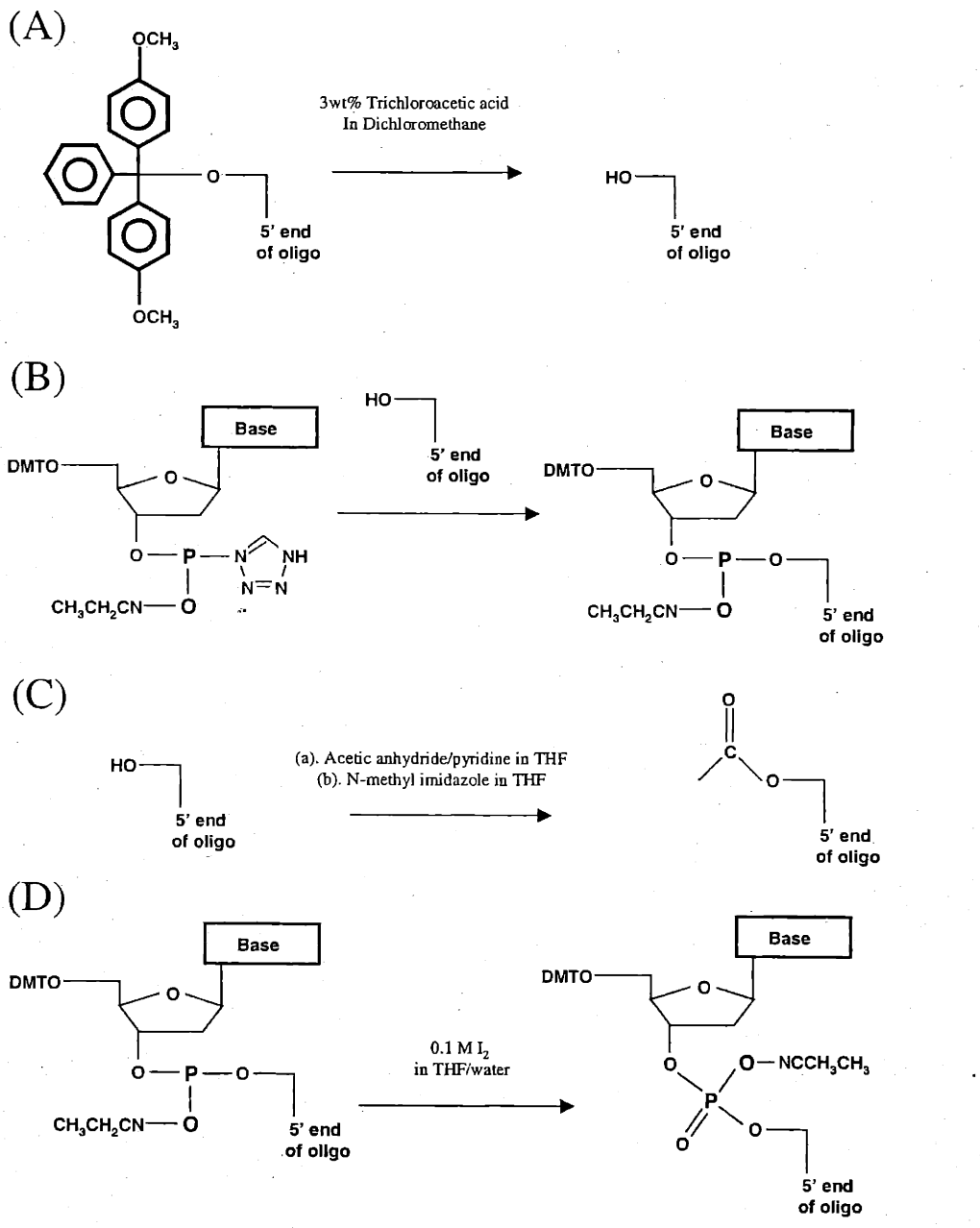

Figure 3-7. The basic reactions of phosphoramidite based synthesis chemistry of oligonucleotides. (a) deprotection of the 5' OH group; (b) coupling reaction attaches an activated phosphoramidite at 5' end; (c) capping reaction protects uncoupled 5' OH groups; (d) oxidation of triphosphate to pentavalent phosphate completes synthesis cycle.

trityl (DMT) protecting group is removed from the 5' end of an immobilized oligo with 3wt% trichloroacetic acid in dimethylformamide (DMF), to expose the reactive hydroxyl group. Next, a phosphoramidite in solution is activated on the 3' end with tetrazole, and the incoming activated tetrazoyl phosphoramidite is coupled to the 5' hydroxyl group of the immobilized oligo. Next, unreacted 5' end hydroxyl groups on the surface are capped with acetic anhydride, activated with n-methyl imidazole to produce an acetylating reagent, to prevent unwanted side reactions that would result in incorrect sequences and shorter chain lengths.

Finally, a 0.1 M iodine in a solution mixture of water and THF is used to oxidize the chemically unstable phosphite triester group to form a stable pentavalent phosphate triester entity, which is not susceptible cleavage by acidic agents such as the trichloroacetic acid/DCM solution subsequently used to deprotect the 5' DMT group of the coupled nucleotide. The oxidation reaction completes the oligo addition cycle, and with each subsequent cycle another oligo is added stepwise to the surface-immobilized oligo chain. Upon completion the oligos are exposed to 28wt% $NH_4OH_{(aq)}$, which cleaved the oligo chain from the surface, removed the cyanoethyl group from the phosphate triester to form an electronegative $P\text{-}O^-$ group, and also removed base protecting groups from the nucleotide bases to expose the amine groups necessary for the formation of hydrogen bonds during DNA hybridization.

3.4.2 Change in substrate reactive site for oligo synthesis

My system differed from standard phosphoramidite chemistry in many ways, based mainly on the critical difference in the product's application, resulting in a radical shift in design philosophy and strategy. Traditionally oligos produced by automated synthesis have been used as short chain PCR primers. Since PCR is a solution-phase reaction, the oligo primers must be readily cleavable from the synthesis support. Therefore the solid support for oligo primer synthesis consisted of long chain alkylaminosilanes (LCAA) derivatized onto a silica surface. Next, the 3' end of the 1st nucleotide to be attached to

the surface is derivatized with succinic anhydride to form and ester bond, then the succinate group is activated and forms a covalent peptide bond with the amino group on the LCAA film). The ester bond is base-labile and easily cleaved with $NH_4OH_{(aq)}$ to release the oligo chain into solution.

However, my system requires that the oligo chains are chemically stable and remain attached to the surface under a variety of conditions. Thus, instead of using LCAA on controlled pore glass, I used hydroxy terminated silanes. I chose the hydroxy groups because they form a phosphate bond with the nucleotides, which is the same bond present in the oligo and dsDNA backbones. Previous research showed that DNA chains are chemically stable in basic conditions of up to pH = 14, therefore the synthesized oligo chain would not be cleaved from the silane SAM surface by a strong base such as $NH_4OH_{(aq)}$. A schematic comparing the two oligo surface attachment chemistries is shown in Figure 3-8.

3.4.3 Change in deprotection chemistry

The next major difference was in the deprotection chemistry. Figure 3-9a shows the various functional groups that protect the primary amines on the nucleoside bases from being exposed during the oligo synthesis reaction, to prevent unwanted side reactions from occurring. The protecting groups are fairly stable and only removed by exposure to a strong ammoniolysis agent such as $NH_4OH_{(aq)}$ at elevated temperatures (80° C) for 1 hour or at room temperature for long periods of time (4-16 hours).

However, the $NH_4OH_{(aq)}$ was also a strong base that readily removed the synthesized oligo chains from the surface[8-10]. This phenomena was observed by researchers such as *Southern*, and was responsible for a 20 fold decrease in oligo surface density after a few hours of exposure and almost complete degradation of the surface in 24 hours or high temperature[8]. Also, *Fodor* determined the surface coverage of their OH silane films was

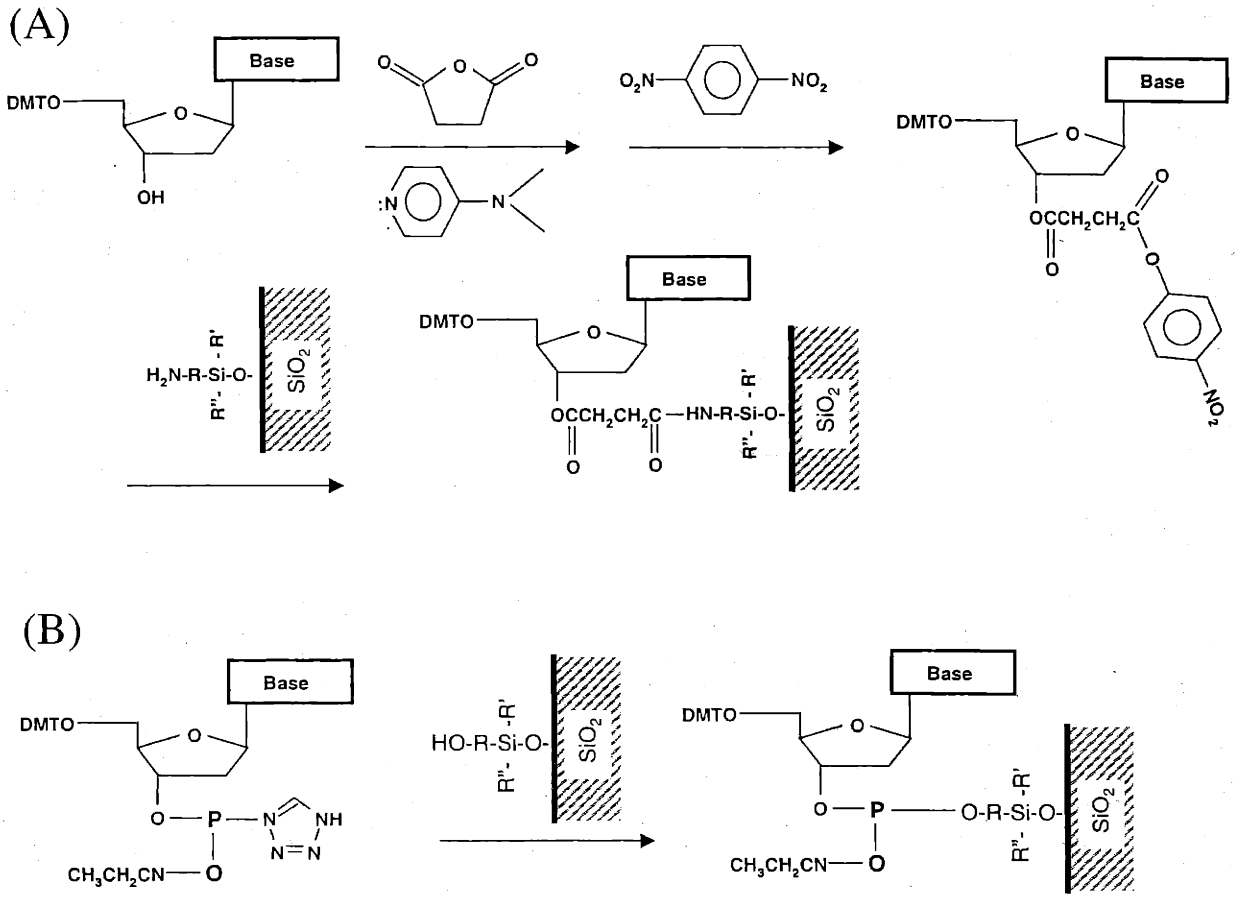

Figure 3-8. A graphical comparison of the nucleotide surface attachment chemistry. (a) standard attachment of phosphoramidites onto CPG substrate via the hydrolytic ester bond; (b) my attachment protocol forms a phosphate bond that is not sensitive to basic solutions.

about $1\text{-}3x10^{-12}$ moles/cm^2. This value is much lower than the approximate monolayer value of $7.2x10^{-10}$ moles/cm^2 I determined using XPS with iodinated propyl silanes. The large discrepancy is possibly due to removal of the majority of OH silane molecules by $NH_4OH_{(aq)}$. I conducted studies on the mechanism for base-induced desorption using oligo surfaces and iodinated silane SAMs, with XPS data from iodine labeled 1st nucleotide surfaces exposed to 28wt% $NH_4OH_{(aq)}$ for various time periods shown in Figure 3-10a, while Figure 3-10b shows results from exposure of iodopropyl silane SAMs to 1 M NaOH for various time periods.

I found that even at room temperature approximately 50% of the surface-attached oligos were removed after 15 minutes of immersion, and the attached oligos were completely removed after 24 hours immersion. Thus the majority of the surface-immobilized oligo chains would be removed into solution even before they are effectively deprotected and useful for hybridization experiments. In addition, I determined that desorption was due to cleavage of the siloxane bond between the silicon atom on the silane chain and the silicon oxide substrate, rather than the stable phosphate bond between the oligo chain and the silane hydroxy group. Since I need to control the oligo surface density for my studies, any damage to the surface was unfavorable. An alternative would be to try and control the extent of oligo desorption by manipulating the exposure time of the oligo surfaces to the basic solution. However, repeated experiments indicated the lack of consistent relationship between the exposure time of the oligo surface to basic solution and the amount of oligos desorbed from the surface, and also indicated that the quality of the oligo surfaces was degraded after prolonged exposure to the 28wt% $NH_4OH_{(aq)}$. Therefore I considered a more reasonable approach of using phosphoramidites with more labile base-protecting groups that could be removed under more mild conditions.

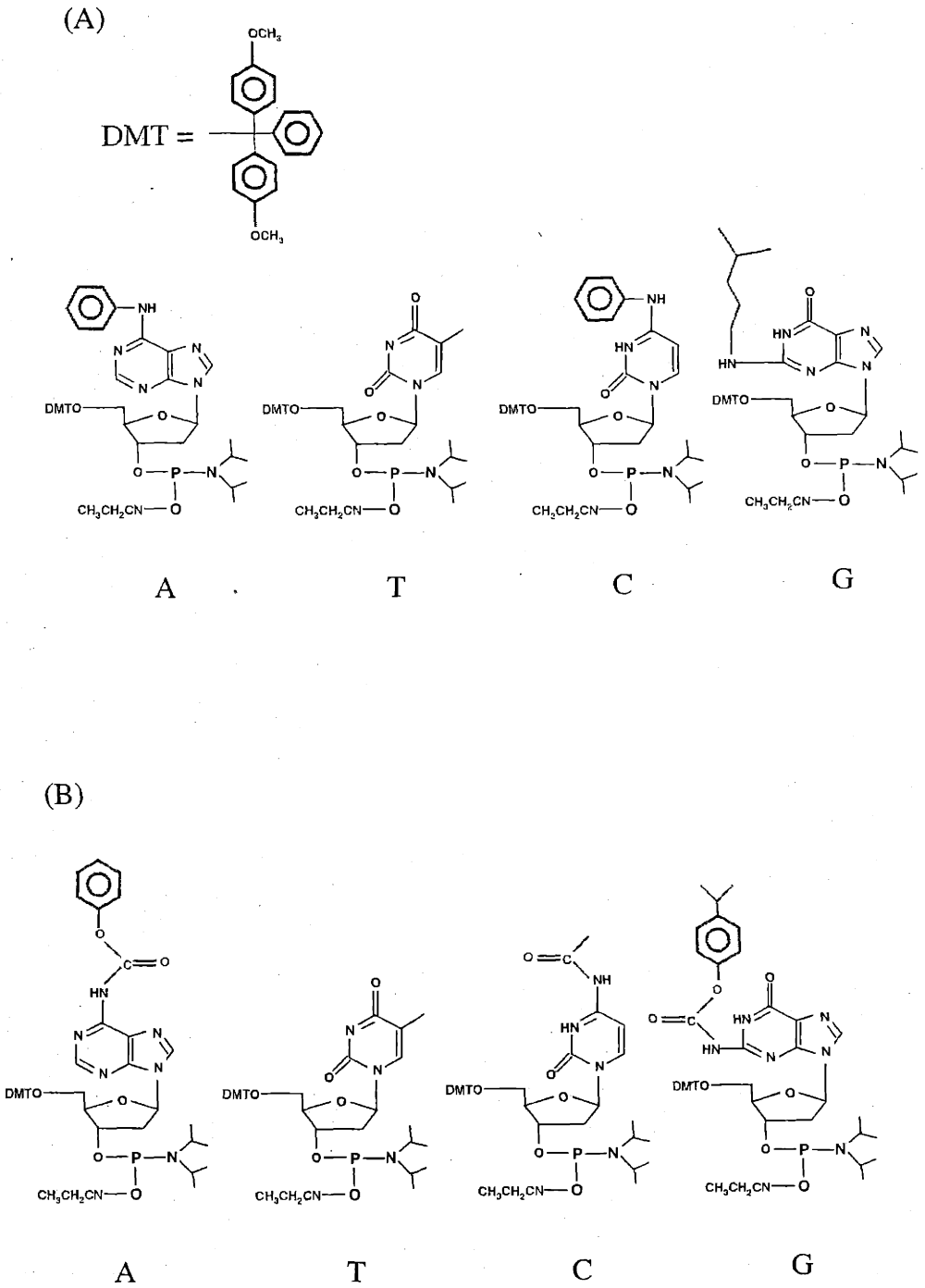

Figure 3-9. Structures of traditional and UltraMILD® phosphoramidite reagents: (a) regular protecting groups are removed by strong bases such as 28 wt% $NH_4OH_{(aq)}$; (b) UltraMILD® protecting groups are more labile and are removed by milder deprotecting agents such as 0.05 M K_2CO_3 in methanol and 20 v/v% piperidine in DMF.

(A)

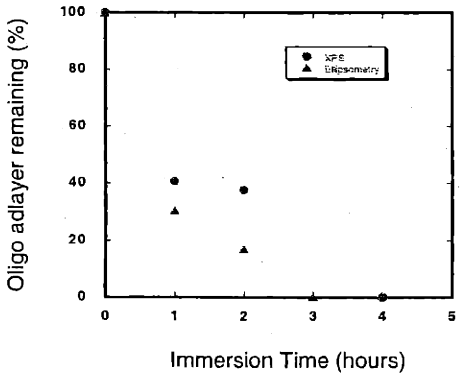

(B)

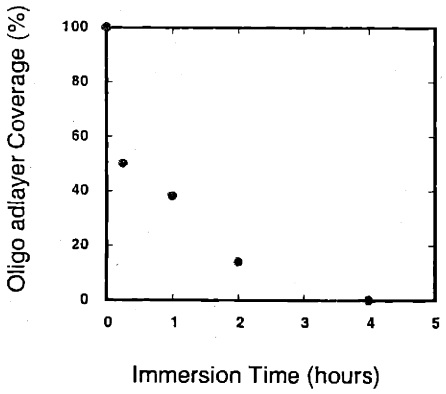

Figure 3-10. Effect of NH_4OH exposure on the stability of oligo surfaces: (a) The oligo surface coverage decreases with increased immersion in $NH_4OH_{(aq)}$, and is totally removed after 3 hours; (b) experiments conducted with iodosilane SAMs immersed in $NH_4OH_{(aq)}$ prove that the silane itself is being desorbed by the strong base.

Thus, my oligo synthesis strategy would be to produce oligo chains with optimal coupling efficiency and sequence fidelity, and choose deprotection protocols that preserved the synthesized oligo chains on the surface, and control the oligo surface density strictly by modifying the silicon substrate with the appropriate silane SAM films to create the proper 1st nucleotide surface density. Instead of using traditional base protecting groups for the phosphoramidites, I used UltraMILD® phosphoramidites, shown in Figure 3-9b. The UltraMILD® groups are more labile compared to the regular base protecting groups, and are removed by a variety of mild chemical agents at room temperature.

Next, four alternative deprotection protocols were studied concurrently using surface-immobilized oligo chains synthesized with UltraMILD® phosphoramidites. Either 0.05 M potassium carbonated (K_2CO_3) in anhydrous methanol (MeOH), or a 28wt% $NH_4OH_{(aq)}$ solution was used to remove the base protecting groups. Next, either 20wt % piperidine in dimethyl formamide (DMF), or 28wt% NH_4OH was used to deprotect the cyanoethyl groups and create the hydrophilic $P\text{-}O^-$ groups. All deprotection reactions were carried out at ambient temperature and pressure. Both XPS and ellipsometry were used to determine the amount of surface-immobilized oligo chains (labeled with iodinated U) remaining after treatment with the various deprotecting protocols, by comparing the data values for the oligo surfaces before, and after chemical deprotection.

In addition, hybridization experiments were performed using ^{32}P-labeled complementary oligo sequences in solution to challenge the surface-immobilized oligo sequence deprotected by the various chemical agents. The amount of radiolabeled oligo hybridized to the complementary oligo surfaces were quantified by liquid scintillation counting to discern whether the deprotection protocols were successful, because only exposed amine groups can form the hydrogen bonds necessary for DNA hybridization. In

addition, the dsDNA double helix will only form if the oligo phosphate backbone contains the electronegative P-O^- group rather than the hydrophobic β-cyanoethyl group.

The complementary target oligo is radiolabeled in solution using the enzyme terminal transferase, which adds the radioactive α^{32}P-dCTP onto the 3' end of the oligo chain, consuming 2 ATP molecules in the process. Terminal transferase was chosen because the synthesized oligo chains are oriented with their 3' end adjacent to the silane surface and their 5' end distal to the surface. Since DNA hybridization occurs in an antiparallel manner, having extra C nucleotides attached at the 3' end of the target oligo should not significantly hinder or restrict the hybridization reaction. In addition, because the effective enzymatic activity of the terminal transferase added to the solution was approximately 100 times higher than what is required to completely attach all the ^{32}P-dCTP to the oligos, the reaction is essential proceeds to completion with a quantitative yield. A 20% acrylamide gel was run on the labeled oligos to confirm the reaction efficiency, and an autoradiograph is shown if Figure 3-11. The single spot corresponds to the radiolabeled oligos, and the lack of radioactive signal downstream of the oligo spot indicates that the reaction efficiency is very close to 100%. Since the amount of oligo added to the terminal transferase solution mixture is known, the activity of the radiolabeled oligo is determined by measuring the radioactive signal equivalent to the amount of ^{32}P-dCTP added to the reaction mixture using scintillation counting, then dividing the signal intensity by the amount of oligo in the solution mix. Furthermore, the lack of free ^{32}P-dCTP in solution after reaction, and the ability to add a surfactant to the labeled oligo solution after the transferase reaction was complete, enabled me to minimize the effects of nonspecific adsorption during the surface hybridization reactions. After the addition reaction I solvated the labeled oligos in an aqueous 7xSSC buffer with 0.1wt% SDS, to form a 0.5 μM oligo solution, and the hybridization reaction was carried out by immersing the oligo surfaces in the oligo solution at 4° C for 24 hours. This protocol was used by *Brown* to hybridize his cDNA target to the surface immobilized probe DNA on his microspot arrays.

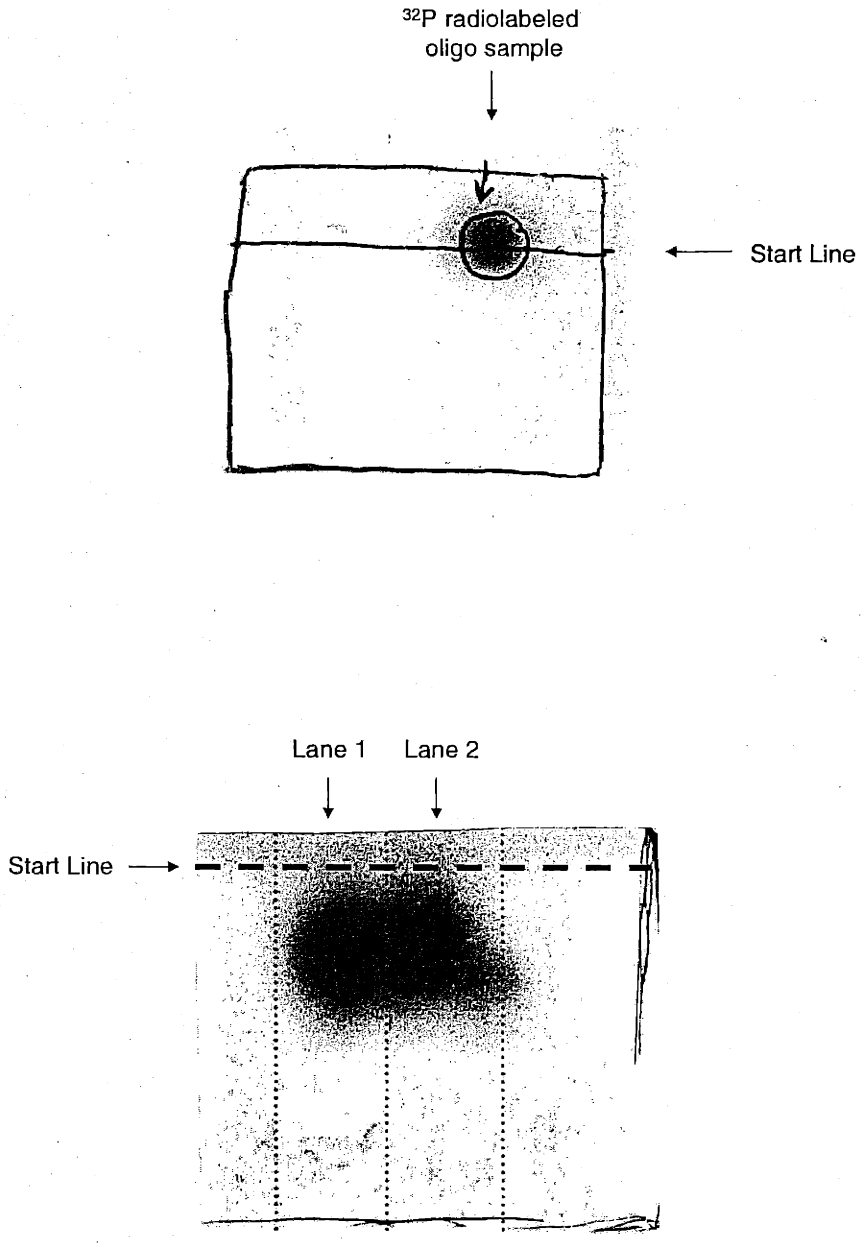

Figure 3-11. Autoradiographs of 20wt% acrylamide gels of 10mer oligos labeled with ^{32}P-dCTP using terminal transferase. Both slides show a discrete spot in each lane corresponding to the labeled oligo chain, and no downstream streaking of the radiaoactive signal, suggesting an absence of free ^{32}P-dCTP molecules.

The results of the tests conducted on the various mild deprotection protocols are presented in Table 3-2. It is clear that regardless of the type of silane surface used as the oligo synthesis substrate, the K_2CO_3/MeOH and piperidine/DMF combination resulted in no loss of surface-attached oligo chains, and also had the highest amount of radiolabeled complementary oligos hybridized to the surface, as determined by the ^{32}P signal from scintillation counting.

On the other hand, the $NH_4OH_{(aq)}$ drastically degraded the oligo surface and had the lowest hybridization signal. This trend was consistently demonstrated for a variety of surface oligo sequences, and the surface degradation was sometimes visible without the aid of microscopy. Finally, control sequences that lacked either the K_2CO_3/MeOH, or piperidine/DMF deprotection protocols had only background radiation signals of about 50 cpm, indicating that the mild deprotecting agents effectively removed the relevant protecting groups and activated the surface-immobilized oligo chains for hybridization. Thus I concluded that the K_2CO_3/MeOH and piperidine/DMF combination effectively deprotects the surface oligos without damaging the oligo adlayer, and provides significantly higher quantities of hybridized oligos than $NH_4OH_{(aq)}$. Finally, the data in Table 3-2 also indicated that oligo surfaces synthesized on the OH-terminated surfaces had higher hybridization signals compared to oligo surfaces synthesized on the glycol-terminated surfaces. This result was repeatedly observed with different oligo sequences, and suggested a possible relationship between the density of the surface-immobilized oligo chains and the amount of solution-phase complementary oligos that could be hybridized to these oligo surfaces.

Table 3-2. A comparison of the various deprotection protocols, including traditional agents used for PCR primer synthesis and the mild agents used to remove the UltraMILD® protecting groups. The remaining oligo coverage (%) is determined by comparing the oligo surfaces before and after deprotection, using XPS with iodinated Uracil, and by ellipsometry. The results show that mild deprotection does not remove the surface oligo chains. Next, hybridization reactions with radiolabeled complementary solution oligos were used to determine whether the deprotected surface oligo chains are functional. Regardless of the silane SAM substrate the deprotected UltraMILD® oligo chains consistently had the best hybridization yields and efficiency, suggesting that the deprotection was successful.

Deprotection Protocol	Coverage Remaining (%)	^{32}P signal on glycol linked oligo (cpm)	^{32}P signal on OH linked oligo (cpm)
K_2CO_3/MeOH & Piperidine/DMF	100	4276	13638
NH_4OH Piperidine/DMF	27	2220	6384
K_2CO_3/MeOH & NH_4OH	45	294	2082
NH_4OH	5	198	2548

* K_2CO_3/MeOH = 0.05 M K_2CO_3 in anhydrous methanol for 8 hrs, Piperidine/DMF = 20 wt% piperidine in dimethyl formamide for 4 hrs, NH_4OH = 28 wt% $NH_4OH_{(aq)}$ for 1-3 hrs

3.4.4 XPS characterization of coupling efficiency

The final difference in my approach compared to traditional primer synthesis is the characterization method for determining reaction yields during the automated synthesis. For traditional PCR primer synthesis the coupling efficiency and reaction yields are determined by UV-VIS spectroscopy. The DMT protecting group is a strong chromophore with λ_{ab} = 498 nm. The DMT groups removed from the oligo surfaces by

trichloroacetic acid in DMF is washed with acetonitrile, and the aliquots are collected and analyzed with a spectrometer. Using Beer's law, amount of DMT in solution is determined:

$$A = E \times C \times L$$

Where A = absorbance , E = extinction coefficient ($M^{-1}cm^{-1}$), C = concentration (M), L = path length (cm).

Assuming that the deprotection efficiency is close to 100%, the DMT concentration is representative of the amount of nucleotides added onto the surface oligo chain in the previous cycle, and by comparing the DMT concentration of different reaction cycles it is possible to calculate the coupling efficiency of the synthesis reaction. However, for my systems the total amount of nucleotides added onto the surface during each reaction cycle is below the minimum detection threshold of the UV-VIS spectrometer. In fact, a very high background absorbance signal was obtained when running control experiments using empty synthesis columns. The DMT signals were the product of phosphoramidite contaminants nonspecifically adsorbed onto polypropylene frits on both ends of the reaction chamber. Thus, I needed to develop an alternative characterization strategy with the appropriate specificity and sensitivity require for quantifying the oligo surface density at any stage or cycle of the oligo synthesis reaction. Once again, I utilized XPS and iodine-labeled U phsophoramidites to characterize the stepwise oligo synthesis efficiency and the resulting oligo surface density.

3.4.5 Oligo surface density determined by XPS

Surface-immobilized oligos of various lengths (10-20 mers) and discrete sequences were synthesized on silicon surfaces with different hydroxyl group densities, to study how the surface density of the 1st nucleotide added to the hydroxyl surface film (as previously determined by iodine-labeled U phosphoramidites and XPS characterization), and the synthesis reaction conditions, could affect both the sequence fidelity of the

surface-immobilized oligos, as well as the surface density of full length oligo chains available for hybridization.

The major factor thought to influence oligo surface density and sequence fidelity during synthesis was the coupling of the incoming activated phosphoramidite in solution to the reactive 5' hydroxy end of the surface-attached oligo chain. The stepwise efficiency of this coupling reaction is critical to the amount of full-length oligo chains produced upon completion of the oligo synthesis. For example, *Fodor* only achieved about 96% coupling efficiency using phosphoramidites with photolabile 5' protecting groups, possibly due to the decreased efficiency of the photoactivated 5' hydroxy deprotection reaction. Therefore after synthesis of a 10 mer only 65% of the surface oligos would be the correct sequence and length. On the other hand the coupling efficiency for traditional PCR primer synthesis on CPG substrates is routinely over 99%, and I would like to achieve the same efficiency on flat silicon substrates as well.

To measure the oligo coupling efficiencies iodine-labeled U phosphoramidites were utilized again, along with XPS characterization. First, a single iodine-labeled U was immobilized onto a hydroxyl surface film, and the 1st nucleotide surface density was determined by its iodine signal using XPS. The iodine signal intensity was measured as I_o. Next, an oligo sequence n bases in length was synthesized onto another hydroxy surface film with the same surface hydroxy group density, and the final nucleotide added was an iodine-labeled U. XPS was again used to determine the iodine signal intensity for the n-mer, as I_n. Subsequently, the coupling efficiency was calculated by the following equation:

$$Efficiency = \left(\frac{I_n}{I_o}\right)^{\frac{1}{n}} \times 100$$

Generally, the iodine signals obtained by XPS had errors within 5 %, and were very reproducible.

$$\%\text{Efficiency} = 100 \times \left(\frac{I_n}{I_o}\right)^{\frac{1}{n}}$$

3.4.6 Effect of steric hindrance on coupling efficiency

Oligo surfaces were produced using standard cyanoethyl cycles with a coupling reaction time of 25 seconds. I used a variety of silane SAMs with different hydroxy group density, including GOPS silane , OH silane and mixed TCS surfaces to study the effect of the steric hindrance on oligo coupling efficiency. The XPS data for coupling efficiency for synthesized 10 mer poly T oligos with respect to the 1st nucleotide surface coverage are presented in Figure 3-12. It is evident from this plot that the coupling efficiency decreases steadily with increasing surface density of the 1st nucleotide attached to the silane films, suggesting that steric hindrance has a significant effect on the oligo coupling efficiency, and consequently on the amount of full length surface oligos available for hybridization.

In addition, the coupling efficiencies also decreased by 1-2% for oligo chains over 12 nt in length, possibly also due to steric hindrance, though for shorter chain oligos there was no decrease in coupling efficiency with length. For coded sequences such as 5'->ATGGTGAGTTTT->3' the efficiencies were generally lower by 1-2 % compared to poly T oligos of comparable length, suggesting there are differences in the reactivity of the different nucleotide bases. This phenomena is supported in the literature by previous studies showing that phosphoramidite reactivity indeed varies with the base species, with T being the most efficient, followed by C, G, and A.

The 92% coupling efficiency for oligos synthesized on the surface is obviously unacceptable, but as the 1st nucleotide surface density decreased the efficiency increased until it reached 99% for silane surfaces with less than 40% of the 1st nucleotide density (4.8×10^{-10} moles/cm^2) compared to GOPS SAMs. By modifying the silane surface films, either by using the OH-terminated surfaces, which has a lower hydroxy surface density, or by using mixed hydroxyl-methyl terminated surfaces as the synthesis substrate, I could produce oligo surfaces with the proper density for achieving a 99% coupling efficiency. However, further tests showed that the oligo coupling efficiency still decreased slightly when synthesizing coded sequences or when the oligo chain length is above 12 nt in

length, even for less densely packed oligo surfaces synthesized on OH silane or mixed TCS surfaces. Perhaps other changes in the reaction protocol could help increase the coupling efficiency in such cases. I manipulated reaction conditions such as reactant concentration or coupling time to increase the coupling efficiency for a particular surface density. For these studies I chose the GOPS silane surfaces to test my hypothesis on the effect of steric hindrance on oligo coupling efficiency because the densely packed hydroxy groups created the maximum possible 1st nucleotide packing density on the surface.

3.4.7 Coupling time and coupling efficiency

Since the nucleotides are already densely packed it should maximize the effect of steric hindrance on coupling efficiencies. Therefore an improvement in coupling efficiency would be remarkable and obvious. Diluting the phosphoramidite concentration by a factor of 2 or 4 did not result in any decrease in the coupling efficiency. This is probably because the phosphoramidite concentration is 0.1M, while the surface density of the reactive hydroxy groups is only about 10^{-11} to 10^{-10} moles/cm^2. Thus, there is a large excess (>1000 fold) of activated phosphoramidites compared to the surface hydroxy group, and a slight dilution should not significantly affect the reaction or diffusion kinetics. On the other hand, efforts to increase coupling efficiency by manipulating the coupling time were successful and are shown in Figure 3-13.

It is clear that as coupling time exceeds 75 seconds the coupling efficiency is optimized even for oligos synthesized on the densely packed, sterically hindered GOPS silane surfaces. Thus, after adjusting the coupling reaction time to above 75 seconds, and using hydroxyl surface films that immobilized less than 40% of the maximum 1st nucleotide surface density (such as the hydroxy-terminated surfaces), higher than 99 % efficiencies were regularly achieved for 20 mer oligos with coded sequences. Consequently, longer chain, discretely coded oligo surfaces could be consistently produced while maintaining a high degree of sequence fidelity.

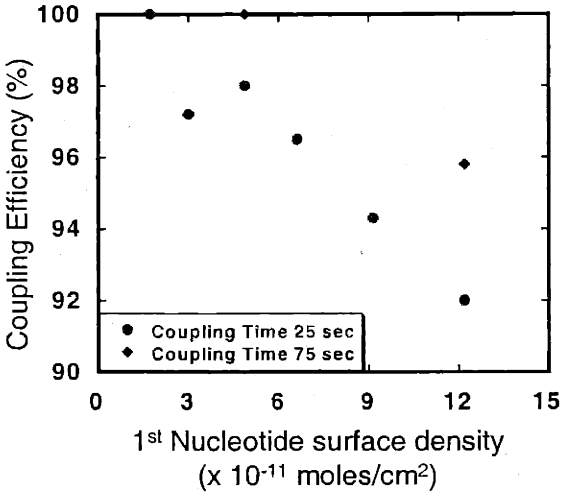

Figure 3-12. Relationship between the stepwise coupling efficiency and the 1st nucleotide surface density during oligo synthesis on the surface. As the surface coverage increases, the coupling efficiency steadily decreases. However, by choosing the appropriate 1st nucleotide surface coverage and increasing the coupling reaction time close to 100% efficiency is achieved.

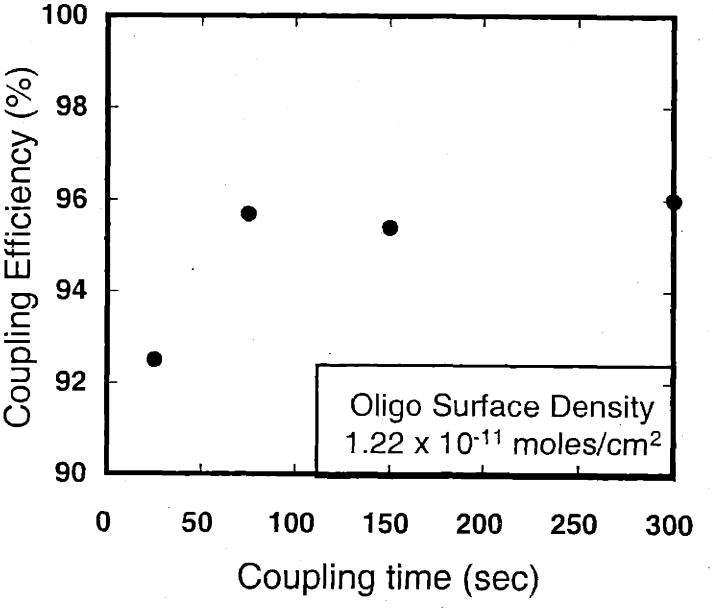

Figure 3-13. Coupling efficiency against coupling time. Iodine-labeled oligos were synthesized on GOPS silane substrates to observe the relationship between the stepwise coupling efficiency and coupling time. GOPS substrate was used because it provides the maximum packing density of 1st nucleotides and the lowest coupling efficiency at 25 second coupling time, possibly due to steric hindrance. Thus the GOPS substrate should be the most sensitive towards changes in coupling time. The results show that the coupling efficiency reaches a maximum at coupling times higher than 75 seconds.

3.4.8 Capping efficiency

The proportion of full-length oligos synthesized is dependent not only on the coupling reaction efficiency, but also on the capping efficiency. The unreacted 5' OH groups on the surface-immobilized oligo chains must be effectively capped with acetyl protecting groups to prevent them from reacting with activated phosphoramidites in solution during subsequent coupling reaction cycles. Such untoward reactions could significantly reduce the sequence fidelity of the surface-immobilized oligo chains. Thus, capping efficiencies were studied for OH silane and GOPS silane surfaces, using iodine-labeled U phosphoramidites and XPS characterization.

First, the oligo synthesis cycle was modified to jump from the 5' OH detritylation step directly to the capping step without running a coupling reaction. Next, the acetyl-capped surface was exposed to an activated iodine-labeled uracil phosphoramidite (I-UPA), and two additional nucleotides were added subsequent to labeling, to displace any nonspecifically adsorbed I-UPA from the oligo surface. The presence of any iodine signal during XPS would indicate a failure in the capping process, and would reduce the proportion of full length oligos produced, as well as degrade the sequence fidelity of the oligo chains. In addition, some samples were produced on capped hydroxyl surface films, where three nucleotides were added prior to the iodine-labeled uracil, to determine if the acetyl protecting groups added to cap the surface hydroxy groups on the silane SAMs remained chemically stable during subsequent synthesis cycles.

The XPS results indicated that the capping efficiencies were consistently at 100%, and that the acetyl protecting groups remained stable to chemical attack during subsequent synthesis. The exception was the capping reaction for the GOPS silane surface after addition of one I-UPA, which was shown to be only 99% effective, and would result in the synthesis of about 6-7 % extra surface oligos that are shorter by one base. This is possibly due to the large number hydroxy groups on the GOPS silane surface, some of which may be sterically hindered from reacting with the acetyl

protecting groups during the short (4 second) reaction time. However, for surface films with lower surface hydroxy densities such as the OH silane surfaces, the capping efficiency improved to 100%, thus minimizing the impact of low capping efficiency to only oligos synthesized on surface films with very high hydroxy density such as GOPS silane surfaces.

3.4.9 Comparison of synthesized oligo surface coverage with literature values

After determining the reaction conditions and the deprotection protocols that provided the optimal sequence fidelity and maximum yield of full-length oligos attached on the silicon surface, I were able to consistently synthesize oligo surfaces with a coverage density of up to $8x10^{-11}$ moles/cm^2. My surface oligo density was at least one order of magnitude higher compared to most flat, 2-D oligo surfaces produced by covalent attachment of an oligo with an amine, thiol, or biotin linker to an activated surface, regardless of the surface chemistry[11-19 20-23].

Two other research groups achieved oligo surface coverages in the 10^{-11}moles/cm^2 range on a flat surface, using bifunctional crosslinkers to immobilize oligos with amino or thiol linkers[24,25]. However, when I tried to reproduce their results I encounter significant difficulties in obtaining the any coverage in aqueous buffers, and when the thiol-linked oligos were dissolved at concentrations in an organic solvent the nonspecific adsorption of oligos outcompeted the surface crosslinking reaction and covered all the reactive sites on the surface, effectively inhibiting the covalent attachment from occurring. In addition, there is the possibility that when using bifunctional crosslinkers or other covalent attachment methods, of side reactions with functional groups on the nucleotide bases instead of the 5' end linkers[15,18].

Other researchers polymerized micron thick-acrylamide gels that incorporated, or covalently attached oligo chains to derivatized and activated polymer fibers or plates. Although these 3-D structures had a higher overall oligo density in the 10^{-9} moles/cm^2

range the actual coverage per layer was about 10^{-12} moles/cm[29,26-31]. In addition, there are questions on what amount of oligos entrapped within the polymer network are available for hybridization, as well as how the target diffusion through the gel or fiber structure would affect the hybridization kinetics. Therefore I concluded that for my purposes stepwise oligo synthesis on the surface provided superior oligo surface density in a consistent and reliable manner, compared to covalent attachment methods.

Southern had achieved similar coverages of synthesized oligos[10,32]. However, since I utilized UltraMILD® phosphoramidites and mild deprotection agents, I are able to preserve the synthesized oligo chains, and thus the effective oligo surface coverage after deprotection was much higher than the oligo surfaces synthesized by Fodor ($3x10^{-12}$ moles/cm^2)[33,34] and Southern ($1x10^{-11}$ moles/cm^2)[35], who used highly basic $NH_4OH_{(aq)}$ for deprotection. Furthermore, my system had higher coupling efficiency (>99%) compared to Fodor's synthesis protocol (96%)[33,36,37]. The most important difference and critical advantage of my approach compared to other oligo synthesis or attachment methods is the ability to control the oligo surface density by manipulating the composition and chemical moeties of the silane SAM formed on the silicon surface.

As mentioned previously, it is not clear how the oligo surface density may affect DNA surface hybridization, either through steric hindrance or electrostatic repulsion, and what oligo surface density would maximize DNA hybridization. Previously *Southern* had shown qualitatively how steric factors affected hybridization, by inserting spacer molecules between the oligo chains and the surface[10]. My oligo synthesis strategy provided us with a powerful tool to systematically study these effects and determine the optimal oligo surface density for maximum DNA hybridization efficiency or yield. This was the topic of my subsequent research.

3.5 Hybridization efficiency

Researchers have performed hybridization studies on immobilized oligo arrays, and have obtained a wide range of data for hybridization amount[26,38-40] and efficiency[12,22-24,26,39,41-43]. However, no researcher has yet quantified the relationship between oligo surface coverage and hybridization. This is the goal for the following experiments.

3.5.1 Hybridization experimental conditions

Hybridization experiments were conducted with ^{32}P radiolabeled complementary oligo sequences in solution to examine the relationship between the oligo surface density and the amount and efficiency of DNA hybridized onto the surface. First, oligo chains with the appropriate sequences were synthesized on silicon surfaces modified with a mixed TCS film with various hydroxy/methyl compositions, to create surface-immobilized oligo chips with different surface densities. Next, 0.5 μM solutions of both complementary and control (noncomplementary) oligo sequences were labeled by the terminal transferase reaction and suspended in a high salt (7xSSC, approximately 1 M sodium chloride) solution with 0.1wt% SDS[27,28,38,39,44]. The high salt (sodium ion) concentrations were chosen to help facilitate DNA hybridization, which is dependent on the sodium ion concentration. The negatively charged surfactant SDS helped to prevent nonspecific DNA adsorption onto the surfaces, as shown in my previous studies. The specific activity of the oligo chains in solution was determined by using scintillation counting to determine the radioactivity of the solution, then dividing the radioactivity by the amount of oligo in solution.

3.5.2 Effect of T_m on hybridization

The hybridization efficiency of short chain oligos is highly dependent on the thermodynamic stability of the dsDNA duplex formed by the reaction. In turn, the stability of the dsDNA is represented by its T_m, which is dependent on a various factors and may be theoretically calculated by a variety of equations, such as the commonly used *Wallace* equation:

$$T_m = 4\times(\#GC) + 2\times(\#AT)$$

Where T_m is the melting temperature (°C), $\#GC$ = number of G or C in the DNA sequence, and $\#AT$ = number of A or T in the DNA sequence.

The most comprehensive T_m equation for short chain oligos was developed by *Jacobs et al.* , and took into account the DNA chain length, solution Na^+ ion concentration and the presence of organic denaturants such as formamide[45]. The equation is shown below:

$$T_m = 81.5 + 16.6 * \log M + 0.41 * (\%GC) - 0.61 * (\%\, formamide) - \frac{500}{L}$$

$$T_m = 81.5 + 16.6 \log\left(\frac{[Na^+]}{1 + 0.7[Na^+]}\right) + 0.41\times(\%GC) - \frac{500}{L} - 0.63\times(\%\, formamide)$$

Where T_m = melting temperature (°C), M = Na^+ ion concentration (M), $\%\ GC$ = percentage of GC content in the DNA sequence, $\%\ formamide$ = percentage of formamide in the solution, and L = DNA chain length.

It is evident from the above equation that the T_m is dependent on the proportion of GC hybrid in the sequence[23,46,47], since a GC hybrid is connected by three hydrogen bonds, and are thus more stable compared to an AT bp, which only has two hydrogen bonds. GC hybrids also have more favorable base stacking conformations, further improving their stability. In addition, the chain length is important since a higher number of hybridized bp increases the bond energy of the duplex, though at lengths above 50 bp or so the contribution of DNA chain length is diminished. Therefore I designed 10 nt oligo sequences with a relatively high GC content for the hybridization experiments to facilitate hybridization. Also, the hybridized oligos do not dissociate easily. In addition, the hybridization experiments were run at 4 °C, a temperature much lower than the T_m-25 °C needed for hybridization to occur. There is a risk of decreased stringency at the lower

hybridization temperature. But the effect of a mismatch on the T_m is high (8-12 °C)[48] for short 10 mer oligos, so the possibility of a mismatch occurring are still low at 4 °C.

In addition, irreversible DNA dissociation occurs at:

$$T_{dissociation} = 94 - \frac{820}{L} - 1.2 \times (100 - h)$$

Where L = oligo length, h=% homology between probe and target[49].

A 10 mer duplex will dissociate when washed by a 12 °C buffer. Thus, the temperature of the TE buffer wash solutions were also maintained at 4 °C to prevent any immobilized oligos from being lost by desorption.

3.5.3 Effect of salt concentration on hybridization

Sodium ion concentration is also a critical factor, and high salt concentrations usually facilitate DNA hybridization[50,51], by shifting the thermodynamic partitioning of the oligo chains away from the aqueous phase in favor of the organic phase (other oligo chains), a so-called "salting out" effect. Also, high ion concentrations screen the negatively charged oligo chains, decreasing the electrostatic repulsion effects that inhibit effective collisions of the oligo chains.

However, there were questions on whether a high (1M) salt concentration would be necessary for surface hybridization, and other researchers had proposed an alternative salt, tetramethyl ammonium chloride (TMACl), which they claimed facilitated DNA surface hybridization[50]. Thus, I hybridized radiolabeled 10mer oligos onto surface oligos produced on an OH silane SAM, using buffers with different salt concentrations and species. The results, shown in Figure 3-14, suggest that the amount of oligos hybridized onto the surface increases with NaCl salt concentration, and the difference is more significant at longer time periods (24 hrs). A comparison between 1M solutions of NaCl

and TMACl show that NaCl buffers result in 50% more DNA hybridization onto the surface, and that NaCl is the superior salt species for DNA surface hybridization.

Finally, organic denaturing agents such as formamide can destabilize the DNA double helix and thus their presence causes a decrease in the T_m[52]. DNA hybridization usually occurs at around T_m-25° C, and some protocols recommend that hybridization experiments be run at approximately this temperature to optimize the hybridization stringency and minimize mismatches. However, I prefer to maximize the amount of DNA hybridized to the surface, since the goal is to use the surface oligo chains as an attachment point for immobilizing a dsDNA instead of a probe molecule. Because the oligo surfaces are short, only about 10 mer in length, the dsDNA duplexes resulting from hybridization are also less thermodynamically stable and are highly dependent on the GC content. I wanted to use all the possible sequence combinations as addressable hybridization sites to form my surface oligo array, a lower hybridization temperature would drive the hybridization reaction towards equilibrium and improve the stability of the dsDNA duplex formed by the hybridization of short chain oligos. It also would diminish the differences in hybridization yield that would result from the different GC content in the 10mer oligo sequences. Therefore I chose a lower hybridization temperature and immersed the oligo surfaces in the radiolabeled oligo solutions for 24 hours at 4° C. The long hybridization times were chosen to drive the reaction towards equilibrium and minimize any kinetic effects. Later on, the kinetics of DNA hybridization as well as the hybridization stringency and the effect of mismatches on the hybridization efficiency will be explored.

3.5.4 Effect of steric hindrance on hybridization

After, the oligo chips were removed from solution and rinsed with cold (4° C) Tris-EDTA buffer to remove any excess solution and nonhybridized labeled oligos, liquid scintillation counting was used to quantify the amount of DNA hybridized onto the various oligo surfaces by comparing the radiation intensity of the ^{32}P labeled oligos

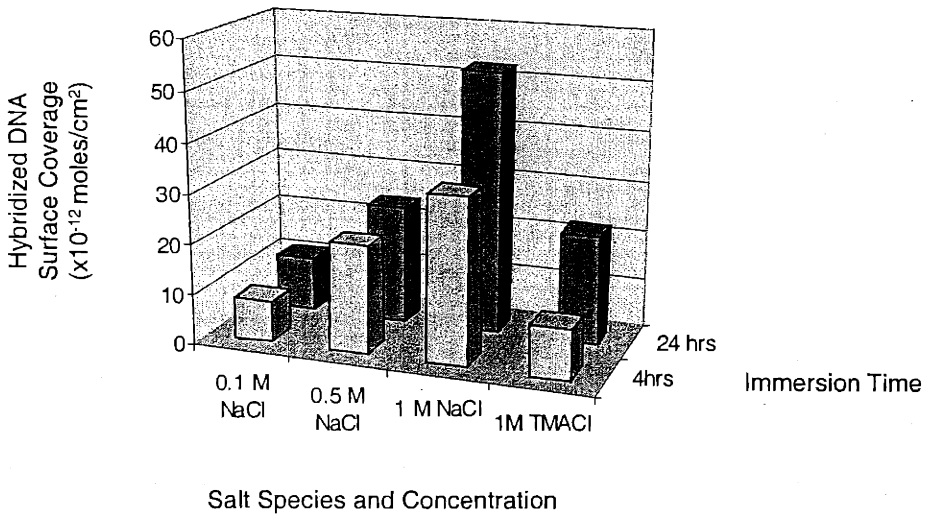

Figure 3-14. Effect of NaCl concentration on surface hybridization. The runs were conducted on oligo surfaces synthesized on OH silane substrates, at 4° C. The results show a consistent increase in surface hybridization with increased NaCl concentration, and that under comparable solution concentrations NaCl is superior to TMACl for affecting surface hybridization.

immobilized on the oligo chips, to the measured specific activity of the radiolabeled oligo solution. Also surface areas for each sample were measured to derive the surface density of the DNA hybridized to the oligo surfaces. The hybridization efficiency was determined by the equation:

$$\text{Hybridization efficiency} = \left(\frac{\text{Hybridized DNA surface density}}{\text{Surface density of full length oligos}} \right) \times 100$$

$$Efficiency = \left(\frac{N_{Rad}}{D \times A} \right) \times 100$$

Where N_{Rad} = number of radiolabeled oligos, D = surface oligo density, and A = sample surface.

The data obtained from hybridization experiments using the surface oligo sequence 5'->ATGGTGAGTTTT->3' are represented in Figures 3-15 and Figure 3-16. The spread in hybridized DNA surface density measured for different samples was between 10 to 15%, which is similar to hybridization experiments with other systems[39].

Figure 3-15 clearly indicates an increase in the hybridization efficiency with decreasing oligo surface density, strongly suggesting that steric effects from the density of the oligo chains on the surface are critical to the hybridization efficiency. As expected, decreasing oligo surface densities resulted in lower steric hindrances to the incoming complementary oligo chains in solution, leading to higher hybridization efficiencies. These results are supported by other research literature[10,22,30]. Hybridization experiments performed using different oligo sequences showed the same trend, further supporting this hypothesis. However, as the oligo surface density decreased, so did the amount of oligo chains on the surface available for hybridization. Consequently there should be an optimal oligo surface coverage that results in the maximum amount of DNA hybridized onto the surface.

From Figure 3-16, it is evident that the maximum hybridization amount occurs at an oligo surface density of about $3\pm0.15 \times 10^{-11}$ moles/cm^2. Further experiments with various oligo sequences indicated that the optimal oligo surface density for DNA hybridization occurs approximately between 3 to 5×10^{-11} moles/cm^2. This value not only is in good agreement with the optimal oligo surface coverage for DNA hybridization presented in previous literature[10,26,28,53], but more importantly, it closely resembles the theoretical maximum density of dsDNA double helices that could be vertically packed on a surface (4×10^{-11} moles/cm^2)[7], assuming the effective double helix diameter is for a dsDNA chain in a 1 M sodium ion solution is approximately 21 Å, and that each DNA molecule is modeled as a 21 Å by 21 Å square.

The match between the empirical oligo surface density that provides the highest amount of hybridized DNA, and the theoretical optimal dsDNA surface density suggests that there are physical spatial limitations on the amount of DNA that can be hybridized onto a surface of immobilized oligo chains. For an oligo chain in solution to hybridize with a strand on the surface, the solution oligo chains must diffuse deep enough into the oligo surface film so that each nucleotide base will effectively contact its complementary base on the surface oligo chain, and thus hybridize to form the double helix. Therefore a 10 mer oligo chain in solution needs to penetrate 35 Å into the surface film of complementary oligo chains in order for all the base pairs to match correctly and achieve hybridization. Even though an increase in oligo chains on the surface increases the collision probability with the complementary oligo strands in solution, this benefit should be greatly outweighed by not only the increased electrostatic repulsion presented by the excess surface oligo chains, but also by steric hindrances due to the presence of multiple excess oligo chains on the surface that prevent the effective penetration of the oligo chains from solution into the surface oligo film.

(A)

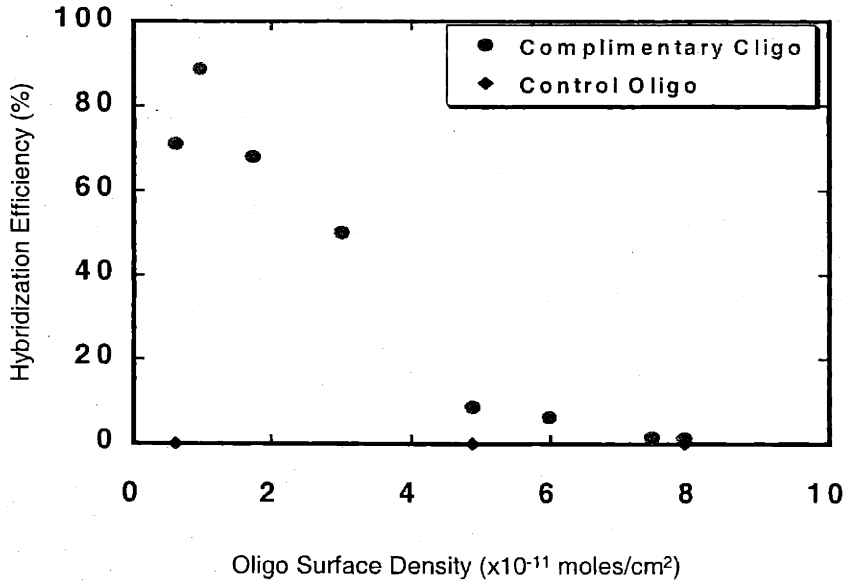

(B)

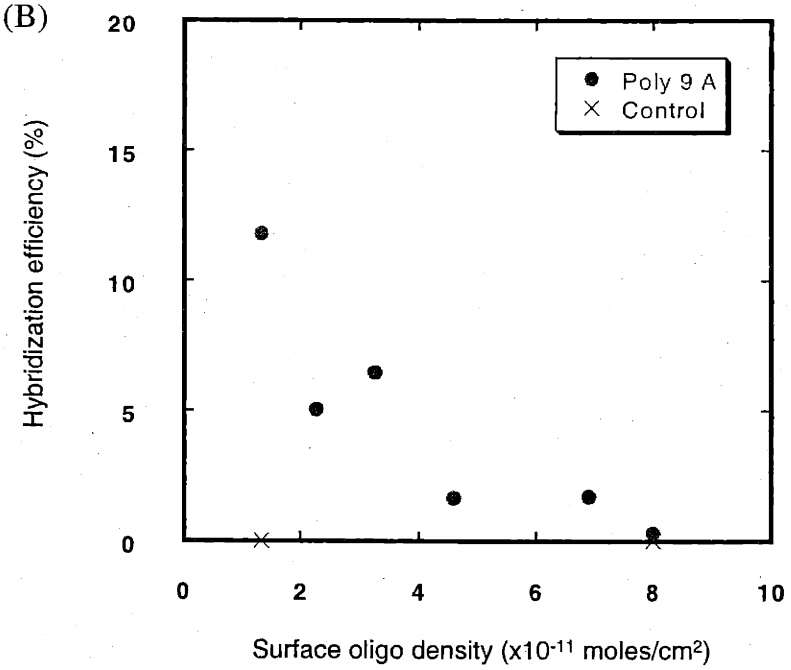

Figure 3-15. Hybridization efficiency for surface hybridization studies. The experiments were conducted by immersing oligo surfaces synthesized on mixed TCA-dodecyl TCS silane substrates, in 0.5 μM ^{32}P-labeled 10mer oligo solution (A = "*" sequence, B = poly 9 A) with 1M NaCl and 0.1 wt% SDS, for 24 hours at 4°C. The hybridization efficiency increases steadily with decreasing oligo surface density, suggesting that steric hindrance affects surface hybridization.

(A)

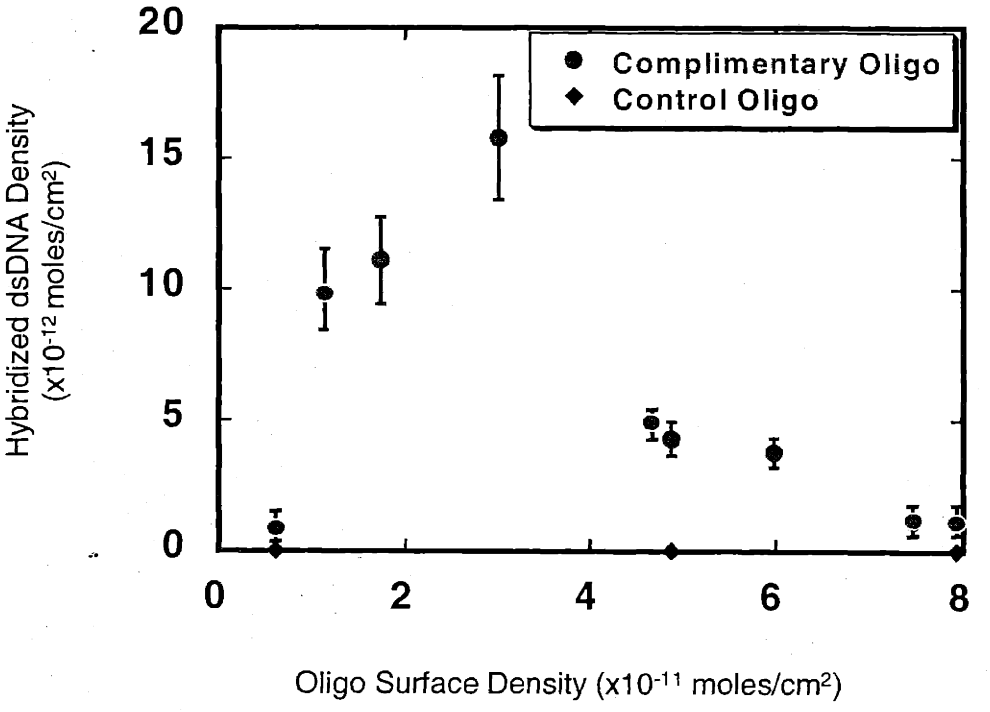

Figure 3-16a. Hybridization amount for surface hybridization studies. Experiments were conducted by immersing oligo surfaces synthesized on mixed TCA-dodecyl TCS silane substrates, in 0.5 μM ^{32}P-labeled 10mer oligo solution ("*" sequence) with 1M NaCl and 0.1 wt% SDS, for 24 hours at 4°C. The optimal surface coverage of hybridized 10 bp dsDNA occurs at an oligo surface coverage of 3-4 x 10^{-11} moles/cm^2, or approximately 40% of the maximum oligo surface coverage, suggesting that although steric factors are critical to hybridization efficiency, it must be balanced by an adequate quantity of surface oligo chains in order to achieve the maximum surface hybridization coverage.

(B)

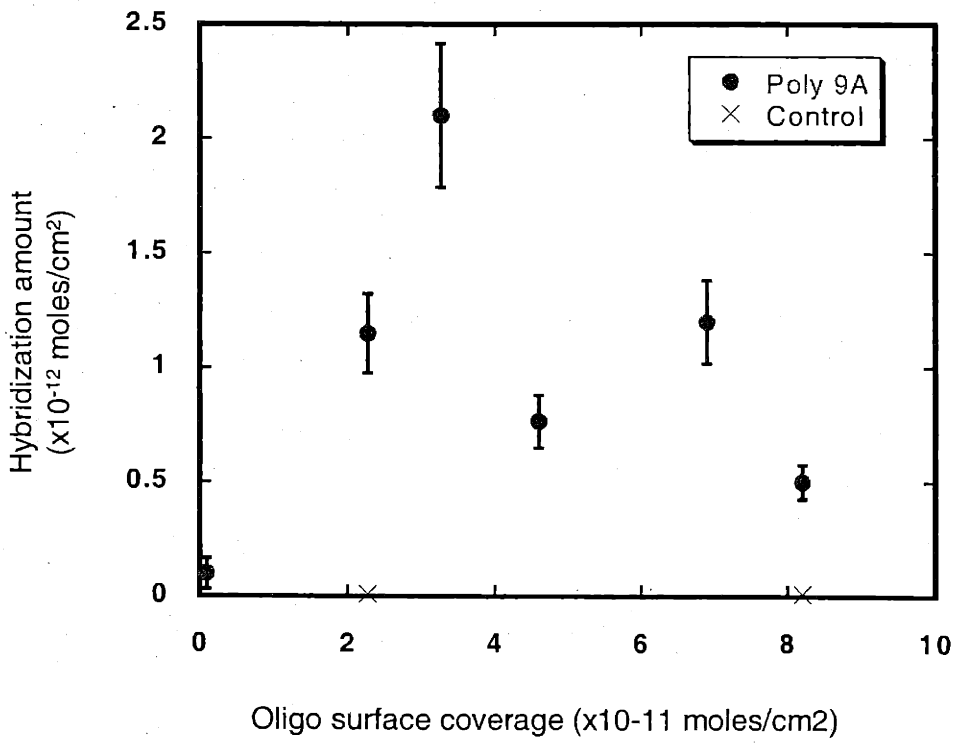

Figure 3-16b. Hybridization amount for surface hybridization studies. Experiments were conducted by immersing oligo surfaces synthesized on mixed TCA-dodecyl TCS silane substrates, in 0.5 μM ^{32}P-labeled 10mer oligo solution (Poly 9A sequence) with 1M NaCl and 0.1 wt% SDS, for 24 hours at 4°C. The optimal surface coverage of hybridized 10 bp dsDNA occurs at an oligo surface coverage of 3-4 x 10^{-11} moles/cm^2, or approximately 40% of the maximum oligo surface coverage, suggesting that although steric factors are critical to hybridization efficiency, it must be balanced by an adequate quantity of surface oligo chains in order to achieve the maximum surface hybridization coverage.

Consequently, when the threshold value of 3-5x10^{-11} moles/cm^2 for surface-attached oligos is surpassed the amount of DNA hybridized to the surface will steadily decrease, as shown by the experimental data. In addition, with some of my oligo surfaces hybridization densities were above 60% at an oligo solution concentration of 0.5 μM, compared to 2-3% for 10 μM for other literature[39]. The vast improvement suggests that controlling the oligo surface density could help optimize the hybridization efficiency of an oligo chip. Therefore the surface oligo density should be controlled to approximately 3-5 x 10^{-11} moles/cm^2, to achieve the optimal density of hybridized DNA.

3.6 Oligo distribution, stability, specificity and recycle

3.6.1 Oligo spatial distribution

After determining the effect of oligo surface density on the amount of DNA hybridized to the surface, and the optimal oligo surface density, the OH silane surfaces were chosen as substrates for the synthesis of the oligo chips used in subsequent experiments regarding DNA hybridization stability, specificity, kinetics, and recycle capability of the oligo chips. This was due to ease of production for OH silane surfaces, and because the oligo surface density for this SAM (about 4.8x10^{-11} moles/cm^2) was close to the optimal oligo surface density. There was a concern regarding the spatial distribution and homogeneity of the oligo chains synthesized onto the OH silane surfaces in the macroscopic scale. The resolution for XPS was only about 1 mm, and it was possible that the OH silane surface or the synthesized oligos were segregated in micron sized islands, creating a heterogeneous system.

I used fluorescent Cy5-labeled phosphoramidites and a confocal microscope fluorimeter to answer this question. The fluorescent phosphoramidite was added to the OH silane surface as the 1st nucleotide, and at the end of a 15mer oligo synthesis

program, and the surfaces were scanned in the fluorimeter. The images shown in Figure 3-17 indicated that the surfaces were homogeneous down to the 10 μm resolution limit of the confocal microscope, suggesting the OH silane molecules and the synthesized oligo chains are both evenly distributed over a micron-level area.

3.6.2 Thermal stability of DNA duplex and hybridization amount

The DNA melting temperature (T_m) represents the thermal stability of a particular DNA sequence, and is related to DNA chain length and the proportion of guanine (G) and cytosine (C) bases, as well as hybridization conditions such as the buffer salt concentration. Thus, for similar hybridization conditions and temperature, DNA sequences with higher T_m should be thermodynamically driven to hybridize onto the oligo surfaces, and also the resulting DNA duplex would be more stable.

Hybridization experiments were conducted with 10 mer oligo surface sequences that had different proportions of G or C content. The T_m values of these oligo sequences were calculated by a variety of different equations. These include the above-mentioned *Wallace* Rule and the *Jacobs* Rule. In addition, another formula is used which takes into detailed account the various free energies of the base stacking conformations generated by different base pairs. The equation is:

$$T_m = \frac{T_a \times \Delta H^\circ}{\left(\Delta H^\circ - \Delta G^\circ + RT_a \ln\left[\frac{C_T}{x}\right]\right)} + 16.6 \log \frac{\left[Na^+\right]}{1+\left[Na^+\right]} - 269.3$$

Where ΔH° = standard heat of formation of a hybrid bp (J/mole), ΔG° = standard free energy of formation of a hybrid bp (J/mole) , C_T = total molar strand concentration (M), R = ideal gas constant (1.987 J/mole-°K), T_a = standard temperature (298 °K), and x = 4 for complementary DNA sequences

The T_m calculated using the above formulas are shown in Table 3-3. Although the values are different depending on the equation, there is a general trend that longer sequences and sequences with higher GC content have higher T_m values.

Table 3-3. The T_m of three oligo sequences determined by various equations.

Equation	Tm (°C)		
	Sequence "*"	Sequence "X"	Sequence "GC"
Wallace	28	38	80
Jacobs	44	52	94
Base stacking	13	35	67

The radiolabeled complementary oligo sequences were solvated at 0.5 μM concentration in an aqueous 1 M 7xSSC buffer with 0.1 % SDS, and the oligo surfaces were immersed in the oligo solutions at 4°C for 24 hours. The amount of DNA hybridized onto the oligo surfaces were determined by scintillation counting. The results presented in Figure 3-18, showed that the amount of DNA hybridized to the surface was directly related to the T_m for the dsDNA strand. For example, an oligo with 100% GC content had 200% higher hybridization efficiency compared to an oligo with 40% GC content synthesized on the same hydroxy-terminated surfaces, and under the same hybridization conditions. In addition, surface oligo sequences with longer chain lengths (20 mer) also have a higher hybridization performance compared to a 10mer oligo chain. This is reasonable since the in general for short chain oligos the dsDNA stability is directly proportional to chain length. Therefore, I can optimize the amount of DNA hybridized onto a surface by modifying the GC content and the chain length of the surface-immobilized oligo chains.

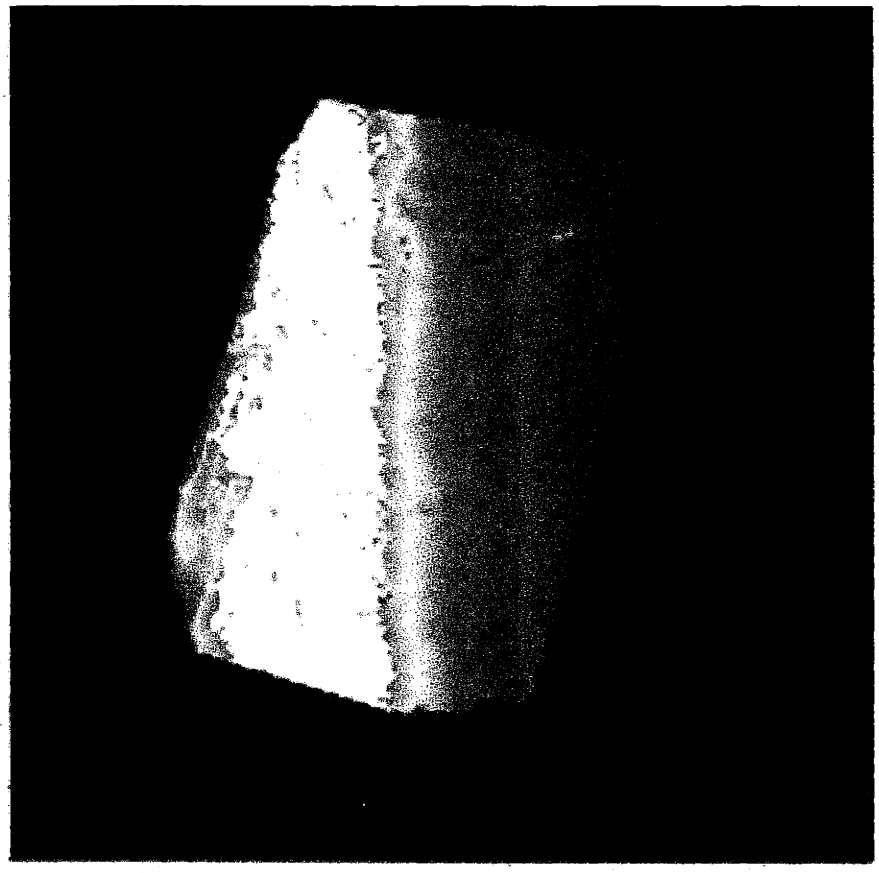

Figure 3-17. Confocal microscopy image of a silicon chip with immobilized Cy5-labeled 1st nucleotides. The pixel resolution is 10 μm x 10 μm, and the objective focal plane is 20 μm in height. The fairly even distribution of fluorescence intensity suggests that the oligo surface is homogenous at the microscale, with no evidence of islands or other localized concentrations of surface oligos. The gradient observed is due to the slight change in sample height due to uneven thickness of underlying adhesive.

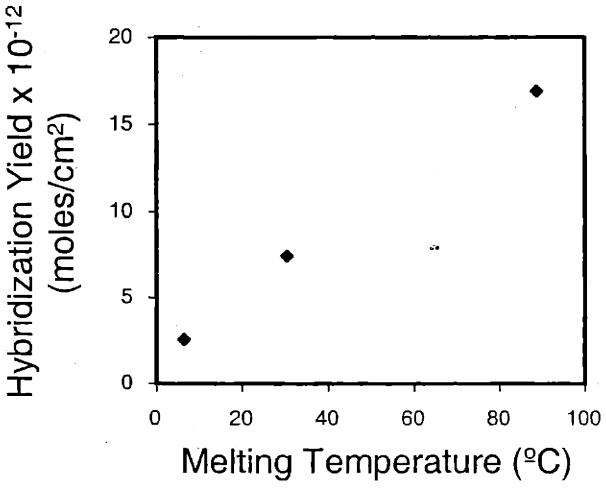

Figure 3-18. Effect of T_m on the hybridization coverage. All the oligo surfaces were synthesized on OH silane substrates, and challenged with 0.5 μM ^{32}P-labeled 10mer oligo solution with 1M NaCl and 0.1 wt% SDS, for 24 hours at 4°C. The oligo chain T_m was controlled by the manipulating the sequence GC content. As the T_m increased, so did the surface hybridization coverage, suggesting that the thermodynamic stability of the oligo sequence affects the amount of surface hybridization.

3.6.3 Effect of mismatches on hybridization amount

Further hybridization experiments were conducted under similar solution concentrations and hybridization conditions as above, using control (noncomplementary) sequences, either in solution or on the surface. Some controls had only one bp mismatch, while others had more than an 80% sequence mismatch. Theoretically mismatches dramatically reduce the stability of short DNA duplexes, with each 1.7% degree in mismatch accounting for a 1 °C decrease in the T_m[49]. For short duplexes 11-25 bp in length, each mismatch causes a 5 °C decrease in the Tm (*Wallace* ,1979). Therefore the stringency for the oligo surface hybridization should be high, even at the low hybridization temperature.

The experimental controls consistently yielded background radiation signals from 50 to 200 cpm, with little distinction in the degree of mismatch present in the oligo sequence. In addition, signal-to-noise ratios for the complementary sequence DNA compared to control sequences were high, between 50 to 500 times, clearly indicating a high level of specificity for the DNA hybridization reactions on the oligo surfaces, especially since the low hybridization temperature (4°C) reduced the hybridization stringency and should thus facilitate the hybridization of sequences with low degree of mismatch. The low background also suggested a lack of nonspecific DNA adsorption, which is reasonable since my previous studies showed that a surface DNA layer would prevent further DNA adsorption unless the solution salt concentration was extremely high (5 M).

3.6.4 Thermal stability and recycle ability of oligo chips

For my application the oligo surfaces would be heated to over 90 °C. Therefore it is critical that the oligo surfaces are thermally stable. Other researchers have produced oligo surfaces with varying degrees of stability: thermally stable covalently bound oligos[9,25,38,39,42,53-55], and chemisorbed oligo-S/Au surfaces. Oligo chips stored dry

at 4°C for over three months did not demonstrate any significant decrease in the amount of DNA hybridized to the surface, indicating that the oligo chips are chemical stable and can be stored for long periods of time prior to use. Tests on the recycle ability of the oligo surfaces were performed by heating an oligo chip with ^{32}P-labeled complementary oligo hybridized onto the surface, to 90 °C in 0.1wt % SDS aqueous solution for 30 minutes, to remove the ^{32}P-labeled oligo chains. Then the oligo chip was rinsed with deionized water and washed again in 90° C 0.1 wt% SDS aqueous solution for 30 minutes, after which only background radiation was detected, indicating complete removal of the ^{32}P-labeled oligo from the surface. Next, the oligo chip was immersed in a fresh solution of complementary, radiolabeled oligo chains, and the amount of oligo hybridized to the oligo chip was measured by liquid scintillation counting. This cycle of DNA melting, removal by wash, and subsequent hybridization was repeated twice, and the results shown in Figure 3-19. For all cycles complete desorption of labeled oligo was observed after heating, and there was no decrease in ^{32}P radiation signal during the subsequent hybridization reactions. This is expected since the oligo surfaces are covalently bound to the silicon substrate, and the nucleotide bases are chemically stable in the absence of enzymes. Further, the results demonstrate the thermal stability and recycle capabilities of the surface immobilized oligo chips.

3.7 Hybridization kinetics

After research on the hybridization efficiency, I conducted studies on hybridization kinetics. *Wetmur* and *Davidson* established that solution phase DNA hybridization had a 2nd order kinetic profile. The solution phase DNA hybridization was dependent on concentration, DNA chain length, and complexity (the number of unique sequences present in the DNA chain). For the 0.5 μM oligo solution concentration I used, the rate constant k = 1-1x10^{5} s^{-1} M^{-1}, or about 180-200 hr^{-1} for a solution phase hybridization reaction. Due to the limited mobility for an immobilized oligo chain, the rate constant values for a surface hybridization are expected to be substantially lower.

There are disparate models on DNA surface hybridization in the research literature. Some models suggested that DNA hybridization on surfaces was reaction-limited and followed a pseudo 1st order kinetic profile[38,47,56]:

$$\theta = 1 - \exp(-kt)$$

Where θ = fractional coverage of hybridized oligos, k = rate constant (s^{-1}), and t = time (s).

For surface hybridization kinetics based on the pseudo first order model, the decreased kinetic order is due to the immobilization of one of the two oligos, which restricts its mobility. The solution phase oligos have to diffuse to the surface to collide with the surface-bound oligos, which are immobile. Thus it is expected that DNA surface hybridization should be slower compared to solution phase hybridization.

On the other hand, *McKenzie*[56] and others theorized that though the oligo surface hybridization is reaction-rate limited. His rationale was based on the fact that the rate constants (k) determined for solution phase hybridizations are in the 10^5 $s^{-1}M^{-1}$ level. But if the reaction were diffusion limited, the theoretical k value is much higher, about 10^{10} $s^{-1}M^{-1}$(based on experimentally derived DNA diffusion constants of $9x10^{-9}$ to $2x10^{-6}$ cm^2/s). The hybridization could be reaction limited due to the lack of conformational flexibility for the immobilized oligo chain. The restricted conformations could reduce the efficiency of the collisions, because hybridization is highly dependent on the position and orientation of the complementary oligo strands. Since the oligo density of *McKenzie's* model is low (about 10^{-13} moles/cm^2), his supposition on the reaction-rate limitations are not based on any interactions or hindrances of neighboring oligo chains on the surface, but to the individual conformational restrictions of each oligo strand. In fact, due to the sparse oligo surface coverage, he theorized that the solution oligos first adsorb onto the silicon surface, and would diffuse laterally before encountering an immobilized oligo and hybridizing with it.

Others suggested that surface hybridization was diffusion limited and followed a Langmuir kinetic profile[41]:

$$\theta = \theta_{final} \times \left[1 - \exp\left(-kt^{\frac{1}{2}} \right) \right]$$

Where θ = coverage of hybridized oligos (moles/cm^2), θ_{final} = final coverage of hybridized oligos (moles/cm^2), k = rate constant (s^{-1}), and t = time (s).

The apparent argument for the diffusion limited model is that due to the sparse surface coverage, there is a lack of interference from neighboring oligo chains, so hybridization reaction is rapid compared to the diffusion of solution oligos to the surface. The two models present opposite reasoning on the effect immobilized oligos have one the surface hybridization kinetics.

Regardless of the proposed models, researches typically used oligo surfaces with sparse coverage, only 10^{-13} moles/cm^2. Thus the neighboring oligo chains do not affect the surface hybridization kinetics. However, much denser surfaces may be required for optimizing the performance of the oligo chip, up to 10^{-11} moles/cm^2. At such surface densities, interactions between neighboring oligos is unavoidable. At dense surface coverage the surface oligos could resist hybridization by both steric effects and electrostatic repulsion, which is amplified on the densely packed and negatively charged oligo surface. Consequently, for my system the surface hybridization kinetics are affected by numerous factors such as oligo length and sequence, oligo solution concentration, sodium ion concentration, and the addition of chemical agents that either facilitate hybridization or destabilize the hybridized dsDNA.

For kinetics studies the hybridization conditions such as sodium ion concentration (1 M), and reaction time (24 hours), with the purpose of optimizing the amount of DNA

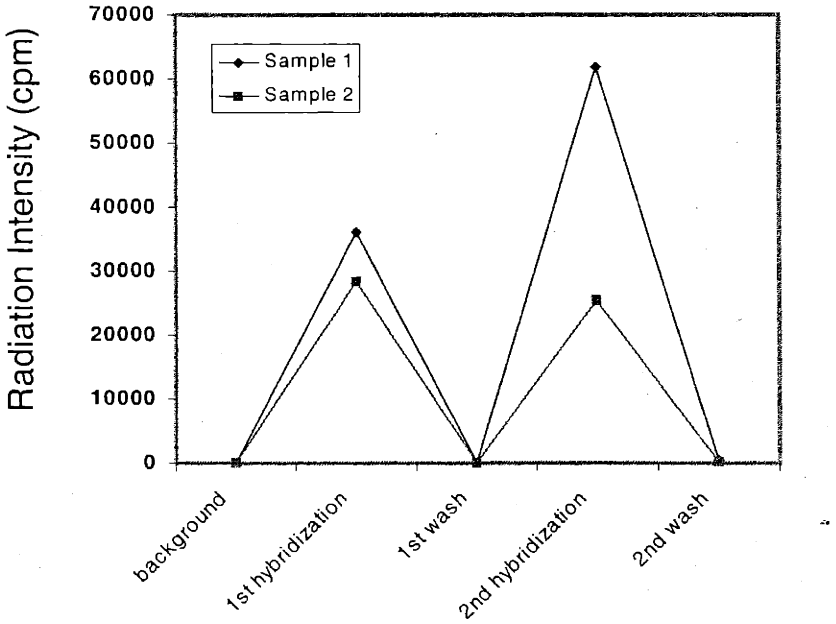

Figure 3-19. Hybridization amount on surface through various recycles. The thermal stability of the synthesized oligo surfaces was tested by observing whether the surface hybridization coverage decreases after the oligo surface was heated to 90° C for 1 hour in TE buffer with 0.2 wt% SDS to remove the hybridized ^{32}P-labeled oligo. After two repeated heating cycles there was no significant decrease in the amount of hybridized ^{32}P-labeled oligo, suggesting that the oligo surface is not degraded by heating and is thermally stable.

hybridized to the surface and to reach an equilibrium state. Standardized oligo chips with the same sequence, synthesized on OH silane surfaces, were used to provide consistent surface properties for performing a series of hybridization experiments to study the above conditions.

Research literature suggests that although DNA hybridization consists of both forward and a reverse reactions, the forward reaction is the predominant factor in deciding the hybridization kinetics, unless the temperature is too close to the T_m of the hybridized dsDNA and the duplex unravels[47]. Since my goal was to observe the reaction kinetics it was imperative to minimize the kinetics of the reverse denaturing reaction. Therefore the hybridization temperature was again set at 4°C..

First, experiments were run using the standard hybridization conditions described above, for reaction times up to 96 hours, and the results are shown in Figure 3-20. The plot suggests that the amount of DNA hybridized onto the surface reaches a maximum at 24 hours, with no further increase in hybridized DNA after 96 hours of immersion. This suggests that the hybridization reaction reaches equilibrium conditions after 24 hours reaction time. Since literature sources suggests that DNA surface hybridization follows pseudo 1st order kinetics, I tried to use a simple 1st order kinetics model to fit the experimental results. Since the quantity of oligos in the solution were at least two orders of magnitude higher than the surface oligo chains, I chose the surface oligo chains as the limiting reactant and used the following equation to model the 1st order kinetics:

$$\frac{C_A}{C_{AT}} = 1 - \exp(-kt)$$

Where C_{AT} = total surface oligo density (moles/cm^2), C_A = surface hybridized oligo density (moles/cm^2), k = rate constant (hr^{-1}), and t = hybridization time (hr)

The results of the kinetics models are shown in Figure 3-21 and Figure 3-22. I observed a reasonable fit between the model and the experimental data at the rate constant value k = 0.25 hrs^{-1}. Further 1^{st} order kinetics curves were generated to fit a separate set of kinetics data from surface hybridization experiments conducted by another group member, Manish Bajaj. There was a reasonable fit when k = 0.03 hr^{-1}, a lower rate constant compared to my run. The reason for the lower rate constant is due to the hybridization reaction conditions. Though I both used oligo surfaces synthesized on OH silane substrates, Manish conducted the hybridization experiments at 25° C, and with a lower oligo solution concentration (0.33 μM).

The thermal stability of the DNA duplex is directly related to T_m of the oligo sequence, and is especially sensitive for chains less than 20 nt in length. Usually hybridization occurs at T_m - 25°C, and the thermodynamic driving force for hybridization increases with lower hybridization temperatures. For my particular oligo sequence the theoretical T_m in 1 M $NaCl_{(aq)}$ is approximately 52° C, with a threshold hybridization temperature of about 27°C. Thus hybridization at 4°C should be more rapid than at 25°C, which is closer to the threshold hybridization temperature. In addition, the difference in oligo solution concentration may also be a factor in the lower rate constant obtained in the data set collected by Manish. However, it is unclear whether either or both factors mentioned above are the cause of the differences in the rate constants, and the extent of their influences. More experiments need to be run at different oligo solution concentrations and hybridization temperatures to determine the effect each variable has on the DNA surface hybridization.

It is also possible to fit the same hybridization kinetics data with a diffusion-limited Langmuir model. The curve fit resulted in rate constants k = 0.2-0.6 $hr^{1/2}$. Since both models fit the data equally well, it is not possible to determine which model is the correct one. Regardless of the theoretical model, the rate constants for surface hybridization are much lower than for solution phase hybridization, which is quite reasonable.

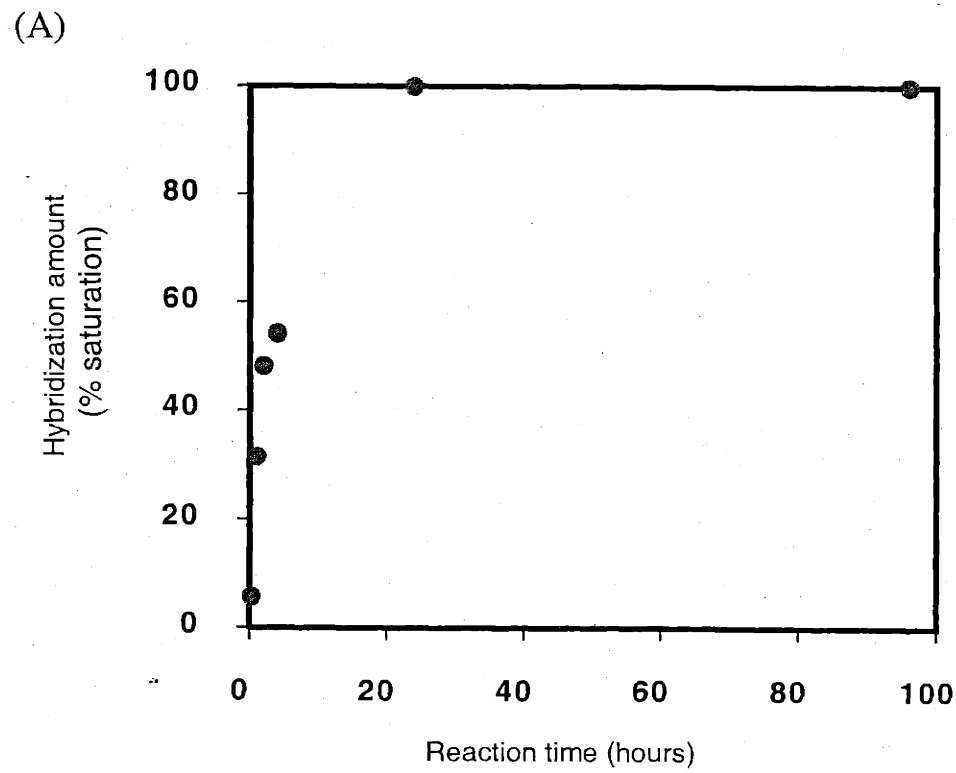

Figure 3-20. Hybridization kinetics of oligo surfaces. Hybridization kinetics were observed with oligo surfaces synthesized on OH silane substrates, immersed in 0.5 μM ^{32}P-labeled 10mer oligo solution with 1M NaCl and 0.1 wt% SDS, at 4°C: (a) The proportion of DNA hybridized to the surface, normalized to the equilibrium surface coverage, with respect to reaction time.

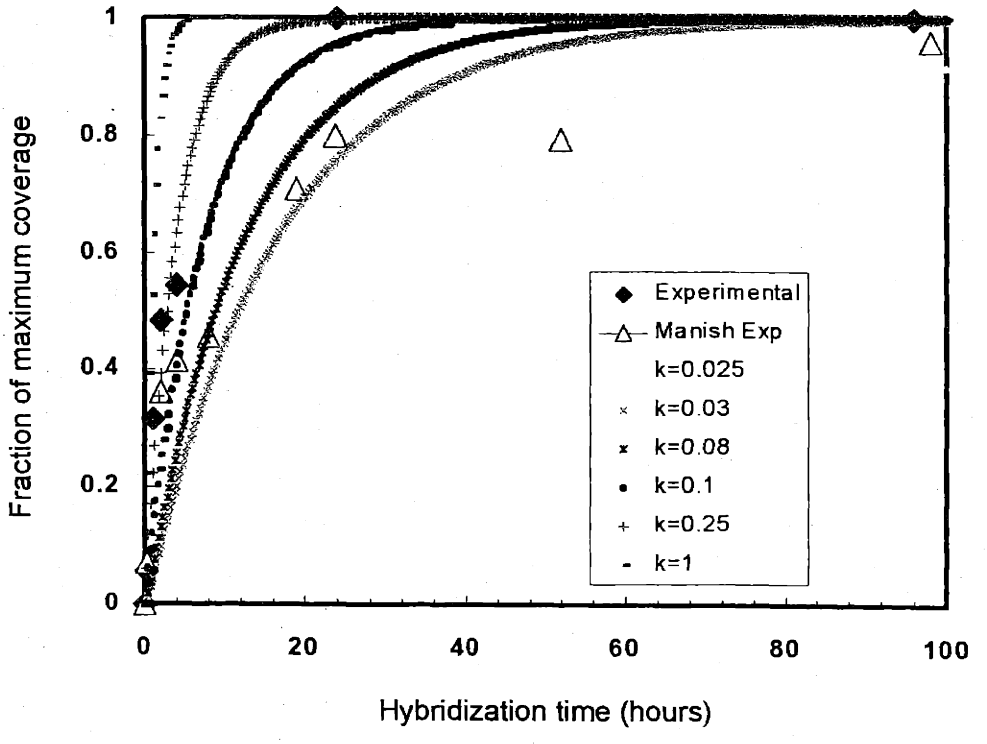

Figure 3-21. Kinetic model for surface hybridization. Hybridization kinetics were observed with oligo surfaces synthesized on OH silane substrates, immersed in 0.5 μM ^{32}P-labeled 10mer oligo solution with 1M NaCl and 0.1 wt% SDS, at 4°C. A simple 1st order (batch) kinetics model was used to fit the experimental data, with an approximate k value of 0.25 hour^{-1}. For comparison, an experiment conducted with 0.3 μM solution oligo concentration, at 25°C is shown, with a k value of 0.03 hour^{-1}.

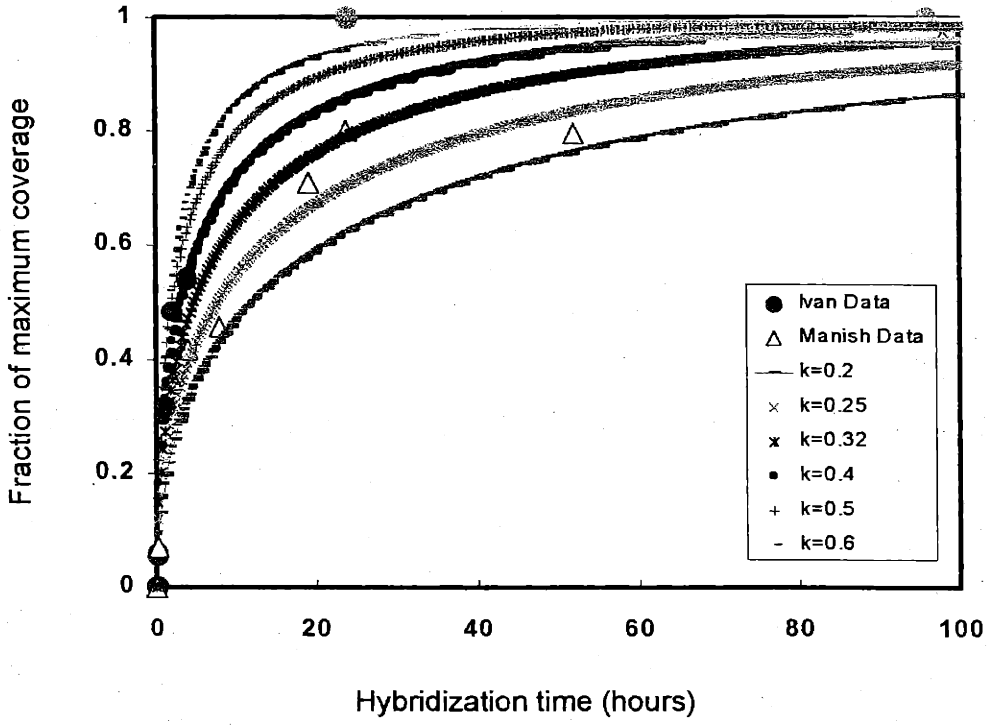

Figure 3-22. Alternative kinetic model for surface hybridization. Hybridization kinetics were observed with oligo surfaces synthesized on OH silane substrates, immersed in 0.5 μM ^{32}P-labeled 10mer oligo solution with 1M NaCl and 0.1 wt% SDS, at 4°C. A diffusion limited Langmuir model was used to fit the experimental data, with an approximate k value of 0.6-0.7 hour$^{-0.5}$. For comparison, an experiment conducted with 0.3 μM solution oligo concentration, at 25°C is shown, with a k value of 0.25-0.32 hour$^{-0.5}$.

Overall, the 1st order kinetics equation and diffusion limited Langmuir equation represent only extremely simplified and idealized models for surface hybridization. The actual hybridization kinetics on an oligo surface is most likely dependent on many factors, including the surface oligo coverage, the oligo solution concentration, the hybridization temperature, and the solution cation concentration and species. The surface oligo coverage could affect hybridization kinetics through both steric hindrance and electrostatic repulsion, which complicates the model design. Furthermore, the solution oligos already hybridized and immobilized on the oligo surface at any time present a dynamically varying amount of steric and electrostatic hindrance towards the incoming solution-phase oligos, resulting in a complex problem for developing a detailed and accurate kinetics model based on first principles.

In addition, the question still remains of whether the DNA surface hybridization kinetics are diffusion limited or reaction rate limited, and some literature has suggested that 2-D diffusion of the solution-phase oligos on the surface may also be a critical factor in determining the surface hybridization kinetics. Clearly much more research should be conducted on the many variables that affect DNA surface hybridization before a more accurate and sophisticated predictive kinetic model can be developed for DNA hybridization on a surface. Attempts to optimize the performance of oligo chips would be greatly aided by the development of a consistent theoretical kinetics model.

3.8 Measurement range, threshold detection level and concentration factors

From the previous section I noted that an increase in solution oligo concentration caused an increase in the amount of oligo hybridized to the surface. Consequently I decided to run a series of hybridization reactions over a wide range of solution oligo concentrations to observe the effects of oligo concentration on the surface hybridization. The experimental data can also be used to determine the threshold detection level and

measurement range of the oligo surfaces if I treat them as immobilized surface probe for detection of target oligos in the solution phase. I started with a 0.5 μM ^{32}P radiolabeled oligo solution in 7xSSC buffer with 0.1% SDS. The oligos were labeled with ^{32}P-dCTP using terminal transferase at an oligo to radiolabel ratio of 30 to 1. For lower concentrations the radiolabeled oligo solution was serially diluted in the appropriate buffer.

The approach for increasing oligo solution concentration was to add unlabeled oligo to the radiolabeled oligo solution to produce a mixture with a higher oligo concentration. Then I immersed oligo surfaces synthesized on OH silane SAMs in the various oligo solutions for 48 hours at 4° C, to achieve equilibrium conditions. The resulting plot of hybridization amount versus solution concentration up to 500 nM is shown in Figure 3-23. My first observation was that the amount of oligos hybridized to the surface initially increased with increasing oligo concentration, but then leveled off and even decreased slightly as the oligo concentration reached the 50 μM point.

The increased hybridization with increased oligo solution concentration is typical of DNA surface hybridization[39,53]. However, the decrease in hybridization for my surface is unusual. On the other hand, the decreasing trend was still evident in repeat experiments. A possible explanation is that the amount DNA surface hybridization has a maximum ceiling where all of the surface oligo chains available for hybridization have been consumed and no further hybridization can occur at the surface.

I also noted that at high solution oligo concentrations (50 μM), the radiation signal intensity actually suggested a decrease in the surface coverage of hybridized DNA, compared to the values I observed at 0.5μM, which I assumed was the saturation concentration. The decrease in density at high oligo concentrations may be due to the large ratio of nonlabeled to labeled oligo chains in solution (3000 to 1). The nonlabeled oligos are shorter and more abundant than the labeled oligos, and are thereby thermodynamically favored over labeled oligos during competitive hybridization with oligo surfaces. Consequently the radioactive signal intensity for surfaces immersed in the

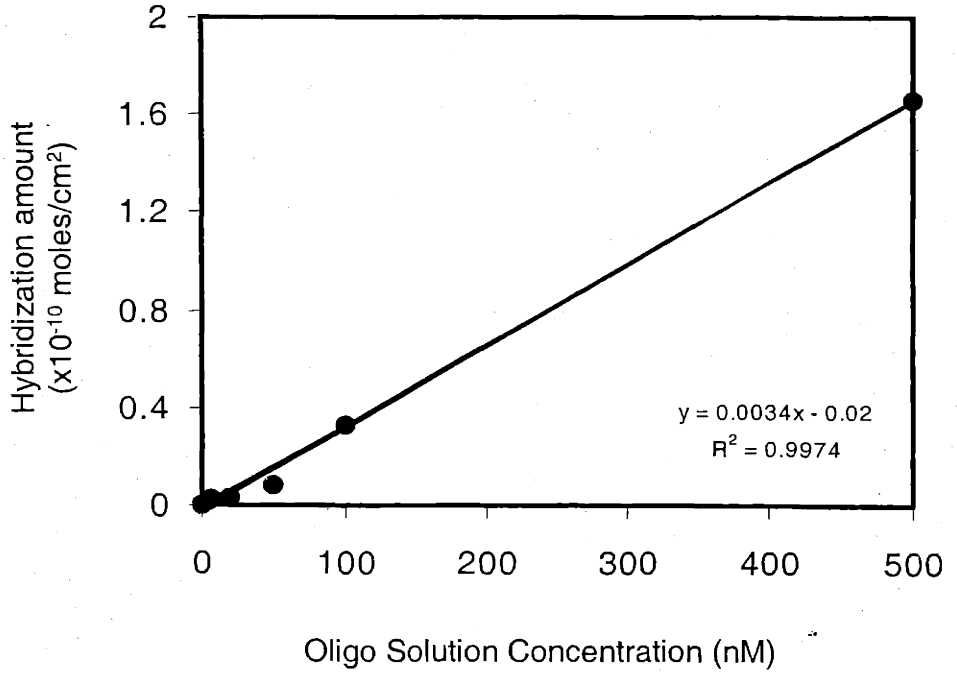

Figure 3-23. Effect of oligo solution concentration on surface hybridization. The surface oligos were synthesized on OH silane surfaces. The radiation signals indicate a threshold detection limit in the nM range. The experimental data were fit with a linear model, with fairly high accuracy.

high oligo concentration solutions would decrease even though the total density of hybridized dsDNA at the surface is the same is comparable to the hybridized DNA surface coverage achieved at lower solution oligo concentrations.

The dramatic decrease in amount of surface hybridization with decreasing solution oligo concentrations suggests that at high solution oligo concentrations the surface hybridization sites are saturated and that the maximum possible DNA surface hybridization coverage is achieved. On the other hand, at lower concentrations the surface hybridization reaction seems to diffusion limited, instead of reaction rate limited, especially since the hybridization conditions have been chosen to optimize the hybridization reaction kinetics (low temperature, 4°C, and high salt concentration, 1 M NaCl).

The data on the plot could be readily fit with a linear model instead of a Langmuir adsorption model. The Langmuir adsorption models usually result in a very high initial hybridization amount, followed by a sharp transition towards and asymptote during saturation. On the other hand, the linear model suggests that there is less hybridization at low solution oligo concentrations, indicating that the hybridization is slower than traditional Langmuir adsorption kinetics, possibly due to steric and electronegative repulsions from the oligo surfaces. This effect may indeed be the case since the oligo surfaces that were used were of high density, approximately $0.8\text{-}1\text{x}10^{-11}$ moles/cm^2. As shown previously, the hybridization efficiency decreases as the surface oligo density increases. Perhaps when using oligo surfaces with lower coverage the steric hindrance will decrease, resulting in less hindrance and a closer resemblance to the Langmuir adsorption model. My adsorption experiments were conducted for 24 hours, so the oligo chains in solution had ample time to diffuse to the oligo layer surface, and to react with the surface oligo chains. The steric hindrance only inhibits the oligo from quickly diffusing into the oligo layer to hybridize with the surface oligos. Thus the hybridization conditions should be very close to equilibrium. However, it is still not possible to determine whether the hybridization is a first order kinetic model or a thermodynamic model, since both models could result in a linear relationship between solution oligo

concentration and hybridization amount. Additional experiments using oligo surfaces with low coverage (to decrease steric effects) may provide an answer to this question.

Finally, from Figure 3-23 the threshold detection limit I could obtain with the current system of radiation scintillation counting was in the low nM (~5 nM) range. This number is comparable to the threshold levels of oligo surfaces produced by other methodologies. Furthermore, since the ratio of nonlabeled to ^{32}P-labeled oligos in solution was 30 to 1, I anticipate a further reduction of the threshold detection limit by a factor of 30 if 100% radiolabeled oligos were used as target DNA. In addition, if a lower detection threshold is required, I can change from the ^{32}P label to alternative nonradioactive labels that provide signal amplification. Some examples include fluorescent probes with high quantum yields such as fluorescein, Cy3, and Cy5; or enzyme linkers such as alkaline phosphotase or horseradish peroxidase, which can produce up to 10000 x signal amplification by generating a chemiluminescent signal through a redox reaction with substrates such as luminol or digoxigen. By controlling the oligo surface density and ensuring high sequence fidelity, one can optimize the performance of the surface oligo probes, so that the limiting factor for determining threshold detection limit would be the characterization method rather than the surface DNA probes. Finally, it is possible to use oligo surfaces with lower surface coverages to increase the sensitivity, due to the decreased steric hindrance for theses surfaces.

3.9 Conclusions

I was able to control the surface density of 1st nucleotides immobilized onto silicon surfaces by synthesizing mixed methyl/hydroxy-terminated silane SAM with different hydroxy group compositions, and I utilized XPS and iodine-labeled phosphoramidites to accurately determine the surface coverage of the 1st nucleotides immobilized onto the derivatized surfaces. These derivatized surfaces were used to study

the effect of 1st nucleotide surface density on oligo chain synthesis efficiency and sequence fidelity By manipulating the surface density of the 1st nucleotide immobilized onto the surface to less than $4x10^{-11}$ moles/cm^2, and the coupling reaction time to above 75 seconds, I achieved coupling reaction efficiencies above 99%, and thus optimized the fraction of full-length oligos synthesized on the surface. The appropriate choice of mild deprotection agents and UltraMILD® base protecting groups prevented any degradation of the synthesized oligo chains, and provided us with thermally stable, reusable oligo chips that had consistent, controlled, and reproducible surface densities, and a high degree of sequence fidelity.

I utilized synthesized oligo chips with different oligo surface coverages to study DNA hybridization on surfaces, and found that the hybridization efficiencies of oligo chains in solution to the complementary surface-immobilized oligo sequences increased with decreasing surface oligo chain density. This trend suggests that hybridization onto the surface is affected by steric hindrance, and also by electrostatic repulsion related to the surface density of the immobilized oligo chains. Furthermore, I determined that the optimal amount of oligos hybridized to the surface occurred at oligo surface densities of approximately between 3 to 5 x 10^{-11} moles/cm^2, which corresponds to the theoretical maximum packing density for dsDNA double helices onto a surface, and is in agreement with the previous literature.

The oligo surface I produced demonstrated psuedo 1st order hybridization kinetics. The thermodynamic stability of the dsDNA duplex due to GC content and chain length, as well as the target oligo solution concentration affected the hybridization performance of the oligo surface. The measurement range of the oligo surface using radiolabeled target oligos spanned 4 orders of magnitude, with a threshold sensitivity limit at the sub nM level.

The ability to produce oligo chips on silicon surfaces with high sequence fidelity, thermal stability and with consistent, controllable surface density not only provided us with model oligo surfaces to study DNA hybridization in a systematic manner, but also

could be the basis for the synthesis of oligo chips with optimal hybridization performance, to immobilize oligo or DNA chains to a flat silicon surface. The oligo surfaces themselves could be as probes to detect complementary oligos are ssDNA in solution, or as the platform to immobilize a longer chain dsDNA to form a surface probe using ssDNA.

3.10 References

1) K. L. Prime; G. M. Whitesides *J.Amer. Chem. Soc.* **1993**, *115*, 10714-10721.
2) T. W. Greene *Protective Groups in Organic Synthesis*; John Wiley & Sons: New York.
3) B. G. Bravo; S. L. Michelhaugh; P. S. Manuel; I. Villegas; D. W. Suggs; J. E. Stickney *J. Phys. Chem.* **1991**, *95*, 5245-5249.
4) P. Gao; M. J. Weaver *J. Phys. Chem.* **1986**, *90*, 4057-4063.
5) R. L. McCarley; A. J. Bard *J. of Phys. Chem.* **1991**, *95*, 9618-9620.
6) X. Gao; J. E. Gregory; F Liu; A. Hamelin; M. J. Weaver *J. of Phys. Chem.* **1994**, *98*, 8086-8095.
7) S. Trohalaki; A. A. Brian; H. L. Frisch; L. S. Lerman *Biophys. J.* **1984**, *45*, 777-782.
8) D. E. Gray; S. C. Case-Green; T. S. Fell; P. J. Dobson; E. M. Southern *Langmuir* **1997**, *13*, 2833-2842.

9) Lisa Henke; Paul A. E. Piunno; Andrea C. McClure; U. J. Krull *Anal. Chimica Acta* **1997**, *344*, 201-213.
10) M. S. Shchepinov; S.C. Case-Green; E. M. Southern *Nuc. Acids Res.* **1997**, *25*, 1155-1161.
11) M. Eggers; M. Hogan; Reich., R. K.; J. Lamture; D. Ehrlich; M. Hollis; B. Kosicki; T. Powdrill; K. Beattie; S. Smith; R. Varma; R. Gangadharan; A. Mallik; B. Burke; D. Wallace *Biotechniques* **1994**, *17*.
12) R. Levicky; T. M. Herne; M. J. Tarlov; S. K. Satija *J. Amer. Chem. Soc.* **1998**, *120*, 9787-9792.
13) M. J. Kozal; N. Shah; N. Shen; R. Yang; R. Fucini; T. C. Merigan; D. D. Richman; D. Morris; E. Hubbell; M. Chee; T. Gingeras *Nat. Med.* **1996**, *2*, 753-759.
14) J. A. Running; M. S. Urdea *Biotechniques* **1990**, *8*, 276-&.
15) S. R. Rasmussen; M. R. Larsen; S. E. Rasmussen *Anal. Biochem.* **1991**, *198*, 138-142.
16) P. Balaguer; B. Terouanne; P. Allibert; P. Cros; A. -M. Boussioux; B. Mandrand; J. -C. Nicolas *Mol. and Cell. Probes* **1993**, *7*, 155-159.
17) P. Cros; R. Kurfurst; P. Allibert; N. Battail; N. Piga; V. Roig; N. T. Thuong; B. Mandrand; C. Helene *Nuc. Acids Res.* **1994**, *22*, 2951-2957.
18) H. Bunemann; P. Weshoff; R. G. Hermann *Nuc. Acids Res.* **1982**, *10*, 7163-7180.
19) I. D. Parsons; B. Persson; A. Mekhalfia; G. M. Blackburn; P. G. Stockley *Nuc. Acids Res.* **1995**, *23*, 211-216.
20) L. A. Chrisey; G. U Lee; E. O'Ferrall *Nuc Acids Res.* **1996**, *24*, 3031-3039.
21) G. U Lee; C. E. O'Ferrall,; L. A. Chrisey *Nuc. Acids Res.* **1996**, *24*, 3031-3039.
22) M. Boncheva; L. Scheibler; P. Lincoln; H. Vogel; A. B. *Langmuir* **1999**, *15*, 4317-4320.
23) U. Maskos; E. M. Southern *Nuc. Acids Res.* **1992**, *20*, 1679-1684.
24) M. J. O'Donnell; K. Tang; H. Koster; C. L.Smith; C. R. Cantor *Anal. Chem.* **1997**, *69*, 2438-2443.
25) L. A. Chrisey; C. E. O'Farrell; B. J. Spargo; C. S. Dulcey; J. M. Calvert *Nuc. Acids Res.* **1996**, *24*, 3040-3047.
26) V. A. Efimov; A. A. Buryakova; O. G. Chakhmakhcheva *Nuc. Acids Res.* **1999**, *27*.
27) R. S. Matson; J. Rampal; S. L. Pentoney, J.; P. D. Anderson; P. Coassin *Anal. Biochem.* **1995**, *224*, 110-116.
28) F. N. Rehman; M. Audeh; E. S. Abrams; W. H. Philip; M. Kenney; T. C. Boles *Nuc. Acids Res.* **1999**, *27*, 649-655.
29) G. Yershov; V. Barsky; A. Belgovskiy; E. Kirillov; E. Kreindlin; I. Ivanov; S. Parinov; D. Guschin; A. Drobishev; S. Dubiley; A. Mirzabekov *Proc. Natl. Acad. Sci. USA* **1996**, *93*, 4913-4918.
30) P. Nilsson; B. Persson; M. Uhlen; P. -A Nygren *Anal. Biochem.* **1995**, *224*, 400-408.
31) P. A. E. Puinno; R. H. E. Hudson; H. Cohen; M. J. Damha; U. J. Krull *Anal. Chem.* **1995**, *67*, 2635-2643.
32) U. Maskos; E. M. Southern *Nuc. Acids Res.* **1992**, *20*, 1679-1684.
33) G. McGall; J. Labadie; P. Brock; G. Walraff; T. Nguyen; W. Hinsberg *Proc. Natl. Acad. Soc. USA* **1996**, *93*, 13555-13560.
34) A. Pease; D. Solas; E. J. Sullivan; M. T. Cornin; C. P. Holmes; S. P. A. Fodor *Proc. Natl. Acad. Sci. USA* **1994**, *91*, 5022-5026.

35) E. M. Southern; K. Mir ; M. Shchepinov *Nat. Genet. Suppl.* **1999**, *21*, 5-9.
36) R. J. Lipshutz; D. Morris; M. Chee; E. Hubbell; M.J. Kozal; N. Shah; N. Shen; R. Yang; S. P. A. Fodor *Biotechniques* **1995**, *19*, 442-447.
37) G. H. McGall; D. B. Anthony; M. Diggelmann; S. P.A. Fodor; E. Gentalen; N. Ngo *J. Amer. Chem. Soc.* **1997**, *119*, 5081-5087.
38) Z. Guo; R. A. Guilfoyle; A. J. Thiel; R. Wang,; L. M. Smith *Nuc. Acids Res.* **1994**, *22*, 5456-5465.
39) D. Guschin; G. Yershov; A. Zaslavsky; A. Gemmell; V. Shick; D. Proudnikov; P. Arenkov; A. Mirzabekov *Anal. Biochem.* **1997**, *250*, 203-211.
40) J. B. Lamture; L. B. Kenneth; B. E. Burke; M. D. Eggers; D. J. Ehrlich; R. Fowler; M. A. Hollis; B. B. Kosicki; R. K. Reich; S. R. Smith; R. S. Varma; M. E. Hogan *Nuc. Acids Res.* **1994**, *22*, 2121-2125.
41) T. M. Herne; M. J. Tarlov *J. Amer. Chem. Soc.* **1997**, *119*, 8916-8920.
42) J. A. Ferguson; T. C. Boles; C. P. Adams; D. R. Walt *Nat. Biol.* **1996**, *14*, 1681-1684.
43) M. Yang; R. Y. C. Kong; N. Kazmi ; A. K. C. Leung *J. Chem. Soc. Japan* **1998**, 257-258.
44) D. Shalon; S. J. Smith; P. O. Brown *Genome Res.* **1996**, *6*, 639-645.
45) J. Sambrook; E. F. Fritsch; T. Maniatis *Molecular Cloning: A Laboratory Manual*; 2 ed.; Cold Spring Harbor Laboratory Press: Cold Spring Harbor NY, 1989.
46) G. U Lee; L. A. Chrisey; R. J. Colton *Science* **1994**, *266*, 771-773.
47) G. H. Keller; M. M. Manak *DNA Probes*; 2 ed.; Stockton Press: New York, 1993.
48) J. W. Nelson; F. H. Martin; I. Tinoco Jr. *Biopolymers* **1981**, *12*, 2509-2531.
49) M. L. M. Anderson *Nucleic Acid Hybridization*; Bios Scientific Publishers: Oxford UK, 1999.
50) U. Maskos; E. M. Southern *Nuc. Acids Res.* **1992**, *20*, 1679-1684.
51) U. Maskos; E. M. Southern *Nuc. Acids Res.* **1993**, *21*, 4663-4669.
52) N. K. Hogan; L. S. Lerman *Personal Communication,* **1999-2000**
53) L. A. Chrisey; O. F. Elizabeth; J. S. Barry; C. S. Dulcey; J. M. Calvert *Nuc. Acids Res. 1996* **1996**, *24*, 3040-3047.
54) C. R. Graham; D. Leslie; D. J. Squirrell *Biosen. and Bioelect.* **1992**, 487-493.
55) A. P. Abel; M. G. Weller; G. L. Duveneck; M. Ehrat; H. M. Widmer *Anal. Chem.* **1996**, *68*, 2905-2912.
56) V. Chan; D. J. Graves; S. F. McKenzie *Biophys. J.* **1995**, *69*, 2243-2255.

Chapter 4: Covalent end-immobilization of dsDNA

4.1 Introduction

After I developed a methodology to produce oligo surfaces with consistent and controllable surface density, and manipulated reaction conditions to optimize the hybridization of solution phase complementary oligo sequences, I had to next immobilize dsDNA onto the oligo surface. As mentioned before some methods for immobilizing dsDNA used acrylamide gels with copolymerized functional groups such as oligos or amines. Mosaic Technologies developed a surface PCR method that used the gel-immobilized oligo chains as PRC primers. When the reaction is complete dsDNA chains would be attached to the oligo chains. Alternatively, $NaIO_4$ was used to oxidize the 3' end nucleotide pentose ring to form reactive aldehyde groups[1], that subsequently reacted with the amine groups in the acrylamide gels. However, for these 3-D gel multiplayer "surfaces" the dsDNA surface density per surface layer was low (10^{-14} moles/cm2)[1,2], so alternative methods were considered.

4.1.1 Polymerase extension method for immobilizing dsDNA

There were a few proposed approaches for attaching dsDNA onto a surface via hybridization to an immobilized oligo chain, but they had various shortcomings or technical difficulties. A schematic diagram describing the systems developed is shown in Figure 4-1. One method involved hybridizing a long chain ssDNA in solution to a surface oligo with a sequence complementary to the 3' end of the ssDNA (Figure 4-1a). Then a DNA polymerase was used to fill in the missing portion of the DNA sequence to obtain a surface immobilized dsDNA strand[3-6].

However, there was a definite upper limit on the maximum possible dsDNA surface density since the dsDNA strands had to be separated by a suitable distance in order for the enzyme to function effectively. In addition, to obtain the ssDNA, I would have to first produce dsDNA through PCR amplification, then use one of numerous protocols to digest one of the two ssDNA chains in a so called asymmetric PCR reaction. The mechanism for PCR is shown in Figure 4-2, and the asymmetric PCR protocol is shown in Figure 4-3. For asymmetric PCR custom PCR primers were produced for one of the ssDNA strands. The custom primer contained a specific chemical group that inhibited to function of an exonuclease enzyme[7]. For instance, T7gene 6 exonuclease does not recognize phosphorothioate nucleotides[8], while λ exonuclease is inhibited by the presence of a 5' phosphorylated PCR primer[9,10]. The custom primers were added to the PCR reaction mix, and after the reaction is completed the dsDNA product is digested with the exonuclease. The ssDNA strand that contains the customized primer is not destroyed and after purification is hybridized to the surface. Or, one of the PCR primers can be labeled with a 5' biotin group, and after PCR the dsDNA is heated to melt the duplex, and filtered through a chromatography column containing streptavidin coated magnetic beads[11]. The streptavidin molecules have an affinity for biotin ($K^d=10^{-15}$ M), and react with the biotinylated ssDNA strands to remove them from the DNA solution.

Regardless of the method, asymmetric PCR increased the number of steps and the complexity of the process, with a consequent reduction in yield and reproducibility, and thus was not considered as a strategy for immobilizing dsDNA onto the surface. However, it was still a good approach for producing labeled target ssDNA onto the surface for testing the probe DNA on the immobilized onto the oligo surface.

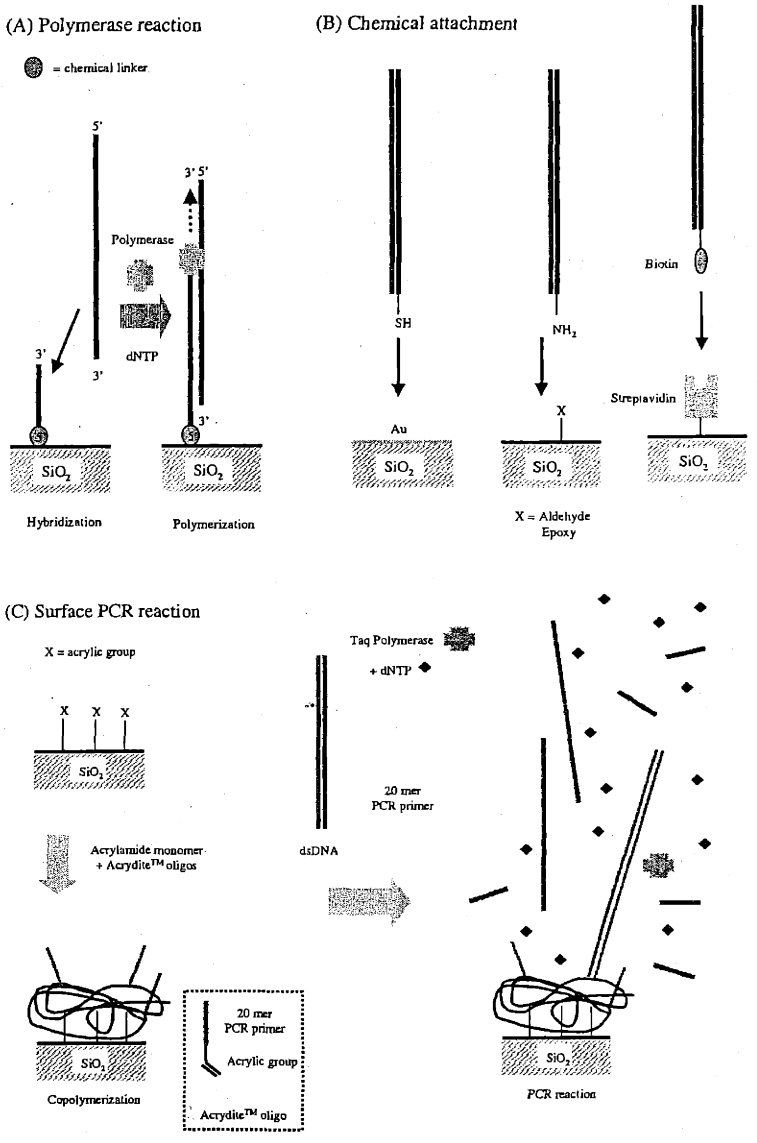

Figure 4-1. A graphic representation of dsDNA immobilization techniques from literature. (a) An ssDNA chain is hybridized to an immobilized oligo and polymerase is used to fill in the complementary sequence; (b) dsDNA with reactive linkers are attached to surfaces by chemical crosslinking reactions; (c) an oligo primer is copolymerized with an acrylamide gel on the surface and the dsDNA is generated by the PCR reaction.

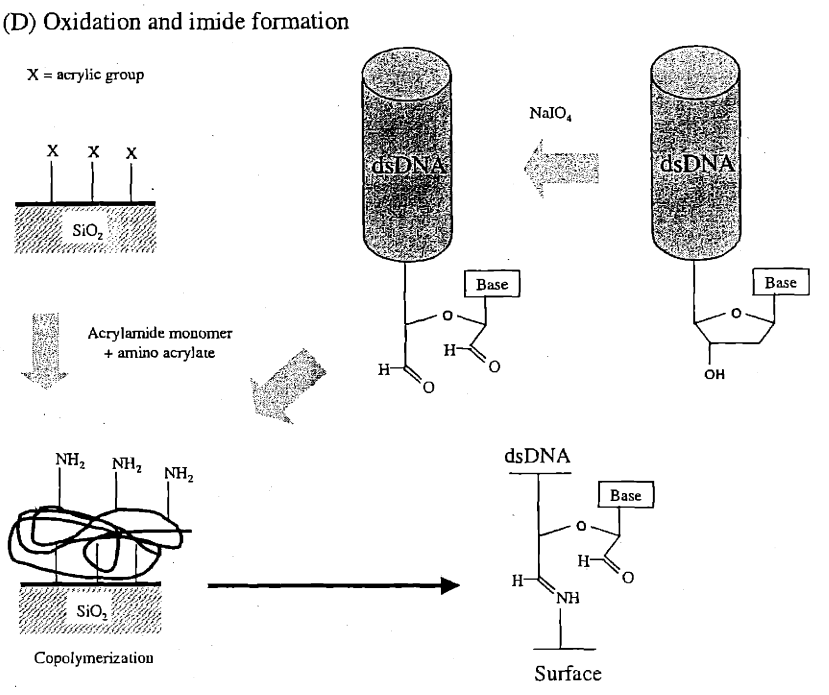

Figure 4-1. A graphic representation of dsDNA immobilization techniques from literature (cont'd). (d) an amine group is copolymerized with an acrylamide gel that is attached to the surface via acrylic-terminated silanes. Next, the 3' pentose ring on a dsDNA molecule (generated by PCR) is oxidized to form aldehyde groups, which then react with the amines on the surface to form imine bonds, or Schiff bases.

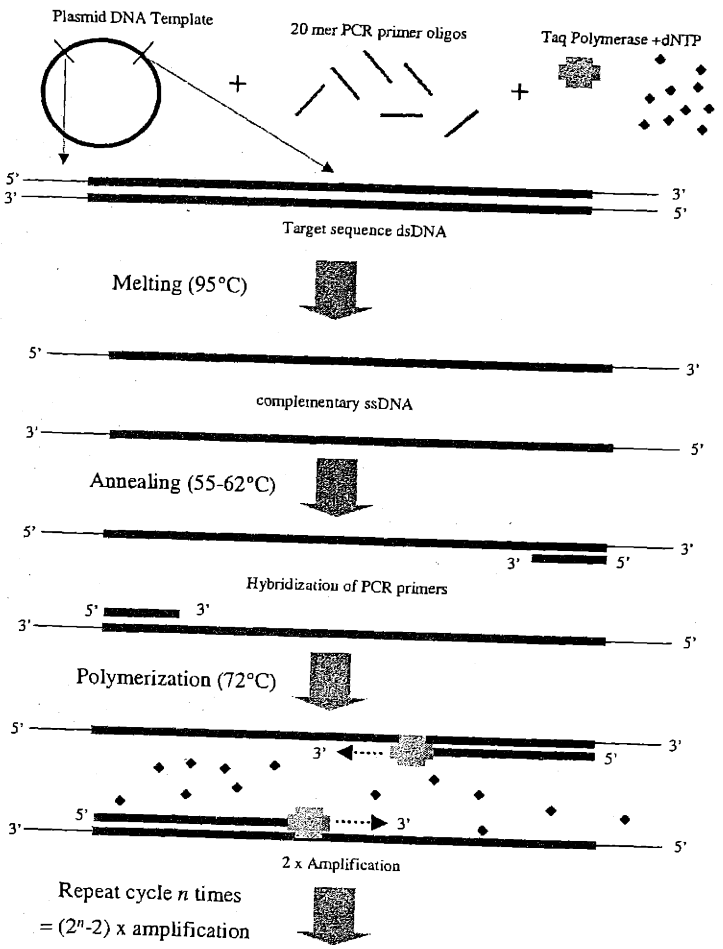

Figure 4-2. A graphic representation of PCR protocol. The template dsDNA (usually incorporated into a circular plasmid DNA form) is heated to separate the two ssDNA strands. Next, the 20 mer oligo PCR primers are hybridized to the ssDNA the 3' ends in the "annealing" process. Finally, the Taq polymerase fills in the complementary strand in the 5' → 3' direction to generate 2 dsDNA chains within the target DNA sequence, usually an exon of an expressed sequence. Each thermal cycle results in a 2 x amplification of the dsDNA.

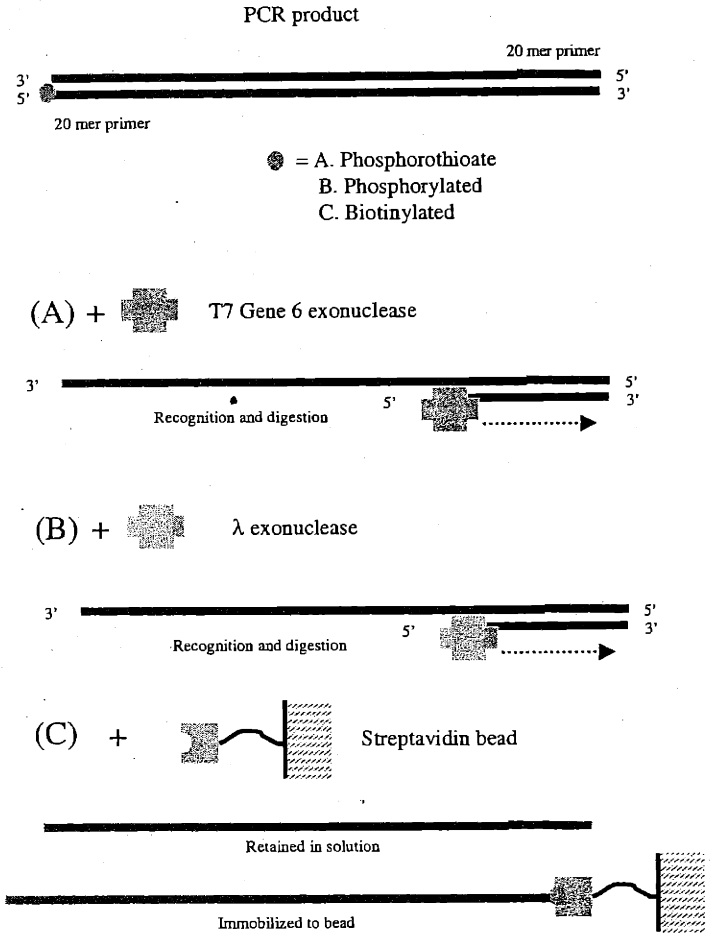

Figure 4-3. A graphic presentation of asymmetric PCR protocol. The dsDNA is generated by PCR with one of the primers modified at the 5' end with specialized functional groups: (a) and (b) the specialized primer is recognized and preferentially digested by certain exonucleases; (c) the dsDNA is heated to melt into two ssDNA strands, and the biotinylated strand is removed by specific conjugation with streptavidin-covered beads. In all cases the ssDNA with the specialized primer is removed or degraded.

4.1.2 Hybridization of dsDNA with 3' dangling end

An alternative would be to amplify the dsDNA by PCR, then use a specific restriction endonuclease to create a dangling oligo overhang that can react with complementary oligo sequences on the surface[12]. This approach is simpler compared to the asymmetric PCR protocol and results in the direct creation of a dsDNA with an overhang oligo available for surface attachment. However, most restriction endonucleases only provide a 4 to 5 nt length overhang, which not in is less thermodynamically stable but also reduces the number of possible discrete sequences ($=4^n$, where n = number of nucleotides on the oligo chain) available for spatially addressing the dsDNA onto the surface. In addition, most restriction endonucleases have a fairly narrow and specific recognition site on the DNA chain, which further restricts the number of choices available for the overhang sequence. One exception is the restriction endonuclease NbstN.I, which creates a 9 mer overhang. Since all endonucleases only recognize and cut specific sequences on the dsDNA chain, and since the recognition sequence usually straddles the actual cleavage site, the possible permutations of the oligo overhang sequence are still somewhat limited. However, the 9mer overhang is more thermodynamically stable and is thus a possible choice for immobilizing dsDNA molecules. First, oligos with 5' end reactive linkers (amino, thiol, biotin) are immobilized onto a derivatized silicon surface. The oligo sequence is complementary to the 3' oligo overhang created by the endonuclease on the dsDNA chain. The dsDNA molecules are attached to the oligo surface by hybridization of the overhang sequence. Then, DNA ligase is used to fill in the single phosphate gap between the oligo molecule and the dsDNA chain, thus covalently immobilizing the dsDNA chain onto the surface[13-15].

4.1.3 Orientation considerations for DNA surface hybridization

However, a common problem with all of the above approaches is that in order to DNA hybridization to proceed, the orientation of the oligo chain on the surface must be 3' end distal to the surface, and 5' end is adjacent to the silane SAM. Since DNA hybridization is antiparallel, the surface oligo must be oriented with the 5' primer adjacent to the solid surface in order for the dsDNA with overhang to effectively hybridize to the surface. Otherwise the long chain dsDNA portion would be directed at the surface instead of towards the solution phase, a structure that is both sterically and thermodynamically unfavorable.

The importance of the orientation of the surface oligo chains to the immobilization strategy is shown in detail in Figure 4-4. The orientation with the 5' end of the oligo facing the solid surface is routinely met by oligo immobilization methods involving covalent attachment of synthesized oligo chains from solution to the surface, since the amine, thiol or biotin functional groups used as the reactive group is added onto the 5' end of the oligo chain during synthesis. The resulting orientation of the oligo chain immobilized by covalent crosslinking is the exact opposite of the orientation I achieved by directly synthesizing the oligos onto the surface. For the DNA polymerase reaction, the enzyme recognizes a 3' OH group and proceeds in the 5' to 3' direction, so an ssDNA chain hybridized to our surface would not have the correct orientation for the polymerase reaction to take place. furthermore, the overhangs created by the various restriction endonucleases are on the 3' end of the dsDNA strand and are also incorrectly orientated for hybridization to oligo chains produced by direct synthesis. For a visual representation of the issues encountered using these methods see Figure 4-5.

4.1.4 Strategy for producing and immobilizing dsDNA with 5' overhang

I had to develop a method that could accommodate the particular orientation of our surface oligo chains, so I decided to try a strategy that involved PCR with a customized PCR primer that created a 5' end overhang instead of the 3' end overhangs produced by restriction endonucleases. I decided to synthesize a PCR primer with the usual 20 nt sequence necessary for incorporation into the PCR dsDNA chain, but also add

a 10 mer oligo sequence to the 5' end of the primer. This oligo overhang would be complementary to the sequence of the oligo surface, and act as the dangling end that hybridizes with the surface oligo chains to immobilize the dsDNA to the surface.

However, the Taq polymerase and other enzymes used for PCR proceed in the 5' to 3' direction and unless they are inhibited in some way would simply fill in the 10mer oligo sequence to create a dsDNA chain 10 bp longer with no overhang available for hybridization to the oligo surface. Previous literature indicated that certain chemical moieties of the correct length inserted in between two oligo sequences would form a "spacer" that the structurally specific enzyme fails to recognize, causing the polymerase reaction to be terminated before the 10 mer oligo overhang is filled in, therefore preserving it for the surface hybridization reaction. I chose a triethylene glycol group as our spacer group because its conformation is dramatically different from a nucleotide and should not be recognized by the polymerase enzymes[16-18], and also because it is freely rotating and highly flexible[7,19], which could be helpful when the bulky and semi-rigid, dsDNA strand is trying to hybridize with the oligo surface chains, which are spatially constricted and have a severely limited range of motion and orientation.

4.1.5 Alternative methods for creating 5' overhang

Another possible approach would be to synthesize a custom oligo PCR primer with a 20mer sequence with UltraMild® protecting groups, and a 10 mer sequence with regular protecting groups. The custom oligo was synthesized on a specialized "Q" support (Glen Research, VA), which allowed the oligo to be cleaved from the support rapidly without removal of the protecting groups. The oligo chain would 1st be exposed to mild deprotection agents that removed the UltraMild® protecting groups on the 20 mer PCR primer sequence but not the 10 mer overhang sequence. Then the oligo was added to the PCR mix, and after completion the dsDNA would have an overhanging 10 mer that

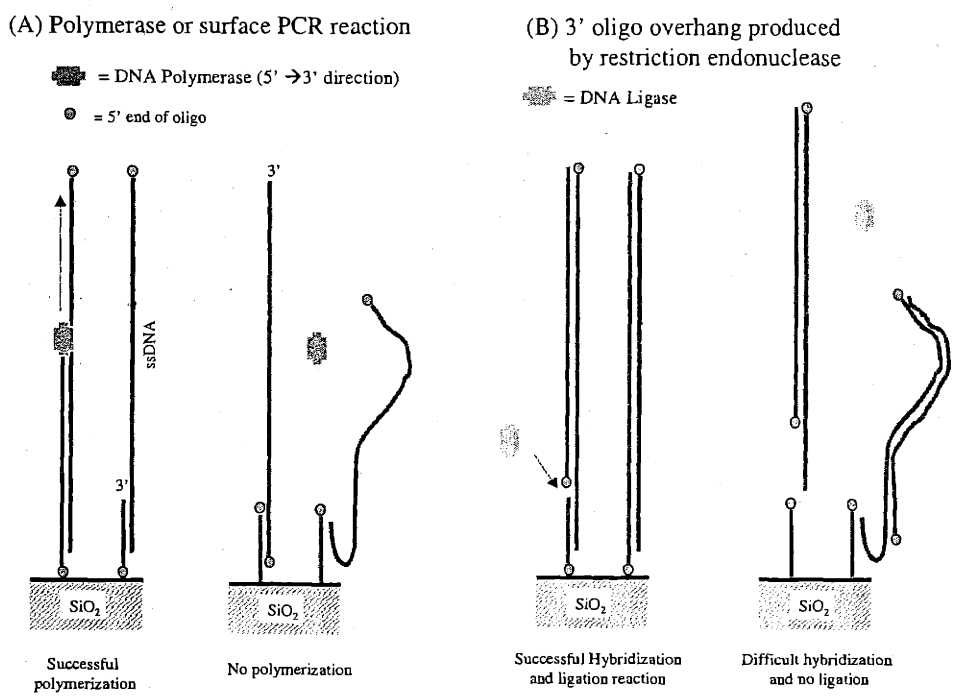

Figure 4-4. The importance of surface oligo orientation for dsDNA hybridization. (a) polymerases operate in the 5'→3' direction and if the oligo is attached to the surface at the 3' end, the ssDNA hybridizes in an orientation that prevents the polymerase action; (b) For dsDNA with 3' overhangs generated by endonuclease digestion, only oligos attached to the surface at the 5' end can hybridize with the dsDNA to create the appropriate 1 nt long gap, which is filled in by a DNA ligase to covalently attach the dsDNA to the surface.

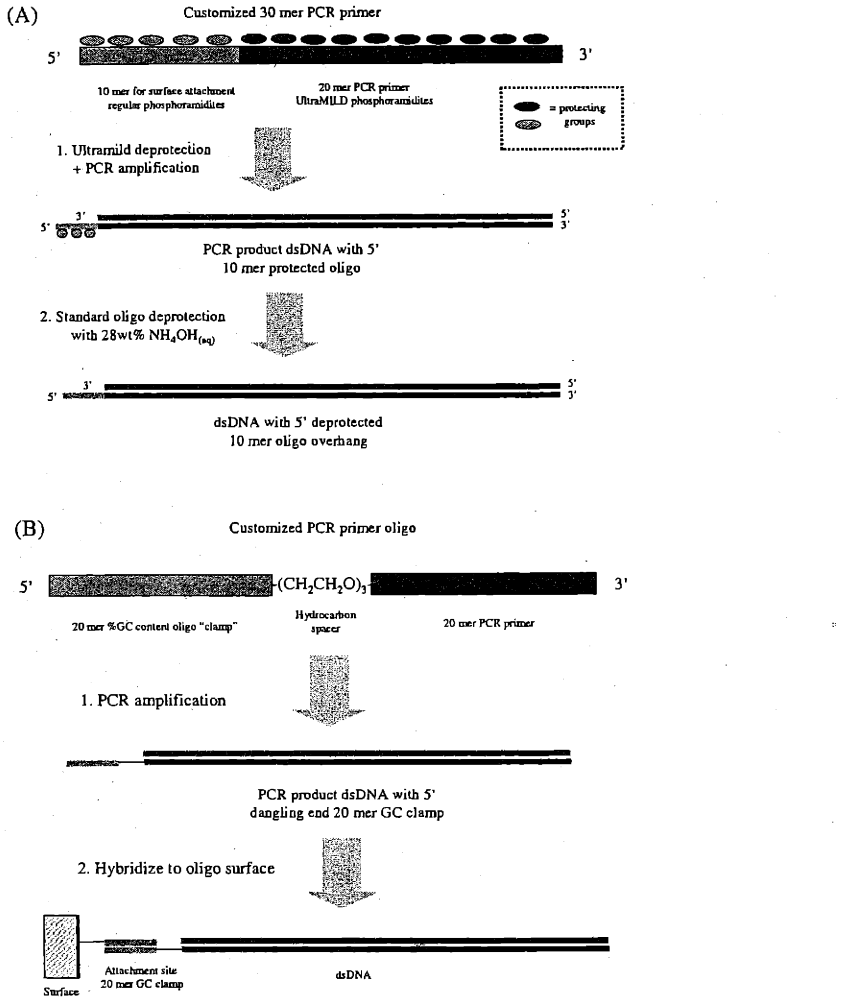

Figure 4-5. Alternative methods for generating 5' dsDNA overhangs, and surface attachment strategies. (a) A 40 mer oligo is generated with UltraMILD® protecting groups on the PCR primer sequence, which are deprotected for PCR. Then the whole dsDNA is immersed in NH_4OH to deprotect the 20 mer 5' overhang; (b) A customized oligo primer is produced with a 20 mer PCR primer portion and a GC sequence, and a hydrocarbon spacer protects the GC sequence from being filled in by the Taq polymerase. After hybridization to the immobilized oligo, the GC sequence acts as a thermally stable "clamp" to immobilize the dsDNA to the surface.

could be deprotected by a strong base such as 28wt% NH_4OH, because the strong base cannot degrade the dsDNA chain.

Although I demonstrated that the customized oligo could participate in PCR to produce the dsDNA chain, by using agarose gel electrophoresis with ethidium bromide dye, problems with effectively removing the base from the dsDNA solution, the lack of a flexible spacer between the 2 oligo sequences (10 mer and 20 mer), and the inherent complexities of the system disfavored this method, and I proceeded with the triethylene glycol spacer approach.

4.1.6 Approaches for creating a thermally stable surface attachment chemistry

The next question was how to covalently attach the dsDNA onto the surface. One proposal was instead of using a chemical crosslinker I would increase the thermal stability of the short dsDNA duplex formed by hybridization of the dsDNA overhang to the surface oligo chain. It is well known that GC hybrids are more thermodynamically stable than AT hybrids. Thus dsDNA duplexes with high GC content (%) have higher T_m values and are more stable to high temperatures. The stability of short dsDNA duplexes are also dependent on chain length. I could design the oligo sequence to have 100% GC content, and increase the length to 20 nt, to improve the thermodynamic stability of the dsDNA duplexes created by hybridization of an oligo overhang and a complementary surface oligo chain. Consequently the T_m would increase, resulting in higher thermal stability for a dsDNA. This method is the so-called "GC clamp" approach[20]. However, using 100% GC content would also limit the variability of the oligo sequences and thus restrict the number of addressable attachments sites on the surface, which is undesirable for DNA microarrays. In addition, I would need to heat the immobilized dsDNA strand over 90° C to effectively unravel the long chain (>300 bp) duplex and expose the probe ssDNA, and it was doubtful whether a 100% GC content dsDNA duplex could withstand the elevated temperatures, because the short chain length (20 mer) placed inherent limitations on thermodynamic stability.

In fact, this DNA melting effect was observed when I was amplifying certain dsDNA sequences (hemoglobin, or Hbglb) with a GC clamp inserted, by PCR. The successful amplification was proof that the GC clamp melted at the 95°C, since the whole Hbglb strand had to melt into ssDNA before the reaction could proceed. Finally, the total length of such a custom oligo would be at least 41mer in length, and despite the high coupling efficiencies for oligo synthesis the effective yield of oligo products with the correct length and sequence does decrease with increasing chain length.

4.1.7 Psoralen crosslinking method for covalent attachment

Therefore I decided instead to use a photoactivated crosslinker molecule psoralen. The structure of psoralen is shown in Figure 4-6a. Psoralen is part of the coumarin family, with a rigid, flat structure that readily intercalates within the dsDNA double helix, preferable between an A-T sequence[21]. Both the furan and pyrone functional groups of the psoralen compound are photolyzed with long wavelength UV light (365 nm)[22,23] to form covalent bonds with particular nucleotide bases. The furan side is 4 times more reactive than the pyrone side an overwhelmingly favors reacting with T nucleotides, though they have limited reactivity also with C and U nucleotides[21,23,24]. The crosslinking can result in the formation of monoadducts or diadducts by varying the wavelength and intensity of the UV illumination source. Finally, the crosslinking is reversible by exposure to short wavelength (254 nm) UV light[23], which appears to cleave the covalent bonds. Researchers have used psoralen or methylated psoralen derivatives to crosslink the two complementary ssDNA strands of a dsDNA duplex together to study DNA structure in solution, and special phosphoramidites with 5' psoralen linkers are commercially available (Glen Research). I decided to try two approaches involving psoralen, either by adding it as the final "nucleotide" on the 5' end of the surface oligo chains, or by adding it to the 5' end of the customized PCR primer, creating an oligo with a 20 mer PCR primer connected to a 10 mer overhang sequence with a flexible spacer

that is inert to the thermophilic polymerases used in PCR, and a photoactive psoralen crosslinker at the end. A cartoon represenation of the structure of the customized PCR primer I acquired from Research Genetics (Huntsville, AL), as well as its position in the PCR product is shown in Figure 4-6b. Figure 4-7 provides a synopsis of the psoralen crosslinking reaction that immobilizes dsDNA with a 5' 10 mer overhang onto oligo surfaces, using both the above-mentioned approaches. The customized primer was used for PCR amplification using a subcloned Hbglb plasmid fragment as the template, and ^{32}P dCTP labels for quantification.

4.1.8 Characterization of PCR product dsDNA using gel electrophoresis

After PCR the dsDNA crude product solution mix was characterized by electrophoresis in a 1% agarose gel with 0.5% ethidium bromide and the results are shown in Figure 4-8. Ethidium bromide is an intercalating dye that is fluorescent when stimulated by long wavelength UV light (365 nm), and is commonly used to detect the present of dsDNA during gel electrophoresis. The dsDNA PCR product forms a band at approximately 400 bp, which is reasonable since the Hbglb sequence is 390 bp in length and the 10 mer overhang adds some extra length as well as extra drag the will cause a slight decrease of the migration rate of the dsDNA in the agarose gel. The lack of other bands of different length and significant streaking suggests the PCR reaction proceeded efficiently. After using a spin column to purify the dsDNA and remove the unreacted primers and dNTP, 1% agarose gel electrophoresis confirmed the presence of dsDNA product in the retentate. The concentration of dsDNA in solution was determined by UV-Vis spectroscopy at 260 nm, and calculated with the equation:

C (μg/ml) =dilution x optical density (O.D.) x activity

Where activity for dsDNA = 50 μg/ml-O.D.

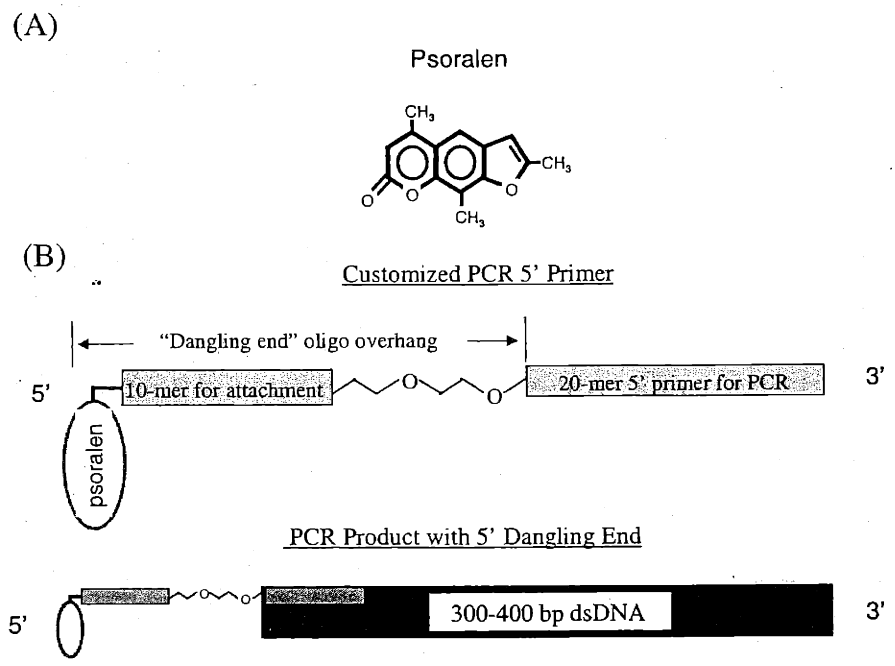

Figure 4-6. Graphic representation of customized oligo overhang and its position in the PRC product dsDNA molecule. (a) Psoralen structure is flat and rigid and readily intercalates within the dsDNA duplex, preferably between A-T sequences; (b) the composition of the customized PCR primer that includes a spacer to protect the 5' overhang oligo from the Taq polymerase during PCR, and the photoactive psoralen molecule. The overhang is incorporated at the 5' end of one of the ssDNA strands and freely rotates due to the spacer.

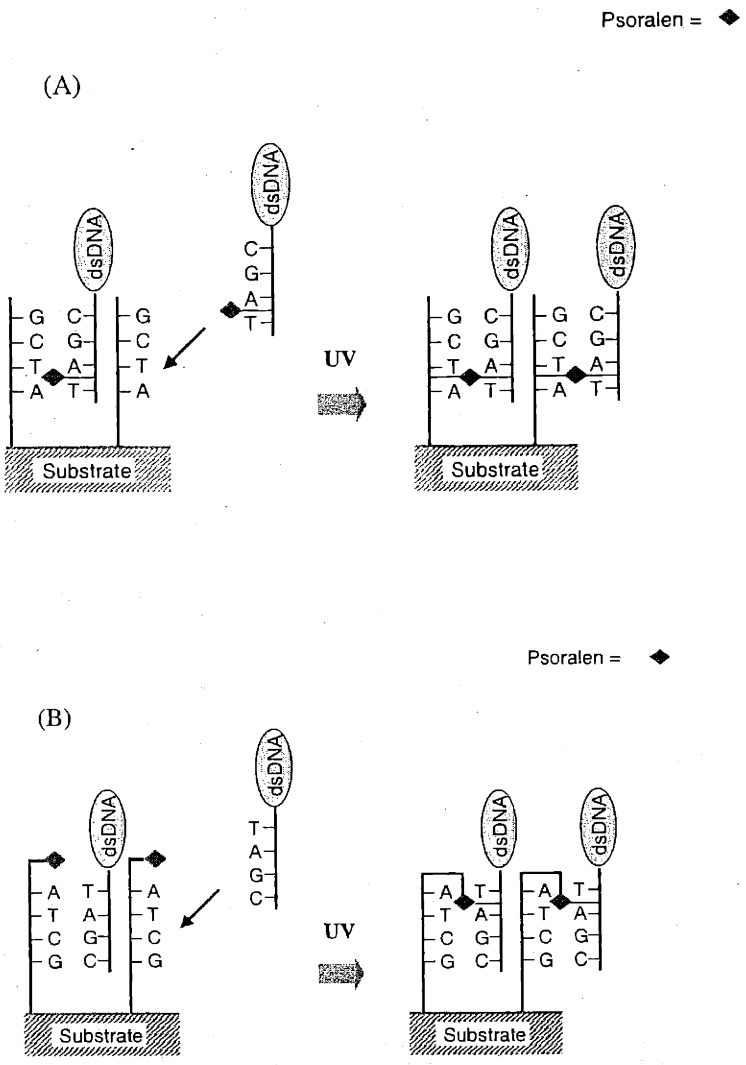

Figure 4-7. Schematic of psoralen crosslinking protocols. (a) Psoralen is incorporated at the 5' end of the incoming dsDNA; (b) Psoralen linker is synthesized on the 5' end of the surface oligo chain. In both cases the psoralen preferentially intercalates in the A-T sequence and is photolyzed to form a covalent bond with a T base.

Then a 1μl aliquot of the radiolabeled dsDNA solution was taken, and the radioactivity determined by scintillation counting. The activity of the radiolabeled dsDNA was calculated by:

Activity (cpm/mole) = Total radioactivity/Total DNA quantity

Where Total radioactivity = total solution volume x radioactivity of 1μl aliquot
And Total DNA quantity = C x total solution concentration /MW of Hbglb
And where MW = 600 Daltons/bp x dsDNA chain length

After I determined the activity of the dsDNA solution, it could be concentrated by lyophilization or purified by ethanol precipitation, then resuspended in the appropriate buffer solution. Since I hose buffers with high salt concentrations (1M NaCl) to facilitate hybridization of the dsDNA overhang to surface oligos, I did not remove the extra Tris and salts present in the original spin column elution buffer. Therefore I preferred lyophilization to ethanol precipitation to prevent product loss. The exception was for thiolated dsDNA PCR product used for experiments in Chapter 2. The thiol links had to be reduced using dithiothreitol (DTT) to protect their reactivity[25]. Consequently, the DTT had to be removed by extraction with ethyl acetate, followed by ethanol precipitation.

I confirmed the presence of the 10mer oligo overhang in our Hbglb PCR product dsDNA produced using the customized primer by challenging an unlabeled dsDNA strand with radiolabeled oligos that had a sequence complementary to the overhang oligo sequence of the dsDNA. The hybridization was conducted in solution, and the unreacted labeled oligos were removed by spin column, then the dsDNA was eluted. Scintillation counting indicated that hybridization had occurred between the dsDNA overhang and the labeled oligo, proving that the overhang was present in the PCR product.

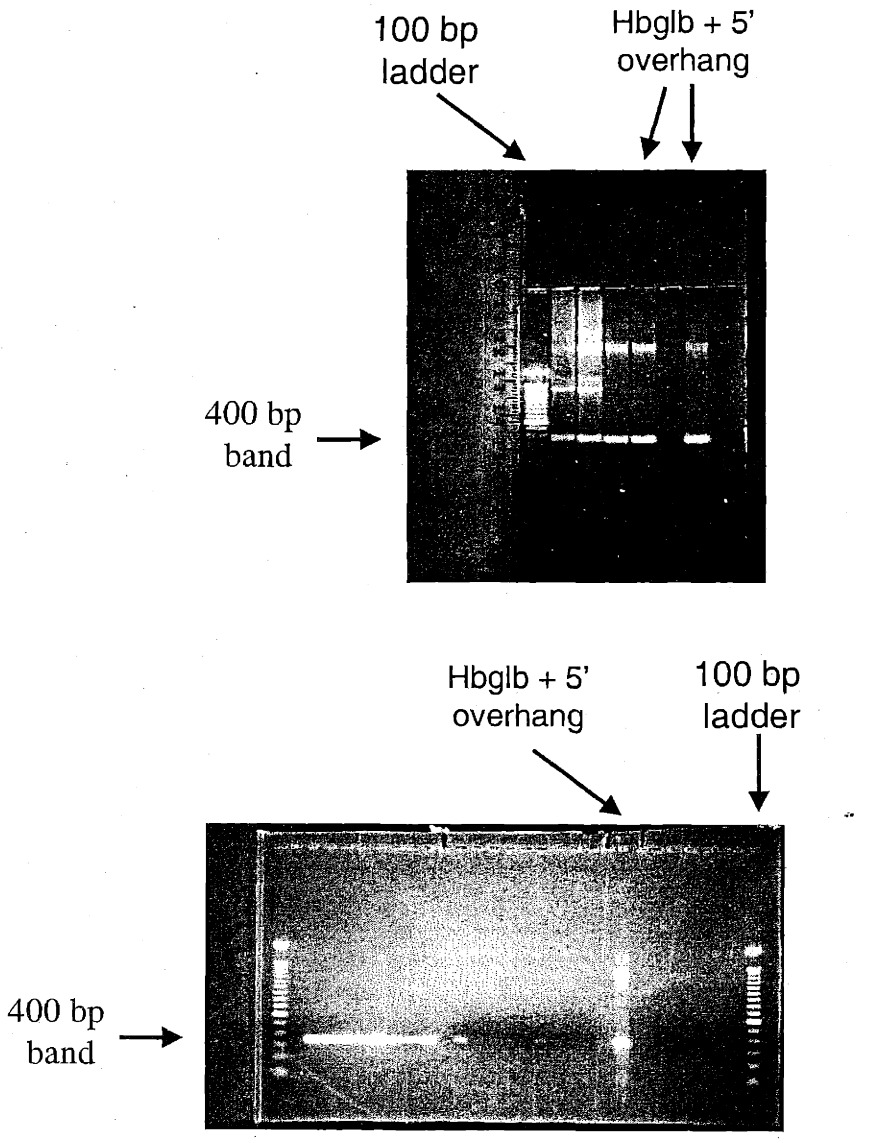

Figure 4-1. Image of 1% agarose gel with PCR product (Hbglb sequence + 5' 10 mer overhang + psoralen crosslinker). The dsDNA is characterized by UV illumination of the intercalating dye Ethidium Bromide. A band appearing at approximately the 400 bp level indicates successful amplification of the Hbglb sequence (390 bp) with a 10 nt oligo overhang.

4.2 dsDNA Immobilization by surface hybridization

4.2.1 Hybridization of dsDNA with 5' overhang to surface oligos

After producing and purifying dsDNA with 5' oligo overhangs, I immobilized the dsDNA onto complementary oligo surfaces under conditions similar to the optimal surface hybridization conditions obtained from previous surface hybridization studies using of 10 mer oligos. The dsDNA was dissolved in 1 M NaCl solution (7 x SSC) at a solution concentration of 0.5 μM, with 0.1 wt% SDS added to prevent nonspecific adsorption of the dsDNA onto the oligo surfaces. Hybridization was carried out at 4° C for 24 hours, following the same protocol as experiments with 10 mer oligos. However, unlike the 10 mer oligo hybridization experiments, where the oligo surfaces were completely immersed in the labeled oligo solution, the amount volume of dsDNA solution was only around 3 to 5 μl, just enough to cover the oligo surface with a thin liquid film. This small volume of liquid was necessary to maintain the dsDNA solution concentration and to conserve the PCR product.

Thus, after the dsDNA solution droplets were added to the oligo surfaces, the samples were placed into improvised polystyrene hybridization chambers. The chambers were sealed almost airtight with tape and parafilm, and inside the chambers were reservoirs containing buffer solutions at lower salt concentrations (1 x TE) than the hybridization buffer (7xSSC). At equilibrium conditions, the reservoir would provide a continuous source of water vapor that would hydrate the sample due to osmotic pressure driving forces created by the differences in salt concentration between the reservoir and the hybridization solution. When using this setup the hybridization solution on the oligo surface did not dry up, but instead the area of the liquid drop slowly expanded until it reached the edges of the silicon chip, fully coverage the oligo surface. In addition, the SDS surfactant added to prevent nonspecific DNA adsorption also helped to reduce the surface tension of the aqueous solution and spread the liquid drop out evenly over the silicon surface instead of being localized into a bead.

4.2.2 Characterization of dsDNA hybridization

Radiation scintillation counting and fluorescence spectroscopy were used to characterize the oligo surfaces after hybridization, to determine whether dsDNA was hybridized to the surface oligos, and the amount of immobilized dsDNA. For this purpose ^{32}P labeled dCTP or fluorescein labeled dCTP were added to the PCR reaction mix so that the labels could be incorporated into the dsDNA backbone during the amplification. The radiolabeled dsDNA can be quantified by scintillation counting, while a CCD or PMT system can be used to characterize the fluorescence signal emitted at 525 nm by the fluorescein dye (illuminated by an Ar laser at 488 nm).

A picture and schematic of the CCD/PMT setup is shown in Figure 4-9a and 4-9b. From the diagram the incident laser light illuminates the oligo chip at an angle of about 60 to 70 degrees from the surface normal, while the CCD or PMT is located directly about the sample chip. This configuration was designed to minimize possible interference of the reflected laser light on the CCD or PMT readings. In addition, highband filters were added to both the CCD and PMT objective lenses to further screen out any reflected or reflected light with wavelengths lower than 500 nm. Finally, the entire optical illumination/detection system was enclosed in a light-tight structure that prevented ambient light from being detected by the PMT or CCD camera, causing unwanted noise or interference with the fluorescence measurements.

To test the specificity of the dsDNA surface hybridization, three sets of dsDNA were produced. One dsDNA sequence had a 5' 10 mer oligo overhang and radioactive labels incorporated. Another dsDNA sequence also had the oligo overhang and had both ^{32}P and fluorescein labels. The third dsDNA sequence was a control sequence with no oligo overhang but both ^{32}P and fluorescein labels. All three sequences were separately hybridized onto oligo surfaces with sequences complementary to the 10mer overhang of the dsDNA molecules. Scintillation counting was used to quantify the sample radioactivity, and the PMT setup was used to determine fluorescence, and the results are tabulated in Table 4-1.

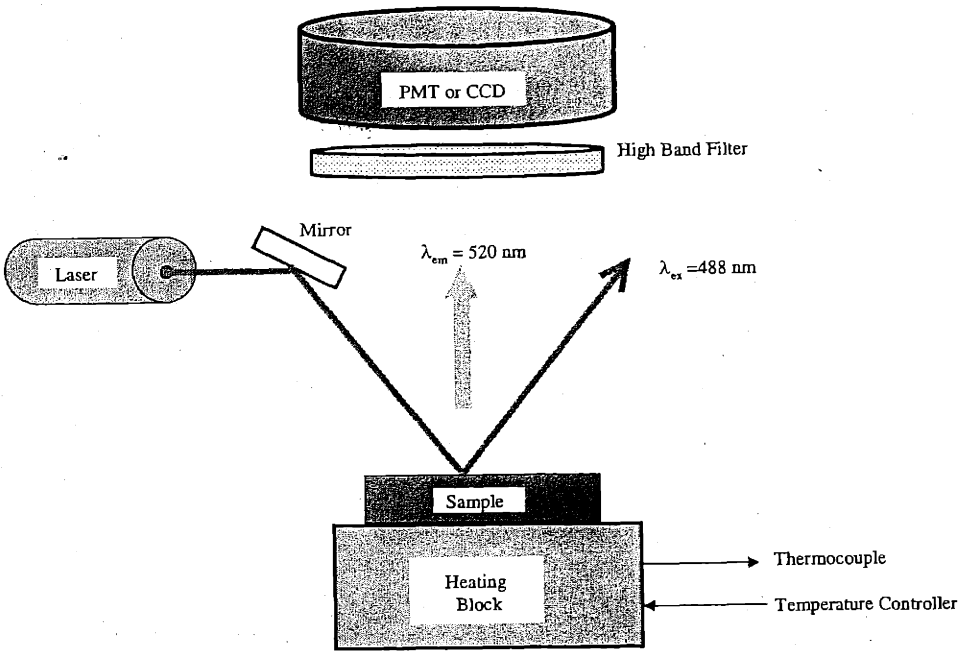

Figure 4-9. Graphic description of the PMT-CCD setup: (A). Schematic diagram shows that the incoming laser illumination is directed by mirror to a 30-40° incident angle to minimize background from scattering or reflection. The fluorescent emissions are passed through a filter to prevent contamination by scattered laser radiation, then collected and quantified by a CCD camera or PMT. The sample may be heated by an underlying heating block.

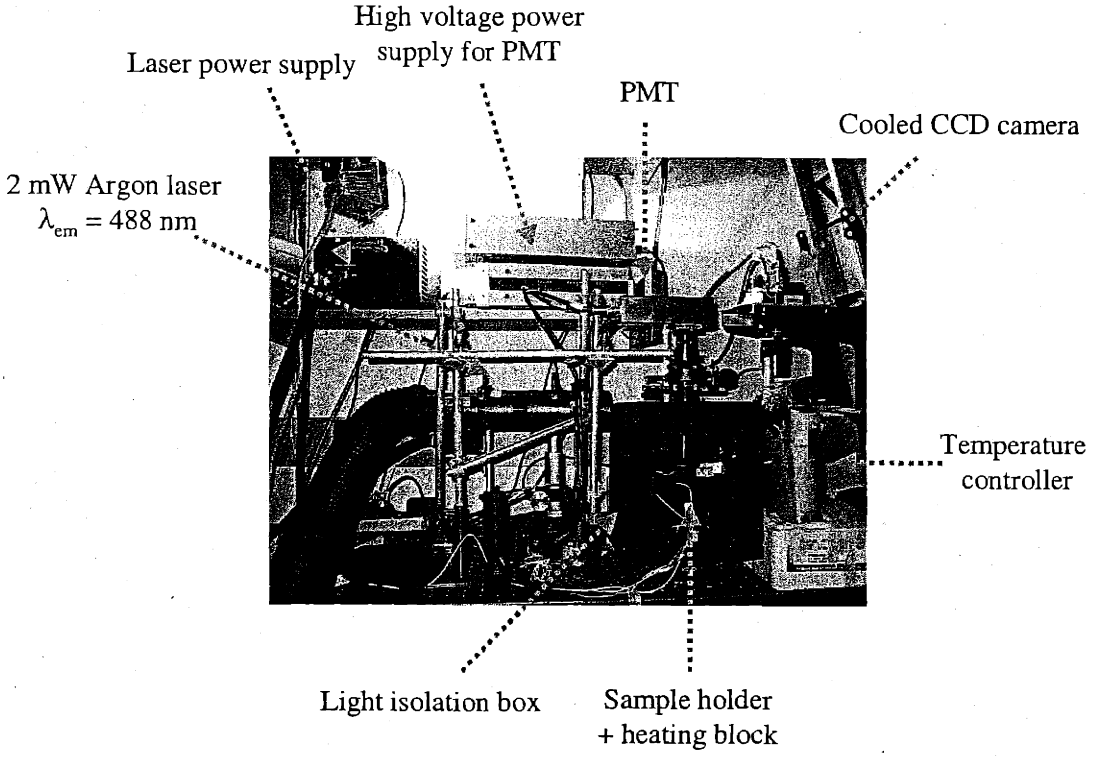

Figure 4-9. (B) Photograph of fluorescence setup, which consists mainly of the cooled CCD device, the PMT device, light tight sample holders with aluminum base plates (capable of generating temperature ramps), and the 2 mW Ar laser (λ_{em} = 488 nm).

From the low radiation and fluorescence background signal produced by the control dsDNA sequence, it is evident that there is very little nonspecific adsorption of the control dsDNA onto the oligo surface. This result is partially due to the SDS surfactant present in the hybridization buffer, and to the electrostatic repulsion of the surface oligo layer.

Conversely, the high radiation and fluorescence signals obtained for oligo surfaces challenged with dsDNA sequences that had a 10mer oligo overhang strongly suggest that the dsDNA has been immobilized to the surface by hybridization. In addition, the oligo surfaces challenged with the control dsDNA with fluorescein and ^{32}P labels had a higher fluorescent signal than the surfaces with hybridized dsDNA (with overhang) that had only ^{32}P labels. This data confirmed that the PMT was working properly and detected only the background fluorescence signal from the small amount of nonspecifically adsorbed control dsDNA chains, while ignoring the hybridized dsDNA with no fluorescein labels. Finally, surface coverage of dsDNA hybridized to oligo surfaces synthesized on OH silane substrates was high enough that the majority of subsequent dsDNA surface hybridization experiments were carried out using oligo surfaces synthesized on OH silane substrates, unless otherwise noted.

4.2.3 Fluorescence with YOPRO™

Alternatively, a buffer solution containing YOPRO™ (oxazole yellow), an intercalating dye, could be added to the oligo surface. Shortly after immersion, the amount of YOPRO™ in solution versus the amount intercalated into the dsDNA double helix reaches an equilibrium condition, resulting, on average, in approximately one intercalated YOPRO™ molecule per 8 to 10 bp. The YOPRO™ solution and the surface were illuminated by 488 nm light from an Argon laser.

Table 4-1. Hybridization of fluorescein-labeled PCR product with dangling 5' 10 mer overhang (in 1 M NaCl buffer with 0.1% SDS) to surface oligos synthesized on OH surfaces. The hybridization proceed for 24 hours at 4°C. The control is a PCR sequence with no overhang. The radioactive scintillation counting and fluorescence intensities all suggest a significant amount of dsDNA hybridized to the surface, and a low background due to nonspecific adsorption.

dsDNA species	Radioactivity (cpm)	Fluorescence (cps)
Fluorescein +^{32}P + overhang	10502	3985
Fluorescein +^{32}P control	73	162

** Immerse for 24 hr at 4° C in 50 μg/ml dsDNA in 1M $NaCl_{(aq)}$, OH silane oligo (40%)*

The presence of immobilized dsDNA on a surface was detected by comparing the fluorescence signal of a sample immersed in YOPRO™ solution with a control (oligo surface or a silane surface) immersed in the same YOPRO™ solution. It is possible to detect DNA hybridization because the intercalated YOPRO™ dye produces a 50-100 times amplification in fluorescent signal, compared to YOPRO™ molecules in solution. Either the CCD or the PMT setup can be used to determine the fluorescence signal of the YOPRO™ dye. For the experiments using YOPRO™ dye, I produced dsDNA PCR

products with incorporated ^{32}P radiolabel and a 5' 10 mer oligo overhang. The dsDNA molecules were used to challenge oligo surfaces containing both oligo sequences complementary to the 10mer overhang, and control surfaces with a noncomplementary oligo sequence.

After the hybridization reaction was completed, the oligo chips were first characterized by scintillation counting, then immersed in a 0.1μM YOPRO™ solution in 7xSSC (1 M NaCl) buffer for 4 hours. The samples, still immersed in the dye solution, were illuminated by an Argon laser (λ_{em} = 488 nm), and a CCD camera was used to measure the fluorescence signal. Representative CCD images are shown in Figures 4-10a and 4-10b. Figure 4-10a was obtained from an oligo chip with dsDNA immobilization confirmed by radiation scintillation counting, while 4-10b represents a control sample with only the oligo surface immersed in the YOPRO™ solution.

4.2.4 CCD Data Processing

Certain adjustments were made to the data acquisition program for the CCD camera, to focus onto the illuminated spot, which was only around 1mm in diameter, and to increase the sensitivity and resolution of the CCD measurements. The protocol was developed by Jeremy Lambert and consisted of two major elements. The original optical field of the CCD camera consisted of a rectangular array with 1024x1000 pixels. The pixels were "binned", or reduced by a factor of 10, which effectively changed the size of the array to 102x100. The binning command also integrated the signal intensities of 10 pixels into 1 pixel, causing a 10 fold increase in the sensitivity of the CCD camera. In addition, manual focusing was used to reduce the optical field of the CCD camera to only a 32x32 pixel square that contained the sample spot illuminated by the laser. The focusing and reduced field decreased the amount of background noise that could be caused by stray light reflected off other nonilluminated areas of the sample. To minimize the amount of photobleaching, 5 to 10 measurements were taken immediately after laser illumination, with 10 millisecond exposure times and 1 second spacing in between exposures.

The captured images had to be processed further, by integrating the total intensity of the spot, then averaging the intensity over the spot area, and a program written by Jeremy Lambert in FORTRAN code, "MOSAV", was used for this purpose. The average intensity for the various samples (in cps), along with their respective radiation intensities, are shown in Table 4-2. The low overall radiation and fluorescence signal from the control sample indicate that the 10 mer overhang of the most likely due to a small amount of nonspecifically adsorbed dsDNA on the noncomplementary surfaces, and serve as background readings. The high radiation and fluorescence signals, and the high signal to noise ratios, obtained from the oligo surfaces with sequences complementary to the dsDNA overhangs suggest that the dsDNA molecules indeed hybridized to the surfaces rather than nonspecifically adsorbed onto the surfaces. The dsDNA chains do not hybridize to noncomplementary surface oligo sequences, suggesting that the surface hybridization reaction is highly specific. The low signals are possibly to nonspecific DNA adsorption. The results from fluorescent and radioactive characterization techniques all indicate that the dsDNA 5' overhangs have hybridized with the surface oligo chains to form end-immobilized dsDNA chains.

4.2.5 dsDNA surface coverage

The amount of dsDNA hybridized to the oligo surfaces was about $2x10^{-13}$ moles/cm^2. This value is comparable to the amount of dsDNA that theoretically could be nonspecifically adsorbed onto a flat surface, assuming monolayer coverage and a 20 Angstrom by 1400 Angstrom footprint for a 390 bp dsDNA chain. Thus the density of hybridized dsDNA is approximately the same as the surface coverage of dsDNA on the adsorbed on the polylysine substrates for the microspot arrays developed by Pat Brown.

(A)

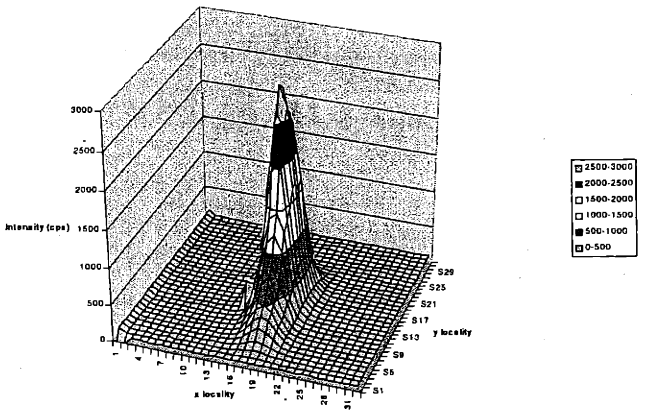

(B)

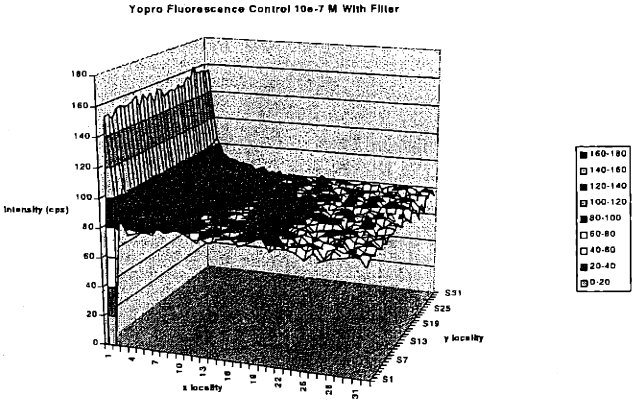

Figure 4-10. Excel plots of CCD camera images of immobilized dsDNA using 0.1 μM YOPRO™ dye in 1 M NaCl buffer at room temperature. (a) dsDNA with 10 mer oligo overhang hybridized to complementary surface oligo; (b) the background from a control sample of dsDNA with 10 mer oligo overhang hybridized to a noncomplementary oligo surface.

Table 4-2. Hybridization of dsDNA PCR product with 5' 10 mer overhang. The dsDNA was solvated at 0.5 μM concentration in 1 M NaCl buffer with 0.1% SDS, and hybridized with the surface oligos for 24 hours at 4°C. The control surface is a noncomplementary oligo sequence. For fluorescence measurements the samples were immersed in a solution of 0.1 μM YOPRO™ dye in 1 M NaCl buffer at room temperature. The scintillation counting provides the surface density of hybridized dsDNA, and the radiation and fluorescence measurements indicate low background resulting from either mismatch hybridization or nonspecific adsorption.

Substrate	^{32}P Intensity (cpm)	Yopro™ Intensity (cps)	Surface Density (moles/cm^2)
OH silane (comp)	4352	1492	2.18×10^{-13}
TCA silane (comp)	8384	2138	?
Control (noncomp)	50-200	80	$<0.1 \times 10^{-13}$

** Immerse for 24 hr at 4° C in 50 μg/ml dsDNA (with overhang) in 1M $NaCl_{(aq)}$*

However, as seen from Figure 4-11, the surface coverage of dsDNA is much lower compared to the densities of either 10 mer oligos, or the 30 mer customized oligos with the 20 mer PCR primers, and to a custom-made 38 nt long oligo aptamer that has some additional secondary structure. The results of the plot suggest that the surface hybridization of DNA is dependent on the length of DNA that is not participating in the surface hybridization (and is therefore not part of the surface attachment site, a 10 bp dsDNA duplex). As the length increases, the surface coverage of hybridized DNA

decreases. One possibility for this decrease in hybridized DNA surface coverage may be due the larger volume of the unhybridized oligo or dsDNA that is not directly hybridized with the 10 surface oligo. These negatively charged DNA oligomers remain suspended in solution but are very close to the oligo surface, and they may create a boundary layer with steric and electrostatic repulsion effects that effectively prevent incoming solution phase DNA strands from reaching the surface immobilized oligo chains and hybridizing with them.

In addition, the negatively charged nucleotides in the all DNA chains are fairly soluble in water. Therefore, the unhybridized DNA the remains in solution has a thermodynamic driving force may result in equilibrium conditions that favor partitioning the DNA molecules in the solution phase instead of on the solid surface. Also, the unhybridized DNA molecules could also reduce the thermodynamic stability of the 10 bp double helical DNA that attaches the DNA onto the oligo surface, resulting in lower surface coverage. Consequently, a 10mer oligo in solution that is complementary to the surface oligo, with no unhybridized nucleotides, has a higher surface hybridization density than a 30 nt custom oligo, since the custom oligo sequence contains a 20 nt long PCR primer portion that is not hybridized. The 390 bp Hbglb dsDNA sequence is not only 39 times longer then a 10 mer oligo but has at least 78 times the amount of nucleotides since it is double-stranded, and the large portion of DNA still solvated in the buffer could repulse incoming dsDNA molecules from diffusing to the oligo surface, or disrupt the stability of the surface hybridization site, so the amount of dsDNA hybridized to the surface is only about 1/50 of the amount of 10 mer oligos.

4.2.6 Optimization of dsDNA surface coverage-dsDNA solution concentration

The next question was whether it was possible to increase the amount of dsDNA hybridized to the surface. The motivation for an increase in surface density was twofold. First, a higher dsDNA surface coverage should result in producing brush-like structures, with the 300 –1,000 bp dsDNA strands oriented upright and away from the surface. I believe that after photoactivated crosslinking and heating to expose the ssDNA chains,

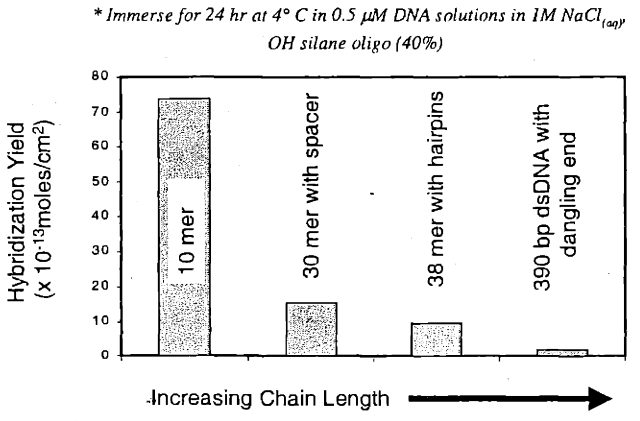

Figure 4-11. Comparison of the surface coverage of oligos or dsDNA hybridized to surface oligos synthesized on OH silane surfaces. The DNA was solvated at 0.5 μM concentration in 1 M NaCl solution with 0.1% SDS, and hybridized with the oligo surfaces for 24 hours at 4°C. The plot indicates a decrease in surface hybridization with increasing oligo length, with a 50 x differential between 10 mer oligos and 390 bp dsDNA. This decreasing trend suggests that longer chain length inhibits surface hybridization possibly due to steric or electrostatic repulsion, or through shifts in the thermodynamic stability of the 10 mer dsDNA surface attachment site.

that a brush-like surface structure should result in improved hybridization efficiency for the surface immobilized long chain ssDNA probes. In addition, since the existing literature showed that the psoralen photolysis reaction used to covalently crosslink the dsDNA chain to the surface is only around 50% efficient in the solution phase, maximizing the surface coverage of dsDNA prior to photolysis should help to increase the amount of dsDNA covalently bound to the surface.

The first consideration I tried was to increase the dsDNA solution concentration, which should create a thermodynamic driving force that would favor hybridization of the dsDNA to the oligo surface. The dsDNA was concentrated by first freezing the purified PCR product (in TE buffer, pH=8.0). The samples were then lyophilized the samples using a speed vac, and finally resuspended at smaller liquid volumes. I was able to produce dsDNA solutions in 7xSSC buffers with concentrations up to 20 times higher than the original 0.5 μM, and after running hybridization experiments with the resuspended dsDNA solutions, I examined the relationship between surface hybridization coverage and dsDNA solution concentration. The experimental data shown in Figure 4-12 indicate that the surface coverage of dsDNA increases with increasing solution concentration, suggesting that it is possible to improve the surface coverage of hybridized dsDNA by using more concentrated dsDNA solutions.

I was able to achieve dsDNA surface hybridization densities at up to $2x10^{-12}$ moles/cm^2, values an order of magnitude higher compared to other dsDNA immobilization methods described in the literature, as well as that obtained from commercially available dsDNA microarrays. In addition, the monolayer coverage of 390bp dsDNA adsorbed flat onto a surface is approximately $6x10^{-13}$ moles/cm^2, according to a 1400Å x 20Å footprint, which is only half of the surface coverage obtained previously. These calculations strongly suggest that the dsDNA molecules immobilized onto the oligo surfaces at a surface coverage of 2×10^{-12} moles/cm^2 shouldn't display a flat conformation, but rather a brush-like structure with the end-immobilized dsDNA strands oriented away from the oligo surface. For the brush-like structure, the dsDNA is attached to the surface only at the 10mer oligo hybridization site, instead of at multiple

points like the nonspecifically adsorbed dsDNA strands used in the Pat Brown microspot arrays.

4.2.7 Optimization of dsDNA surface coverage-dextran sulfate

Next, I studied the dsDNA surface hybridization kinetics and found that it resembled the kinetics profile obtained for surface hybridization of 10 mer solution phase oligos. After an initial sharp increase in the amount of dsDNA hybridized to the surface, the curve starts to flatten out. This decrease could be due to the increased steric and electrostatic repulsion created by the immobilized long chain dsDNA molecules, preventing incoming dsDNA from diffusing to the oligo surface. However, as with the 10mer oligo hybridization seems to have stopped after 24 hr immersion times, suggesting that the system has reached equilibrium conditions.

Literature from previous studies have suggested that the surface hybridization kinetics could be increased by adding 5-10wt% dextran sulfate to the dsDNA solution. Since dextran sulfate is a negatively charged polysaccharide, the theory is that at high concentrations it could exhibit volume exclusion effects that create a thermodynamic driving force that help partition the dsDNA molecules to the oligo surfaces. Solutions containing dsDNA and various concentrations of dextran sulfate were used for surface hybridization studies, and the results are shown in Figure 4-13.

I found that dsDNA solutions with higher than 5wt% concentration of dextran sulfate show up to 125% increase on hybridized dsDNA surface density after 24 hours immersion, suggesting that it is possible to increase the amount of surface hybridized dsDNA by adding at least 5wt% dextran sulfate. However, the plot does not seem to indicate a positive trend for dsDNA surface hybridization when more dextran sulfate is added, so 5wt% should be adequate. Another approach I explored for increasing the

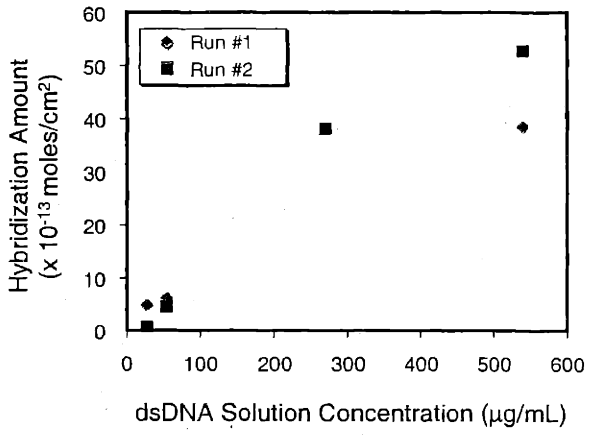

Figure 4-12. Effect of solution dsDNA concentration on surface hybridization. The dsDNA is lyophilized, then resuspended in 7 x SSC (1M NaCl) buffer with 0.1% SDS, and hybridized with surface oligos synthesized on OH silane surfaces for 24 hours at 4°C. It is evident that the surface coverage of hybridized dsDNA increases with increasing solution concentration.

amount of dsDNA hybridized to the surface was to reduce the contact area between the dsDNA solution and the oligo surface, using hydrophobic pinning techniques.

4.2.8 Producing patterned surfaces by soft lithography

I designed 1 or 2 mm diameter circular spot patterns, which were made into photolithographic masks that were used to positively etch silicon chips. Then, polydimethylsiloxane (PDMS) rubber was poured onto the silicon chip positive resists, to produce negative resists used for "soft lithography". In this technique, a thin layer of trichlorosilanes in organic solvent is added onto the surface of the PDMS negative resist. After the solvent evaporates a very thin film of trichlorosilane remains on the PDMS surface. The PDMS resist is then used as a "stamp" to transfer the silanes onto a silicon surface in a particular pattern. The imprinted silane instantly forms a covalent attachment to the silicon surface, creating a surface pattern with modified surface properties. For a schematic of the soft lithography technique please refer to Figure 4-14.

I used octadecyltrichlorosilane (OTS) in dry hexane as the "ink", and printed it onto two surfaces. First, I printed OTS onto bare silicon surfaces, resulting in hydrophobic 1 cm x 1 cm squares surrounding 1mm or 2mm diameter spots of bare silicon. Then I derivatized the bare silicon spot with reactive OH silane, and synthesized oligos on the OH silane surface.

In an alternative approach, oligo surfaces were synthesized. Then the oligo surfaces were imprinted with OTS using the same PDMS stamps as above. Hydrophobic squares with a 1mm or 2mm spots of immobilized oligo chains in the middle were produced using this method. In either case the hydrophobic surfaces successfully prevented the spread of aqueous solutions from the oligo surfaces in the middle to the surround area, ensuring a minimal contact area for hybridization to occur. Since the volume of the drop and the dsDNA solution concentration are unchanged, the hydrophobic pinning would result in an effective increase in the concentration of dsDNA

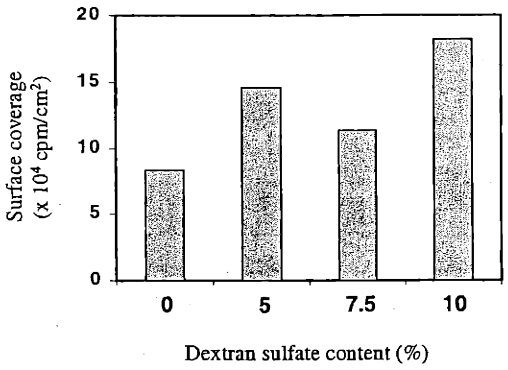

Figure 4-13. The effect of dextran sulfate on dsDNA hybridization. All dsDNA with 5' 10 mer oligo overhangs were solvated at 200 mg/ml in 7xSSC (1M NaCl) buffer with 0.1% SDS and different concentrations of dextran sulfate, from 5-10 wt%. The results suggest that addition of >5% dextran sulfate will result in up to 125% increase in the surface coverage of hybridized dsDNA.

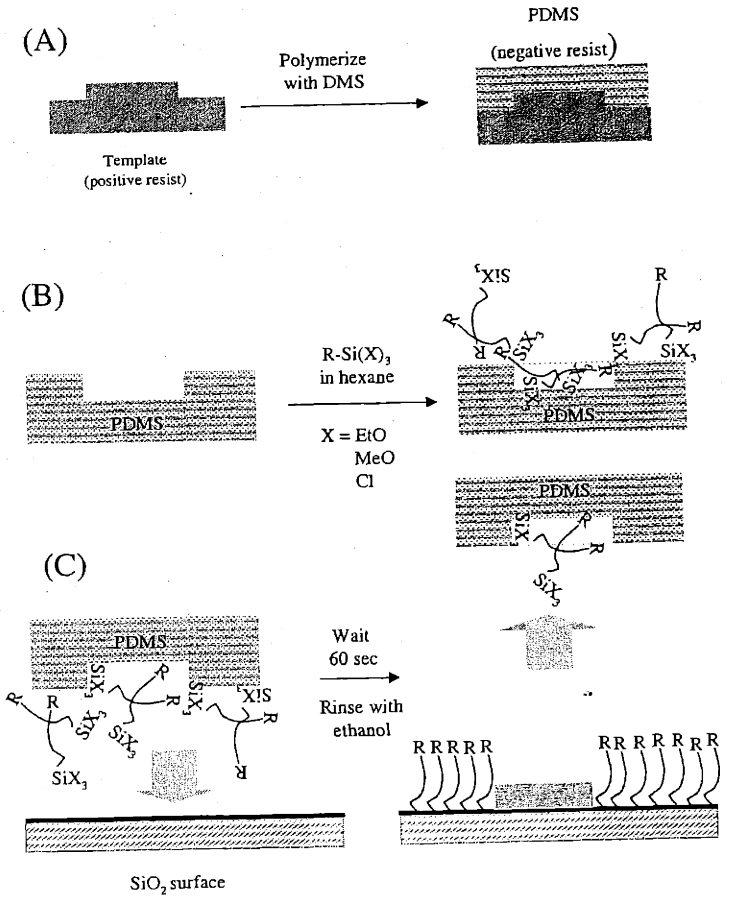

Figure 4-14. Graphic representation of the soft lithography technique. (a) PDMS is polymerized over a silicon resist to create the negative resist "stamp"; (b) a silane solution is added to the PDMS surface and the solvent evaporates to leave a thin silane film; (c) The PDMS stamp is pressed onto the target silica surface for 60 seconds, then removed. A thin silane film is imprinted onto the silica surface, where it reacts to form a monolayer level film with specific physical and chemical surface properties such as hydrophobicity.

at the liquid/solid interface, thereby increasing the chance for hybridization of the dsDNA 10 mer oligo overhang to the surface oligos.

However, I found that aqueous drops would spread across the hydrophobic surface if the surfactant SDS was present in solution, and the SDS is necessary to prevent nonspecific DNA adsorption. Therefore, soft lithography was not used for dsDNA surface hybridization experiments, but in situation where no SDS is present in the aqueous solution, for instance when trying to adsorb DNA nonspecifically onto amine silicon surfaces derivatized with monolayer thick aminosilane films, an improvement on the original polylysine substrates used in the *Brown* protocol for cDNA microspot arrays.

4.2.9 Spatial addressability of immobilized dsDNA

After confirming that dsDNA was immobilized to the oligo surfaces through hybridization of the 10 mer oligo overhang, I had to demonstrate that the oligo surfaces were spatial addressable. Previous hybridization experiments with ^{32}P-labeled 10 mer oligos in solution had already shown that hybridization to the oligo surfaces were highly specific and less than 2% of noncomplementary oligo sequences were immobilized to the surface, whether by nonspecific adsorption or mismatched hybridization. In addition, the oligo surfaces could discern between 10 mer sequences with single nucleotide mismatches, suggesting a high degree of stringency during hybridization.

However, my goal is to create a solid phase array that allows various dsDNA sequences to spontaneously "self-assemble" to the appropriate locations on the surface, with a high degree of specificity, from a solution mixture. The mechanism for localizing the dsDNA sequences to specific sites on the surface would be due to the highly specific hybridization of the 10 mer oligo overhang to its complementary surface oligo sequence. To test this system oligo surfaces with two different sequences, "*" and "X", were synthesized on OH silane surfaces. I confirmed the synthesis of functional surface oligo adlayers by XPS using iodinated Uracil labels, and by hybridization experiments with ^{32}P-labeled 10 mer oligos in solution. The XPS and radiation scintillation counting also

provided us with the surface oligo density and hybridization efficiency for the two surface oligo sequences.

Next, PCR was used to produce 390 bp Hbglb dsDNA chains with 10 mer oligo overhangs. The dsDNA with an overhang complementary to the "X" surface oligo sequence, "compX", was also labeled with ^{32}P-dCTP and Cy5-dCTP incorporated into the DNA backbone. The dsDNA with an overhang complementary to the "*" surface oligo sequence "comp*", was labeled with Cy3-dCTP in its backbone. A 1% agarose gel was run to confirm if PCR amplification was successful, and the PCR product was purified with spin columns to remove any unreacted nucleotides, labels, and PCR primers. The purified "compX" and "comp*" dsDNA solutions were then lyophilized, resuspended in 7xSSC buffer with 0.1% SDS, at a concentration of about 350 μg/ml, and mixed together. The "X" and "*" oligo surfaces were then hybridized with the dsDNA solution mix for 48 hours at 4°C in a hybridization chamber. The radioactivity of the surface oligos were measured by scintillation counting, and then the oligo surfaces were scanned for Cy3 and Cy5 fluorescence in a ScanArray 5000 confocal microscope.

The scintillation counting data are presented in Table 4-3, and the fluorescent image taken in the confocal microscope is shown in Figure 4-15. Ideally, if no hybridization of mismatches or nonspecific adsorption occurred, only the "X" oligo surfaces would show a significant radioactive signal, while the "*" oligo surfaces would only have background level radiation, suggesting that the radiolabeled "compX" dsDNA sequences had hybridized to the "X" oligo surfaces, and not to the "*" surfaces. Segregation of the Cy3 and Cy5 fluorescent signals to the appropriate oligo surfaces would be further proof that the dsDNA sequences were successfully localized onto the oligo surfaces according to their 10mer oligo overhang sequences.

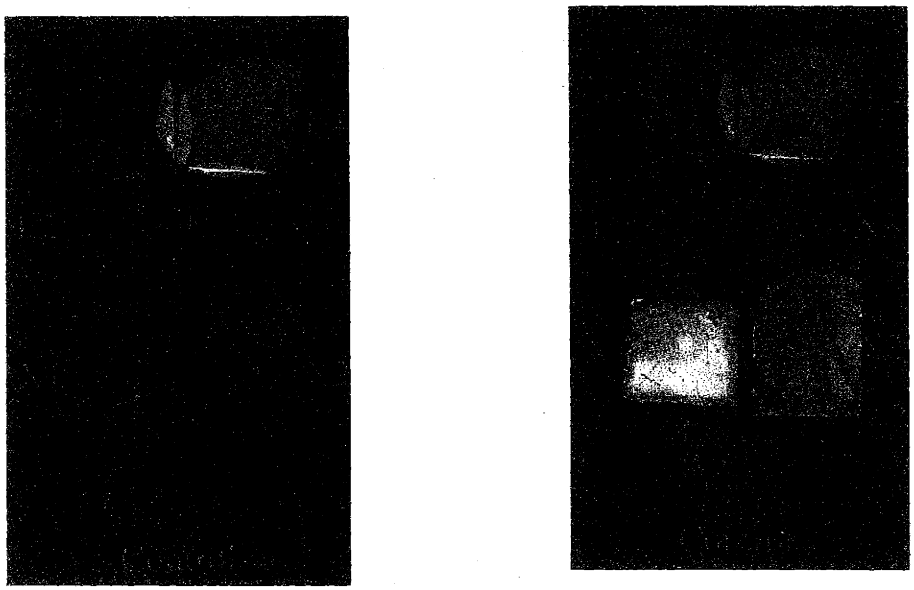

Cy3 Image

Cy5 Image

Figure 4-15. Confocal microscope images for mixed Cy3 and Cy5 labeled dsDNA with 5' 10 mer oligo overhangs, dissolved at 200 μg/ml concentration in 7XSSC (1M NaCl) buffer with 0.1% SDS. Hybridization proceeded for 72 hours at 4°C to ensure equilibrium conditions. The sample numbers correspond with the samples listed in Table 4-3. The internal control sample was E1, a blank silicon chip not immersed in the dye-labeled dsDNA mix. Comparison of the Cy3 and Cy5 images for each sample indicates low background signal from either nonspecific adsorption or mismatch hybridization (X1 and X2) of the dsDNA with the oligo surfaces synthesized on OH silane substrates. Segregation of Cy3 labeled dsDNA onto the "*" sequence surface (E4), and of Cy5 labeled dsDNA onto the "X" sequence surfaces (X3 and X4) is evident, and signal to noise ratios were good, up to 37:1.

Table 4-3. Scintillation counting data for mixed Cy3-Cy5 dsDNA hybridized onto oligo chips, under reaction conditions described in Figure 4-15. The scintillation data correlate well with the fluorescent data, suggesting that the 32P and Cy3 labeled dsDNA preferentially hybridized with "*" surfaces (E4) compared to noncomplementary surfaces (X1-X4). In addition, the generally low background and high signal-to-noise ratio suggests that little mismatch hybridization or nonspecific adsorption occurred.

Sample Name	X1	X2	X3	X4	E2	E4	control
Radiation Intensity (cpm)	755	489	136	320	14592	379	180
Intensity – background (cpm)	525	259	-	90	14362	149	-

4.3 Psoralen crosslinking

4.3.1 Background on psoralen molecules

After I confirmed that the 390 bp length dsDNA were attached to the oligo surfaces through hybridization, I used UV photolysis to induce covalent crosslinking of the dsDNA to the synthesized surface oligo through the psoralen molecule. As mentioned previously, psoralen preferably intercalates between A-T sequences in a DNA chain, and

reacts most favorably with T nucleotides. There during the design of the surface oligo sequence I deliberately added an A-T sequence on both ends of the chain. The A-T located at the 3' end of the oligo adjacent to the silane surface would be used when the dsDNA overhang contains a 5' psoralen linker.

The A-T sequence located at the 5' distal end of the surface oligo sequence could be used when a final psoralen phosphoramidite is added to the 5' end of the oligo chain, creating an oligo surface with a psoralen crosslinker. When using this method the dsDNA 5' oligo overhang does not require a psoralen linker for covalent crosslinking to occur. Schematics for the two different strategies are shown in Figure 4-16. I decided to try psoralen crosslinking at both ends since I wasn't sure whether the location of the psoralen linker had any effect on the crosslinking efficiency when dealing with a surface immobilized dsDNA molecule. For psoralen crosslinking in solution phase, there is no difference in the location of the psoralen molecule, and sometimes even free psoralen molecules are added to a DNA solution to freely intercalate at random sites prior to photolytic crosslinking. However, our system requires that only one of the two ssDNA strands is covalently attached to the oligo surfaces, so control over the psoralen crosslinking site is critical.

4.3.2 Psoralen crosslinking reaction design and methods

After the proper oligo surfaces were produced and hybridization of the dsDNA to the oligo surfaces was completed, the samples were immersed in 7xSSC (1 M NaCl) buffer and placed on an ice bath to prevent the 10 mer dsDNA duplex surface attachment site from melting during the UV illumination process, causing the dsDNA to desorb from the surface before it is covalently bound. The illumination system consisted of 2 parallel 15 W low pressure mercury lamps the provided a fairly even radiation surface, and the glass tubes absorbed the short wavelength (around 254 nm) UV light that is known to cleave the psoralen bond with nucleotides, and reverse the crosslinking reaction. The light source was approximately 3 cm away from the sample surfaces.

Four types of psoralen reactions were tested. First, the customized 30 nt long oligo primers used to created the dsDNA with 5' oligo overhangs were labeled with ^{32}P radiolabel and used for the initial tests of the psoralen crosslinking efficiency after hybridization with complementary oligo surfaces. There were two customized primers, one containing a 5' psoralen linker. This primer was used with regular surface oligo chains. The other customized primer had no 5' psoralen linker, and this was hybridized to surface oligo chains that had 5' psoralen linkers added during the stepwise synthesis reaction.

In addition, after some data and trends were obtained for the psoralen crosslinking using only the labeled customized primers, PCR with ^{32}P-dCTP was used to produce radiolabeled dsDNA product with 5' overhangs. One dsDNA product had a psoralen crosslinker and was hybridized to regular surface oligos, while the PCR product with no psoralen at the 5' end again was reacted with oligo surfaces that had 5' psoralen linkers. Cartoons in Figure 4-16 describe the four different psoralen crosslinking scenarios. Scintillation counting was used to characterize the surfaces. After initial radioactivity readings were taken, the surfaces were illuminated with UV light and then washed twice in TE buffer with 0.2wt% SDS at 60°C for 30 minutes to desorb and remove all unbound oligo or dsDNA molecules. Then the samples were measured again by scintillation counting, and the psoralen crosslinking efficiency was determined by the ratio of radioactivity of the samples before and after photolysis:

Psoralen Crosslinking Efficiency = Intensity after wash/Intensity before photolysis (cpm)

In addition, to further confirm the existence of dsDNA on the surfaces after the UV photolysis and washing, YOPRO™ dye and the CCD camera system was used to characterize the surfaces after wash.

4.3.3 Effect of illumination time on crosslinking efficiency

The first consideration was the illumination times, and experiments were run using radiolabeled primers with 5' psoralen linkers, hybridized to oligo surfaces and then illuminated with UV light for various time periods. The results, shown in Figure 4-17, indicate that psoralen crosslinking efficiency increases with illumination time until at reaches a maximum at 2 hours, then it steadily decreases. This trend was consistent and reproducible with other systems such as labeled primers hybridized to oligo surfaces with 5' psoralen linkers, and also labeled dsDNA with 5' psoralen linkers hybridized to oligo surfaces. It is possible that initially the psoralen crosslinking occurs with UV illumination, but reaches a peak at around 2 hours time, after which further illumination results in some type of degradation in the crosslink, causing the efficiency to decrease. This phenomena also was evident in crosslinking reactions in light proof enclosures, in the absence of contamination by short wavelength UV light from the environment. Thus, the degradation that occurred was not due to the reverse reaction induced short wavelength (254 nm) UV light.

4.3.4 Other variables that could affect psoralen crosslinking

Another question was the reason behind the large difference in psoralen crosslinking, from 40% to 80%, between two sets of experimental runs with the same oligo surface density using OH silane substrates, and the same labeled oligo primer solution concentration used during the hybridization reaction. Some possibilities for the wide range of psoralen crosslinking efficiencies were distance from the sample to the UV light source, the oligo surface density, and the density of hybridized dsDNA duplexes on the surface. I used ^{32}P-labeled 30 mer oligo primers with 5' psoralen linkers to test the various possible causes for the discrepancy in crosslinking efficiency. First, I hybridized the labeled primers to oligo surfaces synthesized onto OH silane surfaces, at various distances from the light source (1 cm to 6 cm).

Since radiation intensity is inversely related to the square of the distance to the radiation source, in this case the UV light source, perhaps there is a large enough difference in the amount of incoming UV light onto the sample surfaces to affect the psoralen crosslinking efficiency.

However, all the samples were crosslinked at approximately the same efficiency, around 58%, suggesting that the distance to the radiation source has no effect on the performance of the psoralen crosslinker, perhaps since the geometry and area of the light source was much larger than the irradiated sample, instead of a point source, thus the radiation energy was uniformly distributed over space and thus a change in distance to the light source did not result in a decrease in the UV radiation flux. Next I tried to hybridize the labeled primer on oligo surfaces synthesized on various silane surfaces with different oligo density, to determine whether the oligo surface density was a factor in psoralen crosslinking efficiency.

The results, shown in Figure 4-18, did show that the crosslinking efficiency increased with illumination time, but there was no definite trend between psoralen crosslinking efficiency and the oligo surface coverage, though the maximum efficiency seemed to occur on oligo surfaces synthesized onto OH silane surfaces. Finally, I tried diluting the labeled primer solution concentration prior to hybridization, resulting in lower coverage of surface hybridized primer. Then the samples of were illuminated with UV light for 2 hours, and the psoralen crosslinking efficiency was quantified by liquid scintillation counting. The average crosslinking efficiency was about 65%, with little spread in the readings and no discernible trend in the efficiency with changes in the coverage of hybridized primers on the oligo surface.

To further study the mechanics and variables of psoralen crosslinking, I hybridized ^{32}P-labeled oligos with no 5' psoralen linker onto oligo surfaces with a 5' psoralen linker; ^{32}P-labeled dsDNA molecules with oligo overhangs and a 5' psoralen crosslinker to regular oligo surfaces; and ^{32}P-labeled dsDNA molecules with 5' oligo

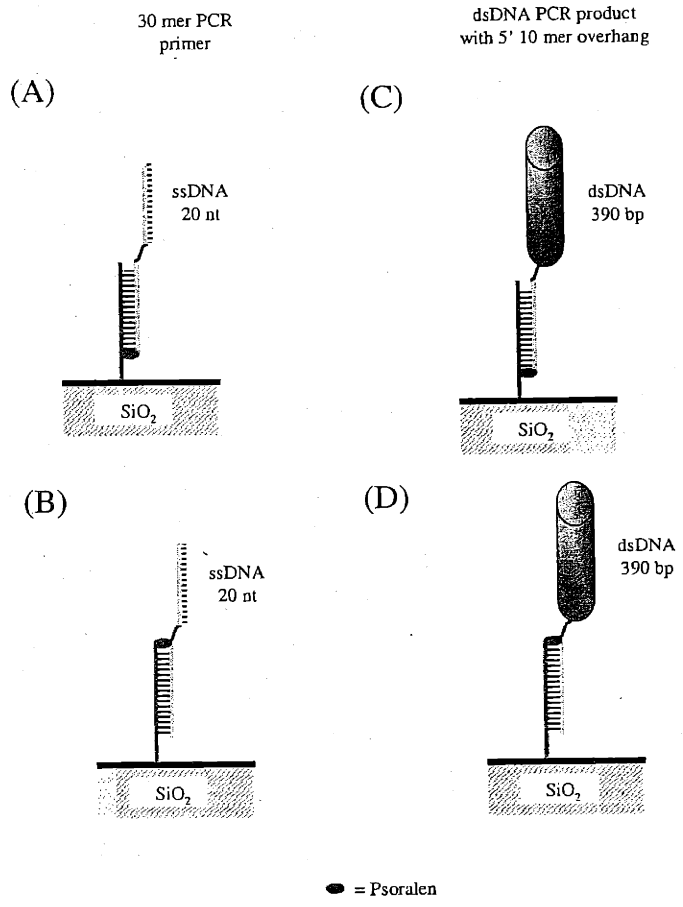

Figure 4-16. A graphical representation of 4 different psoralen crosslinking experiments. (a) 30 mer customized PCR primer with 5' psoralen linker hybridized to surface oligo; (b) 30 mer customized PCR primer hybridized to surface oligo with 5' psoralen linker; (c) 390 bp dsDNA with 5' oligo overhang and psoralen linker hybridized to surface oligo; (d) 390 bp dsDNA with 5' oligo overhang hybridized to surface oligo with 5' psoralen linker.

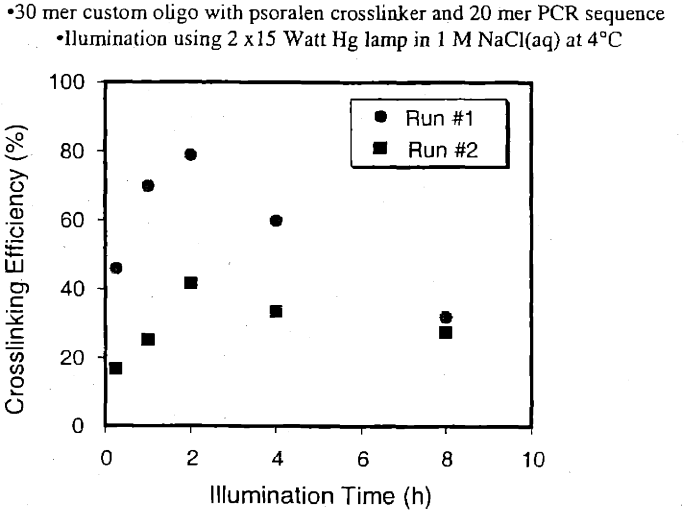

Figure 4-17. Crosslinking efficiency with respect to illumination time. The crosslinking reaction was carried out using 2x15W mercury lamps as the UV illumination source. The samples were immersed in 7xSSC (1M NaCl) and cooled with an ice bath throughout the reaction. Initially the crosslinking efficiency increases with illumination time up to 2 hours, then the efficiency decreases, suggesting the psoralen bond degrades under extended illumination by the mercury lamps.

overhangs but no psoralen crosslinker onto oligo surfaces with a 5' psoralen linker. These combinations are described in Figure 4-16.

4.3.5 Effect of DNA chain length on psoralen crosslinking efficiency

The results of the crosslinking experiments are presented in Table 4-4. It is evident from the data that the psoralen crosslinking efficiency of the 30mer oligo primers was generally higher than the dsDNA with 5' oligo overhangs. The reason for this difference may be similar to the argument for the decrease in surface hybridization coverage with increasing chain length for the solution phase oligo or dsDNA. The psoralen molecule must first intercalate successfully into the DNA double helix before it is effectively photolyzed to crosslink with the T nucleotide.

In addition, the psoralen molecule prefers to intercalate into A-T sequences, which are thermodynamically less stable compared to G-C sequences, and consequently are less easily formed and more easily denatured. Since the Hbglb dsDNA PCR product is 390 bp in length, with more than 78 times the number of negatively charged nucleotides compared to the 30 mer customized oligo primer, it has a much higher thermodynamic driving force to remain in solution, and consequently the 10 mer dsDNA duplex created by hybridization of the overhang to a surface oligo is much less stable compared to the oligo primer, especially at the A-T sequence located at the end of the 10 mer dsDNA duplex. In addition, since the A-T sequence is not bracketed by other nucleotides on both ends, its thermodynamic stability is reduced further and it is likely that when the dsDNA with overhang is hybridized to the surface oligo, that a significant portion of the A-T sequences may not form stable double helices to allow the psoralen molecule to intercalate inside.

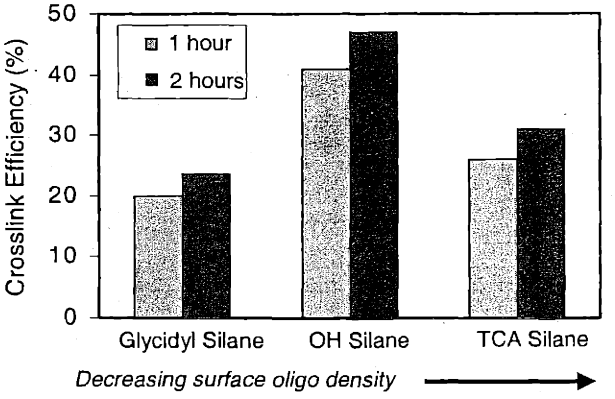

Figure 4-18. Psoralen crosslinking on different oligo surfaces. All hybridizations were carried out for 24 hours at 4°C, using 30 mer customized PCR primers with 5' psoralen linkers dissolved at 0.5 μM concentration in 7xSSC (1M NaCl) buffer with 0.1% SDS. Illumination occurred using 2x15W mercury lamps, with the samples immersed in 7xSSC buffer on ice. There was a consistent trend of increased crosslinking efficiency with illumination time, but no apparent trend correlating to the surface oligo density, except that the oligo surfaces synthesized on OH silane surfaces achieved the best efficiency.

4.3.6 Effect of psoralen linker location on crosslinking efficiency

In turn, these psoralen molecules would not form covalent bonds during UV illumination, resulting in lower crosslinking efficiency for the long chain dsDNA molecules compared to the customized oligo primers. Another general trend that was observed was that the psoralen crosslinking efficiency increased when the psoralen crosslinker was attached to the 5' end of the surface oligo chains, rather then when they were on the 5' end of the customized oligo primers or the dsDNA oligo overhangs. The cause of this difference in crosslinking efficiency could be related to a combination of steric effects and thermodynamic considerations.

First, when the psoralen molecule is located on the 5' end of the solution phase DNA molecule, the intercalation and crosslinking site is at the A-T sequence located at the 3' end of the surface oligo chain, which is imbedded deep inside the oligo adlayer and adjacent to the silane surface. Due to the fairly dense packing of the oligo chains on the silane surface, the A-T sequence at the 3' end of the surface oligo could be sterically hindered from successfully forming a double helix structure, by other oligo chains in the vicinity. Many of the DNA molecules in solution would find it difficult to squeeze the complete 10mer overhang deep into the restricted space between surface oligo chains.

In addition, the A-T bond is less thermodynamically stable compared to G-C bonds. Thus some of the surface hybridization may be incomplete, resulting in DNA being attached to the surface by a DNA duplex that doesn't include the final A-T sequence located at the 3' end of the surface oligo chain (see Figure 4-19a). Consequently, the psoralen molecule would not be able to successfully intercalate and crosslink with the T nucleotide. On the other hand, the A-T sequence located on the distal 5' end of the surface oligo chain is less sterically restricted compared to the 3' end location, and thus the probability of successfully forming a double helix for psoralen molecule intercalation is much higher, resulting in a higher crosslinking efficiency (see Figure 4-19b).

Therefore, I concluded it was possible to improve the psoralen crosslinking efficiency by adding the psoralen molecule to the 5' end of the surface oligo rather than the 5' end of the solution oligo or dsDNA, but that due to thermodynamic stability considerations the psoralen crosslinking efficiency for long chain dsDNA such as the 390 bp Hbglb sequence is inherently lower compared to the shorter 30mer oligo primer molecules.

Table 4-4. Psoralen crosslinking efficiency. The oligos and dsDNA were solvated in 7xSSC buffer with 0.1% SDS. The oligo concentration was 0.5 μM, and the dsDNA concentration was 350 μg/ml concentration. Hybridization reactions took place for 24 hours at 4°C on surface oligos synthesized on OH silane substrates. Psoralen crosslinking was catalyzed by illumination with 2x15W mercury lamps for 2 hours, and the samples were immersed in 7xSSC buffer on an ice bath. The highest efficiency occurred for 30 mer PCR primer hybridized onto oligo surfaces with 5' psoralen linkers, while 390 bp dsDNA with 5' psoralen linkers hybridized onto oligo surfaces demonstrated the lowest crosslinking efficiency.

Psoralen crosslinking efficiency (%)	30 mer customized PCR primer	390 bp PCR product with 5' 10 mer overhang
Psoralen on 5' end of PCR primer	**50-70**	**20-30**
Psoralen on 5' end of surface oligo	**80**	**40-50**

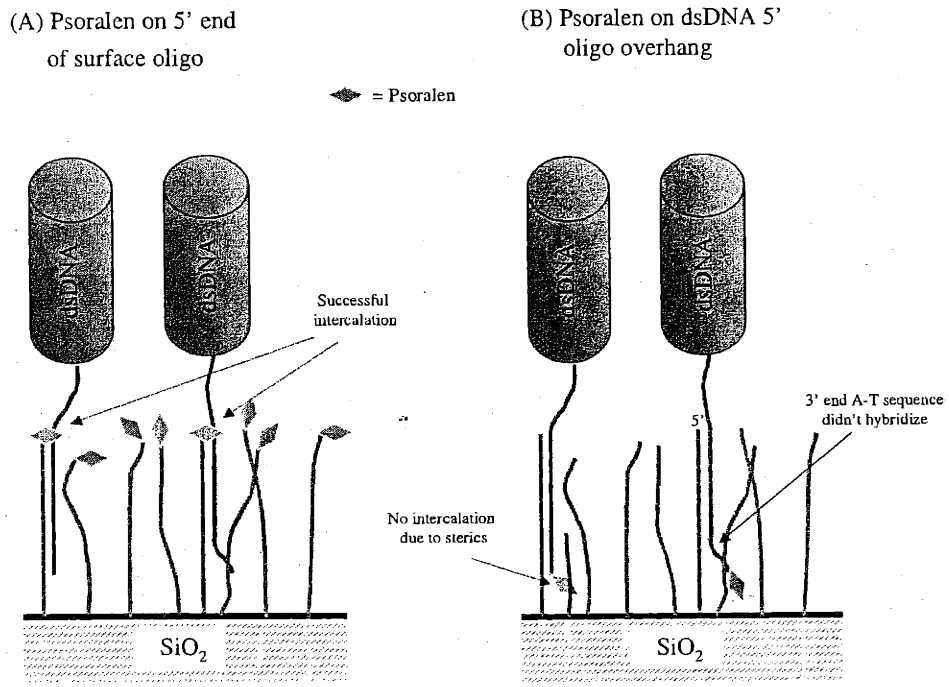

Figure 4-19. Effect of location of 5' psoralen on crosslinking efficiency. (a) when the psoralen linker is attached to the 5' end of the surface oligo through automated synthesis, it is more likely to intercalate into the dsDNA duplex due to lower steric hindrance at the oligo surface, and the increased thermodynamic stability and hybridization efficiency of the 10 mer surface attachment site; (b) on the other hand if the psoralen is at the 5' end of the dsDNA it could be hindered from intercalation by the densely packed surface oligo chains. The high surface density of the oligos may also prevent complete hybridization of the 10 mer surface attachment site, especially the less thermally stable A-T sequence located at the 3' end of the surface oligo chain proximal to the silane substrate. If the A-T sequence duplex doesn't form the psoralen will not intercalate into the dsDNA and consequently would not form a covalent crosslink upon photolysis.

4.4 ssDNA probe formation

4.4.1 Experimental approach for confirming formation of immobilized ssDNA chains

After the psoralen crosslinking of dsDNA to the oligo surfaces were complete, I heated the immobilized dsDNA strands to 90°C in TE buffer with 0.2 wt% SDS to remove the noncrosslinked ssDNA strand, so that the final form of DNA on the oligo surface is a ssDNA 390nt long attached to the surface at its 5' end but with all the nucleotides on its complete length available for hybridization. To confirm that the ssDNA surface was successfully formed, a UV illuminated, and ^{32}P radiolabeled dsDNA sample surface was heated to 60°C in TE buffer with 0.2wt% SDS for 30 minutes, the temperature at which the 10mer DNA duplex that attaches the dsDNA to the surface melts into two oligos. Any noncrosslinked dsDNA strands will desorb from the surface under these conditions. The radiation intensity of the remaining radiolabeled dsDNA was measured by scintillation counting and the results were rationed against the intensity prior to UV illumination to determine the psoralen crosslinking efficiency, as well as the surface coverage of the immobilized dsDNA. Then, the sample is washed twice at 90°C for 30 minutes in TE buffer solution with 0.2wt% SDS, and the radiation intensity measured again after rinsing.

4.4.2 Experimental results

If the dsDNA has melted and one of the ssDNA has desorbed from the surface, the radiation intensity should be approximately 50% of the signal obtained after UV crosslinking and washing at 60°C. The scintillation counting results are shown in Figure 4-20. The data clearly indicate that upon heating the melting temperature of the 390bp Hbglb dsDNA sequence (90°C), approximately half of the radiation signal remains compared to the intensity of the dsDNA surfaces after heating to 60°C. This result strongly suggests that the immobilized dsDNA has melted and that the remaining DNA on the surface is single stranded. An important note is that although the radiation signal

decreases by 50% for ssDNA compared to those of dsDNA immobilized on the surface, the surface coverage of DNA molecules has not decreased. So a 10% signal for ssDNA corresponds to 20% psoralen crosslinking efficiency. In addition, a control sample of noncrosslinked dsDNA that was washed at 60°C has only background radiation levels, showing that if the psoralen crosslinking reaction is not induced by UV illumination, the immobilized dsDNA is not thermally stable at the melting temperature of the 10mer DNA duplex surface attachment site, and that the dsDNA will fully desorb from the surface.

The radiation signals from various experimental runs show from 10-15% signal compared to the sample before a 90 °C hot water wash. In addition, samples heated to only 60 °C usually had 20-30% radioactive signal. This suggests that the psoralen crosslinking efficiency is about 20-30% for hybridized 390 bp length Hbglb chains with 5' end overhangs that end in a psoralen molecule. This efficiency is typical of psoralen when attached at the 5' end of a large dsDNA molecule. As mentioned above, there are various approaches that could improve the crosslinking efficiency, albeit at higher production costs.

4.4.3 Using YOPRO™ to analyze the quality of immobilized ssDNA

The next questions were the quality of the attached ssDNA, and whether it could function as a probe DNA that would hybridize with complementary target ssDNA in solution. One approach to determine the quality of the ssDNA strand covalently attached to the surface is to heat the immobilized dsDNA sample to above its T_m and observe the melting curve. The melting curve may be determined by immersing the dsDNA samples in YOPRO™ intercalating dye. The fluorescence signal of intercalated YOPRO™ dye is 50 to 100 times higher than randomly oriented dye molecules in solution. Thus, when the

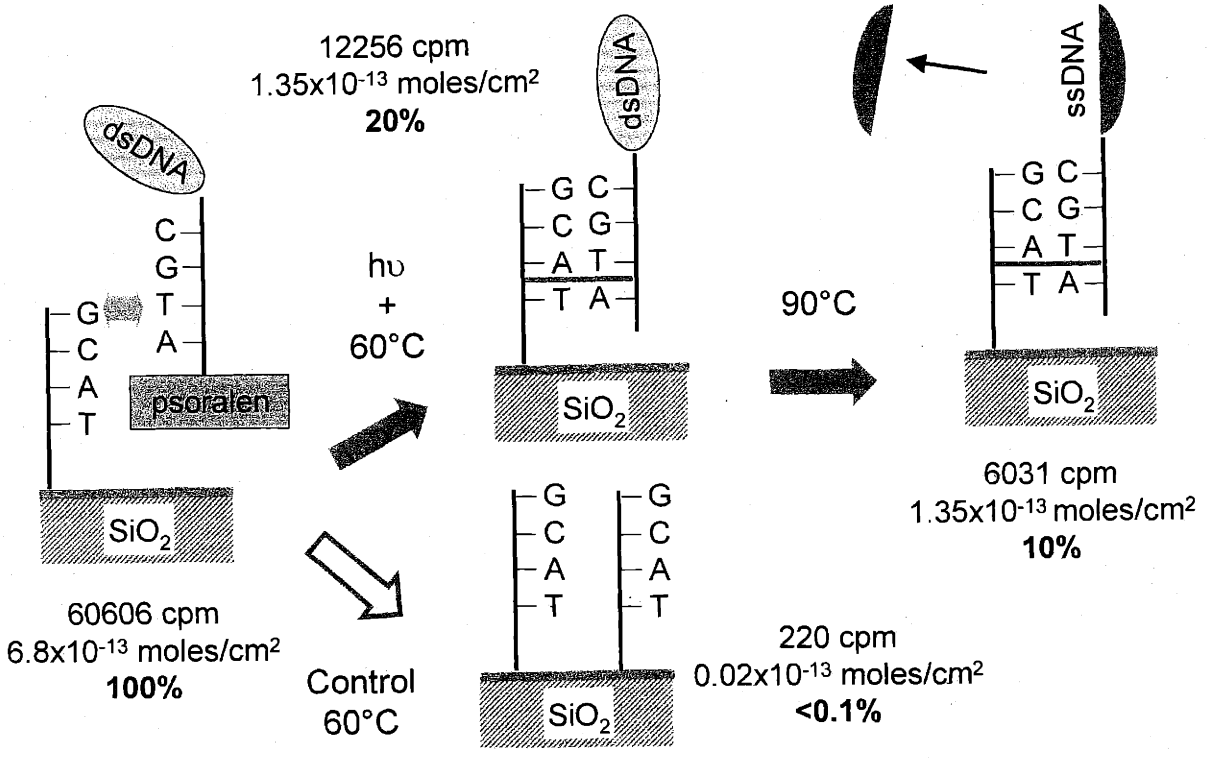

Figure 4-20. Generation of end-immobilized dsDNA and ssDNA chains. All samples heated in TE buffer with 0.2 wt% SDS.

dsDNA unravels into single strands above T_m, the YOPRO™ molecules are no longer intercalated in the DNA duplex, and the fluorescent signal decreases rapidly and dramatically, resulting in a transition that corresponds to the T_m of the dsDNA sequence.

4.4.4 Effects of dsDNA immobilization on DNA melting temperature

An end-immobilized dsDNA that is not attached to the surface at multiple point but floats freely in solution should exhibit melting behavior similar to solution phase, with a sharp Tm transition over a 1° C range. A significant shift in the T_m of the surface immobilized dsDNA sequence compared to values obtained in solution phase melting curve experiments, or a broader, less well-defined T_m transition (with a temperature range over 2° C) would suggest either the dsDNA immobilized to the surface is of incorrect length or sequence, or that the dsDNA is attached to the surface at multiple points other than the oligo overhang site. It is important to determine the quality of the dsDNA immobilized onto the surface, since one of my objectives was to try and attach DNA onto the surface in a manner that allows the full length to remain available for hybridization to target DNA. If the dsDNA is attached to the oligo surface at multiple points, the hybridization efficiency and the stringency of the probe DNA may suffer.

4.4.5 Packing density of dsDNA molecules affects their orientation and interactions

I have demonstrated the ability to immobilized dsDNA on oligo surfaces at surface coverage of up to $2x10^{-12}$ moles/cm^2. Since this density is higher than the theoretical packing density of a monolayer of dsDNA chains laid flat on the oligo surface ($6x10^{-13}$ moles/cm^2), one can assume that the dsDNA chains for a 3-D brush-like structure, where the mutual electrostatic repulsion from the negatively charged dsDNA

required for a brush-like structure, and some of the dsDNA strands can come in contact with the underlying oligo surface.

The oligo surface is also negatively charged and in previous studies DNA did not adsorb onto DNA unless the solution salt concentration was very high, and when SDS was present in the solution the degree of nonspecific adsorption was low, only around 0.5-2%. However, during the sample preparation the dsDNA surfaces were sometimes dry, increasing the possibility of nonspecific adsorption of the dsDNA to the oligo surfaces, and since it would be preferable to store the dsDNA (and also ssDNA) surfaces dry, it is important to try and evaluate the quality of the dsDNA surfaces after psoralen crosslinking, especially with regards to possible multipoint attachment of the dsDNA to the oligo surfaces.

4.4.6 Initial fluorescent experiments on immobilized dsDNA surfaces

Samples of Hbglb dsDNA covalently attached on oligo surfaces were immersed in 10^{-7} M YOPRO™ dye in a 1.5M nicotinamide denaturant solution, and were heated with a heating block controlled by a Lakeshore temperature controller. The heating profile followed a linear ramp, from 50°C to 70°C, above the theoretical Tm for the 390 bp Hbglb sequence. An Ar laser was used to illuminate the sample during heating, and the fluorescence at 510 nm was recorded periodically at 1 Hz via a CCD camera. The resulting melt curve showed a shallow and broad transition over 4°C, but also showed a lower overall signal-to-noise ratio and significant quenching of the fluorescence signal. Subsequent calibration runs with a 10^{-7} M YOPRO™ solution heated from 50°C to 70°C indicated a linear decrease in fluorescence signal with increasing temperature, due to a decrease in the quantum yield during heating. On the other hand, continuous illumination of the 10^{-7} M YOPRO™ solution for 15 minutes by the 2 mW Argon laser yielded no discernable decrease in fluorescence signal, suggesting a lack of significant photobleaching.

By measuring the YOPRO™ fluorescent for serially diluted dsDNA solutions I was able to determine that a minimum immobilized dsDNA surface coverage of $2x10^{-13}$ moles/cm^2 was necessary to obtain an adequate fluorescent signal over noise at 20°C. Though I have achieved this density after psoralen crosslinking, the YOPRO™ fluorescence intensity decreased by almost 65% after heating to 50°C, and a further 15% at 70°C. Therefore, it is important to increase the surface coverage of immobilized dsDNA, in order to achieve the required sensitivity and signal to noise ratio for accurate YOPRO™ fluorescence measurement of the melting curve of the dsDNA molecules. Otherwise, alternative methods need to be explored for determining the quality of the immobilized dsDNA and the subsequent ssDNA strand obtained after psoralen crosslinking and heating.

4.4.7 Alternative approach for evaluating quality of immobilized ssDNA

Another approach for evaluating the quality of the ssDNA is to observe its performance during hybridization reactions with labeled target ssDNA in solution. The efficiency and the specificity of the target-probe interactions between the ssDNA are especially important. The end-immobilized dsDNA molecules could attach to the oligo surface at multiple points if the surface coverage is low, affecting the hybridization efficiency when the chip is heated to produce the ssDNA surface probes. The ssDNA molecules present further complications, since there motion is no longer restricted by the semi-rigid double helix conformation of the dsDNA duplex, so it would behave more like a polymer with random coiling. In addition, the bases on the ssDNA chains are no longer "protected" by hybridization to a complementary ssDNA strand, and are free to interact with the oligo surface and other ssDNA chains, either by hybridization or intermolecular forces that could result in adhesion or adsorption.

From a design viewpoint it is critical not to have complementary sequences within the ssDNA strands that would result in the formation of hairpins or other secondary structures from interactions between neighboring ssDNA chains, or complementary sequences in the surface oligo chains that would allow them to hybridize with any

segment of the immobilized ssDNA chains. However, regardless of design considerations the inherent flexibility and "reactivity" of the ssDNA chains compared to dsDNA chains presents more difficulties in maintaining a brush-like surface orientation with no interactions between the ssDNA chain and the oligo surface. However, it is difficult to ascertain the structure of the ssDNA by techniques such as AFM or STM or ellipsometry. Instead I focused on the consequences of the surface orientation, mainly the ability of the immobilized ssDNA to function effectively as a DNA probe, with regards to its hybridization efficiency and stringency. The hybridization efficiency for immobilized ssDNA probes could be tested using fluorescently-labeled ssDNA.

4.4.8 Approaches for producing target ssDNA molecules

I tried various asymmetric PCR procedures that removed one of the 2 ssDNA strands in the PCR product. I used PCR to amplify a 390 bp Hbglb dsDNA sequence with no 5' oligo overhang, and with Cy5 fluorescent dye incorporated into its backbone. The 3' PCR primers were customized to contain special molecules that were recognized by the exonucleases used to degrade the enzyme. Oligo primers with 4 phosphorothioate nucleotides at the 5' end were used in conjunction with T7 gene 6 exonuclease, and also oligo primers with a phosphorylated 5' end in conjunction with λ exonuclease. The nuclease would not recognize the ssDNA strand with the customized primers and would only digest the other ssDNA chain. The remaining fluorescently-labeled ssDNA molecules could be used as target DNA to test the quality of the immobilized ssDNA chains.

In both cases the enzymes should not degrade the ssDNA chains with customized primers and thus only one of two ssDNA strands would remain as the target DNA to the surface immobilized complementary ssDNA chain. However, in repeated trials using either exonuclease, both enzymes failed to degrade the PCR product. An alternative approach may be used to produce the target ssDNA. Again PCR would used to amplify the template Hbglb sequence, but the 5' PCR primer would contain a biotin linker, allowing one of two ssDNA strands to be removed by a chromatography column

containing streptavidin-coated beads. The biotinylated dsDNA PCR product is first heated to 90°C to melt the dsDNA into two ssDNA strands, and the hot solution is passed quickly through the column before the two complementary strands could reanneal. The biotin-streptavidin bond is highly specific ($K_d=10^{-15}$ M) and effectively removes the ssDNA strand with the nucleotide sequence identical to the ssDNA strand attached to the oligo surfaces, leaving the Cy5 labeled complementary strand in solution. This fluorescently labeled ssDNA target sequence would then be used to challenge the ssDNA chains immobilized on the oligo surfaces.

4.5 Conclusions

I developed a strategy for producing PCR dsDNA product with a 5' oligo overhang that was used for attachment to an oligo surface synthesized from an OH silane substrate, and also a psoralen crosslinker to affect a covalent bond to the surface upon illumination with UV light. Hybridization studies were conducted with the dsDNA PCR product analogous to the experiments previously run using labeled 10 mer oligos in solution. The dsDNA is immobilized onto the oligo surfaces by hybridization of the 10 mer oligo overhang to the surface oligo chains, with a high degree of specificity and very little nonspecific adsorption (0.5-2%).

The hybridization results were confirmed by scintillation counting of the radiolabeled dsDNA molecules as well as fluorescence spectroscopy using fluorescein and YOPRO™ dyes. The hybridization kinetics of dsDNA resembled that of 10 mer oligos in solution, with a maximum coverage reached after 24 hours of immersion time. Compared to 10 mer and 30 mer oligo solutions of the same concentration (0.5 μM), the amount of dsDNA hybridized to the oligo surfaces at equilibrium conditions (>24 hour immersion) was lower by a factor of 10 to 50, suggesting that the surface hybridization density of DNA decreases with increasing size, possibly due to the decrease in thermodynamic driving force for surface hybridization, as well as steric hindrance from the dsDNA already immobilized to the surface towards incoming dsDNA strands.

However, the amount of dsDNA hybridized to the surface increased linearly with increasing dsDNA solution concentration, and coverage of up to $2x10^{-12}$ moles/cm^2 were achieved, which is an order of magnitude higher than the coverage obtained from other methods in literature, and which is larger than a monolayer coverage of dsDNA at 390 bp length ($6x10^{-13}$ moles/cm^2), suggesting that the immobilized dsDNA has a brush-like structure instead of a flat structure. In addition, the T_m of the 10mer dsDNA duplex surface attachment point also affected the equilibrium hybridized dsDNA surface coverage, with increasing coverage obtained using oligo sequences with higher T_m, mirroring the results observed using 10 mer oligos in solution. By adding 5-10% dextran sulfate, the amount of hybridized dsDNA molecules onto the surface increased by 125%, further optimizing the system. Finally, I demonstrated that the system could segregate dsDNA sequences from a solution mixture onto discrete surface sites, confirming that my approach provides spatial addressability, which is the key component for successfully producing microarrays

Once the dsDNA was immobilized the psoralen molecules were photolyzed to crosslink the dsDNA to the surface oligo. Many variables that affected the crosslinking efficiency were studied. I concluded that the optimal UV illumination time was 2 hours, after which the crosslinking efficiency steadily decreased. The decrease in crosslinking efficiency with illumination time suggested that the maximum crosslinking occurred after 2 hours time, and that further exposure to UV light degraded the psoralen bond. Otherwise, the only other factors that consistently affected psoralen crosslinking were the location of the psoralen molecule and the size of the dsDNA chain "brushes" that did not directly participate in the surface attachment process.

Psoralen molecules linked to the 5' end of the surface oligo chains was more effective than those connected to the 5' end of the 10 mer oligo overhang of the dsDNA molecule, possibly due to steric factors. Also, as the length and molecular weight of the DNA sequence increases, the crosslinking efficiency decreases, with strong suggestions pointing to both the thermodynamic stability of the 10 mer surface attachment site and

steric hindrance as the major contributing factors to the performance of the psoralen linker. By the appropriate placement of the psoralen linker, on the 5' end of the synthesized surface oligo chain, and the proper choice of 10mer oligo overhang sequence to increase its T_m, crosslinking efficiencies of up to 50% for dsDNA and up to 80% for the 30mer custom PCR primer were observed.

After crosslinking end-immobilized ssDNA Hbglb sequences were produced after heating the dsDNA surfaces up to 90°C, with densities of around $2x10^{-13}$ moles/cm^2, confirmed by radioactive scintillation counting. Furthermore, I confirmed that dsDNA strands not covalently attached to the surface were effectively removed by immersion in an SDS surfactant solution. There are a variety of potential applications for both ssDNA and dsDNA immobilized onto a surface in a spatially addressable manner.

The end-immobilized dsDNA chains could be used to study DNA interactions with proteins, small molecules and other biomolecules. The dsDNA surfaces could be heated to observe the melting profile, which could possibly be analyzed to discern SNPs within the dsDNA sequence for. This approach towards SNP detection could be applied towards polymorphism screening and research. The ssDNA molecules attached to the surface could be used as a DNA probe library for rapid forensics and pathogen screens as well as quantitative gene expression studies.

However, the critical issue for all the above applications is the surface structure of the immobilized dsDNA and ssDNA molecules, especially in the dry conditions in absence of surfactants such as SDS. Due to the chemical and structural complexity of the DNA molecules and the oligo surfaces, there is a high probability that multiple interactions could occur between the immobilized dsDNA or ssDNA chains and the surface oligos. Will the DNA chains interfere with each other or perhaps adsorb irreversibly onto the oligo surface, degrading the performance of the immobilized DNA probes? Answers to this question are critical for determining how to store and handle the end-immobilized DNA surfaces, as well as how to judge the quality of the experimental data obtained from such systems, but there is a dearth of studies and literature in this area.

Thus, further research focused on the structure and hybridization behavior of the end-immobilized dsDNA and ssDNA molecules should be pursued.

4.6 Methods and Materials

Materials: All materials required for the production of oligos surfaces were mentioned in the previous chapter. 5' psoralen phosphoramidite was purchased from Glen Research (Sterling, VA). All customized PCR primers were purchased from Research Genetics (Huntsville, AL). Hbglb sequence template DNA was kindly donated by Dr. Katherine Hogan from the MIT department of biology. Taq Polymerase and Fluorescein-dATP were purchased from Roche Molecular Biochemicals (Indianapolis, IN). TdT transferase was purchased from New England Biolabs (Boston, MA). ^{32}P-dCTP was purchased from New England Nuclear Bioscience (Boston, MA). Cy3-dCTP and Cy5-dCTP were purchased from Amersham Pharmacia Biotech (Piscataway, NJ). λ exonuclease and T7 gene 6 exonuclease were purchased from USB (Cleveland, OH).YOPRO™ dye was purchased from Molecular Probes (Eugene, OR). All buffer solutions and chemicals required for gel electrophoresis were generously provided by the Lerman lab in the MIT department of biology.

Methods:

1. Terminal transferase (TdT) radiolabeling reaction

   The TdT reaction was performed on a 50 μl basis using TdT enzyme (concentration=20,000 units/ml) were purchased from New England Biolabs (Beverly, MA), and α^{32}P-dCTP radioactive labels was purchased from New England Nuclear Biosciences (Boston, MA). The recipe is as follows:

   5μl 10 x TdT buffer

5μl 2.5mM $CoCl_{2(aq)}$ solution

1μl unlabeled oligo

1μl α^{32}P-dCTP (3000 Ci/mm radioactivity)

0.5μl TdT (in ethylene glycol)

37.5μl ddH_2O

The reaction was carried out in an Ericomp (San Diego, CA) DeltaCyclerI™, or an Applied Biosystems (Foster City, CA) GeneAmp® PCR system 9700 thermocycler, with the following temperature profile: maintain at 37° C for 1 hour, heat to 70° C for 10 minutes to deactivate enzyme, then cool and hold at 4° C indefinitely. After reaction is completed 0.1wt% SDS is added to the labeled oligo solution.

2. Polymerase chain reaction (PCR)

The standard PCR reaction was performed on a 25 μl basis using Taq polymerase (concentration = 5 units/ml) purchased from GIBCO BRL/Life Technologies, or Roche Molecular Biochemicals (Indianapolis, IN). The recipe is as follows:

2.5μl 10 x PCR buffer (with 2mM $MgCl_2$)

2.5μl 10x $dNTP_{(aq)}$ solution (2.5mM each of dATP, dCTP, dGTP and dTTP)

1μl plasmid prep template DNA (Hbglb or SRY sequence)

1μl 5' PCR primer oligo

1μl 3' PCR primer oligo

0.5μl Taq polymerase (in ethylene glycol)

16.5μl ddH_2O

To produce radiolabeled or fluorescently labeled PCR product fluorescein labeled dCTP was purchased from Roche Molecular Biochemicals, Cy3 and Cy5 labeled dCTP were purchased from Amersham Pharmacia (Pisataway, NJ), and α^{32}P-dCTP was purchased from New England Nuclear Biosciences (Boston, MA). The PCR recipe was modified as follows:

2.5μl 10 x PCR buffer (with 2mM $MgCl_2$)

2.5μl 10x $dNTP_{(aq)}$ solution for labeling reaction

(2.5mM each of dATP, dGTP, and dTTP with 2mM dCTP)

1µl plasmid prep template DNA (Hbglb or SRY sequence)

1µl 5' PCR primer oligo

1µl 3' PCR primer oligo

1µl NTP label (2mM fluorescein, Cy3, Cy5 or α^{32}P labeled dCTP)

0.5µl Taq polymerase (in ethylene glycol)

15.5µl ddH_2O

The reaction was carried out in an Ericomp (San Diego, CA) DeltaCyclerI™, or an Applied Biosystems (Foster City, CA) GeneAmp® PCR system 9700 thermocycler, with the following temperature profile: initial heating to 94° C for 3 minutes; followed by 28 thermal cycles, each cycle consisting of 3 steps: a melting step at 94° C for 30 seconds, then an annealing step at 55° C for 30 seconds, then an enzymatic reaction step at 72° C for 30 seconds; next, the solution is held at 72° C for 7 minutes to complete the reaction, then cooled and held at 4° C indefinitely.

3. Agarose gel electrophoresis

A 1% agarose gel was produced by dissolving 0.5 gm of SeaKem (Rockland, ME) ME agarose in 50 ml of boiling Tris-Acetate-EDTA (TAE) buffer, and 2.5 µl of ethidium bromide (EB) from Sigma was added as the fluorophore. All samples were loaded in 10 µl of cyano blue loading dye buffer solution, and 100bp DNA ladders were purchased from Gibco BRL for determining the DNA lengths. The agarose gels were run horizontally in Hoefer Scientfic Instruments (San Francisco, CA) HE 33 mini submarine electrophoresis unit at a potential drop of approximately 80V. The DNA was imaged under a long wavelength UV light source to determine the DNA length by comparing its position relative to the DNA ladder.

4. Acrylamide gel electrophoresis

A premixed a 20v/v% acrylamide gel solution was purchased from. The mixture contained a 29:1 ratio of acrylamide monomer versus the bifunctional crosslinker N,N methylenebisacrylamide. A binary catalyst system of 0.06 wt% ammonium persulfate, and 0.03 wt% TEMED was used to polymerize the acrylamide into a polyacrylamide gel within the vertical gel plates. Upon completion the vertical gel was run using a BioRad Mini-PROTEAN II multicasting vertical gel electrophoresis system at a potential drop of about 100V. The samples were loaded in 5 μl of cyano blue loading dye buffer, and the position of the radiolabeled oligos in the gel was determined using autoradiography with imaging film purchased from Eastman Kodak Co. (Rochester, NY).

5. Ethanol precipitation

For every volume of sample add 0.1 volume of 3M aqueous sodium acetate, and 2 volumes of 100% neat ethanol in a 1.5 ml microfuge tube. Leave the ethanol mixture at –20°C for 24 hours, then spin it in a microfuge at 10,000 g for 15 minutes. Remove the supernatant liquid phase by micropipette, taking care not to remove the precipitated DNA at the bottom of the microfuge tube. Next, add 500 μl of 70% ethanol solution to wash the DNA sample. Leave the sample on ice for 5 minutes, then spin in microfuge at 10,000 g for 7 minutes. Remove the supernatant solution phase, then air dry sample in the tube and resuspend with the appropriate buffer.

6. Spin column purification

The crude PCR product was purified using a Qiagen (Valencia, CA) PCR purification kit, according to the protocols provided. A or Eppendorf microfuge was used at 10,000 g, and the purified DNA product was eluted in Tris buffer (pH=8.5). The purified samples were stored at 4° C.

7. Confocal Microscopy

For imaging DNA labeled with cyanine dyes such as Cy3 (λ_{ex} = 552 nm, λ_{em} = 570 nm) and Cy5 (λ_{ex} = 643 nm, λ_{em} = 667 nm), a ScanArray 3000 (GSI Lumonics, Billerica,

MA) or ScanArray 5000 (GSI Lumonics) confocal microscope was used. The ScanArray 2000 was used for imaging glass samples since the objective lens could only be manually adjusted. The objective lens for the ScanArray 5000 was computer-controlled and thus it was used to scan samples on silicon chips, as long as the thickness was less than 2 mm, the tolerance of the sample holder. The laser intensity was set at 60%, and the PMT efficiency at 70% for the imaging runs.

8. Epifluorescence laser illumination

A 2 mW (class 2) Uniphase (San Jose, CA) model 2212-4SL Argon laser (λem = 488 nm) was used to excite DNA chains labeled with either fluorescein or YOPRO™ (oxazole yellow) dyes. The incident beam angle was approximately 70 degrees to the surface normal. Both a charge-coupled device (CCD) and a PMT were used to characterize the sample fluorescence. The CCD was a liquid cooled model #CH220 purchased from Photometrics Ltd. (Tuscon, AZ). A high band optical filter was added to the lens to remove any incoming light with a wavelength less than 488 nm. The CCD program was custom tailored in FORTRAN code by a previous associate in the biology department, which allowed for characterization of specific locations on the sample surface as well as signal amplification via "binning", or integration of the signal intensity of the pixels covered by the CCD lens. The PMT was a Model #RF1/S MKII from Thorn EMI (CA), run using software developed by Lawson Ltd. (??). A custom-made light isolation box for the PMT apparatus was designed by an associate in biology, Greg, and the complete laser-CCD-PMT imaging setup was custom-built on an optical bench and enclosed in a dark room.

9. Lyophilization

Prior to lyophilization the solution samples were frozen at -20°C. A speedvac was used to lyophilize the samples.

10. UV crosslinking

9. Lyophilization

Prior to lyophilization the solution samples were frozen at -20°C. A speedvac was used to lyophilize the samples.

10. UV crosslinking

Two 15 W low-pressure mercury lamps purchased from Blacklight U.S.A. (#F15T8/BL) were used to illuminate the samples at a distance of 1 cm. The samples were immersed in 1 M NaCl solution and placed onto an ice bath to prevent desorption of the surface-immobilized dsDNA prior to UV crosslinking.

11. UV-VIS Absorbance Spectroscopy

Measurements were conducted using a Varian (Mulgrave, Australia) Cary 1E UV-Visible Spectrophotometer. The blank sample was 1 ml of ddH_2O in a quartz cuvette. All DNA samples were diluted in ddH_2O to a volume of 1ml. The sample absorbance spectra was measured from wavelengths of 240 to 300 nm. The conversion factor was 50 μg/O.D.

4.7 References

1) D. Guschin; G. Yershov; A. Zaslavsky; A. Gemmell; V. Shick; D. Proudnikov; P. Arenkov; A. Mirzabekov *Anal. Biochem.* **1997**, *250*, 203-211.

2) F. N. Rehman; M. Audeh; E. S. Abrams; W. H.Philip; M. Kenney; T. C. Boles *Nuc. Acids Res.* **1999**, *27*, 649-655.

3) M. N. Kuppuswami; J. W. Hoffman; C. K. Kasper; S. G. Spitzer; S. L. Groce; S. P. Bajaj *Proc. Natl. Acad. Sci. USA* **1991**, *88*, 1143-1147.

4) P. Nyren; B. Petterson; M. Uhlen *Anal Biochem.* **1993**, *208*, 171-175.

5) L. Ugozzoli; J. M. Wahlquist; A. Eshani; B. E. Kaplan; R. B. Wallace *GATA* **1992**, *9*, 107-112.

6) A. -C Syvanen; A. Sajantila; M. Lukka *Am. J. Hum. Genet.* **1993**, *52*, 46-59.

7) M. S. Shchepinov; S.C. Case-Green; E. M. Southern *Nuc. Acids Res.* **1997**, *25*, 1155-1161.

8) T. T. Nikiforov; R. B. Rendle; P. Goelet; Y. Rogers; M. L. Kotewicz; S. Anderson; G. L. Trainor; M. R. Knapp *Nuc. Acids Res.* **1994**, *22*, 4167-4175.

9) R. G. Higuchi; H. Ochman **1989**.

10) M. Shon; J. Germino; D. Bastia *J. Biol. Chem.* **1982**, *27*, 13823-13827.

11) T. Hultman; S. Stahl; E. Hornes; M. U. Ulhen *Nuc. Acids Res.***1989**, *17*, 4937-4946.

12)C. Bamdad *Biophys. J.* **1998**, *75*, 1997-2003.

13) U. Landegren; R. Kaiser; J. Sanders; L. Hood *Science* **1988**, *241*, 1077-1080.

14) D. A. Nickerson; R. Kaiser; S. Lappin; J. Stewart; L. Hood; U. Landergren *Proc. Natl. Acad. Sci. USA* **1990**, *87*, 8923-8927.

15) F. Baramy *Proc. Natl. Acad. Sci. USA* **1991**, *88*, 189-193.

16) Z. Guo; R. A. Guilfoyle; A. J. Thiel; R. Wang.; L. M. Smith *Nuc. Acids Res.* **1994**, *22*, 5456-5465.

17) A. Muscate; F. Natt; A. Paulus; M. Ehrat *Anal. Chem.* **1998**, *70*, 1419-1424.

18) H. Bunemann; P. Weshoff; R. G. Hermann *Nuc. Acids Res.* **1982**, *10*, 7163-7180.

19) L. Henke; P. A. E. Piunno; A. C. McClure; U. J. Krull *Analytica Chimica Acta* **1997**, *344*, 201-213.

20) N. K. Hogan; L. S. Lerman *Personal communications*, **1999-2001**.

21) H. I. Elsner; S. Mouritsen *Bioconjugate Chem.* **1994**, *5*, 463-467.

22)P. K. Chatterjee; C. R. Cantor *Nuc. Acids Res.* **1978**, *5*, 3619-3633.

23) H. Gamper; J. Piette; J. E. Hearst *Photochem. and Photobiol.* **1984**, *40*, 29-34.

24) G. D. Cimino; H. B. Gamper; S. T. Isaacs; J. E. Hearst *Ann. Rev. Biochem.* **1985**, *54*, 1151-1193.

25) L. A. Chrisey; C. E. O'Farrell; B. J. Spargo; C. S. Dulcey; J. M. Calvert *Nuc. Acids Res.* **1996**, *24*, 3040-3047.

1. Chapter 5. Future Perspectives

Immobilized oligo probes have been used for a variety of applications such as DNA sequencing, gene expression studies and polymorphism screening. However, there is still a lack of understanding on the fundamentals of DNA surface hybridization. Consequently, it is difficult to optimize the performance of the surface probes. The lack of systematic studies on DNA surface hybridization is due to the absence of a reliable method of producing oligo surfaces with desired densities. My first research goal was to develop a methodology for synthesizing oligo surfaces with controllable surface densities. The oligo surface density was controlled by using mixed compositions of end-funtionalized trichlorosilanes to create a thin surface film on silicon, with a controlled proportion of reactive sites. Oligos were then synthesized stepwise onto the reactive sites to generate surface oligo chains with controlled density. Finally, mild deprotection protocols were used to prevent the loss of oligo chains due to degradation of the silane bond by basic $NH_4OH_{(aq)}$.

In addition to generating the appropriate oligo surfaces, I developed a novel characterization technique to accurately quantify the density of my oligo surfaces using XPS. Iodinated phosphoramidites were used as labels to detect the presence of oligo chains on the surface. The measurement results were normalized against a standard (iodine on Au) to determine the oligo surface coverage.

The idea of synthesizing oligo surfaces was further developed into the alternative use of the oligo chains as highly specific molecular glue instead of just as a probe. The oligo chains would immobilize a long chain dsDNA strand through hybridization. By varying the base pair sequences of the oligos on the surface, it is possible to immobilize DNA strands at specific sites. This ability to spatially address a large number of DNA onto a surface is critical to the design of combinatorial DNA microarrays. Long chain dsDNA molecules with 5' end oligo overhangs were synthesized by PCR. The oligo overhangs were produced by using a customized oligo with a poly ethylene glycol spacer, and a 5' psoralen linker, as one of the PCR primers. The spacer prevented the 5' overhang from being filled in by

polymerase during the extension process. The oligo overhangs were used for surface attachment by hybridization to the oligo surfaces. The dsDNA molecules were then covalently attached to the oligo surface by photolysis of the psoralen crosslinker.

The end-immobilized dsDNA molecules could be used for studying DNA interactions with proteins and small molecules, or for polymorphism studies. Or, the dsDNA could be heated to generate end-immobilized ssDNA chains. The ssDNA molecules could act as probes for research in gene expression, or for pathology screens.

The system I devised would be used primarily for generating surface immobilized DNA probes. The oligo surfaces could be directly utilized as surface probes. Or, dsDNA or ssDNA molecules could be covalently end-immobilized onto the oligo surface, also for use as probes. It is evident that the thrust of my research was in design and optimization of a solid-state DNA assay. The approach was to introduce elements of engineering to a previously biologically oriented field. Thus, my efforts concentrated on the development and proof of concept of the covalently end-immobilized oligo/DNA protocol, as well as some initial optimization studies. This focus is apparent in the application for a patent (Paul E. Laibinis, Ivan H. Lee, and Leonard S. Lerman, "*End-Immobilized DNA Brushes on Solid Supports*", filed May 2, 2000). Further fundamental studies of the kinetics and thermodynamics of DNA surface hybridization using this system will be pursued by colleagues.

There are many important aspects of solid-state oligo/DNA assays that need to be explored and optimized. Critical issues of DNA assay performance are the ability to create combinatory arrays, sensitivity, quantification, kinetics, stringency, and reproducibility. Other important issues are cost, possible reuse, integration, and flexibility. Sometimes it is possible to optimize some aspects of a system at the expense of others, and perhaps the requirements for a system is dependent on the application. For example, a pathology screen may emphasize rapid kinetics and only qualitative results, while sensitive gene expression studies may require more quantification in exchange for a longer measurement time.

But regardless of the application, DNA hybridization is the central reaction to all DNA assays, and the key to optimization lies in how to facilitate surface hybridization. The oligo/DNA probes on a surface are restricted in motion and conformation, resulting in slower kinetics. Furthermore, the close proximity of negatively charged oligo/DNA molecules also inhibits DNA hybridization through steric and electrostatic repulsion. On the other hand, a low surface probe density may affect the ability for a quantitative assay as well as the assay sensitivity. Inconsistent surface probe coverage could be an obstacle to reproducibility, and the length of the DNA probe is also a factor in the performance of the assay. The system I developed could be used to address all these issues.

Spatial addressability

My design philosophy for the oligo surfaces was not to try and immobilize exons for every gene in the human genome. Instead, the oligo surfaces would become a flexible platform for immobilizing only the dsDNA or oligo sequences that a particular researcher was interested in. Even if used directly as probes, the feature size of each oligo "pixel" is not meant to approach the miniaturization obtained by the Affymetrix photolithography system. For lower pixel densities, it is possible to use somewhat less rigorous patterning techniques such as soft lithography and nanoliter scale fluid delivery systems. Initially, the glass or silicon surface would be imprinted with protected hydroxy-terminated alkyltrichlorosilane molecules using a patterned PDMS "stamp". At the sites where the PDMS contacted the silicon surface, the trichlorosilanes would quickly form a thin film onto the silicon surface. It is possible to print an array of round pixels, each a few hundred μm in diameter, onto a surface in this manner.

Next, the stamped surface would be immersed in another silane solution containing end groups with very low surface energy. This second silane would form surface films on the bare silicon sites that surround the pixels created by the PDMS stamp. After deprotection, the phosphoramidite solutions used for stepwise synthesis are transferred from an array of very thin tubes onto the surface. The 4-5 nanoliter-sized droplets would be deposited directly onto

the pixels with reactive hydroxy groups. Since the interfacial energy of the hydroxy surfaces are larger then that of the surrounding area, the droplets are pinned to the pixel by surface tension, and are consequently prevented from spreading out to contaminate adjacent pixels. This type of surface tension pinning may be the technology used to produce the FlexChip arrays made by Protogene Inc (Menlo Park, CA).

Upon completion of synthesis the oligo array could be used directly for some DNA assays. If dsDNA or ssDNA arrays are desired, the dsDNA solutions are again delivered to the surface from thin tubes. The oligo overhang hybridizes with the surface oligos to immobilize the dsDNA. Then the dsDNA is crosslinked to the surface by photolysis with UV light. Alternatively, the whole surface could be immersed into a mixture of all the different dsDNA probes desired for the application. The various probe dsDNA would all have oligo overhangs with different sequences. The different oligo sequences allow the dsDNA molecules to become localized at specific sites on a surface by hybridization with a complementary surface oligo chain. Thus the dsDNA probes would self-assemble from solution onto the surface to form the array in one step. This approach was demonstrated in Chapter 4. Once the dsDNA is immobilized and covalently crosslinked, the sample is heated in a buffer solution containing SDS to remove any unattached molecules. Either end-immobilized ssDNA or dsDNA strands could be generated depending on the heating temperature.

Sensitivity

Even when PCR is used to amplify the target DNA for gene expression studies, the sample amounts for some DNA sequences are still low. Sensors with a low detection threshold and high sensitivity are desirable because they could reduce the possibility of false negatives for genes expressed at low levels. It is important for the surface probe density to be somewhat lower to prevent any steric or electrostatic hindrance to the incoming target DNA. My initial studies using oligo surfaces with high ($0.8–1x10^{-10}$ moles/cm^2) densities achieved detection limits at the nM level. However, I believe that sparser coverage could results in even lower thresholds. Systematic studies using a very dilute target DNA solution and oligo

surfaces with different densities would determine the optimal density that maximizes the detection limit. In addition, sensitivity for an assay could be improved by using the appropriate fluorescent or chemiluminescent probes. These molecules may amplify the signal strength by many orders of magnitude and help increase the sensitivity of the assay. Finally, electric focusing or increasing the salt concentration could also help facilitate DNA hybridization and increase the sensitivity.

Quantification

For a DNA assay to be quantitative, it is crucial for all of the DNA molecules in the sample to contact all of the immobilized DNA probes. Currently for most DNA assays the sample DNA solution is statically applied over the surface. Due to the lack of convection, this detection approach does not guarantee that the DNA molecules in the solution would diffuse to all parts of the surface. Since the different probe sequences are localized, it is very possible that some DNA sequences present in the solution don't come into contact with their complementary probes during the experiment. This would result in either a spurious decrease of the gene expression level or even a false negative result. In addition, the amount of surface DNA probes should theoretically be higher than the amount of sample DNA in solution. The excess of surface probes ensures that the assay will not be saturated.

I could obtain surface oligo densities of up to 1.2×10^{-10} moles/cm^2 by synthesizing oligos onto a silicon surface. However, after systematic studies I determined that the amount of DNA hybridized onto the oligo surface is optimized at oligo surface densities of around 2-4×10^{-11} moles/cm^2. This density is at least an order of magnitude higher than most commercial DNA assays and would help decrease the possibility of saturation.

A recirculating flow system for the sample DNA solution could ensure that the target DNA contacts all of the different surface probe sequences. Some researchers are trying to develop flow systems using an SPR apparatus with specialized multichannel substrate chips. The DNA solution would circulate through all the channels and thereby ensure contact with all the DNA probes immobilized on the channel surfaces. It is possible to synthesize oligos in

each channel and use them directly as surface probes. However, it is difficult to synthesize more than one oligo sequence in each channel. For combinatory assays with up to thousands of target sequences it is impossible to create that number of channels onto a single SPR substrate chip.

An alternative would be to immobilize the probe DNA on the inner surfaces of microcapillary tubes. I could derivatize glass microcapillary tubes with a silane surface film with the appropriate surface composition of reactive hydroxy groups. Subsequent stepwise oligo synthesis would generate oligo chains on the insides of the glass tube. Then either oligos or dsDNA molecules with dangling ends would be introduced to hybridize with the oligo surfaces. The psoralen linkers on the oligos or dsDNA molecules are photolyzed to covalently immobilize the probes inside the microcapillary tubes. A series of tubes, each with a different probe could be connected together, and the target DNA solution would be recirculated through the tubes. If more than one probe sequence is desired in each capillary, it is possible to deliver a plug of oligo or dsDNA probe (with overhang) to a certain location in the tube. After hybridization the solution is rinsed away, and a second probe solution is delivered to a different location in the tube. After all the surfaces in the tube have been hybridized with probe DNA, the tubes are illuminated with UV light to covalently attach the probe molecules. The microcapillary tubes are then connect in series and the target DNA solution is circulated repeatedly through the system.

Regardless of the arrangement scheme for oligo/DNA probes inside the microcapillary tubes, the continuous contact of the target DNA in solution with the probes in the tubes should guarantee that every target sequence would come into contact with all possible complementary sequences on the microcapillary surfaces. When the probe density is in excess and when the target DNA sequences are exposed to all possible probe sequences, the assay should become quantitative.

Kinetics

For some DNA assays it is important to obtain results quickly, especially for diagnostic applications. The ultimate goal is close to real-time measurement rates, if only for a qualitative answer. Speed is also desirable for gene expression studies since many experiments must be performed and a faster speed would result in increased data output. For DNA surface hybridization, the surface oligo density plays a critical role in determining the kinetics. My hybridization studies indicated that after 24-hr immersion, the hybridization efficiency of target oligos to the surface oligos increases as the oligo surface density decreases. This strongly suggests that a sparse coverage could dramatically increase hybridization rates. However, very sparse coverage may also result in saturation of the surface oligo probes, rendering quantitative analysis impossible.

In addition, when the oligo surfaces are used to immobilize dsDNA molecules, favorable hybridization kinetics could help improve the production rate. However, since a brush-like structure is preferred for the end-immobilized dsDNA molecules, the surface coverage of covalently attached dsDNA molecules should not be lower than approximately $5x10^{-13}$ moles/cm^2 for about 500 bp length DNA chains. This value is a practical lower limit for the oligo surface coverage. From the above examples it is evident that although lower surface coverage improves hybridization kinetics, other considerations must be evaluated to produce oligo surfaces with the appropriate balance. Therefore, further research should be conducted on how surface coverage affects DNA hybridization kinetics, and how to optimize the kinetics without sacrificing detection capacity.

Other factors that traditionally affect DNA hybridization in solution also affect its surface hybridization. High salt concentrations, increased DNA chain length, increased target concentration, polymers such as dextran sulfate, and lower hybridization temperatures have all been found to facilitate DNA hybridization, increasing the amount hybridized after 24 hours. Research literature has shown that these factors also affect the hybridization kinetics. Thus, some of these conditions may be applied to improve hybridization kinetics. For instance, it is possible to increase the target DNA concentration at a specific site by using electric focusing techniques similar to those applied by Nanogen. This method was shown to increase hybridization rate to a few seconds. But again, one must carefully consider other

factors before making a change. For example, lowering the hybridization temperature may increase the hybridization rate, but could results in reduced hybridization stringency. Also, using long chain ssDNA probes (instead of short 10-20 mer oligos) on the surface may increase hybridization kinetics. However, it also could increase steric and electrostatic hindrances to successful diffusion of incoming target DNA molecules to their immobilized counterparts. Again, research in these areas would also be beneficial for improving the kinetics of solid-state DNA assays.

Stringency

Stringency is critical to the accuracy of DNA assays. Having a false positive on a gene expression study could radically affect the focus of analysis and future research. For short chain oligo probes (10-25 mer), a single base pair mismatch would results in a large difference in the T_m of the DNA duplex, greatly reducing its stability. This effect is the best protection against mismatch hybridization for oligo probes. On the other hand, a single base pair mismatch on a long chain ssDNA probe would not result in a large reduction in the duplex stability. Consequently immobilized ssDNA probes would not be useful SNP screening. However, it is still possible to effectively use ssDNA probes for gene expression studies, because the existence of an appropriately expressed mRNA sequence suggests that the SNP has not affected the expression of that gene.

The primary concern for stringency using long chain ssDNA probes is the partial hybridization of the incorrect target DNA sequence to a probe that shares a partially complementary band. Perhaps there is a 15 bp overlap for two separate DNA sequences, so that target "A" sequence would partially hybridize with probe "B", resulting in a false positive signal. However, this could be remedied by simply increasing the hybridization temperature to above the T_m for all 20 bp duplexes. Since there is rarely any overlap of complementary sequences above 20 bp, this approach should ensure the stringency for hybridization of long chain ssDNA.

Reproducibility

The lack of reproducibility between different production lots of commercial DNA assays has plagued researchers using either Affymetrix chips or cDNA microspot arrays. In both cases, controlling the oligo or cDNA surface density is a key to having reproducible results between runs. For oligos surfaces, the mixed alkylsilane method I developed would control the number of reaction sites available for oligo synthesis. The appropriate synthesis conditions (coupling efficiency >99%) would ensure the fidelity of the oligo chains as well as maximize the number of generated full-length oligos. Finally, mild deprotection protocols would ensure that the synthesized oligo chains are not removed from the surface. By combining the above techniques it is possible to produce oligo surface probes with high sequence fidelity and controlled surface density. For an oligo probe system, another consideration for improving the assays' reproducibility is to minimize steric and electrostatic repulsion for incoming target. This may also be implemented with the mixed alkylsilane methodology.

Immobilized cDNA probes share some of the same issues with oligo surfaces, such as controlled surface probe density. However, for cDNA probes the orientation and structure of the probe molecules is an additional consideration. If the probes are attached randomly to the surface at multiple points, it is difficult to reproduce results since the target DNA hybridized to surface probes at different lengths and locations along the sequence. End-immobilized brush-like structure is favorable for reproducibility of assays using long chain ssDNA surface probes. The ssDNA surfaces I produce are covalently attached at one end to the surface. When solvated in buffer solution with SDS surfactants, the ssDNA chains will not adsorb onto the resistant oligo surface. Therefore the complete length of the ssDNA probe is available for hybridization to the target, as opposed to only partial hybridization for adsorbed DNA probes. Another advantage of a brush-like orientation is that the space between neighboring ssDNA strands is more consistent. Consequently, the electrostatic repulsion and steric hindrance between neighboring ssDNA molecules is more consistent. Thus a brush-like end-immobilized scheme for attaching ssDNA probes should result in higher reproducibility.

Cost

The fabrication cost of DNA arrays vary widely, depending on the techniques and approaches used. The Affymetrix system is expensive primarily due to the design and fabrication costs for the photolithographic masks, and the photolabile deprotection chemistry. In contrast, the cost of Pat Brown cDNA arrays lies in the cDNA probes, which are produced by PCR. The automation and miniaturization techniques for delivering the cDNA probes to the glass surfaces are well developed and fairly inexpensive. My end-immobilized ssDNA probes are also produced by PCR. However, my custom primers contain psoralen linkers and ethylene glycol spacers, which increases the cost of the PCR reaction. But the increase is slight, since a $350.00 batch of customized primer yields about 200 μg of product, which may be used for about 2000 PCR reactions. For arrays with a few hundred sequences the cost increase would not be very high, but if all the genomic sequences are incorporated (30,000-60,000 genes) the cost would be prohibitive. Consequently, the end-immobilized ssDNA arrays I developed are better applied to more focused gene expression studies involving a few hundred to a 1,000 probe sequences rather than the full complement of genomic DNA sequences.

Reuse of DNA assays

The ability to reuse a DNA assay would not only reduce costs, but more importantly could result in better reproducibility of the experimental data between runs. If many runs are performed on the same recycled chip, the data are readily compared without concerns about differences between chips or production lots. The first condition for reusability is that all target DNA must be removed from the assay surface. This is possible for my oligo surfaces since the negatively charged oligos naturally resist adsorption by other oligos or DNA molecules. Previous experiments showed that the target DNA is removed by heating the surfaces in a buffer containing SDS, leaving only 0.01-0.1% background signal. In addition, the immobilized oligos or ssDNA chains must not be removed during the heating process. I have shown that the covalently attached surface oligos are not removed during repeated heating cycles, suggesting that after the target DNA is removed the oligo surfaces can be

used again with consistent performance. No equivalent experiments were performed on the end-immobilized dsDNA and ssDNA chains, but the psoralen crosslinking was shown to resist prolonged exposure to heated buffer solutions. Therefore, I am confident that the ssDNA surfaces are also reusable.

Integration

Many researchers and companies are developing integrated assay systems that combine sample preparation/purification, amplification, and assay all on the same chip. Some of these "lab-on-a-chip" concepts have been proposed for gene sequencing, medical diagnostic screens, and polymorphism studies. A good candidate for the substrate of such an integrated chip would be silicon. The main reason is the ease of fabricating micron-level features on silicon, using techniques used in the semiconductor industry. The ability for patterning is complemented by the ability for adding chemical dopants, which could be used to modify the electrical and thermal conduction properties of the silicon substrate. Thus electric fields or thermal energy could be readily introduced to the system. My oligo system is readily synthesized on silicon surfaces, and could become part of an integrated DNA assay package.

Flexibility

The system I developed was designed to be inherently flexible. The approach was to synthesize a surface array of a few hundred to a thousand different oligo sequences. The oligo sequences are then used as a specific molecular adhesive to end-immobilize various dsDNA chains onto the surface. The dsDNA chains are produced by PCR with a customized primer to generate the 5' end oligo overhang used for hybridization with a surface oligo chain. The oligo arrays are intended as a general platform, to be tailored towards different applications. Researchers would only need a thermocycler and an automated oligonucleotide synthesizer to produce the dsDNA chain required for their experiments. In addition, it is possible to attach oligo chains onto other biomolecules such as enzymes, antibodies and haptens using protein conjugation techniques. These biomolecules could then also become

immobilized onto a surface for assay purposes. Thus, it is possible to use the oligo arrays to produce a multifunctional diagnostic package tailored to the individual.

Another area of flexibility is the system itself. I can use my approach to produce either oligo surfaces, end-immobilized dsDNA surfaces, or end-immobilized ssDNA surfaces. Each of these surfaces could be utilized for different applications. Also, the applications of oligo surfaces are not limited to DNA assays. It is possible to make a temperature sensitive gene delivery system by immobilizing oligo chains with a specific sequence onto the Au pellets used in biolistic guns. The oligo sequence would be designed to have a T_m of less than body temperature under physiological conditions. The DNA to be delivered is produced by PCR, using a custom primer to create oligo overhangs. The DNA is hybridized to the surface oligos at a low temperature, and loaded into the biolistic gun. Once the pellets penetrate the target cells, the DNA desorbs from the gold pellets and is successfully delivered into the cytoplasm. Another possible application of oligo surfaces is molecular architecture. *Seeman* has generated a variety of geometries[1-4] (cruciforms, two, three, four-armed junctions, cubes, octagons) by the hybridization of appropriately designed oligo sequences with "sticky ends". It is possible to immobilize some of these forms onto the surface by hybridization of a sticky end to a surface oligo chain. Since the oligo surface density is controllable, it is possible to assemble a variety of geometric forms at desired intervals onto a surface. In turn, these immobilized DNA geometric forms could act as molecular "scaffolds" that form the basis of nano-scaled surface architectures. The mixed end-functionalized alkylsilane films used for oligo synthesis could be used to generate surfaces with controlled coverage of a particular reactive site. The active sites could be used to synthesize various oligopeptides, or to immobilize small molecules that facilitate cell adhesion. The immobilized biomolecules could then direct cells to adhere at specific sites on patterned surfaces

In conclusion, the central theme of my approach to producing end-immobilized oligo and DNA surfaces is flexibility. The mixed end-functionalized alkylsilane film methodology could be used to control the surface coverage of different functional groups, which in turn could be used for various chemical reactions, or for immobilizing other biomolecules. The

synthesized oligo chains, end-immobilized ssDNA and dsDNA surfaces all have commercial applications in areas such as diagnostics, drug discovery, genomics, and forensics. The XPS method for quantifying oligo surface coverage could also be used to detect and measure other biomolecules such as proteins, antibodies, enzymes, saccharides, antigens, and various small molecules on surfaces.

Furthermore, the various oligo and DNA surfaces are also applicable to fundamental research in the thermodynamics and kinetics of DNA surface hybridization. The results would increase our understanding of the behavior of DNA at interfaces. The gained knowledge could then be utilized to further optimize the performance of solid-state DNA assays, or to devise more novel applications for end-immobilized oligos and DNA. Thus, my work represents the beginning, rather than the end, of systematic research and optimization for immobilized oligo and DNA probes. Perhaps further development and research of my system could lead to techniques or approaches that become applied in the creation of an integrated, automated, multifunctional bioassay system that operates in real-time. This future goal is closer than you think.

5.1 References

(1) L. Furong; R. Sha; N. Seeman *J. Amer. Chem. Soc.* **1999**, *121*, 917-922.

(2) M. L. Petrillo; C. J. Newton; R. P. Cunningham; R.-I. Ma; N. R. Kallenbach; N. C. Seeman, *Biopolymers* **1988**, *27*, 1337-1352.

(3) R.-I. Ma; N. R. Kallenbach; R. D. Sheardy; M. L. Petrillo; N. C. Seeman, N. C. *Nuc. Acids Res.* **1986**, *14*, 9745-9753.

(4) N. Seeman *J. Theor. Biol.* **1982**, *99*, 237-247.

Appendix I. Alkanethiol SAMs on Hg/Au surfaces

A.1 Introduction

Thin organic films formed by functionalized alkanethiol self-assembled monolayers (SAM) on Au substrates have been used to modify the chemical and physical property of surfaces, creating model organic surfaces used for interfacial science research. Linear alkanethiol molecules adsorb onto Au substrates from solution phase under ambient conditions, forming densely-packed, well ordered monolayers with a 3 x 3 crystal lattice, all *trans* configuration, and cant angle of 30° to normal[1 2 3 4 5]. The alkanethiol SAMs are fairly robust and possess consistent surface structure and properties that have been thoroughly characterized by standard surface science techniques such as XPS, grazing angle reflectance FTIR, wetting measurements, STM, AFM, and ellipsometry. In addition, by manipulating the chemical species and compositions of end-functionalized alkanethiols, the SAMs can be used to modify the surface properties of the underlying substrate, with various potential application such as the formation of thin barrier films [6 7] to pacify the surface and prevent corrosion, new photolithography techniques, adhesion mediums [8 9 10 11], and as an immobilization method for attaching biomolecular probes to surfaces.

In addition to Au, other metals with affinity to sulfur compounds have also been studied as candidate substrates for alkanethiol SAM formation, such as silver [4 12 13 14 15 16 17 18,19] and copper[4 12 19 20]. Hg has also been the subject of a few studies, but since it is a liquid under ambient conditions and possesses a high vapor pressure, it has been difficult to characterize SAMs on Hg with traditional surface science techniques. Research has been limited to alkanethiol monolayer formation on bulk Hg sessile drops[21 22]or electrode[23 24 25 26 27 28 29], using STM [21], CV[26 28 29 22]and capacitance[24 25] for characterization. Alkanethiols adsorbed on Hg substrates formed highly impermeable, insulating SAMs following a Langmuir isotherm[29]. Structural studies with X-ray

diffraction and reflectivity suggested that alkanethiol SAMs on bulk Hg have no long-range order, possibly due to the dominance of the Hg-S bond strength over interchain forces[23].

One approach that circumvents the problems of using liquid Hg as a substrate is to deposit it onto another substrate such as Au, which amalgamates readily with Hg. Au-stabilized Hg substrates would not only provide a more stable, robust and practical platform on which to conduct research, but an amalgam may also possess surface properties superior to the pure component metals. For instance, alkanethiol SAMs formed on silver-modified Au substrates have demonstrated higher resistance to thermal desorption than either on pure Au or Ag substrates[18].

Two techniques previously used for depositing Hg onto Au have been underpotential deposition (UPD) of Hg cations from an electrolyte solution onto a Au electrode[30 31 32 33 34]; or, using a forced stream of carrier gas such as N_2 or air to deposit Hg vapor onto the Au surface[35 36 37 28 29 22 38]. However, Hg was observed to amalgamate with Au to form dendrite structures when coverage exceeded one monolayer[39 40 41 42 38,43], so it is crucial to control the amount of Hg deposited on Au at the sub-monolayer level. For UPD Hg films on Au, there has been disagreement on the adlayer lattice structure, the possibility of contamination by the coadsorption of oxygen or sulfate molecules present in the system, and on the reaction conditions affect adlayer structure[31 32 33 34]. In addition, Hg deposition under forced flow was very rapid and often resulted in the formation of multilayer amalgamates. Therefore we decided to try and reduce the deposition rate of Hg on Au by using vapor deposition under natural convection, a simple and direct adsorption method.

Presently, no research has been conducted on the properties of alkanethiol SAMs on a Hg modified Au substrate. Our goal is to deposit Hg onto Au substrates under ambient temperature and pressure at submonolayer coverage. Alkanethiol SAMs formed on this substrate will be observed with standard surface science techniques such as XPS,

FTIR, wetting measurements, ellipsometry, and CV. Our research will focus on the alkanethiol SAM structure, order, surface properties, and how these properties change with reaction conditions. Specifically, we will look into the thermal stability of alkanethiol SAMS on Hg modified Au surfaces, to determine whether such a system can be used to stabilize adlayers of thiolated biomolecules subjected to elevated temperatures.

A.2 Experimental Section

Materials: Au shot (99.99%) and chromium-coated tungsten filaments were obtained from Americana Precious Metals Co. (East Rutherford, NJ) and R.D. Mathis (Long Beach, CA), respectively. Elemental Hg (99.9995%), octadecanethiol, dicyclohexane, and hexadecane were obtained from Aldrich and used as received. Ethyl alcohol (95%, Pharmco) and isooctane (EM science) were reagent grade. Docosanethiol, undecanethiol, 11-(2,2,3,3,3 pentafluoropropyloxy)-undecanethiol[12] and octadecanethiol-d_{37} [44] were available from previous studies.

Sample preparation: Chromium (100 Å) and Au (1000 Å) were sequentially evaporated at 1.5 Å/s and 4 Å/s, respectively, onto 100 mm silicon (100) wafers (Silicon Sense) in a diffusion-pumped vacuum chamber at an operating pressure of 2×10^{-6} torr. The wafers were cut into 1 x 3 cm^2 slides, washed with ethyl alcohol, dried with N_2, and transferred into an N_2-filled glove box. The samples were inserted vertically into a 20 ml scintillation vial with the Au-coated surface facing a Hg reservoir located at the bottom of the vial. Alkanethiol SAMs were formed by immersing the Hg modified Au surfaces in 1mM alkanethiol solutions (in ethanol or isooctane) for various periods of time at ambient conditions. The samples were removed from solution, washed sequentially with isooctane and ethyl alcohol, and dried with N_2 before characterization. Exposure time to the Hg vapor, and the alkanethiol solutions, and to air during assembly of the SAM system were varied to determine its sensitivity to the preparative conditions.

Methods of characterization: General instrumental parameters and methods for characterization of SAMs by XPS, FTIR, wetting measurement, ellipsometry, and electrochemistry, have been previously described.[45]

XPS binding energies were referenced to Au ($4f_{7/2}$) = 84.00 eV. Samples were stored in N_2 and exposed to air for less than 5 min prior to XPS characterization. Reflectance infrared spectra were obtained at grazing angles 80° from normal. A Au sample with octadecanethiol-d_{37} monolayer was used as background, and 1024 scans were performed with polarized light at 2 cm^{-1} resolution.

Ellipsometry thickness was calculated using a refractive index of 1.45. Baseline Ns, Ks values were taken on Au samples deposited with Hg in N_2, with less then 5 min exposure to air. All cyclic voltammetry (CV) scans were run in an electrochemical cell with 0.8 cm^2 area aperture, in 0.1 M $H_2SO_{4(aq)}$ solution using a supported Au film as counterelectrode and silver wire as reference electrode.

Stability studies: XPS was used to determine the Hg coverage on Hg modified Au samples. Next, the samples were oxidatively stripped by voltage ramped from +50 mV to +1050 mV. Subsequently the sample was scanned for Hg coverage by XPS. The same process was repeated with alkanethiol SAM covered samples and the data compared.

Hg modified Au and Au samples were immersed in 11-(2,2,3,3,3 pentafluoropropyloxy)-undecanethiol solution for 30 min, then placed in dihydronaphthalene and heated by an oil bath to 85 °C. At various time intervals, samples were removed, rinsed with isooctane and ethanol, and the fluorine (1s, 270eV) and Hg ($4f_{7/2}$, 100eV) intensities measured by XPS.

A.3 Results and discussion

A.3.1 Hg deposition on Au

Hg deposition on Au: To establish deposition conditions for producing submonolayer Hg coverage, we exposed the evaporated Au samples to a vapor of elemental Hg under natural convection for 1 minute to 4 hours time. A schematic of the experimental setup is shown in Figure A-1. The Hg deposition was conducted in a nitrogen-filled glove box to prevent the Hg adlayer on Au from oxidization. The samples were characterized by XPS to determine the level and rate of Hg adsorption, and the results are shown in Figure A-2. The observed Hg coverage increased dramatically within the first 5 min of deposition, then gradually leveled out in the 10 min to 1 h time range. After 2 h of deposition, silver-colored dots were observed (optically) scattered on the sample surface, suggesting that Hg was amalgamating with Au into islands.

Subsequently, Hg coverage was calculated from the XPS data using the equation presented by Jennings and Laibinis[45]:

$$\phi_{upd} = \left\{ \left(\frac{I_{Au}}{I_{upd}} \right) \left(\frac{I^{\circ}_{upd}}{I^{\circ}_{Au}} \right) C_{SAM} \left[1 - \exp\left(\frac{-a_{upd}}{\lambda_{upd(KE_{upd})} \cos\Theta} \right) \right] + \left[1 - \exp\left(\frac{-a_{upd}}{\lambda_{upd(KE_{Au})} \cos\Theta} \right) \right] \right\}^{-1}$$

where C_{SAM} is approximately 1, $\Theta = 55°$, and $a_{upd} = 3.5$ A.

The equation is based on the attenuation in the XPS signal intensity of the underlying substrate by the adlayer, which reduces the intensity of the incoming X-ray beam that impacts the substrate, by interacting with a portion of the incoming X-ray beam. In the case of Hg deposition on Au, certain constants were determined. First, the empirically derived XPS sensitivity factors were determined for Au (I_{Au}° = 10.7) and Hg (I_{Hg}° = 11.6). For Hg monolayer on Au without SAM, the inelastic mean

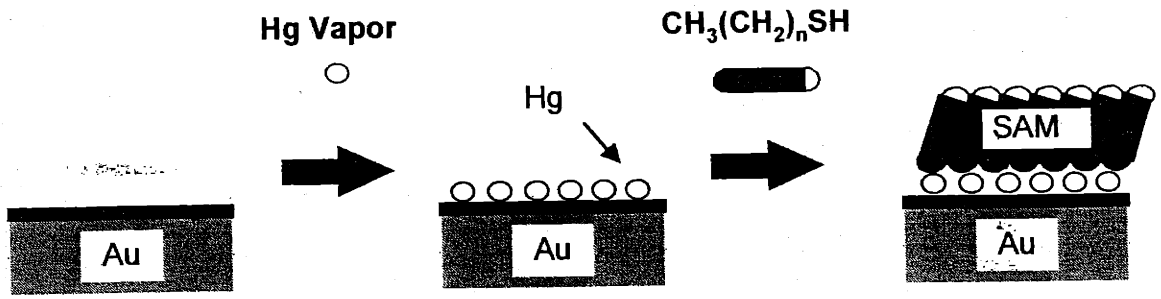

Figure A-1: Procedure for alkanethiol SAM formation on Au/Hg substrate

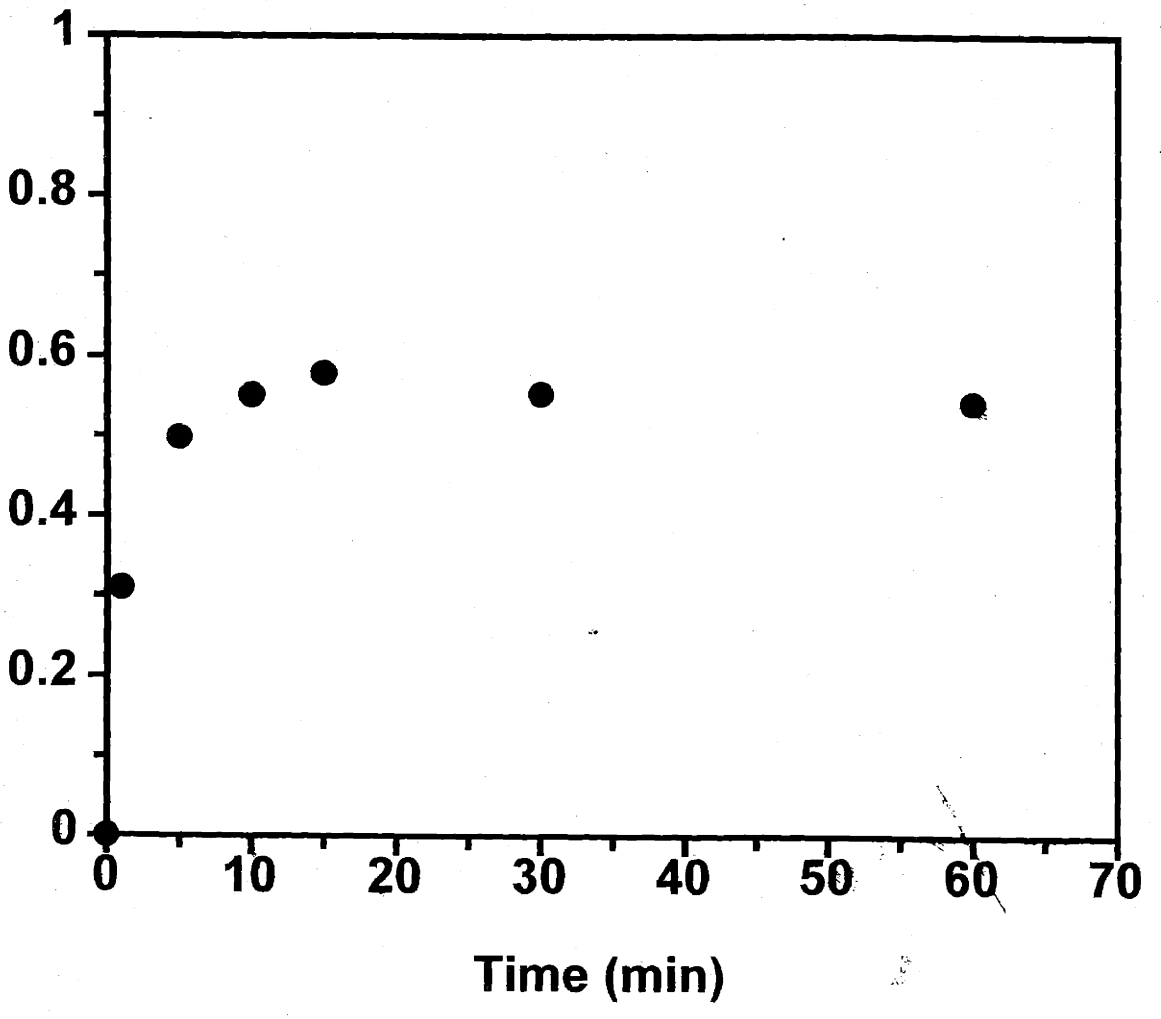

Figure A-2: Hg coverage on Au vs. deposition time determined by XPS

free path of Hg ($\lambda_{upd(KEupd\ Au)}$) was assumed to be approximately equivalent to Au ($\lambda_{upd(KEupd\ Hg)}$), and determined at 1000 eV energy to be 12.9 Å[46]. Attenuation factors for SAM monolayers on Au ($\lambda_{SAM(KE\ Au)}$) and Hg ($\lambda_{SAM(KE\ Hg)}$) were determined by the equation presented by Laibinis,[47] which resulted in 39.8 A for Au, and 39.4 A for Hg, respectively. I_{Au} and I_{Hg} represent the integrated XPS intensities corresponding to Au ($4f_{7/2}$) and Hg ($4f_{7/2}$). Cyclic voltammetry was also used to determine Hg coverage, by charge density measurements obtained from oxidative stripping of Hg from Au. Romeo and Posadas[41] have determined the charge density of monolayer Hg to be 340 $\mu C/cm^2$, with 1.6-1.7 exchange electrons per Hg atom, which were used as the basis for coverage calculations.

From XPS and CV data the Hg adlayer was determined to be approximately 0.65 +/- 0.15 of a monolayer for 30-minute deposition times. This rate was much slower than the results of George and Glaunsinger[30] who observed single monolayer Hg coverage after 60 seconds of Hg deposition. A possible explanation for this is the use of natural convection rather than forced airflow[30] for Hg deposition, which resulted in slower Hg diffusion kinetics to the Au surface. Despite the spread in coverage, Hg was consistently deposited at submonolayer coverage over a time range of 15 minutes to 1 hour, without amalgamating with Au. Therefore a 30-minute deposition time was chosen as the standard for creating the Hg modified Au substrates used for alkanethiol SAM surface property and stability studies.

An XPS survey scan of octadecanethiol SAM on Hg/Au surface (Fig. A-3) confirmed that Hg remained on the Au surface after SAM formation. The lack of oxygen peaks suggests that the Hg was not oxidized. This is supported by the absence of binding energy shift for Hg before (99.88 eV), and after (99.80 eV) SAM formation, from XPS data.

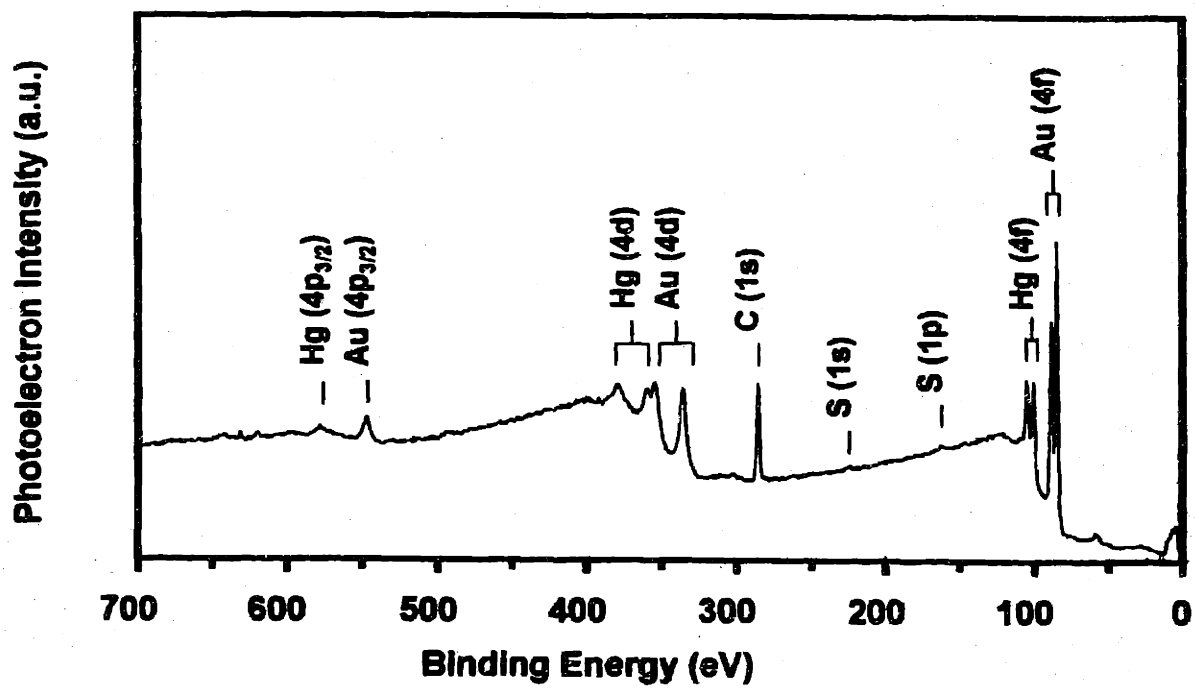

Figure A-3: XPS survey scan of octadecanethiol SAM on Hg-modified Au surface

A.3.2 Alkanethiol SAM formation on Hg/Au substrate

Ellipsometry: From ellipsometry, the thickness of an octadecanethiol (C18) SAM was determined at 23+/-2 Å, versus 19+/-2 Å for a C18 SAM formed on pure Au substrate, suggesting that the C18 formed a SAM onto the Hg modified Au surface with close to normal orientation.[17] The film thickness measured by ellipsometry for other alkanethiol SAMs such as those formed by undecanethiol (14+/-2 Å) and docosanethiol (27+/-2 Å) suggests a linear relationship between the SAM thickness and alkane chain length.

Contact Angles: Contact angles were measured for undecanethiol, octadecanethiol, and docosanethiol under a variety of conditions, with consistent θ_a values of 110-112°, θ_{ret} of 95-97° for water; and θ_a values of 42-45°, θ_{ret} of 34-37° for hexadecane. Natural variances (+/- 2°) aside, the angles are only slightly lower than for pure Au (θ_a of 114-116°, θ_{ret} of 95-97° for water; θ_a of 44-45°, θ_{ret} of 31-33° for hexadecane), with comparable hysteresis values, suggesting the thiol monolayers are well ordered and closely packed, with few defects. These results are in agreement with Demoz and Harrison for SAM on bulk Hg.[25]

FTIR: The infrared spectra of octadecanethiols on a Hg modified Au substrate resembled that of those formed on silver modified Au (UPD) [30] and pure silver[30] substrates. (See Figure A-4), and a computer program developed by Atul[10] was utilized to fit the IR profile for C18 on Hg modified Au substrates (See fig. A-5). C18 SAMs on Hg modified Au substrates had cant angles between +12° to + 15°, and twist angles between 45° to 50°. The IR results were reproducible and consistent, and were supported by ellipsometry data that suggested that the orientation of the alkyl chains was almost normal to the surface. In addition, the dichroic ratio of CH_2 asymmetric to

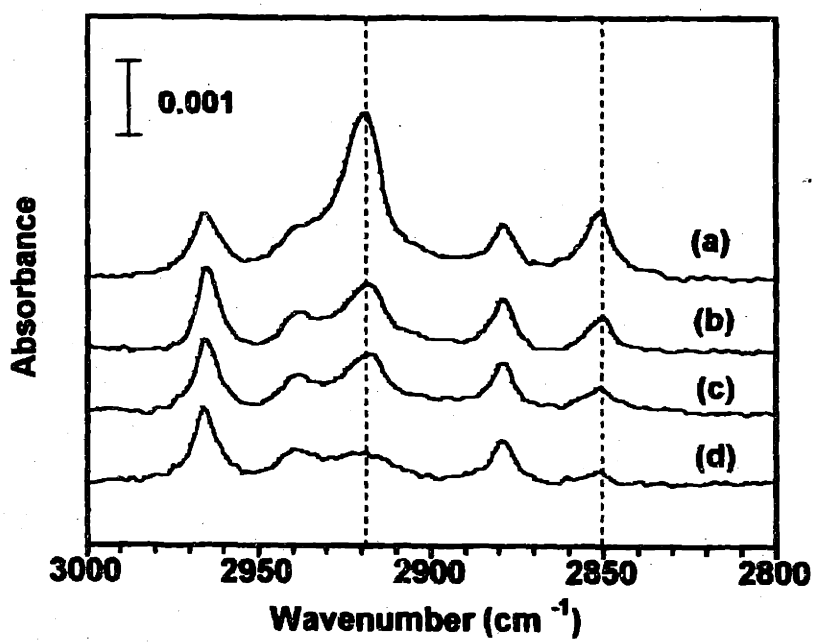

Figure A-4: IR Spectra obtained for octadecanethiol SAM on: (a) Au surface; (b) Ag surface; (c) Au/Hg surface, maximum cant angle; (d) Au/Hg surface, minimum cant angle

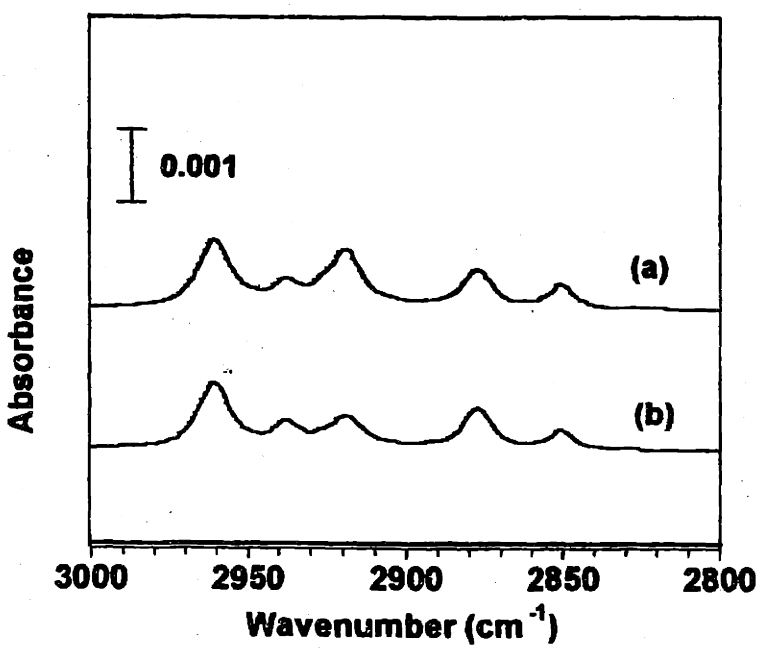

Figure A-5: Computer-fitted IR spectra for alkanethiol SAM using Atul's program: (a) cant 15°, twist 50°; (b) cant 12°, twist 45°

symmetric IR peak intensities was observed at between 2.0 to 2.3, indicating a twist angle of 50°.

The fitted cant angles are lower than the perpendicular orientation determined for alkanethiol SAMs on liquid elemental Hg[23 24]. Perhaps this is because the substrate consists of a Hg adlayer of submonolayer thickness on Au, which is in effect a homogenous mixture of Hg and Au atoms on the adsorption surface, resulting in cant angles being moderated between pure Hg and pure Au. The wavenumber of the CH_2 asymmetric stretching peak was observed at 2920 cm^{-1}, vs. 2918 cm^{-1} for at C18 SAM on Au substrate, suggesting a less crystalline structure for alkanethiol SAMs formed on Hg modified Au substrates compared to those formed on pure Au substrates. This result concurred with Ocko's findings that alkanethiol SAMs formed on Hg surfaces lack long-range order.[23]

Consistent IR profiles were observed with different solvents (ethyl alcohol vs. isooctane), Hg deposition times, air exposure times prior to SAM formation, and immersion times in alkanethiol solution for up to 1 h, suggesting that robust and consistent SAM structures are formed under nonrigorous conditions. In addition, experiments in which Hg deposited on Au in ambient air, and those for 1 minute SAM formation times also yielded IR spectra consistent with the standard procedure of 30 minutes of Hg deposition on Au in N_2 followed by 30 minutes of immersion in the alkanethiol solution, leading to the following conclusions. First, the rate of Hg oxidation in air is very slow. This was supported XPS data on Hg to oxygen intensity ratios, which remained constant with respect to air exposure time; Furthermore, the SAM forms almost instantaneously, which agrees with Demoz and Harrison's conclusion that SAM forms on Hg within one minute[25] of immersion. From the above results, it is reasonable to conclude that alkanethiol SAMs on Hg/Au can be produced under ambient conditions in atmosphere.

The consistency of contact angle measurements and IR spectra, when subjected to variations in deposition conditions previously mentioned, add to the argument that alkanethiol monolayer properties are not significantly influenced by the following

operational factors: Hg deposition times between 15 minutes to 1 hour; immersion times in thiol solutions between 1 minute to 2 hour; air exposure for up to 1 hour prior to immersing the Hg modified Au sample in the alkanethiol solution; either isooctane or ethyl alcohol solvents.

A.3.3 Stability studies

SAMs of octadecanethiol and docosanethiol in air were periodically observed by FTIR for 12 days, with no change in the IR spectra, suggesting that the monolayer remained stable with exposure to air. This conclusion was further supported by the constant Hg coverage observed by XPS, which indicated a lack of Hg evaporation or diffusion into the Au substrate.

When immersed in solution for 12 hours, spots were observed on the SAM coated sample surface, suggesting degradation of the organic film due to etching. This is supported by a large increase in the IR spectra CH_2 asymmetric peak intensity, equivalent to an increase in cant angle from 12° to 30°. Therefore it is reasonable to conclude that alkanethiol SAMs on Hg modified Au substrates are not stable after long periods of immersion in alkanethiol solutions.

XPS measurements of Hg coverage after oxidative potential was applied on Hg modified Au substrates with and without SAMs indicated that Hg was removed from the Au surface on the bare Hg modified Au sample, whereas there was no change in for samples coated with C18 SAMs. The results suggest that the alkanethiol monolayer formed a nonpermeable, resistive barrier, which prevented the Hg from being stripped off the Au surface.

We conducted thermal stability studies by forming a 11-(2,2,3,3,3, pentafluoropropyloxy)-undecanethiol SAM on the Hg modified Au substrates and on pure Au subtrates. The fluorine labeled SAM was highly hydrophobic, with a θ_a of approximately 125°. Then we heated the SAM coated samples to 85°C and observed by XPS how the fluorine intensities at 269eV changed with respect to immersion time, and the results are shown in Figure A-6. The XPS data showed a steady decrease in the fluorine signal intensity with time, for Hg modified Au substrates, until it reached zero at around 4 h immersion at 85° C, suggesting total desorption of the 11-(2,2,3,3,3, pentafluoropropyloxy)-undecanethiol SAM.

This conclusion was supported by the recurrence of surface wetting against ethanol and H_2O, for Hg modified Au samples removed from DHN solution after 4 hours immersion time at 85° C. Also from XPS, the Hg coverage showed no decrease with time, suggesting that the main desorption mechanism was cleavage of the Hg-S bond. This hypothesis is supported by the Hg-S bond strength [48], which is weaker than the Au-S bond strength[49], perhaps explaining why alkanethiol SAMs on Hg modified Au substrates are less stable compared to those on pure Au at elevated temperatures. The inferior thermal stability of the alkanethiol SAMs formed Hg modified Au surfaces decreases its potential as a substitute for Au for DNA assays using adsorbed thiolated dsDNA as probes, since the surfaces needed to be heated to above 90°C for extended periods of time to ensure that the DNA duplex melts and a ssDNA strand is exposed to form the probe molecule.

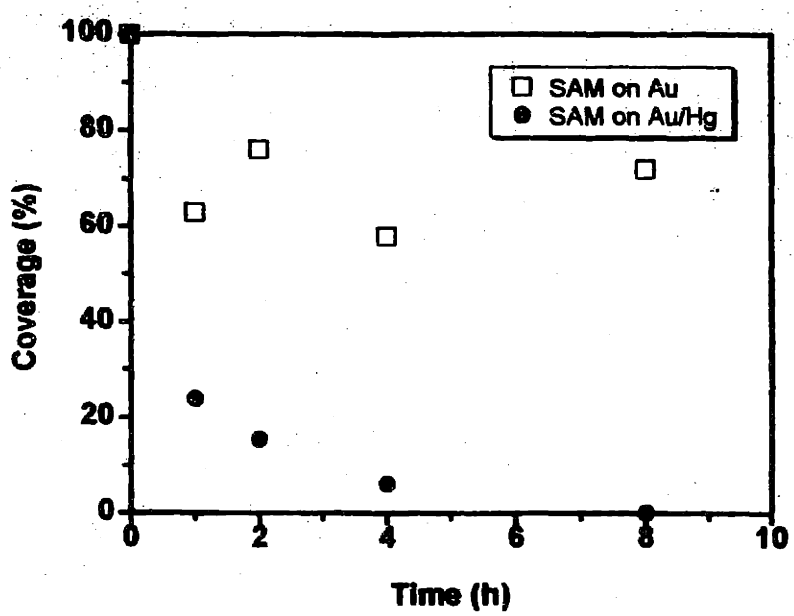

Figure A-6: $CF_3CF_2CH_2O(CH_2)_{11}SH$ **SAM coverage vs. time on Au and Au/Hg surfaces at 85° C in dihydronaphthalene, determined by XPS**

A.4 Conclusion

Elemental Hg was vapor deposited onto Au surface under natural convection, with surface coverage of 0.60+/-0.15 monolayers, and no Hg/Au amalgamates formed at deposition times less than 1 hour. Alkanethiols formed SAMs on the Hg/Au surface, with thickness of 23+/-2 Å (for octadecanethiol) and close to normal orientation. Contact angles in water were: θ_a of 110-112°, θ_{ret} of 94-97°; hexadecane angles were θ_a of 42-45°, θ_{ret} of 34-37°. The contact angles in water for the SAMs formed on Hg modified Au surfaces were very close to those formed on Au surfaces, which was expected, and the low degree of hysteresis suggested that the SAM layer was well ordered and homogenous.

IR spectra for C18 SAMs formed on Hg modified Au substrates showed cants of +12-+15°, and twist angles of between 45-50°, resembling that of SAMs on UPD silver on Au and pure silver systems. IR spectra and contact angles were consistent and reproducible for a 1 minute to a 1 hour immersion times in alkanethiol solutions, up to 1 hour exposure to air, and different solvents. In addition, alkanethiol SAMs on Hg deposited in air yielded IR spectra and contact angles consistent with those done in N_2, suggesting that Hg deposition on Au can be performed in atmosphere without significant affect on the surface properties of the alkanethiol SAM subsequently formed on the Hg modified Au surface. SAMs on Hg modified Au surfaces were shown to be stable in air and to oxidative stripping, but will be etched if immersed in the alkanethiol solution for a 12 hour period. At 85° C, alkanethiol SAMs formed on Hg modified Au substrates were less thermally stable compared to SAMs formed on a pure Au surface. Therefore we could not use Hg modified Au surfaces to replace pure Au surfaces as a platform for immobilizing thiolated dsDNA chains.

A.5 References

1) A. Ulman *An Introduction to Ultrathin Organic Films From Langmuir-Blodgett to Self-Assembly*; Academic Press: Boston, 1991.

2) L. H. Dubois; R. G. Nuzzo *Annu. Rev. Phys. Chem.* **1992**, *93*, 437-463.

3) A. Ulman *Chem. Rev.* **1996**, *96*, 1533-1554.

4) P. E. Laibinis; G. M. Whitesides; D. L. Allara; Y. -T. Tao; A. N. Parikh; R. G. Nuzzo *J. Am. Chem. Soc.* **1991**, *113*, 7152-7167.

5) C. D. Bain; E. B. Troughton; Y. -T. Tao; J. Evall; G. M. Whitesides; R. G. Nuzzo *J. Am. Chem. Soc.* **1989**, *111*, 321-325.

6) P. E. Laibinis; G. M. Whitesides *J. Am. Chem. Soc.* **1992**, *114*, 9022-9028.

7) J. D. Swalen; D. L. Allara; J. D. Andrade; E. A. Chandross; S. Garoff; J. Israelachvili; T. J. McCarthy; R. Murray; R. F. Pease; J. F. Rabolt; K. J. Wynne; H. Yu *Langmuir* **1987**, *3*, 932-950.

8) C. N. Sayre; D. M. Collard *Langmuir* **1995**, *11*, 302-306.

9) M. J. Tarlov *Langmuir* **1992**, *8*, 80-89.

10) R. J. Wilicut; R. L. McCarley *J. Am. Chem. Soc.* **1994**, *116*, 10823-10824.

11) D. R. Jung; A. W. Czanderna *Crit. Rev. Solid State Mater. Sci.* **1994**, *19*, 1-54.

12) P. E. Laibinis; G. M. Whitesides; D. L. Allara; Y. -T. Tao; A. N. Parikh; R. G. Nuzzo *J. Am. Chem. Soc.* **1992**, *114*, 1990-1995.

13) M. M. Walczak; C. Chung; S. M. Stole; C. A. Widrig; M. D. Porter *J. Am. Chem. Soc.* **1991**, *113*, 2370-2378.

14) M. A. Bryant; J. E. Pemberton *J. Am. Chem. Soc.* **1991**, *113*, 3629-3637.

15) P. Fenter; P. Eisenberger; J. Li; N. Camillone III; S. Bernasek; G. Scoles; T. A. Ramanarayanan; K. S. Liang *Langmuir* **1991**, *7*, 2013-2016.

16) A. Dhirani; M. A. Hines; A. J. Fisher; O. Ismail; P. Guyot-Sionnest *Langmuir* **1995**, *11*, 2609-2614.

17) P. E. Laibinis; M. A. Fox; J. P. Folkers; G. M. Whitesides *Langmuir* **1991**, *7*, 3167-

3173.

18) G. K. Jennings; P. E. Laibinis *Langmuir* **1996**, *12*, 6173-6175.

19) G. K. Jennings; P. E. Laibinis *J. Am. Chem. Soc.* **1997**, *119*, 5208-5214.

20) M. Nishizawa; T. Sunagawa; H. Yoneyama, *Langmuir* **1997**, *13*, 5215-5217.

21) J. Janata; C. Bruckner-Lea; J. Conroy; A. Pungor; K. Caldwell *Proc. Am. Chem. Soc.* **1994**, 175-185.

22) C. Bruckner-Lea; R. J. Kimmel; J. Janata; J. F. T. Conroy; K. Caldwell, *Electrochimica Acta* **1995**, *40*, 2897-2904.

23) O. M. Magnussen; B. M. Ocko; M. Deutsch; M. J. Regan; P. S. Pershan; D. Abernathy; G. Grubel; J. F. Legrand *Nature* **1996**, *384*, 250-252.

24) K. Slowinski; R. V. Chamberlain; R. Bilewicz; M. Majda *J. Am. Chem. Soc.* **1996**, *118*, 4709-4710.

25) A. Demoz; D. J. Harrison *Langmuir* **1993**, *9*, 1046-1050.

26) N. Muskal; I. Turyan; D. Mandler *J. of Electroanal. Chem.* **1996**, *409*, 131-136.

27) M. G. Paneli; A. N. Voulgaropolous *Electroanalysis* **1995**, *7*, 292-294.

28) T. T. Mercer *Anal. Chem.* **1979**, *51*, 1026-1030.

29) R. J. Forster *Langmuir* **1995**, *11*, 2247-2255.

30) M. A. George; W. S. Glaunsinger *Thin Solid Films* **1994**, *245*, 215-224.

31) E. Herrero; H. D. Abruna *Langmuir* **1997**, *13*, 4446-4453.

32) C. H. Chen; A. A. Gewirth *Physical Review Letters* **1992**, *68*, 1571-1574.

33) J. Inukai; S. Sugita; K. Itaya *J. Electroanal. Chem.* **1996**, *403*, 159-168.

34)C. H. Chen; A. A. Gewirth *Ultramicroscopy* **1992**, *42-44*, 437-444.

35) M. Levlin; H. E. -M. Niemi; P. Hautojarvi; E. Ikavalko; T. Laitinen *Fres. J. Anal. Chem.* **1996**, *355*, 2-9.

36) M. A. George; W. S. Glaunsinger; T. Thundat; S. M. Lindsay *J. Microscopy* **1988**, *152*, 703-713.

37) M. A. Butler; A. J. Ricco; R. J. Baughman *J. Appl. Phys.* **1990**, *67*, 4320-4326.

38) C. Battistoni; E. Bemporad; A. Galdikas; S. Kaciulis; G. Mattogno; S. Mickevicius; V. Olevano *Appl. Surf. Sci.* **1996**, *103*, 107-111.

39) L. A. Schadewald; T. R. Lindstrom; W. Hussain; E. E. Evenson; D. C. Johnson *J. Electrochem. Soc.* **1984**, *131*, 1583-1587.

40) M. Shay; S. Bruckenstein, *Langmuir* **1989**, *5*, 280-282.

41) F. M. Romeo; R. I. Tucceri; D. Posadas *Langmuir* **1990**, *6*, 839-842.

42) G. Salie; K. Bartels *J. Electroanal. Chem.* **1988**, *245*, 21-38.

43) G. Salie *J. Electroanal. Chem.* **1989**, *259*, 315-319.

44) P. E. Laibinis; R. G. Nuzzo; G. M. Whitesides *J. Phys. Chem.* **1992**, *96*, 5097-5105.

45) G. K. Jennings; P. E. Laibinis *J. Am. Chem. Soc.* **1997**, *119*, 5208-5214.

46) S. Tanjuma; C. J. Powell; D. R. Penn *Surface and Interfacial Analysis* **1988**, *11*, 577-589.

47) P. E. Laibinis; C. D. Colin; G. M. Whitesides *J. Phys. Chem.* **1991**, *95*, 7017-7021.

48) A. K. Rappe; C. J. Casewit; K. S. Colwell; W. A. Goddard III; W. M. Skiff *J. Am. Chem. Soc.* **1992**, *114*, 10024-10035.

49) R. C. Weast; M. J. Astle; W. H. Beyer *CRC Handbook of Chemistry and Physics*; 66th ed.; Weast, R. C.; Astle, M. J.; Beyer, W. H., Ed.; CRC Press: Boca Raton, 1986.

Undefined references

9) Atul's paper on IR program

17) An ellipsometer was used to measure the thickness of octadecanethiol monolayer on pure Au and on Hg covered Au substrates, and the thickness compared. For pure Au substrate SAM thickness 19 +/-2 □, corresponding a 30° cant angle. By multiplying SAM thickness with cosecant^{-1}(30°), a value of 22 +/-2 Å was obtained for octadecanethiol at 0° cant. The thickness for octadecanethiol monolayer on Hg/Au substrate was measured at 23 +/-2 Å indicates that it is close to the surface normal when compared to octanethiol at 0° cant.

1. Appendix II. Sequences of oligos and template DNA

1. Sequence name: *"*"*

Application: Used as the standard sequence for conducting most surface hybridization experiments and for studying oligo synthesis efficiency.

Sequence:

Surface: 5'→ATGGTGAGTTTT→3'
Solution: 3'→TACCACTCAA →5'

2. Sequence name: *"Poly 9A"*

Application: Used as the alternative sequence for conducting surface hybridization experiments and for studying oligo synthesis efficiency.

Sequence:

Surface: 5'→TTTTTTTTTTTT→3'
Solution: 5'→AAAAAAAAA →3'

3. Sequence name: *"X"*

Application: Used for immobilizing "P" sequence customized primer, or dsDNA PCR product (with a 5'oligo overhang).

Sequence:

Surface: 5'→ATGCGGCCTGTATTTT→3'
Solution 3'→TACGCCGGACATA →5'

4. Sequence name: *"C9"*

Application: Customized PCR primer with ethylene glycol spacer and 5' psoralen linker. Hybridizes with "*" sequence surface oligos.

Sequence: solution

5'→C2 psoralen-AACTCACCAT-C9 spacer-ATCCTCTAGAGTCCCGCGCC→3'

5. Sequence name: *"P"*

Application: Customized PCR primer with ethylene glycol spacer and 5' psoralen linker. Hybridizes with "X" sequence surface oligos. Used as a second oligo sequence when attempting to spatially address dsDNA with overhangs onto patterned oligo surfaces.

Sequence: solution

5'→C2 psoralen-ATACGCCGGACAT-C9 spacer-ATCCTCTAGAGTCCCGCGCC→3'

6. Sequence name: *"GC"*

Application: Used for studying the effect of GC content on surface DNA duplex stability. Also considered as a method for immobilizing dsDNA onto oligo surfaces with some degree of thermal stability.

Sequence:

Solution: 5'→GGGCGCGGGGCGCGGGCGGC→3'

Surface: 5'→GCCGCCCGCGCCCCGCGCCCTTT→3'

7. Sequence name: *"Hbglb"*

Application: Template dsDNA used for PCR amplification. Can incorpate either "C9" or "P" primers. 390 bp in length.

Sequence:

5'→acgttgtaaa acgacggcca gtgaattcga gctcggtacc cggggatcct ctagagtccc gcgccccccgtg
ccccccgcccc gcccgccgga ctgcagtttt gatCCCTGGG CAGGTTGGTA TCAAGGTTAC
AAGACAGGTT TAAGGAGACC GGGCATGTGG AGACAGAGAA
GACTCTTGGG TTTCTGATAG GCACTGACTC TCTCTGCCTA TTGGTGTATT
TTCCCACCCT TAGGCTGCTG GTGTCTACC CTTGGACCCA GAGTTCTTT
$(A)_{10}$CTCGG TGCCTTTAGT GATGGcgcgc aagctttccc→3'

8. Sequence name: *"3' primer"*

Application: Used as 3' primer for the PCR amplification of Hbglb sequence.

Sequence:

Solution: 5'→TACGCCAAGCTCTAATACGACTCA→3'